UNIVERSITÀ DEGLI STUDI DI CATANIA
Dipartimento di Fisica e Astronomia
International PhD in Nuclear and Particle Astrophysics

Armando Puglisi

Transport coefficients and early time dynamics of the Quark-Gluon Plasma created in ultra-relativistic heavy ion collisions

Ph.D. Thesis

Ph.D. Coordinator:
Chiar.mo Prof. Stefano Romano

Tutor:
Chiar.mo Prof. Vincenzo Greco
Dott. Marco Ruggieri
Dott. Salvatore Plumari

Ciclo XXVIII 2012/2015

Contents

To my family

with A Tramontana breeze.

"So once you do know what the question actually is, you'll know what the answer means".
Deep Thought

"Do. Or do not. There is no try."
Yoda

"Sometimes it's a little better to travel than to arrive"
Robert M. Pirsig,
Zen and the Art of Motorcycle Maintenance

Abstract

The phase diagram of QCD, the gauge theory that describes the strong interaction, is actually under exploration both theoretically and experimentally searching for the phase transition from ordinary matter to a deconfined phase of quarks and gluons, namely the Quark-Gluon Plasma. Being a remarably complex theory, such a task is very difficult however there are several indications that the phase transition occurs as indicated by Lattice QCD calculations, in the low baryon density region, at a critical temperature of $T_c \sim 155\, MeV$. Phenomenological models predict also a phase transition at high density and low temperature, like in the interior of neutron stars. On the experimental side, the only way to access the QGP in a laboratory is to collide heavy ion collision at ultra-relativistic energies as actually carry out at LHC at CERN and at RHIC at BNL.

One of the most amazing discovery was that the system created in these collisions behaves like a perfect fluid. Indeed hydrodynamics calculations show that the large anisotropic flows measured are in agreement with a shear viscosity to entropy density ration η/s close to the minimum value predicted by AdS/CFT $\eta/s = 1/4\pi$.

In this thesis we discuss about two main subjects of Quark-Gluon Plasma (QGP) produced in ultra-relativistic heavy ion collisions. The first one is a sistematic study of transport coefficients, in particular shear viscosity and electric conductivity of QGP. The second one regards a modeling of initial fields and their early time dynamics of the system produced in such collisions.

Our challenge is to develop a very precise transport based approach with a fixed value of η/s, being the physical quantity that describes a fluid in strong coupling, instead of dealing with all the specific amplitudes scattering one has to consider in the collision integral of the Boltzmann equation. In order to achieve such a task, we compute the shear viscosity solving the Relativistic Boltzmann Transport equation and using the Green-Kubo relation that, being not affected by any kind of approximation, gives us the possibility to find the correct formula among the analytical derivations in Relaxation Time Approximation and in Chapman-Enskog scheme.

Using our numerical solution to the Relativistic Boltzmann Transport equation we also compute the electric conductivity σ_{el} of the QGP. This transport coefficient, the inverse of the electric resistence, represents the response of the system to an applied external electric field and only very recently has captured the attention in the field of QGP due to the strong electric and magnetic fields present in the early stage of the collision. Our focus was to characterize the relation between the σ_{el} and the relaxation time τ. Moreover we

study the relationship between the shear viscosity and the electric conductivity investigating the ratio between η/s and σ_{el}/T, taking into account the QCD thermodynamics, and predicting that the ratio supplies a measure of the quark to gluon scattering rates.

Once we have developed a transport based approach describing a fluid with a given η/s, our interest moved into describing, using a single consistent approach, the fireball created in ultra-relativistic heavy ion collisions starting from the initial time. According to the understanding of the early time dynamics of the collisons, at $t = 0^+$ strong longitudinal color electric and color magnetic flux tubes, known as Glasma, are produced which then decay to a plasma as the system expands. We modelled the early time dynamics considering only a color electric field which decays to pair particles thanks to the Schwinger mechanism. We extended our code in order to couple the dynamical evolution of the initial color field and the many particles system produced by the decay.

Our studies focused on the isotropization and thermalization of the system in the early stage in order to quantify the isotropization time, which is assumed to be $\tau_{iso} = 0.6 \div 0.8\, fm/c$ in hydrodynamics calculations. We investigate in a sistematic way different systems: the static box, the longitudinal expanding system and the 3+1D expanding case. We compute the ratio P_L/P_T, with P_L (P_T) the longitudinal (transverse) pressure, finding that for the relevant cases of 1+1D and 3+1D the system reaches $P_L/P_T \simeq 1$, which characterizes the isotropization of the system, in about $1\, fm/c$ for $\eta/s = 1/4\pi$ while for higher value of shear viscosity the ratio P_L/P_T is quite smaller than 1, meaning that the system does not isotropize.
Moreover, using our approach, we study also the effects of η/s on the elliptic flow v_2 and the impact of the non-equilibrium initial condition on the formation time of v_2. The first studies show that the final v_2 developed by the system is not significantly affected by the strong early non-equilibrium dynamics. Hence, such a result provides a justification of the assumptions exploited in hydrodynamical approach.

List of Papers

I S. Plumari, **A. Puglisi**, F. Scardina and V. Greco,
Shear Viscosity of a strongly interacting system: Green-Kubo vs. Chapman-Enskog and Relaxation Time Approximation
Phys. Rev. C **86** (2012) 054902

II **A. Puglisi**, S. Plumari and V. Greco,
Electric Conductivity from the solution of the Relativistic Boltzmann Equation
Phys. Rev. D **90** (2014) 11, 114009

III **A. Puglisi**, S. Plumari and V. Greco,
Shear viscosity η to electric conductivity σ_{el} ratio for the Quark-Gluon Plasma
Phys. Lett. **B751** (2015) 326-330

IV M. Ruggieri, **A. Puglisi**, L. Oliva, S. Plumari, F. Scardina, and V. Greco
Modeling early stages of relativistic heavy ion collisions: Coupling relativistic transport theory to decaying color-electric flux tubes
Phys. Rev. C **92** (2015) 064904

Introduction and motivations

Quantum Chromodynamics (QCD) is the gauge theory that, within the Standard Model, describes the strong interaction. The elementary constituents of QCD, quarks and gluons that carry the color charge field, have all been observed in deep inelastic electron-proton scattering or jet production in electron-positron annihilation and proton-antiproton collisions, at up to TeV center of mass energies. At high energies, providing a very high momentum transfer, the asymptotic freedom of the theory, i.e. the decreasing of the running coupling constant, allows to treat partonic interactions in a perturbative QCD framework. On the contrary, QCD at lower energies remains one of the open sectors of the Standard Model. In particular, the confinement-deconfinement transition between hadrons and partons. These are of fundamental importance toward the understanding of the primordial cosmological expansion that passed through the QCD color phase transition to hadrons at about $10 \div 20$ microseconds after the Big-Bang, creating all the matter in the present universe. In addition to the QCD confinement-deconfinement phase transition, a further characteristic of QCD phase transition is involved in hadronic matter close to the critical energy density: the restoration of chiral symmetry in QCD matter. This is an invariance of the QCD Lagrangian, at least for the near-massless light quarks that constitute all matter in the universe. It is spontaneously broken in the transition from partons to massive hadrons, this breaking being the origin of allmost the entire hadron mass. Chiral symmetry is expected to be restored at high temperature indicating a phase transition being the order parameter the quark condensate $\langle \bar{q}q \rangle$.
The phase diagram of strongly interacting matter is actually under scrutiny both theoretically and experimentally searching for the phase transition from ordinary matter to the deconfined phase of quarks and gluons, namely the Quark-Gluon Plasma (QGP). The most important non-perturbative approach that shed light on the low density and high temperature region of the phase diagram is Lattice QCD which consists in solving numerically QCD in a discretized spacetime grid. Lattice calulations have shown that the phase transition is located at a critical temperature of $T_c \sim 155\, MeV \sim 10^{12}\, K$ for vanishing baryon density. Phenomenological models show that there is also a phase transition for small temperature and very high density, conditions that are reached in astrophysical objects like neutron stars.

The only way to study the QGP in laboratory is to perform ultra-relativistic heavy ions collisions. Such kind of experiments are actually carried out at Large

Hadron Collider (LHC) at CERN (European Organization for Nuclear Research) and at Relativistic Heavy Ion Collider (RHIC) at BNL (Brookhaven National Laboratory). Experiments at RHIC with energies up to $200\,A\,GeV$ have given clear indications of the formation of the QGP. Further confirmations as well as new measurements are currently undergoing at LHC experiments, that, started in 2010, can reach energies up to $5.5\,A\,TeV$ and an initial temperature $T \sim 3 \div 4\,T_c$.
However, the observables experimentally accesible are hadrons and consequently the study of the partonic behaviour is partially shadowed by the hadronization process that is yet not completely understood. Nevertheless there are a lot of observables, such as particle spectra, particle multiplicity and collective flows, that permit to identify the formation and the properties of the QGP. Such observables are ideally influenced by different phases of the evolution of the QGP, therefore it is important to identify observables that are able to probe one particular phase of the system without being influenced by the other phases, having in this way the possibility to extract information about a particular phase of the evolution.

One of the most amazing discovery was that the system created under such extreme conditions exhibits a nearly *perfect fluid* behaviour. This statement is a consequence of the observation of large anisotropic flows developed in the collision, in particular the large value of the elliptic flow v_2, which is a measure of the azimuthal asymmetry in momentum space. This observable encodes informations in particular about the properties of the matter created in heavy ion collision, the equation of state and the shear viscosity to entropy density ratio η/s.
The value measured of v_2 in ultra-relativistic heavy ion collisions is the largest ever seen and can be described by ideal hydrodynamics suggesting the idea of an almost perfect fluid with the smallest shear viscosity to entropy density ratio η/s ever observed in nature. In fact, the η/s evaluated from the collective flows is close to the lower bound $\eta/s = 1/4\pi$ predicted by supersymmetric Yang-Mills theory in the infinite coupling limit.
First developments of relativistic viscous hydrodynamics have shown that a value of $\eta/s \sim 0.1 \div 0.2$ is sufficient to produce a sizable effect on the v_2, in particular on its dependence on transverse momentum p_T and also it has been possible to provide a first estimate for the shear viscosity to entropy density ratio $\eta/s \leq 0.4$. However viscous hydrodynamics has a limited range of validity in momentum space in particular as the viscosity increases like the one that could be present in the cross-over region of the transition or at very large temperatures.

Another natural approach is based on Relativistic Boltzmann Transport equation where the system is described in terms of a one body distribution function

$f(x,p)$. The Boltzmann equation is a space-time evolution equation for the distribution function and accounts in a natural way non-equilibrium states and relaxation toward the equilibrium.
At variance with hydrodynamics this is a microscopic approach to study the dynamics of the system and the dissipative dynamics produced by a finite viscosity is taken into account within a finite cross sections. However usually kinetic theory is applied to the study of heavy ion collisions starting from the microscopic details of fields and cross sections and it is not discussed directly in terms of viscosity of the system, which is a key transport coefficient as shown by hydrodynamics. This has lead more recently to develop a transport theory based approach at fixed η/s that allows to have a direct link to the viscous hydrodynamic language. Moreover kinetic theory can allow to investigate the non-equilibrium and dissipative effect in a wider range of validity respect to hydrodynamics for both η/s and the momenta of the particles. First attempts in this direction have been already developed and applied to the study of the QGP dynamics however such an approach asks for a knowledge of the exact relation between the shear viscosity η and temperature, cross section, mass and density.

The first part of the thesis is dedicated to a study of the shear viscosity solving numericaly the Relativistic Boltzmann Transport equation in order to find the correct shear viscosity dependence on physical details such as cross section, temperature, density. The result obtained allow us to describe the QGP dynamics in a more precise transport approach developing a numerical code to solve the relativistic Boltzmann equation for the parton distribution function using a fixed shear viscosity to entropy density ratio η/s.
In literature there are several method for computing the shear viscosity, the most employed being the Relaxation Time Approximation and the Chapman-Enskog scheme. The first is based on an ansatz for the collision integral in the Boltzmann equation and it does not allow to have under control the precision of the approximation. The second one is instead based on a linearization of the collision integral that in principle allows to obtain solutions with an arbitrary accuracy which depends on the order of approximation used.
On the other hand Green-Kubo relation, in the framework of Linear Response Theory, give us an exact formula to estimate the transport coefficients. We compare the two main analytical approximation schemes with the results obtained evaluating the Green-Kubo correlator solving numerically the Relativistic Boltzmann Transport equation. This approach gives us the opportunity of quantify the validity of each approximation scheme.
We will show that for all the case of interest the Chapman-Enskog formula is a pretty good approximation to the exact viscosity providing the correct analytical relation between $\eta \leftrightarrow T, \sigma(\theta), \rho, M$. Such analytical relation supplies a way to construct a kinetic theory at fixed $\eta/s(T)$ with a very large accuracy

especially for the case of non-isotropic cross section and massive quasi-particles both of interest for a realistic description of quark-gluon plasma and hadronic matter.

Within the same framework used for computing the shear viscosity, we calculate also the electric conductivity of the QGP. Only very recently the electric conductivity has captured a significative importance in the field of strongly interacting matter on the theoretical side as well as on the experimental one. The electric conductivity, the inverse of the electric resistence, represents the response of a system to the applied electric field. On the experimental side, Heavy Ion Collisions are able to produce very strong electric and magnetic fields ($eE \simeq eB \simeq m_\pi^2$, with m_π the pion mass) which are produced by the charge carried by the two nuclei and decay in about $1\, fm/c$, however the decay time depends on the value of the electric conductivity of the QGP.
The value of σ_{el} would be of fundamental importance for the strength of the Chiral-Magnetic Effect, a signature of the CP violation of the strong interaction. It has also been shown that in mass asymmetric collision the electric field has a privileged direction generating a current whose effects can be observed in collective flow and are directly related to σ_{el}. Moreover σ_{el} can be related to the emission rate of soft photons accounting for their raising spectra. The electric conductivity σ_{el} can be computed from first principles on the Lattice from correlation function.
We will evaluate the electric conductivity solving the Transport Boltzmann Equation and, in details, study the relationship between σ_{el} and the relaxation time τ. In particular we will show that for a generic anisotropic cross section, the Drude relaxation time $\tau = 1/\rho\sigma$, with ρ the density and σ the cross section, underestimates the correct value of relaxation time. We will also compare our numerical results to the analytical formula derived in Relaxation Time Approximation in order to quantify how good is such a crude approximation. Being interested in a more realistic case and in having an approach also able to account for the Lattice QCD results, we employed a quasi-particle model to take into account the thermodynamics of strongly interacting matter.
We discuss the relation between the shear viscosity and electric conductivity investigating for the first time the ratio between η/s and σ_{el}/T taking into account the Lattice QCD equation of state. We predict that the ratio supplies a measure of the quark to gluon scattering rates whose knowledge would allow to significantly advance in the understanding of the QGP phase.

Our calculations of transport coefficients can be extendend to the bulk viscosity as well as to the color-conductivity which are of fundamental importance in ultra-relativistic heavy ion collisions. The bulk viscosity, which represents the friction of the system to a rapid expansion, only very recently has been included in hydrodynamic calculations while the color conductivity is of particular interest

in the early time dynamics of the QGP when are present strong chromoelectric and chromomagnetic fields.
Our interest, after the shear viscosity and electric conductivity studies, moved into applying our very precise transport approach at fixed η/s to the early time dynamics of ultra-relativistic heavy ion collision. In particular using our transport approach we want to study, in a quantitative way, how the system, starting from the non-equilibrium initial condition, reaches a state characterized by thermalization and isotropization in order to quantify the isotropization time, usually assumed $\tau = 0.6 \div 0.8\, fm/c$ in hydrodynamics calculations.
The understanding of early times dynamics is one of the most interesting problems of heavy ion collisions at ultrarelativistic energy actually under investigation. According to the standard picture of such collision processes, immediately after the collision, strong longitudinal color electric and color magnetic flux tubes, known as Glasma, are produced. Such fields, due to quantum fluctuations, decay to a plasma as the system expands reaching, in a very short time, a state characterized by thermalization and isotropization which is the initial state for hydrodynamics description. Our main interest is to investigate the problem of isotropization and thermalization of such a system using our transport approach toghether with the effects of shear viscosity.

One mechanism responsible for the initial fields decay might be the one introduced by Schwinger in the context of Quantum Electrodynamics, known as the Schwinger effect, which consists in a vacuum instability towards the creation of particle pairs by a strong electric field. We develop a code that couple the dynamical evolution of the initial color electric field to the dynamics of the many particles system produced by the decay within the Relativistic Boltzmann Transport equation.
Besides being the first study in which a Monte Carlo method is used to simulate the Schwinger effect in the context of early times dynamics of high energy collisions, we improve previous studies which mainly rely on Relaxation Time Approximation (RTA) or on a linearization of the conductive electric current, by avoiding any ansatz both on the electric current and on the collision integral in the Boltzmann equation which permits to go beyond the RTA. Moreover, in our simulations we are able to fix the ratio η/s thanks to the study of shear viscosity discussed in the first part of this thesis.

Our study focuses on computing quantities which serve as indicators of thermalization and isotropization of the plasma and evaluate how these processes are affected by the η/s. We investigate in a sistematic study different systems starting from the static box case. On one hand such a case can be viewed as only of achademic interest however, on the other, it represents the guideline for interpreting the physical results obtained like for example the decay of the color electric field on about $1\, fm/c$ and the isotropization of the longitudinal

pressure P_L over the transverse pressure P_T in $1\,fm/c$ for $\eta/s = 1/4\pi$. The cases with higher value of η/s show plasma oscillations and require a larger time to isotropize.
Then we consider a system with a longitudinal expansion which has a greater physical interest than the static box because it is closer to the picture of the early times dynamics of relativistic heavy ion collisions. In this case we will show that the electric field exhibits a rapid decay for small η/s while for intermediate and high value of shear viscosity strong oscillations during the time evolution. The ratio P_L/P_T shows that the system reaches a state of isotropization in about $1\,fm/c$ for $\eta/s = 1/4\pi$. For $\eta/s = 3/4\pi, 10/4\pi$ the ratio experiences several oscillations and the aymptotic value of P_L/P_T is quite smaller than 1 indicating that the system does not isotropize.
Finally we extend the longitudinal expansion study to a the three dimensional case which is of great interest being more realistic. In particular, within this framework, we study the isotropization and thermalization of the fireball showing that the transverse expansion affects both plasma oscillations and istropization. Moreover using our approach we are ablo to describe the fireball evolution starting from the initial time $t = 0^+$, when only fields are present, to the develop of collective flows in only one consistent scheme. We will compute the elliptic flow and in particular we will show the effects of η/s on v_2 and how the initial non-equilibrium condition affects the formation time of v_2.

The thesis is structured as follows. In Chapter 1 we discuss about the general properties of QCD and the phase transition from ordinary matter to quark-gluon plasma by mean of ultra-relativistic heavy ion collisions. In Chapter 2 we present Transport Boltzmann equation from the classical case to the quantum-relativistic generalization discussing its numerical implementation. In Chapter 3 the reader can find Linear Response Theory, Green-Kubo relations and analytical approximation to the Boltzmann equation for the shear viscosity and electric conductivity. In Chapter 4 we show our results about shear viscosity dependence on microscopic physical quantities and the more realistic case of shear viscosity of a quark-gluon plasma using the equation of state of Lattice QCD. In Chapter 5 we present similar results for the electric conductivity studying furthermore the ratio between shear viscosity and electric conductivity and pointing out that their relation is determined by the relative interaction between quarks and gluons. In Chapter 6 we study early times dynamics by an initial color electric field which decays to a plasma by the Schwinger effect showing different case of interest: static box, 1+1D expansion and also the realistic case of 3+1D expansion.

1

Quantum-Chromo Dynamics and Quark-Gluon Plasma

"May the (strong) force be with you"

Contents

In this chapter we discuss about the general properties of Quantum-Chromo Dynamics (QCD), namely the Standard Model sector describing the strong interactions. The asymptotic freedom at high energy makes the theory weakly coupled; on the other hand at low energy the coupling becomes large and no perturbative calculation can be reliable. Color confinement, acting in normal conditions of temperature and density, is the phenomenon hindering color charged particles to be isolated singularly, and therefore directly observed. The most important theoretical tool to investigate the QCD properties is to solve the QCD in a space-time lattice, Lattice QCD. Lattice calculations show that there is a phase transition from ordinary matter to a quark-gluon plasma (QGP) phase where quarks and gluons are no longer confined. These new state of matter is reached for extremely high temperature, $T \simeq 10^{12}\,K$, like in the early stage of the universe, or at very high density like the ones that can be found in compact stellar objects (e.g. neutron stars). The only way to produce this state of matter on Earth is to perform ultra-relativistic heavy ions collisions. In such kind of experiments the high multiplicity of particles produced, as their average energy, shows that a temperature higher than the critical one is reached. Such a statement is corroborated by the study of their momentum spectra and collective flows in hydrodynamical framework. Then other several observables probe that the QGP is formed. Moreover, collective flows, in particular the elliptic flow, indicate that the QGP behaves like a fluid with the lowest value of shear viscosity ever observed in nature, close to the lower bound predicted by AdS/CFT $\eta/s = 1/4\pi$.

1.1 Quantum-Chromo Dynamics

The fundamental interaction governing nuclear physics is the strong force. It is one of the four fundamental forces in nature, along with electromagnetism, weak interaction and gravitation. Theoretically strong interactions are described by a non-abelian gauge theory called quantum chromodynamics (QCD). The charge associated with this gauge theory is referred to as color and can take three different values as the underlying symmetry group is $SU(3)$, a special unitary group of degree three. It is the invariance under local $SU(3)$ symmetry transformations in the color space whose gauging leads to QCD. The color charge is carried by spin$-1/2$ fermions called quarks, subatomic particles that, to the best of our current knowledge, have no substructure and are the fundamental particles of QCD. The strong force between the quarks is mediated by gluons, the exchange particles of QCD. Due to the non-abelian nature of the theory, the gluons carry color charge and are thus subject to interactions

via the strong force themselves. This is a feature quite distinct from quantum electrodynamics (QED), where the exchange photons do not couple to each other directly, and leads to wide consequences. Gluons are spin-1 vector bosons and come in eight types, corresponding to the color octet generated by SU(3). In general, for a SU(N) symmetry there are $N^2 - 1$ force carriers. The QCD Lagrangian has the following form:

$$\mathcal{L} = \frac{1}{4}\sum_a F^a_{\mu\nu}F_a^{\mu\nu} + \sum_f^{N_f}\bar{\Psi}_f\left(i\gamma^\mu\partial_\mu - g\gamma^\mu\sum_a A^a_\mu\frac{\lambda^a}{2} - m_f\right)\Psi_f \tag{1.1}$$

where Ψ_f are the quarks fields, being $f = u, d, s, c, b, t$ the quark flavour index, and A^a_μ are the gluon fields with $a = 1, \ldots, 8$ the color index. In Eq. (1.1) g is the strong coupling constant, γ^μ are the Dirac matrices, and λ^a are the Gell-Mann matrices:

$$\lambda^1 = \begin{pmatrix} 0 & 1 & 0 \\ 1 & 0 & 0 \\ 0 & 0 & 0 \end{pmatrix} \qquad \lambda^2 = \begin{pmatrix} 0 & -i & 0 \\ i & 0 & 0 \\ 0 & 0 & 0 \end{pmatrix}, \quad \lambda^3 = \begin{pmatrix} 1 & 0 & 0 \\ 0 & -1 & 0 \\ 0 & 0 & 0 \end{pmatrix},$$

$$\lambda^4 = \begin{pmatrix} 0 & 0 & 1 \\ 0 & 0 & 0 \\ 1 & 0 & 0 \end{pmatrix}, \qquad \lambda^5 = \begin{pmatrix} 0 & 0 & -i \\ 0 & 0 & 0 \\ i & 0 & 0 \end{pmatrix},$$

$$\lambda^6 = \begin{pmatrix} 0 & 0 & 0 \\ 0 & 0 & 1 \\ 0 & 1 & 0 \end{pmatrix}, \qquad \lambda^7 = \begin{pmatrix} 0 & 0 & 0 \\ 0 & 0 & -i \\ 0 & i & 0 \end{pmatrix},$$

$$\sqrt{3}\lambda^8 = \begin{pmatrix} 1 & 0 & 0 \\ 0 & 1 & 0 \\ 0 & 0 & -2 \end{pmatrix}$$

The generators of $SU(3)$ group, satisfy the commutation relations:

$$\left[\frac{\lambda_a}{2}, \frac{\lambda_b}{2}\right] = if_{abc}\frac{\lambda_c}{2} \tag{1.2}$$

which defines the Lie algebra of the $SU(3)$ group. The coefficients f_{abc} are the structure constants of the Lie Algebra and they are totally antisymmetric with respect to the permutation of a, b, c being different from zero the list in Table 1.1.

$f^{123} = 1, \quad f^{147} = \frac{1}{2}, \quad f^{156} = -\frac{1}{2}, \quad f^{246} = \frac{1}{2}, \quad f^{257} = \frac{1}{2}$

$f^{345} = \frac{1}{2}, \quad f^{367} = -\frac{1}{2}, \quad f^{458} = \frac{\sqrt{3}}{2}, \quad f^{678} = \frac{\sqrt{3}}{2}$

Table 1.1: Structure constant of the Lie Algebra of $SU(3)$ group.

The non-linear gluon field strength in the QCD Lagrangian is defined by:

$$F_a^{\mu\nu} = \partial^\mu A_a^\nu - \partial^\nu A_a^\mu - g f_{abc} A_b^\mu A_c^\nu. \tag{1.3}$$

For each flavour the quark wave function has three components $\Psi = (\psi_{red}, \psi_{green}, \psi_{blue})$, being each of them a Dirac spinor, and the local $SU(3)$ gauge transformation is:

$$\Psi \to \Psi' = U(x)\Psi, \qquad U(x) \in SU(3). \tag{1.4}$$

The QCD Lagrangian is invariant under the above local transformation if the gluon fields change according to:

$$A^\mu = A_a^\mu \frac{\lambda_a}{2} \to A'^\mu = U(x) A^\mu U^{-1}(x) - \frac{i}{g} U(x) \partial^\mu U^{-1}(x). \tag{1.5}$$

Only $T^3 \equiv \lambda_3/2$ and $T^8 \equiv \lambda_8/2$ commute so they can be viewed as the operators of the color charge carried by quarks: they are called *color isotopic charge* and *color hypercharge*. The values of the quark charges are obtained as the eigenvalues $\varepsilon_i^{(3)}$ and $\varepsilon_i^{(8)}$

$$T^3 \Psi_i = \varepsilon_i^{(3)} \Psi_i, \qquad T^8 \Psi_i = \varepsilon_i^{(8)} \Psi_i \tag{1.6}$$

where Ψ_i represents the normal basis in the color space $\Psi_1 = (\Psi_{red}, 0, 0)$, $\Psi_2 = (0, \Psi_{green}, 0)$ and $\Psi_3 = (0, 0, \Psi_{blue})$. The solution to the eigenvalue equation above is:

$$\varepsilon_1 = \frac{1}{2}\left(1, \sqrt{\frac{1}{3}}\right), \quad \varepsilon_2 = \frac{1}{2}\left(-1, \sqrt{\frac{1}{3}}\right), \quad \varepsilon_3 = \left(0, -\sqrt{\frac{1}{3}}\right) \tag{1.7}$$

that are two-dimensional vectors in the space of color isotopic charge and color hypercharge. The vectors ε_i are the mathematical representation of three different color charges.

The color charges are also carried by gluons. The gluon field represented by $A^\mu \equiv A_a^\mu \lambda_a/2$ form the basis for the adjoint representation. Charge operators

for gluons can be defined as follows:[1]

$$Ad\,T^3 = \left[T^3, \cdot\right], \qquad Ad\,T^8 = \left[T^8, \cdot\right]. \tag{1.8}$$

Only the generators $\tau_3 = T^3$ and $\tau_8 = T^8$ are the eigenstates of the new operators $Ad\,T^3$ and $Ad\,T^8$ with zero eigenvalues. Other eigenstates are:

$$\tau_{12} = \tfrac{1}{\sqrt{2}}(T_1 + iT_2) = \tfrac{1}{\sqrt{2}} \begin{pmatrix} 0 & 1 & 0 \\ 0 & 0 & 0 \\ 0 & 0 & 0 \end{pmatrix}, \quad \tau_{12} = \tfrac{1}{\sqrt{2}}(T_1 - iT_2) = \tau_{12}^\dagger$$

$$\tau_{13} = \tfrac{1}{\sqrt{2}}(T_4 + iT_5) = \tfrac{1}{\sqrt{2}} \begin{pmatrix} 0 & 0 & 1 \\ 0 & 0 & 0 \\ 0 & 0 & 0 \end{pmatrix}, \quad \tau_{31} = \tfrac{1}{\sqrt{2}}(T_4 - iT_5) = \tau_{13}^\dagger$$

$$\tau_{23} = \tfrac{1}{\sqrt{2}}(T_6 + iT_7) = \tfrac{1}{\sqrt{2}} \begin{pmatrix} 0 & 0 & 0 \\ 0 & 0 & 1 \\ 0 & 0 & 0 \end{pmatrix}, \quad \tau_{32} = \tfrac{1}{\sqrt{2}}(T_6 - iT_7) = \tau_{23}^\dagger$$

In a more compact view:

$$\left[T^3, \tau_{ij}\right] = \eta_{ij}^{(3)} \tau_{ij}, \qquad \left[T^8, \tau_{ij}\right] = \eta_{ij}^{(8)} \tau_{ij} \tag{1.9}$$

where the charges η_{ij} have the form

$$\eta_{ij} = \varepsilon_i - \varepsilon_j \tag{1.10}$$

The three charges, that will be used in the flux tube model in Chapter 6, are:

$$\eta_{12} = (1, 0), \qquad \eta_{13} = \left(\frac{1}{2}, \frac{1}{\sqrt{3}}\right), \qquad \eta_{23} = \left(-\frac{1}{2}, \frac{1}{\sqrt{3}}\right) \tag{1.11}$$

while the remaining three charges are obtained by $\eta_{ji} = -\eta_{ij}$. The gluon field in the basis of τ generators has the form:

$$\begin{aligned} A &= \frac{1}{2} A_a \lambda_a = A^3 \tau_3 + A^8 \tau_8 + \\ &\quad \left[\frac{A^1 - iA^2}{\sqrt{2}} \tau_{12} + \frac{A^4 - iA^5}{\sqrt{2}} \tau_{13} + \frac{A^6 - iA^7}{\sqrt{2}} \tau_{23} + h.c.\right] \end{aligned} \tag{1.12}$$

or

$$\begin{aligned} A &= G^3 \tau_3 + G^8 \tau_8 + G^{12} \tau_{12} + G^{13} \tau_{13} \\ &+ G^{23} \tau_{23} + G^{21} \tau_{21} + G^{31} \tau_{31} + G^{32} \tau_{32} \end{aligned} \tag{1.13}$$

G^3 and G^8 are neutral since they commute with T^3 and T^8 while the fields G^{ij} carriy the color charge η_{ij}. In the new basis the quark-gluon interaction term in the QCD Lagrangian is written as:

$$\begin{aligned}\mathcal{L}_{int} &= -g\bar{\Psi}\left(\tau_3\gamma_\mu G_3^\mu + \tau_8\gamma_\mu G_8^\mu\right)\Psi \\ &\quad -g\left[\bar{\Psi}\left(\tau_{21}\gamma_\mu G_{21}^\mu + \tau_{31}\gamma_\mu G_{31}^\mu + \tau_{32}\gamma_\mu G_{32}^\mu\right)\Psi + h.c.\right] \quad (1.14)\end{aligned}$$

Last equation shows that the color charge of a quark does not change during the interaction with gluon fields G^3 and G^8, so these types of gluons can be treated in a similar way as photons in QED; on the other hand interaction between quarks and gluon field G^{ij} changes the color state of quarks: absorption of gluon G^{ij} by a quark with charge ε_j produces a quark with charge ε_i. The separation of the gluon field into charged and neutral part is gauge dependent, however, fixing the gauge, this method can be applied and it is very useful for the physical interpretation of many processes.

1.1.1 Asymptotic freedom

One particular feature of QCD, not present in QED, is the asymptotic freedom, that is a general property of non-Abelian gauge theory.[2,3] The strength of the interaction decreases as the transfer momentum increases, or equivalently as the distance decreases.

In field theories, the quantum corrections calculated in perturbation theory have ultraviolet divergences with high momenta. For renormalizable field theories, like QED and QCD, these divergences can be absorbed in renormalized parameters. The energy scale where this happens is the renormalization point. The physical observables do not depend on the renormalization point but the coupling $\alpha_s = g^2/4\pi$ depends on it. In the case of QCD, with $N_f = 6$, the coupling α at leading order is:

$$\alpha_s(Q^2) = \frac{4\pi}{\left(11 - \frac{2}{3}N_f\right)\log\left(Q^2/\Lambda^2\right)} \quad (1.15)$$

where Λ_{QCD} is the energy scale of the strong interaction. In Fig. 1.1 from Ref.[4] it is shown α_s as a function of Q: symbols represent experimental measurements while lins are QCD predictions. The asymptotic freedom of the strong interaction allows to set up the perturbation theory for high transfered momentum (pQCD) while for energy comparable with $\Lambda = 200\,MeV$ the coupling is too large to apply any perturbative calculation.

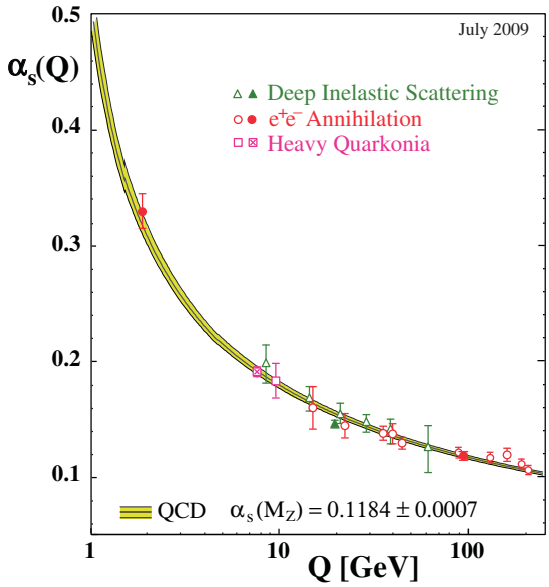

Figure 1.1: Summary of measurements of α_s as a function of the respective energy scale Q from Ref.[4]

1.1.2 Confinement

One of the most peculiar feature of the QCD is the colour confinement: hadrons can exist only in colorless states and quarks can only exist as confined in hadrons. Wheter the QCD vacuum leads to quark confinement can be tested by studying the expectation value of the Wilson loop:

$$\langle W(C)\rangle \equiv \left\langle tr\mathcal{P}e^{ig\oint_C dz_\mu A\mu}\right\rangle \tag{1.16}$$

$$\propto e^{-V(R)\mathcal{T}} \simeq \exp\left[-\left(KR + b + \frac{c}{R} + \dots\right)\mathcal{T}\right] \tag{1.17}$$

where the path C has been chosen as rectangular. $V(R)$ represents the potential between a heavy quark Q and anti-quark $\bar{Q}$, $K \neq 0$ implies the existence of a strong-like linear confining potential and also the area law of the Wilson loop $\langle W(C)\rangle \sim \exp(-KA)$ with $A = R \times \mathcal{T}$ the area inside the path C. The previous equation is valid only if one has heavy colour sources in the medium (the so called quenched approximation): indeed in the case of full QCD with light quarks, the linear rising potential becomes flat because of $q\bar{q}$ virtual pairs which break the string $Q\bar{Q} \to (Q\bar{q})(q\bar{Q})$. In general the $Q\bar{Q}$ potential as a

function or R is defined as

$$V(R) = -\lim_{\mathcal{T}\to\infty}\left(\frac{\log\langle W(C)\rangle}{\mathcal{T}}\right)_{\mathcal{T}\gg R}. \tag{1.18}$$

Non-perturbative numerical simulation on the lattice give us a clear evidence of the linear rising $V(R)$ at zero temperature as shown by black line in Fig. 1.2 from Ref.[5] In Fig. 1.2 are shown quark anti-quark free energy as a function of distance for different value of temperatures: at large distances the free energy approaches a constant temperature dependent value while, in the opposite limit, tends to the potential $V(r)$. In Fig. 1.3 the screening radius as a function of temperature from Ref.:[5] as the temperature increases, the screening radius becomes shorter meaning that the quark anti-quark bound states is influenced by the medium indicating a transition temperature.

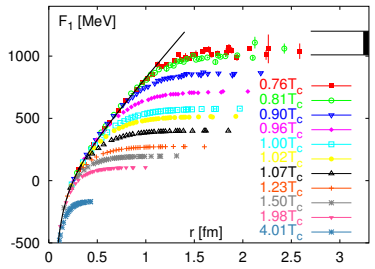

Figure 1.2: The colour singlet quark anti-quark free energies, $F_1(r,T)$, at several temperatures as function of distance in physical units from Ref.[5] The solid line represents the $T = 0$ heavy quark potential, $V(r)$.

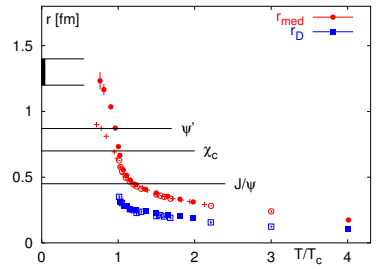

Figure 1.3: The screening radius as function of T/T_c from Ref.[5] estimated from the inverse Debye mass, $r_D \equiv 1/m_D$ ($N_f = 0$: open squares, $N_f = 2$ filled squares). The horizontal lines give the mean squared charge radii of some charmonium states, J/ψ, χ_c and ψ'.

1.1.3 Further symmetries of QCD

In this subsection we discuss further simmetries of QCD; namely chiral and dilatational simmetries.

- *Chiral symmetry* In the limit of vanishing masses the left- and right-handed quarks become decoupled from each other and QCD becomes invariant under their interchange so that left and right-handed quark current are separately conserved. From a mathematical point of view, the

lagrangian of a system has the chiral symmetry if it is invariant under the global $SU(N_f)_L \times SU(N_f)_R$ transformation:

$$SU(N_f)_L : q_L \to e^{i\theta_L^a \frac{\lambda_a}{2}} q_L, \qquad SU(N_f)_R : q_R \to e^{i\theta_R^a \frac{\lambda_a}{2}} q_R \tag{1.19}$$

where λ_a are the generators and $q_L = \frac{1}{2}(1-\gamma_5)q$, $q_R = \frac{1}{2}(1-\gamma_5)q$ are respectively the left-handed and right handed fields. The symmetry implies that also each state of the theory should have a degenerate partner of the opposite parity. However hadrons have well defined parity. This is the case of a spontaneous breakdown of chiral symmetry: the chiral symmetry of the interaction is broken by the true ground state of the theory. According to Goldstone theorem, spontaneous breaking of any continuous symmetry is connected with the existence of soft modes which, in the case of QCD, correspond to pions. In reality, pions have small mass (so they are called pseudo-Goldstone bosons): this is due to the non-zero mass of up and down quark so chiral symmetry is approximate. Chiral symmetry is expected to be restored in the quark-gluon plasma.

- *Dilatation symmetry* The QCD Lagrangian, for massless quarks, is invariant under the following scale transformation:

$$x_\mu \to \varepsilon^{-1} x_\mu, \quad q(x) \to \varepsilon^{3/2} q(\varepsilon^{-1}x), \quad A_\mu^a(x) \to \varepsilon A_\mu^a(\varepsilon^{-1}x) \tag{1.20}$$

that is the dilatation symmetry, while the current associated is

$$\langle T_\mu^\mu \rangle = \varepsilon - 3P = \frac{\alpha_s}{12\pi} \langle F^{\mu\nu} F_{\mu\nu} \rangle + m \langle \bar{\Psi}\Psi \rangle \tag{1.21}$$

which is the trace of energy momentum tensor. The expectation value $\langle F^{\mu\nu} F_{\mu\nu} \rangle$, considering the quantum corrections, is different from zero leading to the trace anomaly.

1.2 Lattice QCD

The most important theoretical non-perturbative approach, used to extract information about the phase transition and also, as we will see in Chapter 3, about transport coefficients like shear viscosity and electric conductivity, is the numerical study of QCD on a discretized space time, namely the Lattice QCD. In Lattice QCD approach the partition function is computed by Monte-Carlo methods. In order to define the gauge field on the lattice and maintain gauge invariance on the discretized space-time, it is necessary to introduce link

variable that is the discretized version of Wilson line defined as follows:

$$U_p(x,y;A) = \mathcal{P}\exp\left(ig\int_p dz_\mu\, A_\mu\right) \tag{1.22}$$

where $\mathcal{P}$ is the path-ordered symbol. The shortest Wilson line on the lattice is the one connecting the site n with site $n+\hat{\mu}$:

$$U_\mu(n) = \exp\left(igaA_\mu(n)\right) \tag{1.23}$$

The smallest closed loop is:

$$U_{\mu\nu}(n) = U_\nu^\dagger(n)U_\mu^\dagger(n+\hat{\nu})U_\nu(n+\hat{\mu})U_\mu(n) \tag{1.24}$$

which transforms covariantly under a local gauge transformation and, in the continuum limit $a\to 0$, it approaches to the field strength tensor $U_{\mu\nu}(n)-1 \to ia^2gF_{\mu\nu}(n)$. The trace $tr\,U_{\mu\nu}(n)$ is a minimal gauge-invariant called plaquette is used to construct a gauge invariant gluon action:

$$\begin{aligned} S_g &= \frac{2N_c}{g^2}\sum_p\left(1-\frac{1}{N_c}\Re\, tr\,U_{\mu\nu}(n)\right) \\ &\to \frac{1}{4}\int d^4x\, F^a_{\mu\nu}(x)F_a^{\mu\nu}(x) \end{aligned} \tag{1.25}$$

In analogous way one can write the Wilson fermion action

$$\begin{aligned} S_W = a^4\sum_n\Bigg[&m\bar{q}(n)q(n) - \frac{1}{2a}\sum_\mu \bar{q}(n+\hat{\mu})\Gamma_\mu U_\mu(n)q(n) \\ &-\frac{r}{2a}\sum_\mu\left(\bar{q}(n+\hat{\mu})U_\mu(n)q(n) - \bar{q}(n)q(n)\right)\Bigg] \\ &\to \int d^4x\,\bar{q}(x)\left(m - i\gamma\cdot D - \frac{ar}{2}D^2\right)q(x) \end{aligned} \tag{1.26}$$

where Γ_μ are the hermitian γ-matrices satistying $\{\Gamma_\mu,\Gamma_\nu\} = 2\delta_{\mu\nu}$. The parameter r vanishes in the continuum limit and avoids the fermion-doubling problem on the lattice.

Once the actions have been set up the theory can be quantized by functional integral over quarks and gluons. The partition function is given by:

$$\begin{aligned} \mathcal{Z} &= \int d[U][d\bar{\Psi}][d\Psi]\, e^{-S_g(U)-S_q(\bar{\Psi},\Psi,U)} \\ &= \int d[U]\, Det\, F[U] e^{-S_g(U)} \end{aligned} \tag{1.27}$$

where the general form $S_q = \sum_{n,n'} \bar{\Psi}(n')F(n',n)\Psi(n)$ has been used. The determinant is computed for all indices of F. Setting $Det\,F[U] = const$ is the *quenched approximation* which ignores the virtual quark-anti-quark excitations.

1.2.1 Polyakov loop

The study of the phase transitions is facilitated by comparing the symmetry of the phases and introducing appropriate order parameters. The step which started the systematic investigation of the deconfinement phase transition was the construction of an order parameter for confinement called Polyakov loop at finite temperature:

$$L(x) = \mathcal{P} \exp\left[i \int_0^\beta d\tau\, A_4(\mathbf{x}, \tau) \right] \tag{1.28}$$

The Polyakov loop can be thought of as representing a static fermion test charge which probes the screening properties of the surrounding gluonic medium. Its expectation value is related to the free energy $F_q(T)$:

$$e^{-F_q(T)/T} \simeq \langle L \rangle \tag{1.29}$$

induced by the presence of the source in the gluonic heath bath. In absence of dynamical quarks, a single colored charge cannot be screened in the confined phase so its free energy F_q is infinite and $\langle L \rangle = 0$. In the confined phase, however, F_q is finite and $\langle L \rangle \neq 0$. The expectation value $\langle L \rangle$ is thus an order parameter for the deconfinement phase transition in the pure $SU(3)$ gauge theory. The discretized version of the Polyakov loop in lattice calculations is

$$L(\mathbf{x}) = \frac{1}{N_c}\, tr \prod_{n_4=0}^{N_t-1} U_4(n_4, \mathbf{x}). \tag{1.30}$$

The existence of the deconfinement transition at high temperature was discussed in the context of lattice gauge theory.[6,7] It was later proved that for $SU(N_c)$ lattice gauge theory there exists a phase transition to the deconfinement phase at high temperature.[8] In particular for $N_c = 2$ the transition is of second order while for $N_c = 3$ the transition is of first order, so that the expecation value of Polyakov loop has a discontinuity at the critical temperature and there is the coexistence of the two phases. However in presence of light quarks the expectation value of L exihibits a cross-over as shown in Fig. 1.4 from Ref.[9]

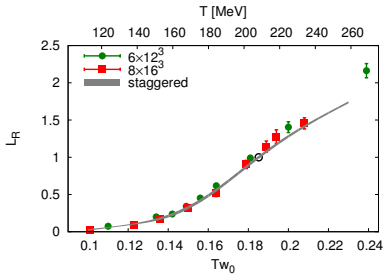

Figure 1.4: Polyakov loop as a function of temperature from Ref.[9]

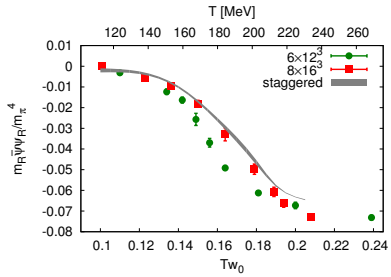

Figure 1.5: Chiral condensate as a function of temperature from Ref.[9]

The other quantity that plays the role of an order parameter is the chiral condensate $\langle\bar{\Psi}\Psi\rangle$. In the limit of vanishing quark masses the chiral condensate is different from zero if the chiral symmetry is spontaneously broken and becomes zero when the symmetry is restored. In the case of finite quark masses the chiral symmetry is only approximate and therefore $\langle\bar{\Psi}\Psi\rangle$ does not vanishes at high temperature but still manifest a critical behaviour as shown in Fig. 1.5 from Ref.[9]

1.2.2 Mass spectrum of light hadrons

On the lattice, the masses of mesons and baryons can be calculated directly. Hadron masses in the quenched approximation are calculated from the operator $calM = \bar{q}(x)\gamma q(x)$ with γ an arbitrary γ-matrix. The correlation function of such operators in Euclidean space is given by

$$D(\tau) = \int d^3x \, \langle \mathcal{M}(\tau, \mathbf{x}) \mathcal{M}^\dagger(0) \rangle \underset{\tau\to\infty}{\longrightarrow} |Z|^2 e^{-m\tau} \tag{1.31}$$

where m is the mass of the lightest bound state with the same quantum number as the operator $\mathcal{M}$ and Z is the pole residue. If the temporal extent of the lattice is infinite, the hadron mass can be extracted using $m = -(1/\tau)\log D(\tau)|_{\tau\to\infty}$. In Fig. 1.6 the mass spectrum for mesons and baryons composed of u, d and s quarks are shown: black circles are the lattice data with s quark mass fixed by the experimental kaon mass while white circles with the ϕ-meson mass. Simulation data and the experiments agree at 11% even in the quenched approximation.

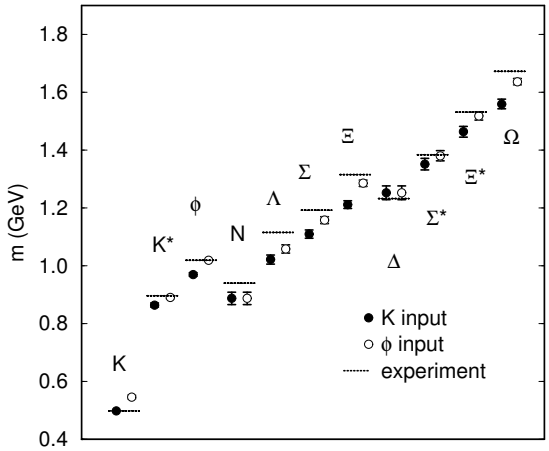

Figure 1.6: Light hadron mass spectrum. Horizontal dashed lines are the experimental masses, while black and white circles are the Lattice QCD data from Ref.[10]

1.2.3 Equation of state

Once the partition function is known, it is possible to compute thermodynamical quantities like the energy density, the pressure and entropy density thanks to the standard thermodynamical relations:

$$\varepsilon = \frac{T}{V}\left(\left.\frac{\partial \log \mathcal{Z}}{\partial \log T}\right|_V\right), \qquad P = T\left.\frac{\partial \log \mathcal{Z}}{\partial V}\right|_T \tag{1.32}$$

$$s = \frac{1}{V}\left(1 + \frac{\partial}{\partial \log T}\right)\log \mathcal{Z}\Big|_V \tag{1.33}$$

In Fig. 1.7 we show recent lattice results[11] for the pressure p/T^4 as a function of the temperature T. In Fig. 1.8 we report recent lattice results continuum extrapolated of entropy density rescaled by T^3 and energy density ε rescaled by T^4 as a function of temperature. In the inset of Fig. 1.8 the speed of sound $c_s^2 = dp/d\varepsilon$ is shown. These results are computed with $2+1\,N_f$. One can observe that near a critical temperature T_c the energy density grows up indicating an increasing of the effective number of degrees of freedom, signal of a transition from hadronic matter to a deconfined system of quarks and gluons. Both pressure and energy density are quite below the Stefan-Boltzmann limit for an ideal gas meaning that also for high temperature there is strong interaction among quarks and gluons. These deviation from the ideal gas behaviour can be expressed in terms of effective thermal masses of quarks and

gluons as proposed in the quasi-particle model employed in Chapter 4 and Chapter 5 in order to compute the shear viscosity and electric conductivity of the quark-gluon plasma.

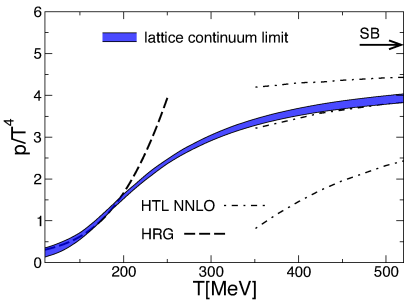

Figure 1.7: Continuum extrapolated result for the pressure with Nf = 2 + 1 flavors.[11]

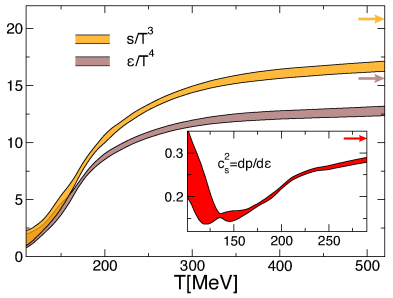

Figure 1.8: Entropy and energy density. The insert shows the speed of sound.

1.3 Phase diagram of QCD

Using the informations coming form Lattice QCD calculations and from phenomenological models it is possible to sketch the phase diagram for the stronlgy interacting matter as shown in Fig. 1.9. In the horizontal axis there is the baryon chemical potential μ_B while in vertical axis the temperature. From Lattice QCD it has been shown that the matter undergoes a cross-over from the confined phase to a deconfined phase of quarks and gluons (quark-gluon plasma) for a critical temperature of about $T_c = 155\,MeV$. This phase existed in the early universe up to a time of about $10 - 20\,\mu s$ after the Big-Bang. In the region of finite μ_B, phenomenological models and recent lattice QCD calculations have also shown a phase transition towards the QGP phase. A possible place where QGP may exist for non zero μ and low temperature is in very compact objects such as neutron star. The phase transition in this region seems to be of first order and many efforts have been making in order to find the critical point for which the first order phase transition becomes a cross-over.[12–14] The unique possibility that we have in order to study the QGP in laboratory is to collide ultra-relativistic heavy ions as we will discuss in the next section.

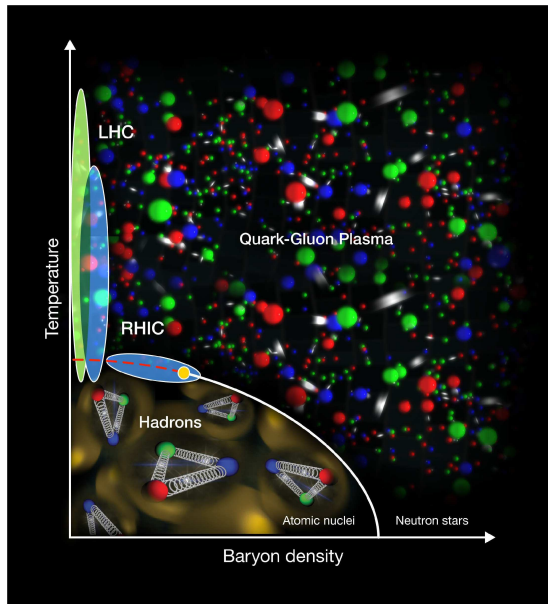

Figure 1.9: Phase diagram of QCD from *https://www.bnl.gov/rhic*

1.4 Quark-Gluon Plasma in heavy ion collision

The first experiments with the ultra-relativistic heavy ions, with energy of $10\,GeV$ per nucleon, took place at the Brookhaven National Laboratory (BNL) and at the European Organization for Nuclear Research (CERN) in 1986. The Alternating Gradient Synchroton (AGS) at BNL accelerated beams up to ^{28}Si at $14\,GeV$ per nucleon while at CERN the Super Proton Synchroton (SPS) accelerated ^{16}O at $60 - 200\,GeV$ per nucleon. In 1995 completely new experiments took place at CERN with ^{208}Pb at $158\,GeV$ per nucleon. These were really ultra-relativistic heavy ions collisions producing large volumes and lifetime of the reaction zone. In 2000 the first data from Relativistic Heavy Ion Collider (RHIC) at BNL were collected accelerating fully stripped Au ions to a collision energy of $200\,GeV$. There are four experiments at RHIC: BRAHMS (particles identification over a broad range of rapidity), PHOBOS (total charged particle multiplicity and particle correlations), PHENIX (electrons, muons, hadrons and photons) and STAR (hadron production over a large solid angle). The first proton run at the Large Hadron Collider (LHC) at CERN ended on 4 November 2010. A run with lead ions started on 8 November 2010, and ended on 6 December 2010 allowing the ALICE experiment to study

matter under extreme conditions similar to those shortly after the Big Bang. Seven detectors have been constructed at the LHC, located underground in large caverns excavated at the LHC's intersection points: ATLAS (signs of new physics, including the origins of mass and extra dimensions), CMS (same purpouse as ATLAS), ALICE (quark-gluon plasma), LHCb (antimatter), TOTEM (yotal cross section, elastic scattering and diffraction dissociation at the LHC), MoEDAL (Monopole and exotic particle detector at the LHC) and LHCf (measurement of neutral π^0 meson production, in order to understand ultra high energy cosmic rays). At full design energy the protons will each have an energy of 7 TeV, giving a total collision energy of 14 TeV. At this energy the protons have a Lorentz factor of about 7,460 and move at about 0.999999991 c, or about 2.7 metres per second slower than the speed of light. It will take less than 90 μs for a proton to travel once around the main ring of 27 Km

The main challenge of the ultra-relativistic heavy ion collision is the observation of the two phase transitions predicted by QCD, the deconfinement and the chiral phase transitions. Increasing temperature or increasing baryon density, a phase transition may occur to the state where quarks and gluons become the correct degrees of freedom.

The present experimental evidence indicates that in such experiments an extended and very dense system of strongly interacting matter is formed. Moreover, such system shows high level of thermalization and also collective behaviour.

1.4.1 Collision dynamics

At ultra-relativistic energy, the energy per nucleon in the center of mass frame is much larger than the nucleon mass, so they are Lorentz contracted along the beam direction. In the center of mass frame they appear as two tiny disk of tickness $2R/\gamma_{CM}$, being R the nuclear radius and $\gamma_{CM} = 1/\sqrt{(1 - p_z^2/E_{CM}^2)}$. At such energies simple geometric concepts are often used. Assuming that all nucleons of each incoming nucleus propagate along straight line then the nucleons that do not meet any other nucleons are called *spectator* while the nucleons that interact are called *partecipants*. Only the spatial distribution of nucleons in the nuclei and the nucleon-nucleon cross section have relevance for the nucleus-nucleus collision. The vector connecting the centers of colliding nuclei is called *impact vector* **b** and its modulus is the impact parameter b. The coordinate system used has the z-axis parallel to the beam axis and the impact vector **b** points the $x-$direction. The reaction plane is individuated by the x and z axes. The value of impact parameter determines the number of the

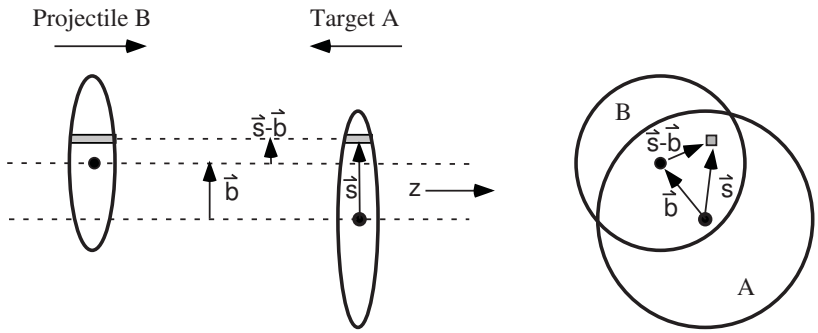

a) Side View b) Beam-line View

Figure 1.10: Schematic representation of the Glauber model geometry.

partecipants, N_{part}, and also the number of spectators N_{spec}. Experimentally, the value of N_{spec} can be extracted from the measurement of the energy deposited in the zero-degree calorimeter (ZDC) and coincidens between the ZDC counters play the role of the trigger for the collision events.

The number of of partecipant nucleons can be evaluated by the Glauber Model which has been succesfully applied in the description in the description of high-energy nuclear reactions. It is a semi-classical model treating the nucleus-nucleus collision as a multiple nucleos-nucleon interactions: a nucleon of incident nucleus interacts with target nucleons with a given density distribution. The nucleon-nucleon inelastic cross-section σ_{NN}^{in} is assumed to be the same as the one in vacuum. It is usefull to introduce the nuclear overlap function $T_{AB}(\mathbf{b})$ with impact parameter $\mathbf{b}$:

$$T_{AB}(\mathbf{b}) = \int d^2\mathbf{s}\, T_A(\mathbf{s}) T_B(\mathbf{s}-\mathbf{b}) \tag{1.34}$$

where the thickness function is defined as

$$T_A(\mathbf{s}) = \int dz\, \rho_A(z,\mathbf{s}). \tag{1.35}$$

in the last equation ρ_A is the nuclear mass number density normalized to mass number A:

$$\int d^2\mathbf{s}\, T_A(\mathbf{s}) = A, \qquad \int d^2\mathbf{b}\, T_{AB}(\mathbf{b}) = AB. \tag{1.36}$$

In the case of interest such as gold and lead nuclei, the Wood-Saxon parametrization is used fro the nuclear density:

$$\rho_A(r) = \frac{\rho_{nm}}{1+\exp((r-R_A)/a)}. \tag{1.37}$$

The number of partecipant nucleons, N_{part}, and the number of nucleon-nucleon collisions, N_{binary}, in the Glauber model are defined as

$$N_{part}(b) = \int d^2\mathbf{s}\, T_A(\mathbf{s}) \left(1 - e^{-\sigma_{NN}^{in} T_B(\mathbf{s})}\right) + \int d^2\mathbf{s}\, T_B(\mathbf{s}-\mathbf{b}) \left(1 - e^{-\sigma_{NN}^{in} T_A(\mathbf{s})}\right), \tag{1.38}$$

$$N_{binary}(b) = \int d^2\mathbf{s}\, \sigma_{NN}^{in} T_A(\mathbf{s}) T_B(\mathbf{s}-\mathbf{b}). \tag{1.39}$$

Monte-Carlo calculations of the Glauber Model are often employed: nucleons of both nuclei are randomly distributed according to the nuclear density profile; at given impact parameter $\mathbf{b}$, each nucleons pairs will interact if the nucleon-nucleon impact parameter $\mathbf{s}$ is less than $\sqrt{(\sigma_{NN}^{in}/\pi)}$.

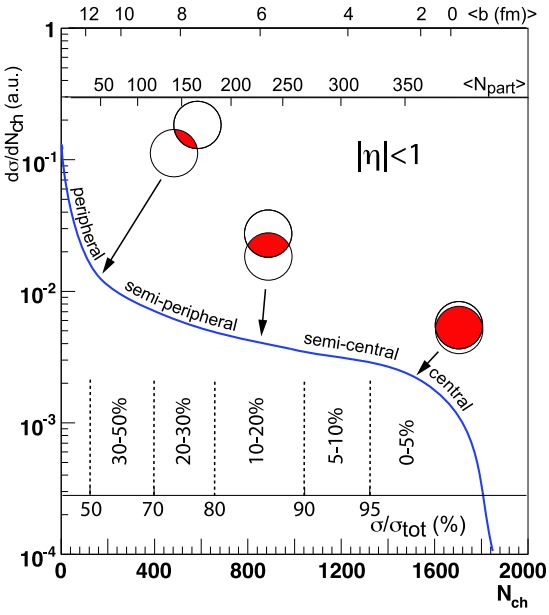

Figure 1.11: Qualitative behavior of the correlation of the final state observable N_{ch} with Glauber calculated quantities (b, N_{part}).

1.4.2 QGP space-time evolution

The result of the multiple nucleon-nucleon collisions is that the two colliding nuclei evolve into an hot and dense system of quarks and gluons. There exists several models to describe this transition: QCD string breaking, QCD parton cascades, color-glass condensate evolving into glasma and later into quark-gluon plasma.

In string breaking model, the nuclei pass through each other and the collisions of the nucleons produce color strings. In a similar way to the quark-antiquark static potential, the strings in nucleon-nucleon collisions can be viewed as quark-diquark pairs connected by the color field: such a system may be treated as the excited nucleons. Then strings decay or fragment forming quarks, antiquarks or hadrons.

Parton cascade models are based on perturbative QCD. The colliding nuclei are treated as clouds of quarks and gluons which penetrate through each other. Multiple hard scatterings between partons and gluons radiation produce large energy and entropy density. The initial state is viewed as an ensemble of quarks and gluons determined by the quark and gluon distribution functions $q_f(x, Q^2)$ and $g(x, Q^2)$, with x is the Bjorken variable. The time evolution of parton phase-space distributions is governed by the relativistic Boltzmann equation with a collision term that contains dominant perturbative QCD interactions. Our approach is close to parton model, however, instead of considering the dominant perturbative QCD interactions, we are able to fix the shear viscosity of the system: this procedure corresponds to a resummation of all relevant channels that produce the η/s, which represents the most important physical quantity of a fluid and determines the space-time evolution of the system.

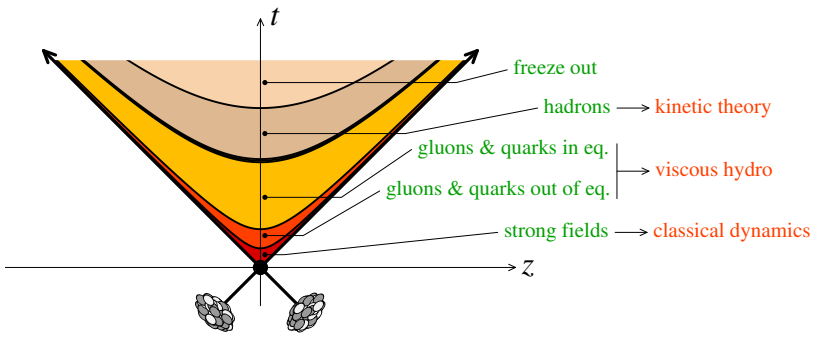

Figure 1.12: The space-time diagram of ultra-relativistic nuclear collisions.[15]

- *Color Glass Condensate* - The color-glass condesate[16–21] is considered the universal form of matter that controls the high-energy scattering of strongly interacting matter. The idea of color-glass condensate was motivated by the rapidly rising of the gluon density as a function of x for large Q^2 as shown in Fig. 1.13 from Ref.[22] This small x behaviour of gluon density needs to be improved since a continuous increase would violate unitarity. As a matter of fact, gluons with typical transverse size of $1/Q$ may eventually overlap each other and saturate. In other words, the gluons form a classical coherent field configuration called color glass condensate (CGC). The saturation scale Q_s is defined as

$$Q_s^2 \sim \alpha_s(Q_s^2)\frac{xg(x,Q_s^2)}{\pi R^2} \tag{1.40}$$

being R the radius of the nucleon. The term color refers to the gluons

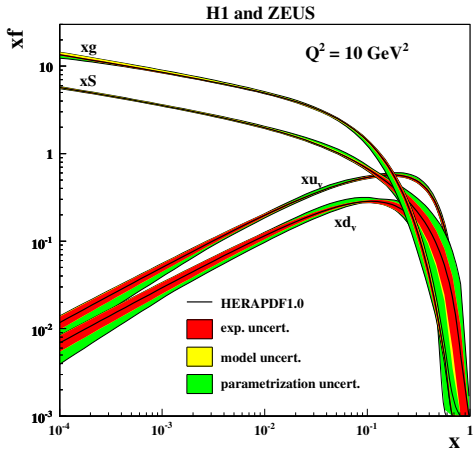

Figure 1.13: Parton distributions of a proton, at the resolution scale $Q2 = 10\,GeV^2$ from Ref.[22]

that are colored, glass describes the property of the low x gluons whose evolution is slow compared to other time scales present in the problem, condensate reflects the large gluon occupation numbers.

The fast gluons are Lorentz contracted and redistributed on the two very this sheets representing the two colliding nuclei. The fast gluons produce the color electric and color magnetic fields which also exist only in the sheets and are mutually orthogonal, as shown qualitatively in Fig. 1.14. Just after the collision of the two gluonic sheets, the longitudinal color electric and color magnetic fields are produced. This form of matter is called *glasma*. The glasma fields decay due to the classical rearrangment

of the fields into radiation of gluons with $p_T \sim Q_s$. Also the decaye due to quantum pair creation are possible. In this way the quark-gluon plasma is produced. In Chapter 6 we will study a color flux tube model

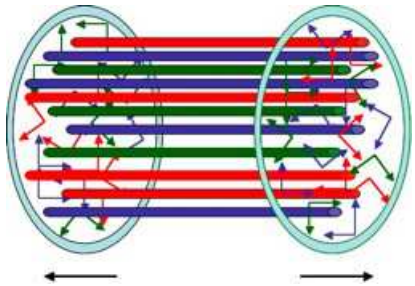

Figure 1.14: Color electric and color magnetic fields after the collision of the two nuclei.[23]

in the framework of the Relativistic Boltzmann Transport equation: we start with a single color longitudinal electric field which decays to pairs particle thanks to the Schwinger mechanism. We couple the dynamical evolution of the initial color field to the dynamics of the many particles system produced by the decay. We will focus on pressure isotropization and thermalization starting from the achademic case of a static box, to a 1+1D expanding flux tube, to the more realistic situation of a 3+1D expanding geometry. In the last case we compute also the elliptic flow

- *Thermalization* - The data observed in experiments suggest a very short thermalization time $\tau_{thermalization} < 1\, fm/c$ supported by the hydrodynamical simulations with an early starting time. The most common view is that the equilibration of the system is an effect of parton rescattering. An interesting phenomenon could be that the equilibration is speeded-up by plasma instabilities:[24] instabilities are much faster than the collisions in the weak coupling regime. Another physical scenario could be that thermalization is a consequence of the chaotic dynamics of the non-Abelian classical color fields.[25] Different approaches to the early-time thermalization problem are agree with a $\tau_{thermalization} \simeq 1\, fm/c$.

  We will show our results on this problem in Chapter 6.

- *Hydrodynamics expansion* - If the thermalization rate is sufficiently fast, a locally thermalized quark-gluon plasma is created and the evolution of the system can be described by the relativistic hydrodynamics equations. These equations are energy momentum and current conservations togheter with the equation of state, taken by Lattice QCD. In this way hydrodynamics represent a link between first principle QCD calculations and dynamical properties of the expanding fireball.

- *Chemical freeze-out* - As the hadronic system cools down the inelastic collisions between its constituents stop before the elastic collisions. The moment when the inelastic collisions stop is defined as the *chemical freeze-out* and the temperature T_{chem} is greater then the thermal freeze-out T_{therm}. As the system evolves from chemical to thermal freeze-out the dominant process are elastic collisions and strong decays of heavier resonances. With this scenario on can describe the measured ratios of hadron abundances by few parameter characterizing the matter at the chemical freeze-out.

- *Thermal freeze-out* - Thermal or kinetic freez-out is the stage when hadrons stop to interact. It is a transition from a strongly coupled system to a weakly coupled one. The expansion of the system causes a rapid growth of the mean free path λ_{mfp} of particles. The thermal freez-out happens when the timescale connected with the collisions becomes larger than the expansion timescale. Particles with different cross section may have different freeze-out points so they decouple from the rest of the system at different times. The momentum distributions of particles are frozen and do not change in time: in this case the measurement of the transverse-momentum spectra reveals information about the state of matter just before the thermal freeze-out.

- *Hadronization* - When the energy density reaches the critical value $\varepsilon_c = 1\,GeV/fm^3$ partons hadronize. There are two different mechanism of hadronization: the fragmentation and the coalescence. In the first one each parton fragment into a jet of hadrons which carries a fraction of momenta of the initial parton. The other mechanism consists of recombination of two or three quarks that respectively form mesons and baryons. In the hadronic phase the hadrons rescatter until the distance between them is larger than the range of strong interaction $d_R \sim 1\,fm$. Therefore at densities $\rho < d_R^{-3}$ all scattering stop and the hadrons decouple and free stream to the detector (kinetic freeze-out). In the hydrodynamic description the hadronization is introduced through a freeze-out algorithm (Cooper Frye formula) which stop the hydrodynamic evolution and translates the hydrodynami output into hadron spectra, making use of the statistical model. Many efforts have being done in last years in the transport theory developing in order to describe both the QGP phase and the hadronization.

1.5 Physical Observables

In this section we resume a list of the principal physical observables that give a signature of the formation of the QGP. Each observables are affected, or can tell us information about, by different stage of the evolution of the QGP. Therefore it is important to identify which observable can shed light on a particulare phase without being influenced by other stages in such a way to have information about a particular phase of the evolution.

- *Global observables* - The rapidity distribution of particles dN/dy and transverse energy density dE_T/dy allow for the determination of temperature, entropy and energy density of the system created in a heavy ion collision, comparing experimental observations to hydrodynamics model. The transverse energy density dE_T/dy is related to the energy density ε by the formula:

$$\varepsilon = \frac{1}{\tau_f S}\frac{dE_T}{dy} \simeq \frac{3}{2}\frac{\langle m_T\rangle}{\tau_f S}\frac{dN_{ch}}{dy} \tag{1.41}$$

  where τ_f is the formation time, conventionally taken as $\tau_f \simeq 1\, fm/c$, S is the transverse overlap area of the colliding nuclei (for a centra collision of two identical nuclei of radius R this is simply $S = \pi R^2$) and $\langle m_T\rangle$ is the mean value of the transverse mass of secondary particles, and N_{ch}/dy is the measured density of charged particles per unit of rapidity.

  The net-proton rapidity distribution of particles dN/dy in Fig. 1.15 from Ref.[26] In details Fig. 1.15 shows the net-proton rapidity distribution for different experiment at different energies. AGS experiments with $Au-Au$ at $11.4\, GeV$ per nucleon measures a gaussian net-proton distribution indicating a large *stopping power*, i.e. baryons are stopped in the middle of the reaction plane and a dense baryon-rich matter is produced at midrapidity. On the other hand, in *transparent collisions*, such as RHIC experiments at $200\, GeV$ per nucleon, the two baryon-rich regions are separated from each other as in the case of RHIC. In transparent collision the system produced in the central region has a very small net baryon number and practically zero baryon chemical potential.

- *Electromagnetic probes* - During the evolution of a nuclear collision are created photons and dileptons that can be used to probe the QGP. The importance of such probes is due to the fact that they do not interact through strong interactions so they could give informations relative to the phase of the evolution when they are originated. However there are so

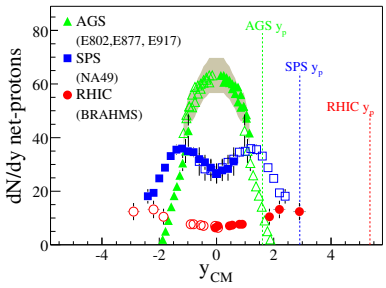

Figure 1.15: The net-proton distribution measured in different experiments from Ref.[26]

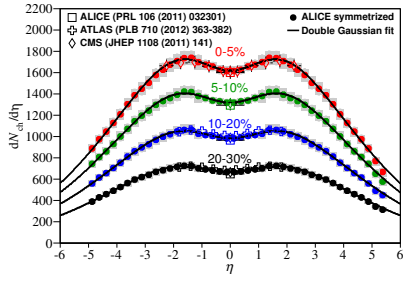

Figure 1.16: Pseudorapidity distribution of charged particles for different centralities from Ref.[27]

many sources which can produce photons and dileptons that the analysis of such kind of observables is quite difficult.

- *Strangeness enhancement* - This phenomenon refers to the increased production of strange particles (Λ, Ξ, Ω) in heavy ion collisions respect to those produces in proton-proton collisions. This signal was predicted in Ref.[28] as a consequence of partons interaction in the QGP.

- *J/ψ suppression* - J/ψ are particles bound states of charm and anti-charm quark ($c\bar{c}$). They are produced moslty by the hard scatterings in the first stage of the collision. They are also created in $p+p$ collisions where they can freely escape from the collision region. Instead, in the case of nucleus-nucleus collisions, the J/ψ are produced in the QGP phase and feel the screening effects of the medium. Even if the J/ψ is a thightly bound particle, in the QGP environment the $c\bar{c}$ potential is screened (Debye screening). As a consequence, the interaction between the $\bar{c}$ and c quarks becomes weaker when $r_{c\bar{c}} > \lambda_D$, being λ_D the Debye screening lenght. For sufficiently high density λ_D is so small that the J/ψ dissociates leading to a suppression of the observed yield compared to the proton-proton or proton-nucleus collisions.[29]

- *Jet quenching* - In the first stage of ultra-relativistic heavy ion collision are produced particles with high transverse momentum that propagate through the plasma interacting with the bulk and loosing their energy via elastic scatterings and radiating gluons in a similar way to the bremsstrahlung photons emitted in QED. The main difference with QED is the non-Abelian nature of QCD, so the emitted gluons carries color charges and again interaact with the color charges of the medium. For high parton energy, the radiative mechanism is the main process for the parton energy loss. The energy loss of high p_T partons causes an attenuation or disappearance of the hadrons jet resulting from the

fragmentation of these high partons. This phenomenon of suppression is called *jet quenching* and is one of the most important probe of the formation of the QGP. The suppression is quantified by the nuclear modification factor R_{AA} which is given by the ratio between the spectrum of partons produced in nucleus-nucleus (AA) collision and the one relative to proton-proton collisions multiplied by the scaling factor N_{coll}

$$R_{AA}(p_T) \equiv \frac{d^2N^{AA}/dp_T d\eta}{N_{coll} d^2N^{pp}/dp_T d\eta}. \tag{1.42}$$

A $R_{AA} = 1$ means that AA collision is only a superposition of pp collisions. One of the open challenge regarding the jet quenching is to explain the difference in the suppression between the different hadron species.

1.5.1 Collective Flows

For non-central collision, the overlap region between the two nuclei is strongly deformed in the transverse plane as qualitatively shown in Fig. 1.17. A measure of such deformation is given by the spatial eccentricity:

$$\varepsilon_x(b) = \frac{\langle y^2 - x^2 \rangle}{\langle y^2 + x^2 \rangle} \tag{1.43}$$

which depends on the impact parameter b. The interactions inside the plasma transfer the spatial deformation into an anisotropy in momentum space. Hence the initial eccentricity influences the azimuthal momentum distribution of the emitted particles. Experimentally, the azimuthal distribution of particle emission is analyzed with respect to the reaction plane in terms of a Fourier expansion as:

$$E\frac{d^3N}{d^3p} = \frac{d^2N}{2\pi p_T dp_T dy}\left(1 + \sum_{n=1}^{\infty} 2v_n \cos\left[n(\phi - \Psi_R)\right]\right) \tag{1.44}$$

where ϕ is the azimuthal angle of the particle and Ψ_R is the azimuthal angle of the reaction plane in the laboratory frame. The first two coefficients in the Fourier decompositions above are called *directed* and *elliptic flow*.

- *Direct Flow* - At low energies, the directed flow is manifested by the reflection of incoming matter by the first produced regions of highly compressed nuclear matter. The nucleons moving with positive rapidities are deflected towards positive x values, while those moving with negative rapidities are deflected towards negative x values. The magnitude of

deflection probes the compressibility of the nuclear matter. It also carries information of the system at early time because the deflection takes place during the passing time of colliding nuclei. At RHIC energies the directed flow of charged particles is negative while the v_1 of spectators is positive: this trend suggests different behaviour of the matter created in the central region and in the target fragmentation regions. At midrapidity the directed flow measured by RHIC is very small, of the order of 1%.

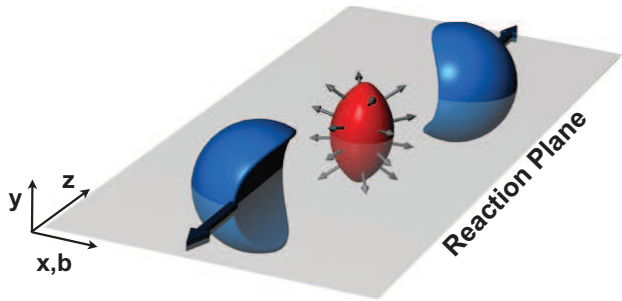

Figure 1.17: Initial space eccentricity, *almond shape*, in non-central collisions.[30]

- *Elliptic flow* - The elliptic flow v_2 characterizes the azimuthal asymmetry of the momentum distributions. At low energies v_2 is negative showing that more momentum is transferred in the direction perpendicular to the reaction plane. At higher energies the elliptic flow becomes positive, hence an excess of momentum is observed in the reaction plane. The enrgy dependence of v_2 can be interpreted in the following way: at low energy the spectators block the expansion of matter in the reaction plane so the matter is squeezed out of the reaction plane; at high energies the spectators move sufficiently fast to leave free space for in-plane expansion of matter.

  The first measurements of v_2 at RHIC showed that v_2 is quite large and very close to the perfect hydrodynamics predictions. The origin of non-zero elliptic flow is the interaction between particles produced in the initially asymmetric region of space (almond-like shape formed by the two overlapping nuclei in non-central collisions) which lead to momentum anisotropy. From the hydrodynamic approach largest pressure gradient acts in the reaction plane.

  Both hydrodynamical and parton cascade calculations have shown that the generation of the elliptic flow saturates in the first $4-5\,fm/c$ making this observable sensitive on the QGP phase without any contaminations by the subsequent hadronic phase. In Fig. 1.18 are shown results of v_2 measured at RHIC as a function of transverse momentum for different

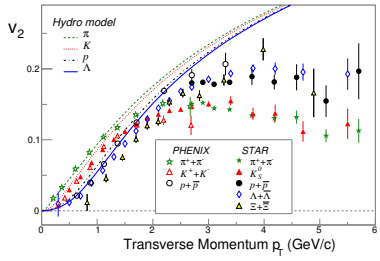

Figure 1.18: Elliptic flow for a variety of particles for Au+Au collisions at $\sqrt{s_{NN}} = 200\,GeV$ measured by the STAR[31] and PHENIX[32] collaborations. Curves show the results from hydrodynamic model calculations[33,34]

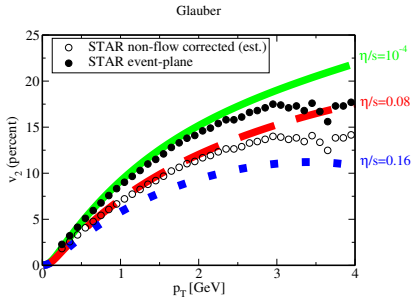

Figure 1.19: Elliptic flow v_2 as a function of transverse momentum p_T: different lines correspond to different value of η/s.[35]

hadrons compared to hydrodynamical calculations. In the region of low transverse momenta $p_T \leq 2\,GeV$ the v_2 is in agreement with ideal hydrodynamical description: this evidence gave the name of *perfect fluid* to the QGP meaning that a very low viscosity fluid was created in ultra-relativistic heavy ions collisions. The fall of the hydrodynamic predictions for $p_T > 2\,GeV$ indicates a break-down of the local thermal equilibrium for particles with high momenta and, on the other hand, the inclusion of a dissipative term in hydrodynamics equations.

There is another important information: baryons have larger v_2 with respect to mesons. This difference can be explained by the coalescence model for hadronization which predicts that the v_2 of any hadron species follows the partonic flow scaled by the number n_q of constituent quarks in the hadron under consideration, i.e. $v_2^{hadron}(p_T) \simeq n_q v_2^{quark}(p_T/n_q)$ with $n_q = 2$ for mesons and $n_q = 3$ for baryons.[36,37] Such a scaling indicates that the flow is developed at the quark level, thus quarks are the true degrees of freedom of the created matter.

2

Boltzmann Transport Equation

Wherever you will go, Boltzmann equation by yourself you will transport.

Contents

In this chapter we discuss about the Transport Boltzmann equation starting from the classical equation to the quantum-relativistic generalization. We also show the numerical implementation of the transport equation. The Transport Theory is useful because, being constructed on a one-body distribution function, allows for a direct tratment of hadronization at variance with the hydrodynamics framework. Moreover the transport approach can describe non-equilibrium states treating in a unified way short range interactions, due to collisions between particles, and long range interactions, associated to mean field effects responsible for the equation of state. Using the Transport Boltzmann equation it is also possible to take into account particles production due to the decay of color flux tubes in the early stage of the collisions, as we will show in Chap. 6., treating in a self-consistent way the fields and the particles dynamics. This means that we can follow the space-time evolution of the system created in heavy ion collisions at ultra-relativistic energy using a single framework. Moreover, as discussed in Chapter 4, we have developed a scheme to fix the shear viscosity to entropy density ratio η/s in our transport simulations overlooking the microscopic details and employing the same language of hydrodynamics.

2.1 Classical Boltzmann Equation

In classical kinetic theory the system under study is a set of N particles in a box of volume V. Particles interacts through collisions whose nature is defined in the cross section σ. The purpose of the theory is not to solve the equation of motion for each particle but to find the distribution function $f(\mathbf{x}, \mathbf{p}, t)$. Being $d^3x d^3p$ the phase space volume element, $f(\mathbf{x}, \mathbf{p}, t) d^3x d^3p$ represents the number of particles that at time t have coordinates in the volume d^3x around $\mathbf{x}$ and momenta in the volume d^3p around $\mathbf{p}$. It has to be noticed that the volume elements d^3x and d^3p are finite volume elements, wide enough to contain a large number of particles and at the same time small enough to be considered as infinitesimal with respect to the macroscopic dimension of the system. Under these assumptions the distribution function $f(\mathbf{x}, \mathbf{p})$ is a continuos function of its arguments.[38, 39]

The normalization condition is:

$$\int f(\mathbf{x}, \mathbf{p}) d^3x d^3p = N. \tag{2.1}$$

In the case of uniform distribution in space coordinate we have:

$$\int f(\mathbf{x},\mathbf{p})\, d^3p = \frac{N}{V}. \tag{2.2}$$

Tha spatial density $\rho(\mathbf{x})$ is obtained integrating the distribution function $f(\mathbf{x},\mathbf{p})$ over momenta:

$$\rho(\mathbf{x}) = \int d^3p\, f(\mathbf{x},\mathbf{p}). \tag{2.3}$$

Average value of a physical observable $O(\mathbf{x},\mathbf{p})$ is computed as follows:

$$\langle O(\mathbf{x})\rangle = \frac{1}{\rho(\mathbf{x})}\int d^3p\, O(\mathbf{x},\mathbf{p}) f(\mathbf{x},\mathbf{p}) \tag{2.4}$$

where, in general, $\langle O\rangle$ can be time-dependent.

The aim of kinetic theory is to describe the space-time evolution of the distribution function $f(\mathbf{x},p)$, so the first step is to obtain the equation of motion for f. Let us consider for simplicity the case of no collisions ($\sigma = 0$): a particle having coordinates $(\mathbf{x},\mathbf{p})$ at time t will be in $(\mathbf{x}+\mathbf{v}\delta t, \mathbf{p}+\mathbf{F}\delta t)$ at time $t+\delta t$, being $\mathbf{F}$ an external force applied to particles and $\mathbf{v} = \mathbf{p}/m$ the particles velocity. In this way, all particles in the volume element $d^3x\, d^3p$ around $(\mathbf{x},\mathbf{p})$ at time t, will be in $d^3x' d^3p'$ around $(\mathbf{x}+\mathbf{v}\delta t, \mathbf{p}+\mathbf{F}\delta t)$ al tempo $t+\delta t$. Hence, if there are no collisions, we have:

$$f(\mathbf{x}+\mathbf{v}\delta t, \mathbf{p}+\mathbf{F}\delta t, t+\delta t)\, d^3x' d^3p' = f(\mathbf{x},\mathbf{p})\, d^3x d^3p \tag{2.5}$$

that can be written as

$$f(\mathbf{x}+\mathbf{v}\delta t, \mathbf{p}+\mathbf{F}\delta t, t+\delta t) = f(\mathbf{x},\mathbf{p}). \tag{2.6}$$

Expanding the left hand side to the first ordet in δt, we obtain the equation of motion for the distribution function:

$$\left(\frac{\partial}{\partial t} + \frac{\mathbf{p}}{m}\cdot\nabla_{\mathbf{x}} + \mathbf{F}\cdot\nabla_{\mathbf{p}}\right) f(\mathbf{x},\mathbf{p}) = 0 \tag{2.7}$$

Considering also collisions between particles ($\sigma > 0$), Eq. (2.6) has to be modified as:

$$f(\mathbf{x}+\mathbf{v}\delta t, \mathbf{p}+\mathbf{F}\delta t, t+\delta t) = f(\mathbf{x},\mathbf{p}) + \mathcal{C}[f] \tag{2.8}$$

where $\mathcal{C}[f]$ is the collision integral and it is a functional of the distribution function. The collision integral takes into account the change of f in time due to collisions. Expanding the left hand side to first order in δt, as in the

previous case without collisions, we obtain:

$$\left(\frac{\partial}{\partial t} + \frac{\mathbf{p}}{m} \cdot \nabla_{\mathbf{x}} + \mathbf{F} \cdot \nabla_{\mathbf{p}}\right) f(\mathbf{x}, \mathbf{p}) = \mathcal{C}[f]. \tag{2.9}$$

In order to write an explicit form for the collision integral $\mathcal{C}$ we have to consider the number of particles that go in or outside the volume element $d^3x d^3p$ in the unit of time. Denoting with $R\,\delta t d^3x d^3p$ the number of collisions that take place during $t + \delta t$ and t when one of the initial particle is in $d^3x d^3p$ around $(\mathbf{x}, \mathbf{p})$, and with $\bar{R}\,\delta t d^3x d^3p$ the one with one of the final particle is in $d^3x d^3p$ around $(\mathbf{x}, \mathbf{p})$, collision integral can be written in this way:

$$\mathcal{C}[f]\delta t = \left(\bar{R} - R\right)\delta t. \tag{2.10}$$

As we can see from the last equation, the collision integral is a balance term for the transport equation: it takes into account the change of phace-space density due to collisions.

2.1.1 Collision integral derivation

In order to obtain an explicit form for the collision integral, let us assume that particles interact through binary collisions and there are no external forces. A collision is a transition from an intial state to a set of final states. The probability transition to final states in the infinitesimal momenta volume $d^3p_1' d^3p_2'$ can be written as:

$$\begin{aligned} dP_{12\to 1'2'} &= d^3p_1' d^3p_2' \delta^4(P_f - P_i) \left|\mathcal{M}_{fi}\right|^2 \\ \delta^4(P_f - P_i) &\equiv \delta^3(\mathbf{P} - \mathbf{P'})\delta(E - E') \end{aligned} \tag{2.11}$$

where $\mathcal{M}_{fi}$ is the transition amplitude for the scattering process and $\delta^4(P_f - P_i)$ is the energy-momentum conservation, because we are considering elastic scattering. The number of transitions $12 \to 1'2'$ in the volume d^3p around $\mathbf{x}$ due to collisions during δt is

$$dN_{12} dP_{12\to 1'2'} \delta t \tag{2.12}$$

where dN_{12} is the initial number of colliding pairs $(\mathbf{p}_1, \mathbf{p}_2)$. The two-particle correlation function is defined as:

$$dN_{12} = \hat{f}(\mathbf{x}, \mathbf{p}_1, \mathbf{p}_2, t) d^3x d^3p_1 d^3p_2. \tag{2.13}$$

Using Eq. (2.11), R can be written as

$$R = \int d^3p_2 d^3p_1' d^3p_2' \delta^4(P_f - P_i) |\mathcal{M}_{fi}|^2 \hat{f}(\mathbf{x}, \mathbf{p}_1, \mathbf{p}_2, t) \tag{2.14}$$

similarly $\bar{R}$

$$\bar{R} = \int d^3p_2 d^3p_1' d^3p_2' \delta^4(P_f - P_i) |\mathcal{M}_{if}|^2 \hat{f}(\mathbf{x}, \mathbf{p}_1', \mathbf{p}_2', t). \tag{2.15}$$

Finally Eq. (2.10), considering $|\mathcal{M}_{if}| = |\mathcal{M}_{fi}|$, assume the following form:

$$\mathcal{C}[f] = \left(\bar{R} - R\right) = \int d^3p_2 d^3p_1' d^3p_2' \, \delta^4(P_f - P_i) \, |\mathcal{M}_{if}|^2 \left(\hat{f}_{1'2'} - \hat{f}_{12}\right) \tag{2.16}$$

where $\hat{f}_{12} = \hat{f}(\mathbf{x}, \mathbf{p}_1, \mathbf{p}_2, t)$. The last equation is exact but it contains the correlation function $\hat{f}$. Boltzmann postulated there are no correlations between particles before each collision (molecular chaos assumption), so Eq. (2.16) becomes:

$$\hat{f}(\mathbf{x}, \mathbf{p}_1, \mathbf{p}_2, t) \approx f(\mathbf{x}, \mathbf{p}_1, t) \, f(\mathbf{x}, \mathbf{p}_2, t). \tag{2.17}$$

Eq. (2.17) means that the probability to find two particle momenta in d^3x is equal to the product of probability to find them individually. Under this assumption, the transport Boltzmann equation is written in a closed form as:

$$\left(\frac{\partial}{\partial t} + \frac{\mathbf{p}_1}{m} \cdot \nabla_x + \mathbf{F} \cdot \nabla_{p_1}\right) f_1 =$$
$$\int d^3p_2 d^3p_1' d^3p_2' \, \delta^4(P_f - P_i) \, |\mathcal{M}_{fi}|^2 \, (f_2' f_1' - f_2 f_1) \tag{2.18}$$

which is a non linear integro-differential equation for the distribution function.

2.2 Relativistic Transport Theory

In relativistic kinetic theory, macroscopic quantities are defined thanks to a scalar distribution function $f(x, p)$ which depends on space-time coordinates $x = x^\mu = (t, \mathbf{x})$ and four momentum $p = p^\mu = (p^0, \mathbf{p})$ which satisfies the mass-shell relation $p^0 = \sqrt{\mathbf{p}^2 + m^2}$.[40,41] The spatial density of Eq. (2.3) is not a Lorentz scalar but it transforms as the time component ($\mu = 0$) of the following four-vector:

$$N^\mu(x) = \int \frac{d^3p}{p^0} p^\mu \, f(x, p). \tag{2.19}$$

while $\mu = 1, 2, 3$ are the components of the current $\mathbf{j}$ The transport equation derivation in the relativistic case is similar to the classical case except for appropriate formal changes. In the following we will derive the transport equation for a system of N relativistic particles non interacting. In this case the distribution function can be written as:

$$f(x,p) = \sum_{i=1}^{N} \delta^4(x_i(t) - x)\delta^4(p_i(t) - p) \tag{2.20}$$

where $x_i(t)$ and $p_i(t)$ denotes coordinates and momenta of the i-th particle at time t. The time evolution of the phase space density is described by the Liouville Theorem: if there are no dissipative forces, the phase space density is a conserved quantity, i.e. $df(x,p)/dt = 0$. Using the Liouville theorem, it is possible to obtain the equation of motion for $f(x,p)$:

$$\begin{aligned}\frac{d}{dt}f(x,p) &= \sum_{i=1}^{N}\left[\frac{dx_i^\mu}{dt}\frac{\partial}{\partial x^\mu} + \frac{dp_i^\mu}{dt}\frac{\partial}{\partial p^\mu}\right]\delta^4(x_i(t) - x)\delta^4(p_i(t) - p) \\ &= \left(\frac{1}{m}p^\mu\frac{\partial}{\partial x^\mu} + F^\mu(x)\frac{\partial}{\partial p^\mu}\right)f(x,p)\end{aligned} \tag{2.21}$$

where $F^\mu(x)$ represents an external force. In this way $df(x,p)/dt = 0$ becomes

$$\left(\frac{1}{m}p^\mu\frac{\partial}{\partial x^\mu} + F^\mu(x)\frac{\partial}{\partial p^\mu}\right)f(x,p) = 0. \tag{2.22}$$

Eq. (2.22) is the relativistic Vlasov equation which in the classical limit gives the Boltzmann transport equation:

$$\left(\frac{\partial f}{\partial t} + \frac{\mathbf{p}}{m}\cdot\nabla_{\mathbf{x}} + \mathbf{F}\cdot\nabla_{\mathbf{p}}\right)f(\mathbf{x},\mathbf{p}) = 0. \tag{2.23}$$

The Vlasov equation can describe systems with conservative forces while it does not permit to take into account dissipative effects. In presence of two body scatterings in fact the phase space density is no more a conserved quantity ($df(x,p)/d\tau \neq 0$) but changes as a consequence of the collisions. It is possible to derive the equation of motion for $f(x,p)$ adding the collision term $\mathcal{C}[f]$ on the right hand side of Eq. (2.22):

$$\left(\frac{1}{m}p^\mu\frac{\partial}{\partial x^\mu} + F^\mu(x)\frac{\partial}{\partial p^\mu}\right)f(x,p) = \mathcal{C}[f](x,p) \tag{2.24}$$

where $\mathcal{C}[f]$ has to be specified. Eq. (2.24) with no external forces is written as follows:

$$p^\mu\partial_\mu f(x,p) = \mathcal{C}[f](x,p) \tag{2.25}$$

which is the equation that we solve numerically for the determination of shear viscosity and electric conductivity of the Quark-Gluon Plasma taking into account only two body collisions. In this case the collision integral is denoted by $\mathcal{C}_{22}[f]$.

Collision term in Eq. (2.25), as well as in Eq. (2.18), can be approximated as:

$$\mathcal{C}[f] \simeq \frac{f - f_0}{\tau_r} \tag{2.26}$$

where τ_r is the relaxation time of the system, i.e. the time scale required to the system to approach the equilibrium state described by f_0. This scheme of approximation is the so famous relaxation time approximation (RTA) which is very useful to obtain analytical results which otherwise are impossible due to the complexity of the Boltzmann equation. In this thesis we will show also how good is the relaxation time approximation for the calculation of shear viscosity and electric conductivity comparing the analytical formula to the numerical results evaluated using Green-Kubo relations which give an exact estimation for transport coefficients.

As shown previously, in order to take into account the dissipative effects that arise from the collisions, it is necessary to add the collision term $\mathcal{C}$ to the Vlasov equation. Let us consider a system of relativistic particles interacting via two body collision and assume there are no correlation before each collisions (molecular chaos), the collision integral $\mathcal{C}_{22}$ is written in terms of distributions functions as follows:[42]

$$\begin{aligned}\mathcal{C}_{22} = &\frac{1}{2E_1}\int \frac{d^3p_2}{(2\pi)^3 2E_2}\frac{1}{\nu}\int \frac{d^3p_1'}{(2\pi)^3 2E_1'}\frac{d^3p_2'}{(2\pi)^3 2E_2'} f_1' f_2' \\ &\times |\mathcal{M}_{1'2'\to 12}|^2 (2\pi)^4 \delta^{(4)}(p_1' + p_2' - p_1 - p_2) - \frac{1}{2E_1} \\ &\times \int \frac{d^3p_2}{(2\pi)^3 2E_2}\frac{1}{\nu}\int \frac{d^3p_1'}{(2\pi)^3 2E_1'}\frac{d^3p_2'}{(2\pi)^3 2E_2'} f_1 f_2 \\ &\times |\mathcal{M}_{12\to 1'2'}|^2 (2\pi)^4 \delta^{(4)}(p_1 + p_2 - p_1' - p_2')\end{aligned} \tag{2.27}$$

where $\nu = 2$ if we are considering indistinguishable particles, otherwise $\nu = 1$. $\mathcal{M}_{f\to i}$ is the transition amplitude scattering.

2.3 Quantum Transport Theory

As shown in the previous section, the fundamental element of kinetic theory is the phase space distribution function whose evolution is described by the Vlasov or by the Boltzmann equation if dissipative phenomena are present. In order to find the analogous equations in quantum mechanics it is necessary to define a quantity that can play the same role of $f(x,p)$. Such a quantity is the Wigner function defined as follow:

$$f_w(r,p,t) = \frac{1}{(2\pi\hbar)^3}\int ds e^{-ip\cdot s/\hbar}\left\langle r+\frac{s}{2}\right|\hat{\rho}\left|r-\frac{s}{2}\right\rangle \tag{2.28}$$

and Fourier transforming:

$$f_w(r,p,t) = \frac{1}{(2\pi\hbar)^3}\int dq e^{+iq\cdot r/\hbar}\left\langle p+\frac{q}{2}\right|\hat{\rho}\left|p-\frac{q}{2}\right\rangle \tag{2.29}$$

where $\hat{\rho}$ is the density operator $\hat{\rho} = |\Psi\rangle\langle\Psi|$. It can be seen as a change of variables from $\langle r|\hat{\rho}|r'\rangle = \rho(r,r') \to f_w(r,p,t)$. Using the explicit expression for the density operator the above equation becomes:

$$f_w(r,p) = \frac{1}{(2\pi\hbar)^2}\int ds e^{-ip\cdot s/\hbar}\Psi^*\left(r+\frac{s}{2}\right)\Psi\left(r-\frac{s}{2}\right). \tag{2.30}$$

The Wigner function, in analogous way to the classical distribution function, allows to calculate the probability distribution in x and p, integrating over x and p respectively one obtains:

$$\rho(r) = \int f_w(r,p)\,dp \quad ; \quad \rho(p) = \int f_w(r,p)\,dr \tag{2.31}$$

and also average value of physical observable O

$$\langle O(r)\rangle = \int \frac{drdp}{2\pi\hbar} O(r) f_w(r,p) \tag{2.32}$$

e.g. the average value of kinetic energy

$$\int dp f_w(r,p)\frac{p^2}{2m} = \langle\psi|T|\psi\rangle \tag{2.33}$$

Once the Wigner function has been defined, one can obtain the quantum version of Vlasov equation performing a Wigner transformation of the Scröedinger equation or, equivalently, of the Heisenberg equation as will be shown below.

Let us start from the equation of motion for the density operator $\hat{\rho}$:

$$\frac{\partial \hat{\rho}}{\partial t} = \left[\hat{\rho}, \hat{H}\right] \tag{2.34}$$

where $\hat{H} = \hat{T} + \hat{U} = \hat{p}^2/2m + \hat{U}$. Let us write explicitely the folowing derivatives of the Wigner function :

$$\frac{\partial f_w}{\partial p} = -\frac{is}{\hbar} f_w, \qquad \frac{\partial f_w}{\partial r} = \frac{iq}{\hbar} f_w \tag{2.35}$$

while, using Eq. (2.34) the time derivative can be written as follows:

$$\dot{f}_w(r,p,t) = \frac{1}{(2\pi\hbar)^3} \int dq e^{iq\cdot r/\hbar} \left\langle q + \frac{p}{2}\right| \frac{1}{i\hbar} \left[\hat{H}, \hat{\rho}\right] \left| p - \frac{q}{2}\right\rangle \tag{2.36}$$

Let us now compute the kinetic part $\left\langle q + \frac{p}{2}\right| \frac{1}{i\hbar} \left[\hat{T}, \hat{\rho}\right] \left| p - \frac{q}{2}\right\rangle$:

$$\begin{aligned} &= \frac{1}{(2\pi\hbar)^3} \int dq e^{iq\cdot r/\hbar} \left\langle q + \frac{p}{2}\right| \frac{1}{i\hbar} (\hat{T}\hat{\rho} - \hat{\rho}\hat{T}) \left| p - \frac{q}{2}\right\rangle = \\ = \frac{1}{(2\pi\hbar)^3} &\int dq e^{iq\cdot r/\hbar} \left(\frac{(p+q/2)^2}{2m} - \frac{(p-q/2)^2}{2m} \right) \left\langle p + \frac{q}{2}\right| \hat{\rho} \left| p - \frac{q}{2}\right\rangle \end{aligned} \tag{2.37}$$

So finally we get the kinetic part of the time derivative of the Wigner function:

$$\dot{f}_w^T(r,p,t) = \frac{1}{(2\pi\hbar)^3} \frac{1}{\hbar} \int dq e^{iq\cdot r/\hbar} \left(\frac{p\cdot q}{m}\right) \left\langle p + \frac{q}{2}\right| \hat{\rho} \left| p - \frac{q}{2}\right\rangle = -\frac{p}{m} \frac{\partial f_w}{\partial r}. \tag{2.38}$$

Let us evaluate the $\hat{U}$ part in Eq. (2.36) in the coordinate space representation:

$$\begin{aligned} \dot{f}_w^U &= \frac{1}{(2\pi\hbar)^3} \frac{1}{i\hbar} \int ds\, e^{-ip\cdot s/\hbar} \left\langle r + \frac{s}{2}\right| \left[\hat{U}, \hat{\rho}\right] \left| r - \frac{s}{2}\right\rangle = \\ = \frac{1}{(2\pi\hbar)^3} \frac{1}{i\hbar} &\int ds e^{-ip\cdot s/\hbar} \left[U\left(r + \frac{s}{2}\right) - U\left(r - \frac{s}{2}\right)\right] \left\langle r + \frac{s}{2}\right| \hat{\rho} \left| r - \frac{s}{2}\right\rangle \end{aligned} \tag{2.39}$$

Expanding U in r:

$$\begin{aligned} U\left(r + \frac{s}{2}\right) &= U(r) + \frac{s}{2}\frac{\partial U}{\partial r} + \frac{1}{2}\left(\frac{s}{2}\right)^2 \frac{\partial^2 U}{\partial r^2} + \cdots = \left(e^{\frac{s}{2}\nabla}\right) U \\ U\left(r - \frac{s}{2}\right) &= U(r) - \frac{s}{2}\frac{\partial U}{\partial r} + \frac{1}{2}\left(\frac{s}{2}\right)^2 \frac{\partial^2 U}{\partial r^2} + \cdots = \left(e^{-\frac{s}{2}\nabla}\right) U \end{aligned} \tag{2.40}$$

Using the above expansion the U term of the time derivative of f_w can be written as:

$$\dot{f}_w^U = \frac{1}{(2\pi\hbar)^3}\int ds\, e^{-ip\cdot s}\frac{1}{2i}\left(e^{i\frac{\hbar}{2}\nabla_r\nabla_p} - e^{-i\frac{\hbar}{2}\nabla_r\nabla_p}\right) U\left\langle r+\frac{s}{2}\right|\hat{\rho}\left|r-\frac{s}{2}\right\rangle = \frac{2}{\hbar}\sin\left(\frac{\hbar}{2}\nabla_r\nabla_p\right)Uf \tag{2.41}$$

where ∇_r acts on U while ∇_p has to be applied to f_w. Finally, using all the terms evaluated, we obtain the following equation:

$$\frac{\partial f_w}{\partial t} + \frac{\partial f_w}{\partial r}\frac{p}{m} - \frac{2}{\hbar}\sum_{k=0}^{\infty}\frac{(-1)^k}{(2k+1)!}\left(\frac{\hbar}{2}\nabla_r\nabla_p\right)^{2k+1} Uf_w = 0 \tag{2.42}$$

where $\sin(ax) = \sum_{k=0}^{\infty}(-1)^k(ax)^{2k+1}/(2k+1)!$ No approximation has been made to find this equation and it is exactly equivalent to the Heisenberg equation or to the Schroedinger equation. If the gradient of the potential is not too strong, the summation over k index can be truncated at the first term, that does not contain any $\hbar$ terms, and the previous equation can be written as:

$$\frac{\partial f_w}{\partial t} + \frac{\mathbf{p}}{m}\frac{\partial f_w}{\partial r} + \vec{\nabla}_r U\cdot\vec{\nabla}_p f_w = 0 \tag{2.43}$$

which has the same form of the classical transport equation but for the Wigner function. We notice also that Eq. (2.43) remains exact for linear or quadratic potential.

2.4 Transport Theory in Quantum Field Theory

In relativistic field theory, the Wigner function corresponds to the ensemble average of the Wigner operator:

$$\hat{W}_{\alpha\beta} \equiv \int \frac{d^4y}{(2\pi)^4} e^{-ip\cdot y}\bar{\psi}_\beta(x)e^{\frac{1}{2}y\cdot\partial^\dagger}e^{-\frac{1}{2}y\cdot\partial}\psi_\alpha(x) \tag{2.44}$$

where $\partial^\dagger$ (∂) play the role of translation generator acting to the left (right). The spinors are Heisenberg operators. $\hat{W}_{\alpha\beta}$ is a 4×4 matrix whose indices are spinor indices. The Wigner function is then:

$$W(x,p) \equiv \langle : \hat{W}(x,p) : \rangle. \tag{2.45}$$

The brackets indicate ensemble averaging and the colons normal ordering with respect to the vacuum state. The physical interpretation of the Wigner function is made clear if we note that in terms of the four momentum operator $\hat{p}_\mu = \frac{1}{2}i(\partial_\mu - \partial_\mu^\dagger)$ the integration over y gives formally

$$W_{\alpha\beta}(x,p) = \langle : \bar{\psi}_\beta(x)\delta^4(p-\hat{p})\psi(x)_\alpha : \rangle. \tag{2.46}$$

In this way $tr\, W(x,p)$ measures the scalar density at space-time point x_μ with momentum p_μ.

In general the Wigner function can be expanded in terms of 16 independent generators of the Clifford algebra whose basis consists of the matrices $1, i\gamma_5, \gamma_\mu, \gamma_5\gamma_\mu, \frac{1}{2}\sigma_{\mu\nu}$, so it can be decomposed as:

$$\hat{W} = \mathcal{F} + i\gamma_5\mathcal{P} + \gamma^\mu\mathcal{V}_\mu + \gamma^\mu\gamma_5\mathcal{A}_\mu + \frac{1}{2}\sigma^{\mu\nu}\mathcal{S}_{\mu\nu}. \tag{2.47}$$

The pseudo-scalar $\mathcal{P}$ and axial-vector $\mathcal{A}_\mu$ parts vanishes in the case of locally spin-saturated system[43] and in classical limit the tensor part can be neglected[44] so the Wigner function in this case can be written as:

$$\hat{W}(x,p) = \mathcal{F}(x,p) + \gamma^\mu\mathcal{V}_\mu(x,p). \tag{2.48}$$

The procedure to derive the transport equation i.e. the equation of motion for the Wigner function is similar to that used in the previous section in order to derive the transport equation in quantum mechanics. Thus one has to do a Wigner transformation of the field's equation of motion. For the purpose of our work we are interested to a system described by a fermionic field which interacts trough a scalar field and hence we will derive the transport equation in this simplified case. The Lagrangian of such a system is

$$\mathcal{L} = \bar{\psi}(x)[i\gamma_\mu\partial^\mu - g_s\sigma]\psi(x) - \frac{1}{2}m_s^2\sigma^2. \tag{2.49}$$

from the lagrangian we derive the equation of motion for the fermionic fields:

$$[i\gamma_\mu\partial^\mu - (m - g_s\sigma)]\psi(x) = 0. \tag{2.50}$$

At this point one makes the Wigner transformation of the equation of motion obtaining

$$\int \frac{d^4y}{(2\pi\hbar)^4} e^{-\frac{ipy}{\hbar}} \bar{\Psi}_\beta(x_+)[i\gamma_\mu\partial^\mu - (m - g_s\sigma)]\Psi_\alpha(x_-) = 0 \tag{2.51}$$

where $x_\pm = x \pm \frac{y}{2}$ and after some operations one gets

$$(\gamma \cdot p - \frac{i}{2}\gamma \cdot \partial - m)_{\beta\rho}\, \hat{W}_{\rho\alpha}(x,p) + \int \frac{d^4y}{(2\pi\hbar)^4}\, e^{-\frac{ipy}{\hbar}} \langle : \bar{\Psi}_\beta(x_+)\Psi_\alpha(x_-)\sigma(x_-) : \rangle = 0. \tag{2.52}$$

Eq. (2.52) is equivalent to the equation of motion (2.50). Considering the scalar field as a classical function, i.e. ignoring the quantum fluctuations (mean field approximation), one can compute the expectation value. Moreover, using the semi-classical approximation, the field can be Taylor expanded to first order, if gradients are not too large, obtaining:

$$\sigma(x_-) = \sigma(x) - \frac{y^\mu}{2}\partial^x_\mu \sigma(x). \tag{2.53}$$

Using the last equation in Eq. (2.52) we have:

$$\{\frac{i}{2}\gamma \cdot \partial + \gamma \cdot p - m^*(x) + \frac{i}{2}\partial^\mu_x \sigma(x)\partial^p_\mu\}\hat{W}(x,p) = 0 \tag{2.54}$$

where $m^* = m - \sigma(x)$ is the effective mass. The real part of Eq. (2.54) is

$$[\gamma \cdot p - m^*(x)]\hat{W}(x,p) = 0 \tag{2.55}$$

while the imaginary part

$$[\gamma_\mu \partial^\mu - m^*(x)\partial^x_\mu m^*(x)\partial^\mu_p]\hat{W}(x,p) = 0. \tag{2.56}$$

Being the one body distribution function $f(x,p) = W_s(x,p)/m(x)$ one obtains:

$$\left(p^\mu \partial_\mu + m^*(x)\partial_\mu m^*(x)\partial^\mu_p\right) f(x,p) = 0 \tag{2.57}$$

which is the Vlasov equation that describes the space time evolution of $f(x,p)$ for fermions interacting through the scalar field σ.
In order to take into account dissipative effects that arise from collisions, one has to include also the collision integral $\mathcal{C}[f]$ on the right hand side of Vlasov equation:

$$\left(p^\mu \partial_\mu + m^*(x)\partial_\mu m^*(x)\partial^\mu_p\right) f(x,p) = \mathcal{C}[f](x,p). \tag{2.58}$$

The above equation describes the motion of particles considering collisions, i.e. short range physics, and mean field, i.e. long range effects.

2.5 Numerical implementation

In this section we discuss about the numerical implementation of the Transport equation. In details we discuss about the *test-particles method*, in order to sample the distribution function, and the *stochastic method*, in order to solve the collision integral.

2.5.1 Test-particles method

In order to solve the transport equation we use the *test particle method*, introduced by Wong[45] and used in almost all transport calculations.[46–48] The test particle method consists in sampling the phase space distribution function by a large number of test particles. Usually the test particles are chosen point-like, i.e. δ function in coordinate and momentum space, hence the phase space distribution can be written as a sum of the δ test particle distribution:

$$f(\mathbf{x},\mathbf{p},t) = A\sum_{i=1}^{N_{test}} \delta^3(\mathbf{x}-\mathbf{x}_i(t))\delta^3(\mathbf{p}-\mathbf{p}_i(t)) \tag{2.59}$$

where $\mathbf{x}_i(t)$ and $\mathbf{p}_i(t)$ are respectively the position and the momentum of the i-th test particle; N_{test} is the total number of test particles while A is a normalization factor that is related to the total number of particles in a way that the integral over the phase space of the distribution function is equal to the total number of particles:

$$\int d^3x \int \frac{d^3p}{(2\pi)^3}\, f(\mathbf{x},\mathbf{p},t) = \frac{A}{(2\pi)^3} N_{test} = N_{particles} \tag{2.60}$$

where $(2\pi)^3/A$ is equal to the number of test particles per real particles. Once the test particles have been introduced, the solution of the transport equation reduces to solve the classical equation of motion for the test particles. The $i-$th test particles in momentum space belongs to the mass-shell hypersurface $p_\mu p^\mu = m^2$. It can be shown, using the Liouville theorem, that the phase space distribution given as a collection of point-like test particles is a solution of the Boltzmann-Vlasov equation (2.58) if the positions and momenta of test particle obey the relativistic Hamilton equations:

$$\dot{\mathbf{x}}_i = \frac{\mathbf{p}_i}{E_i}; \qquad \dot{\mathbf{p}}_i = -\nabla_{\mathbf{x}} E_i + coll \tag{2.61}$$

where the term *coll* indicates the effect of the collision integral, whose numerical implementation will be described in the next subsection. The equation of motion that are solved numerically are:

$$\begin{aligned} \mathbf{p}_i(t+\Delta t) &= \mathbf{p}_i(t-\Delta t) - \nabla_{\mathbf{x}} E_i + coll \\ \mathbf{x}_i(t+\Delta t) &= \mathbf{x}_i(t-\Delta t) - 2\Delta t \frac{\mathbf{p}_i(t)}{E_i(t)} \end{aligned} \tag{2.62}$$

where index i refers to i-th test particle and Δt is the time discretization.

2.5.2 Stochastic Method

In this subsection we will discuss the numerical implementation of the collision integral based on the stochastic method implemented by Ref.[49] and Ref.[42] In this method a probability collision P_{22} is associated to particles: if probability is grater than a random number between 0 and 1 the collision takes place. The P_{22} can be derived from the collision term of the Boltzmann-Vlasov equation Eq. (2.27). The probability in unit volum $\Delta^3 x$ and unit time Δt can be defined as the ratio between the number of collisions that happen in such volume $\Delta^3 x$ during the time Δt and the total number of pairs present in the same unit volume:

$$P_{22} = \frac{\Delta N_{coll}^{2\to 2}}{\Delta N_1 \Delta N_2} \tag{2.63}$$

where $\Delta N_{coll}^{2\to 2}$ is simply derived from the collision integral in Eq. (2.27), that in discretized form can be written as:

$$\begin{aligned} \frac{\Delta N_{coll}^{2\to 2}}{\Delta t \frac{1}{(2\pi)^3} \Delta^3 x \Delta^3 p_1} &= \frac{1}{2E_1} \frac{\Delta^3 p_2}{(2\pi)^3 2E_2} f_1 f_2 \times \\ \times \frac{1}{\nu} \int \frac{d^3 p_1'}{(2\pi)^3 2E_1'} \frac{d^3 p_2'}{(2\pi)^3 2E_2'} &\left|\mathcal{M}_{12\to 1'2'}\right|^2 (2\pi)^4 \delta^4(p_1 + p_2 - p_1' - p_2'). \end{aligned} \tag{2.64}$$

Let us introduce the definition of cross section for a particle of mass m_i

$$\sigma_{22} = \frac{1}{4F} \frac{1}{\nu} \int \frac{d^3 p_1'}{(2\pi)^3 2E_1'} \frac{d^3 p_2'}{(2\pi)^3 2E_2'} \left|\mathcal{M}_{12\to 1'2'}\right|^2 (2\pi)^4 \delta^4(p_1 + p_2 - p_1' - p_2') \tag{2.65}$$

where $F = \sqrt{(p_1 \cdot p_2)^2 - m_1^2 m_2^2}$ is the so called *invariant flux*. Using the definition of cross section, $\Delta N_{coll}^{2\to 2}$ becomes:

$$\Delta N_{coll}^{2\to 2} = \frac{1}{(2\pi)^3} f_1 \Delta^3 p_1 \frac{1}{(2\pi)^3} \Delta^3 p_2 \Delta^3 x \Delta t \, \sigma_{22} \frac{F}{E_1 E_2}. \tag{2.66}$$

The total number of pair present in a unit volum is given by:

$$\Delta N_1 \Delta N_2 = \frac{1}{(2\pi)^3} f_1 \Delta^3 p_1 \Delta^3 x \frac{1}{(2\pi)^3} f_2 \Delta^3 p_2 \Delta x. \tag{2.67}$$

The relative velocity is defined as:

$$v_{rel} = \frac{F}{E_1 E_2} = \frac{\sqrt{[s-(m_1+m_2)^2]\,[s-(m_1-m_2)^2]}}{2E_1E_2} \tag{2.68}$$

where $s = (p_1 + p_2)^2$ is the Mandelstam variable. Combining Eqs. (2.66) (2.67) (2.68) in the definition of probability P_{22} Eq. (2.63) we finally obtain:

$$P_{22} = v_{rel}\sigma_{22}\frac{\Delta t}{\Delta^3 x}. \tag{2.69}$$

If one uses the test particle method the probability has to be multiplied by $1/N_{test}$. In the limit $\Delta t \to 0$ and $\Delta^3 x \to 0$, P_{22} is a Lorentz invariant and the stochastic method converges to the exact solution of the Boltzmann equation. The space-time discretization has to be choosen smaller than the typical scales of spatial and temporal inhomogeneities of particles densities. Only particles being in the same cell can collide each other, and the collision probability has to be calculated for each pair inside the cell and compared with a random number. Strickly speaking, such collisions have not to be considered as real collisions but as a way to map the evolution of the phase space induced by the matrix element $\mathcal{M}_{i\to f}$ (sampled stochastically).

2.6 The code in the box

Once the code has been developed, it is necessary to test the code with some cases whose solution is known analytically. Hence we performed simulations in a static box of volume V with periodic boundary conditions.

2.6.1 Relaxation toward equilibrium

The first check represents the relaxation toward the equilibrium state: the transport equation is a space-time evolution equation for the distribution function having as fixed point the equilibrium distribution function. The equilibrium distribution function is the Boltzmann-Jüttner function in our case,

but the relativistic Boltzmann integral can be easily extendend to have as a fixed point the Fermi-Dirac or the Bose-Einstein distribution function.
If the system is in a non-equilibrium state then in the limit $t \to \infty$ it will evolve to the equilibrium denoted by f_0. In this case we considered a system of massless particles so the transport equation to be solved is:

$$p^\mu \partial_\mu = \mathcal{C}[f](x,p) \tag{2.70}$$

which we solved using the stochastic algorithm and the test particle method previously described. For such a system in a volume V the particle number can be computed as:

$$N = \rho V = V \frac{\gamma}{(2\pi)^3} \int dp\, 4\pi p^2 e^{-p/T} = \gamma V \frac{T^3}{\pi^2} \tag{2.71}$$

where γ is the degeneracy factor and T is the temperature. Using the previous equation and considering a box of $V = 3 \times 3 \times 3\, fm^3$ one obtains $N = 365$ particles. Particles are distributed uniformly in coordinate space while in momentum space we choose the following distribution:

$$\frac{dN}{N dp_T dp_z} = \delta(p_{xy} - p_{xy}^{init})\delta(p_z) \tag{2.72}$$

in such a way to be far from the equilibrium state described by the Maxwell-Boltzmann distribution function. Eq. (2.72) means that at initial time particles have no momentum along the z direction ($p_z = 0$) while $p_{xy} = \sqrt{p_x^2 + p_y^2} = p_{xy}^{init}$, so all particles have finite momentum only in the xy plane. At the equilibrium state the energy per particle is $E = 3T$: choosing $p_{xy}^{init} = 1.2\, GeV$ for each particle the equilibrium temperature will be $T = 0.4\, GeV$. The equilibrium distribution function is the Boltzmann distribution:

$$\frac{dN}{N E^2 dE} = \frac{1}{2T^3} e^{-E/T}. \tag{2.73}$$

In Fig. 2.1 we show a simulation performed using a total cross section $\sigma_{tot} = 10\, mb$ constant and isotropic, $N_{test} = 1000$, $\Delta t = 0.01\, fm/c$ and $\Delta x \simeq 0.1\, fm$: as we can see such a system approaches the equilibrium state for $t > 0.8\, fm/c$.

2.6.2 Equation of State

Another test to be performed in order to check the validity of the code is the reproducibility of thermodynamical quantities such as pressure and energy

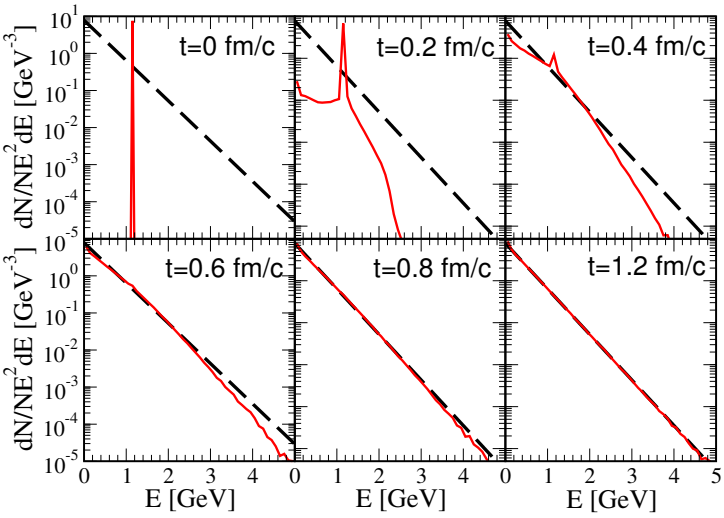

Figure 2.1: Evolution of the distribution function as a function of energy at different time. Dashed line is the Boltzmann equilibrium distribution. For details of the simulation see the text.

density of the system under consideration. In this case we consider a system of particles in a volume V.

The partition function for a relativistic ideal gas of particles with finite mass m is given by:

$$Z(N,T,V) = \frac{1}{N!}\left(\gamma\frac{V}{2\pi^2}\left(Tm^2\right)K_2\left(\frac{m}{T}\right)e^{m/T}\right)^N \tag{2.74}$$

where γ is the degeneracy factor and $K_2(m/T)$ is the modified Bessel function. The free energy is $F = -T\ln Z$:

$$F(N,T,V) = -N\left[T\ln\left(\frac{\gamma}{2\pi^2}\frac{VTm^2}{N}K_2\left(\frac{m}{T}\right)\right) + m + T\right]. \tag{2.75}$$

Once F is known the pressure is simply given by:

$$P = \rho T \tag{2.76}$$

with $\rho = N/V$ the particle density, while the energy density is

$$\varepsilon = \rho m\left(\frac{K_1(m/T)}{K_2(m/T)} + 3\frac{T}{m}\right) \tag{2.77}$$

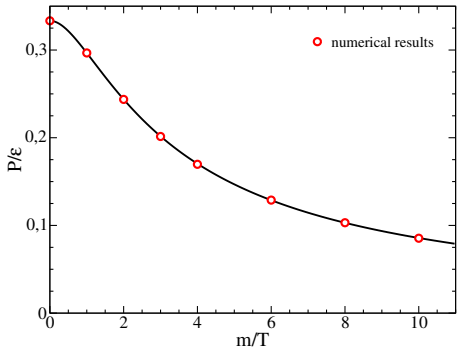

Figure 2.2: Equation of state P/ε as a function of m/T. Red circles represent numerical results while the black line is the analytical prediction of Eqs. (2.76-2.77)

.

In tranport theory the energy-momentum tensor can be written as:

$$T^{\mu\nu} = \int \frac{d^3p}{(2\pi)^3} \frac{p^\mu p^\nu}{p^0} f(p) = \frac{1}{V} \sum_i \frac{p_i^\mu p_i^\nu}{p_i^0} \tag{2.78}$$

where on the right hand side we have used the distribution function for point-like particle Eq. (2.59). Using the last equation it is possible to compute the energy density as $\varepsilon = \langle T^{00} \rangle$ and the pressure $P = \langle T^{11} + T^{22} + T^{33} \rangle /3$. In Fig. 2.2 we show the equation of state P/ε as a function of m/T computed in the box: red circles are the numerical results evaluating the energy-momentum tensor Eq. (2.78) that are in excellent agreement for all the cases of m/T explored with the black line that represent the analytical prediction of Eqs. (2.76-2.77).

Once we know energy density and pressure, the entropy density is given by the Gibbs relation:

$$s = \frac{\varepsilon + P}{T} \tag{2.79}$$

which will be useful in order to compute the ratio of shear viscosity to entropy density ratio.

2.6.3 Collision Rate

One of the most important quantity to keep under control in solving the transport equation is the collision rate. The stochastic method, used to solve the transport equation, as discussed in previous section, is based on the probability collision P_{22} so it is obvious that a fundamental quantity that

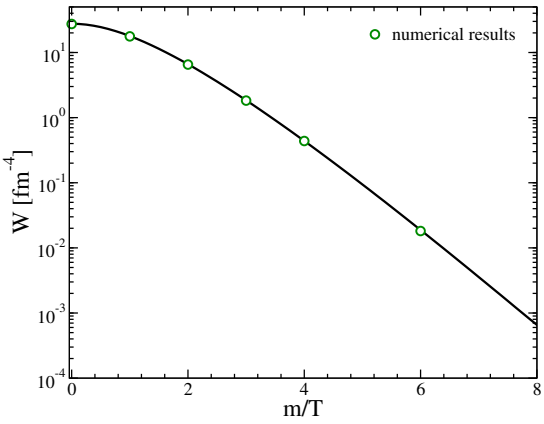

Figure 2.3: Collision rate W as a function of m/T. Green circles are numerical results while the black line is the analytical prediction of Eq. (2.81)

determines the validity of the algorithm is just the collision rate, i.e. the number of collisions in the unit of time. Moreover the collision rate controls the time scale of relaxation that drives the thermalization of the system. Being interested in all these aspects with the aim to compute transport coefficients and thermalization, isotropization of the QGP created in relativistic heavy ion collisions, it is mandatory to compute the collision rate in order to validate our simulations and results.

The collision rate per unit volume W, Lorentz invariant, is defined as follows:

$$W = \frac{\Delta N_{coll}}{V \Delta t} \tag{2.80}$$

which means the number of collisions per unit of time Δt and volume V. The collision rate can be computed analitically[50]

$$W = \frac{8T^6}{\pi^4} \sigma_{tot} \int_{2m/T}^{\infty} dx \left(x^2 \left(\frac{2m}{T} \right)^2 \right) K_1(x) \tag{2.81}$$

In FIg. 2.3 we show collision rate W as a function of m/T: circles are numerical results while solid line is the analytical formula Eq. (2.81). As we can see there is a very good agreement in all the range of temperature and masses explored: this means that the numerical implementation of the sthocastic method is under control and validate our simulations presented in this works.

3

Transport Coefficients

"It's the job that's never started as takes longest to finish."
J.R.R. Tolkien, The Lord of the Rings

Contents

In this Chapter we discuss about the Linear Response Theory which allows us to compute the change of physical observables due to an external small perturbation. The theory predicts that the response of the system can be computed using equilibrium correlation functions not dependent on the external source. For instance, if the perturbation is an external electric field, the system respond generating an electric current proportional to the electric field via the electric conductivity coefficients while if the perturbation is a stress to the fluid, the system will respond generating a velocity flow proportional to the shear viscosity coefficients. Both transport coefficients can be computed using the Green-Kubo formulas in the framework of Linear Response Theory. We also discuss other analytical derivations in Transport Theory like for example Relaxation Time Approximation and Chapman-Enskog method. Finally we briefly report Lattice QCD shear viscosity and electric conductivity results along with a brief primer of AdS/CFT calculations.

3.1 Linear Response Theory

Suppose to apply an external field to a system which is in equilibrium. The aim of Linear Response Theory is to compute the change of the ensemble average value of an operator $Y(\mathbf{x},t)$ caused by the external field.[51] Let the Hamiltonian be:

$$H'(t) = H + H_{ext}(t) \tag{3.1}$$

where H is the unperturbed Hamiltonian, which can contain also interactions, and $H_{ext}(t)$ is the perturbation. The exact equation of motion for Y is

$$\frac{\partial Y(\mathbf{x},t)}{\partial t} = i\left[H'(t), Y(\mathbf{x},t)\right]. \tag{3.2}$$

The expectation value of Y in a eigenvector $|j\rangle$ of H is

$$\begin{aligned} \frac{\partial \langle j|\, Y(\mathbf{x},t)\, |j\rangle}{\partial t} &= i\langle j|\left[H'(t), Y(\mathbf{x},t)\right]|j\rangle \\ &= i\langle j|\left[H_{ext}(t), Y(\mathbf{x},t)\right]|j\rangle . \end{aligned} \tag{3.3}$$

Assuming that H_{ext} will cause only a small perturbation, it is possible to integrate the previous equation to first order in H_{ext}:

$$\begin{aligned} \delta\langle j|\, Y(\mathbf{x},t)\, |j\rangle &= \langle j|\, Y(\mathbf{x},t)\, |j\rangle - \langle j|\, Y(\mathbf{x},t_0)\, |j\rangle \\ &= i\int_{t_0}^{t} dt'\, \langle j|\left[H_{ext}(t'), Y(\mathbf{x},t)\right]|j\rangle . \end{aligned} \tag{3.4}$$

Taking the ensemble average

$$\delta\langle Y(\mathbf{x},t)\rangle = \frac{\sum_j e^{-\beta H}\delta\,\langle j|\,Y(\mathbf{x},t)\,|j\rangle}{\sum_j e^{-\beta H}} \tag{3.5}$$

and using Eq. (3.3) one obtains

$$\delta\langle Y(\mathbf{x},t)\rangle = i\int_{t_0}^{t} dt'\,Tr\left\{\hat{\rho}\left[H_{ext}(t'),Y(\mathbf{x},t)\right]\right\} \tag{3.6}$$

which expresses the change in the ensemble average value of Y in terms of the commutator H_{ext} and Y computed in the unperturbed ensemble represented by $\hat{\rho}$. Let suppose to consider a real scalar field ϕ that is coupled to an external source $J(\mathbf{x},t)$ via

$$H_{ext}(t) = \int d^3x\,J(\mathbf{x},t)\hat{\phi}(\mathbf{x},t). \tag{3.7}$$

The ensemble average of $\hat{\phi}$ is

$$\delta\langle\hat{\phi}(\mathbf{x},t)\rangle = -i\int_{t_0}^{t} dt'\int d^3x'\,J(\mathbf{x}',t')Tr\left\{\hat{\rho}\left[\hat{\phi}(\mathbf{x},t),\hat{\phi}(\mathbf{x}',t')\right]\right\}. \tag{3.8}$$

Recalling that the retarded Green's function is

$$iD^R(\mathbf{x},t;\mathbf{x}',t') = Tr\left\{\hat{\rho}\left[\hat{\phi}(\mathbf{x},t),\hat{\phi}(\mathbf{x}',t')\right]\right\}\theta(t-t') \tag{3.9}$$

it is possible to rewrite Eq. (3.8) as

$$\delta\langle\hat{\phi}(\mathbf{x},t)\rangle = \int_{-\infty}^{\infty} dt'\int d^3x'\,J(\mathbf{x}',t')D^R(\mathbf{x},t;\mathbf{x}',t'). \tag{3.10}$$

For a system in thermal equilibrium, D^R depends only on $\mathbf{x}-\mathbf{x}$**'** and $t-t'$ so one can fourier transform the corrispondent Green's function and current obtaining:

$$\delta\langle\phi(\omega,\mathbf{k})\rangle = J(\omega,\mathbf{k})D^R(\omega,\mathbf{k}) \tag{3.11}$$

which is the equivalent of Eq. (3.10) in frequency-momentum space.

Real time Green's function required in linear response approach are related to the imaginary time propagators:

$$\begin{aligned}\mathcal{D}(\mathbf{x},\tau) &= \langle\hat{\phi}(\mathbf{x},\tau)\hat{\phi}(0)\rangle \\ &= \frac{1}{Z}\sum_n e^{-\beta E_n}\,\langle n|\,\hat{\phi}(\mathbf{x},\tau)\hat{\phi}(0)\,|n\rangle \\ &= \frac{1}{Z}\sum_{m,n} e^{-\beta E_n}\,\langle n|\,\hat{\phi}(\mathbf{x},\tau)\,|m\rangle\,\langle m|\,\hat{\phi}(0)\,|n\rangle\,.\end{aligned} \tag{3.12}$$

Using the time evolution of the field in imaginary time $\hat{\phi}(\mathbf{x},\tau) = e^{H\tau}\hat{\phi}(\mathbf{x},0)e^{-H\tau}$ and Fourier transforming the previous equation, one obtains

$$\begin{aligned}\mathcal{D}(\omega_n,\mathbf{k}) &= \int_0^\beta d\tau \int d^3x\, e^{-i(\mathbf{k}\cdot\mathbf{x}+\omega_n\tau)}\mathcal{D}(\mathbf{x},\tau) \\ &= \frac{1}{Z}\sum_{m,n}(2\pi)^3\delta(\mathbf{k}-\mathbf{p}_m+\mathbf{p}_n)\,\langle n|\,\hat{\phi}(0)\,|m\rangle\,\langle m|\,\hat{\phi}(0)\,|n\rangle \\ &\times \frac{e^{-\beta E_m}-e^{-\beta E_n}}{E_n-E_m-i\omega_n} \qquad (3.13)\end{aligned}$$

where ω_n are the Matsubara frequencies $\omega_n = 2\pi nT$ for bosons ($\omega_n = (2n+1)\pi T$ for fermions). The above equaiton can be written in terms of spectral density as

$$\mathcal{D}(\omega_n,\mathbf{k}) = \int_{-\infty}^{\infty}\frac{d\omega}{\omega+i\omega_n}\rho(\omega,\mathbf{k}). \qquad (3.14)$$

In this way the propagators can be computed from the finite-temperature propagator by analytical continuation and the spectral density determines both real time and imaginary time propagators.

3.1.1 Green-Kubo formulas

Many physical systems, from the universe to high energy nuclear collisions, can be described using fluid dynamics. The state of the fluid can be described in terms of temperature and chemical potentials with an equation of state relating the pressure and energy density. When variations of temperature and chemical potential become appreciable over length scales that are not large compared with thermal wavelengths or correlation lengths then gradients in thermodynamic variable must be taken into account leading to viscous fluid dynamics where the dissipative terms added to energy momentum tensor or to currents are written in terms of gradients and transport coefficients, namely shear and bulk viscosity, thermal and electric conductivity. It is possible to derive these dissipative coefficients from the microscopic theory in particular using linear response theory and the formulas obtained are the Green-Kubo formula, derived indipendently by R. Kubo[52] and M. S. Green[53] In the following we will briefly derive the Green-Kubo formula for shear viscosity and electric conductivity.

In order to compute the shear viscosity, one has to set up a shear flow. Suppose to stress a fluid with a tangential force in order to develop a velocity flow only in the x direction $u_x(y)$ which depends only on y, i.e. on the transverse coordinate to the direction of the perturbation. In this case two layers of fluid

at y and $y + \Delta y$ have different fluid velocities because the velocity flow will be damped by dissipative effects of the fluid. For such a system the perturbing Hamiltonian is:

$$\delta\hat{H}(t) = -\int d^3x e^{\varepsilon t}\hat{T}^{x0}(t,\mathbf{x})\beta_x(y) \tag{3.15}$$

where $\hat{T}^{x0}$ is the $x0$ component of the energy momentum tensor, $\beta_x(y)$ represents the perturbed flow of the fluid. The corresponding linear response is

$$\delta\langle T^{x0}(t,k_y)\rangle = \beta_x(k_y)\int_{-\infty}^{\infty} dt'\,\theta(-t')e^{\varepsilon t'}G_R^{x0,x0}(t-t',k_y) \tag{3.16}$$

where the retarded Green's function is computed at the equilibrium. It can be shown that the retarded Green's function can be parametrized as[54]

$$G_R^{xy,xy}(\omega,k_y) = \frac{\omega^2(\varepsilon + g_T(k_y) + i\omega A_T(\omega,k_y))}{k_y^2 - i\omega/D_T(\omega,k_y) - \omega^2 B_T(\omega,k_y)} - P \tag{3.17}$$

and

$$G_R^{x0,x0} = \frac{k_y^2(\varepsilon + g_T(k_y) + i\omega A_T(\omega,k_y))}{k_y^2 - i\omega/D_T(\omega,k_y) - \omega^2 B_T(\omega,k_y)} - \varepsilon \tag{3.18}$$

where P and ε respectively the pressure and energy density, $g_T(k_y) = G_R^{x0,x0}(0,k_y)$ and the functions A_T, B_T and D_T have the the form $D_T(\omega,k_y) = D_T^R(\omega,k_y) - i\omega D_T^I(\omega,k_y)$. For small ω and k_y, the evolution of T^{x0} is determined by $i\omega = D_T k_y^2$, or, in configuration space:

$$\left(\partial_t - D_T\partial_y^2\right)T^{x0}(t,y) = 0 \tag{3.19}$$

where the momentum diffusion constant is defined as $D_T = D_T^R(0,0)$. The last equation combined with the conservation law implies

$$T^{xy}(t,y) = D_T\partial^y T^{x0}(t,y) = \eta\partial^y u^x \tag{3.20}$$

where $\eta = D_T(\varepsilon + P)$ is the shear viscosity. The last equation can be generalized to

$$\pi_{NS}^{ij}(t,\mathbf{x}) = \eta\left(\partial^i u^j + \partial^j u^i - \frac{2}{3}g^{ij}\partial_l u^l\right) \tag{3.21}$$

where NS indicates the Navier-Stokes shear tensor. The π_{NS}^{ij} tensor can be derived from simple physical considerations. Taylor expanding the flow velocity of a fluid $u(\mathbf{x})$ around $\mathbf{x}$:

$$u(\mathbf{x} + d\mathbf{x}) = u(\mathbf{x}) + \frac{du}{d\mathbf{x}}d\mathbf{x} + \dots \tag{3.22}$$

where $du/d\mathbf{x}$ is the Jacobian having $\partial u_i/\partial u_j$ as elements. Considering only the linear term in the expansion, it follows that viscous forces are functions of

$\partial_j u_i$. The term $\partial_j u_i$ can be decomposed in a symmetric and antisymmetric term obtaining:

$$u_j(\mathbf{x}+d\mathbf{x}) = u_j(\mathbf{x}) + \frac{1}{2}\left(\partial_i u_j - \partial_j u_i\right) dx_i + \frac{1}{2}\left(\partial_i u_j + \partial_j u_i\right) dx_i. \tag{3.23}$$

The second term on the r.h.s of the last equation is the antisymmetric part and represents the rigid rotation of the fluid around $\mathbf{x}$ with angular velocity $\omega = \frac{1}{2}\nabla \wedge \mathbf{u}$, being a rigid rotation does not produce any viscous effects. The symmetric part of the expansion Eq. (3.23) is responsible for the viscosity and can be decomposed as:

$$\frac{1}{2}\left(\partial_i u_j + \partial_j u_i\right) = \frac{1}{3}\delta_{ij}\partial_k u_k + \left[\frac{1}{2}\left(\partial_i u_j + \partial_j u_i\right) - \frac{1}{3}\delta_{ij}\partial_k u_k\right] \tag{3.24}$$

where the first term represents the expansion of the fluid while the term in parenthesis represents the effects of shear, i.e. a transverse dissipation respect with to each component of the flow velocity. The stress tensor, indicating the i-th component of the force that acts in the unit area with j unit vector $dF_i = \pi_{ij} dA_j$, has the form of Eq. (3.21), where in general there is also an extra term $\zeta\delta_{ij}\partial_k u_k$ for the bulk viscosity.

Finally the Kubo formula for shear viscosity is

$$\eta = \lim_{\omega\to 0}\lim_{k_y\to 0}\frac{1}{\omega} G_R^{xy,xy}(\omega, k_y) \tag{3.25}$$

or in terms of the full shear tensor correlation function

$$\eta = \lim_{\omega\to 0}\lim_{\mathbf{k}\to 0}\frac{1}{10\omega} G_R^{\pi_{ij},\pi_{ij}}(\omega, \mathbf{k}). \tag{3.26}$$

In a similar manner one can obtain an expression for the electric conductivity. Perturbing the system with an external electric field $E_x = i\omega A_x$ which couples via $\delta H = \int d^3x A_x J^x$, being J^x the x-component of the electric current, the response of the system is

$$\delta\langle J_x(\omega, \mathbf{k})\rangle = G_R^{JJ}(\omega, \mathbf{k})\frac{E_x}{i\omega}. \tag{3.27}$$

with G_R^{JJ} the retarded Green's function

$$G_R^{JJ}(\omega, \mathbf{k}) = -i\int d^4x\, e^{-ik\cdot x}\theta(t)\langle J^x(t, \mathbf{x}) J^x(0, \mathbf{0})\rangle. \tag{3.28}$$

Using the Ohm's law $J_x = \sigma_{el} E_x$, one obtains[51]

$$\sigma(\omega, \mathbf{k}) = \frac{G_R^{JJ}(\omega, \mathbf{k})}{i\omega}. \tag{3.29}$$

Finaly the electric conductivity σ_{el} is obtained as:

$$\sigma_{el} = \lim_{\omega \to 0} \frac{G_R^{JJ}(\omega, \mathbf{k} = \mathbf{0})}{i\omega} \tag{3.30}$$

3.1.2 Green-Kubo formula for shear viscosity

In this subsection we will derive the Green-Kubo formula for shear viscosity for a system of N particles starting from the classical case. The equation of motion for each particle under a shear flow along the x, $\mathbf{v}(y) = \gamma y \hat{\mathbf{e}}_1$ direction are:

$$\begin{aligned} \dot{\mathbf{x}}_i &= \frac{\mathbf{p}_i}{m} + \gamma y_i \hat{\mathbf{e}}_1 \\ \dot{\mathbf{p}}_i &= \mathbf{F}_i - \gamma p_{y_i} \hat{\mathbf{e}}_1 \end{aligned} \tag{3.31}$$

where γ is the shear rate. The applied stress will create an asymmetry in the internal pressure. The pressure tensor $p_{\alpha\beta}$ can be written in general as

$$p_{\alpha\beta} = \frac{1}{V} \sum_{i=1}^{N} \left[\frac{(\mathbf{p}_i \cdot \hat{\mathbf{e}}_\alpha)(\mathbf{p}_i \cdot \hat{\mathbf{e}}_\beta)}{m} + (\mathbf{x}_i \cdot \hat{\mathbf{e}}_\alpha)(\mathbf{F}_i \cdot \hat{\mathbf{e}}_\beta) \right] \tag{3.32}$$

being $\hat{\mathbf{e}}_\alpha$ the unit vector in the α direction, $\alpha = x, y, z$. The isotropic pressure can be computed via $P = \frac{1}{3} \sum_\alpha P_{\alpha\alpha}$. As already shown, P_{xy} is related to the velocity flow by $P_{xy} = -\eta \partial v_x / \partial y = -\gamma\eta$. Solving for η one has $\eta = -\lim_{t\to\infty} \langle p_{xy}(t) \rangle / \gamma$. According to the classical linear response theory, the change of $\langle p_{xy} \rangle$ can be computed via:

$$\langle p_{xy}(t) \rangle = \langle p_{xy} \rangle_0 - \beta\gamma V \int_0^t ds \langle p_{xy}(0) p_{xy}(t-s) \rangle_0 \tag{3.33}$$

where the underscript 0 means evaluated at the equilibrium state. The shear viscosity is

$$\eta = \frac{V}{kT} \int_0^\infty dt \, \langle p_{xy}(0) p_{xy}(t) \rangle \tag{3.34}$$

where the average $\langle \dots \rangle$ is computed at the equilibrium state. The last equation is formally the same used in our calculation for shear viscosity in Chapter 4 the only difference being the pressure tensor which has to be replaced by the

relativistic energy momentum tensor:

$$T^{\mu\nu} = \int \frac{d^3p}{(2\pi)^3} \frac{p^\mu p^\nu}{p^0} f(x,p) = \frac{1}{V} \sum_i \frac{p_i^\mu p_i^\nu}{p_i^0}. \tag{3.35}$$

3.1.3 Green-Kubo formula for electric conductivity

In this subsection we will briefly derive the Green-Kubo formula for electric conductivity that will be used in Chapter 5.

The electric conductivity is definded as

$$\vec{j} = \sigma \vec{E} \tag{3.36}$$

where $\vec{j}$ is the electric current and $\vec{E}$ is the external applied electric field. The electric current density can be written as

$$j^\mu = \int \frac{d^3p}{(2\pi)^3} \frac{p^\mu}{p^0} q(x) f(\mathbf{x}, \mathbf{p}) = q \frac{1}{V} \sum_{i=1}^{N} \frac{p_i^\mu}{p_i^0} \tag{3.37}$$

where $q(\mathbf{x})$ is the electric charge density at space point $\mathbf{x}$ and in the final expression we refer to a discrete system of N particles. Therefore, using the language of the previous section, the electric current density plays the role of the dynamical quantity we are interested to observe. The interaction Hamiltonian for this system is:

$$\mathcal{H}'(t) = -q \sum_{i=1}^{N} \mathbf{x} \cdot \vec{E}(t). \tag{3.38}$$

Assuming $\vec{E} = E\hat{z}$, the electric current density can be written as

$$j^z = E^z \int dt \phi_{BA} \tag{3.39}$$

with $\phi_{BA} = \beta V \langle j(0) j(t) \rangle$, obtaining for the electric conductivity

$$\sigma_{el} = \frac{V}{T} \int_0^\infty dt \, \langle j_z(t) j_z(0) \rangle. \tag{3.40}$$

The last equation is the Green-Kubo formula we use in our simulations in order to compute the electric conductivity as we will see in Chapter 5.

3.1.4 Time-correlation functions

In the following we will discuss about the computation of transport coefficients developed on the base of time-correlations function of the pertinent physical quantities. Let consider a physical quantity B which characterize the system in thermal equilibrium. The average value $\langle B \rangle$ is defined as

$$\langle B \rangle = \int dpdq\, B\rho(p,q). \tag{3.41}$$

However each member of the statistical ensemble fluctuates around the mean value and the fluctuations are distributed as a gaussian with mean value equals to $\langle B \rangle$. The time correlation function $C(t,t')$ is defined as the product of $B(t)$ times $B(t')$ averaged at the equilibrium:

$$C(t,t') = \langle B(t)B(t') \rangle. \tag{3.42}$$

In the followig some general properties of time correlation function are reported:

- computing the correlation function at fixed time t one obtains:

$$C(t,t) = \langle B(t)B(t) \rangle = \langle B^2 \rangle \tag{3.43}$$

- the long time behavior of the time correlation function is:

$$\lim_{t\to\infty} C(t,t') = \langle B^2 \rangle \tag{3.44}$$

- for a system in equilibrium, the time-correlation functions does not depends on the value t and t' but only on the difference:

$$C(t,t') = C(t-t',0) \equiv C(t) \tag{3.45}$$

The average of B, for a system at thermal equilibrium, can be written as a temporal average

$$\overline{B}_i = \lim_{t\to\infty} \frac{1}{t} \int_0^t dt'\, B_i(t') \tag{3.46}$$

where the index i refers to each member of the ensemble. It is possible to define the autocorrelation function as the temporal average over a trajectory,

i.e. over the temporal evolution of B:

$$\overline{B_i(t)B_i(0)} = \lim_{t\to\infty} \frac{1}{t} \int_0^t dt'\, B_i(t+t')B_i(t') \tag{3.47}$$

and then one has to perform the ensemble average

$$C(t) = \langle \overline{B(t)B(0)} \rangle = \left\langle \lim_{t\to\infty} \frac{1}{t} \int_0^t dt'\, B_i(t+t')B_i(t') \right\rangle . \tag{3.48}$$

In numerical simulations, in order to perform the ensemble average, a set of N events are generated so that the previous equation becomes a mathematical average. If the system is slightly far from the equilibrium value, one can consider to expand B to the first order obtaining a linear equation of motion:

$$\frac{dB}{dt} = -\lambda B \tag{3.49}$$

with λ constant and positive. The previous equation describes the relaxation to equilibrium of the quantity B, being the relaxation time $1/\lambda$. One can calculate the correlation function in this case:

$$C(t) = \langle B^2 \rangle e^{-\lambda t} = C(0)e^{-t/\tau}. \tag{3.50}$$

The last equation will be verified in our cases of interest for shear viscosity in Chapter 4 and for electric conductivity in Chapter 5.

3.2 Shear Viscosity

Viscosity is a key property of a fluid, representing a measure of its dissipative behaviour. A liquid, for example, flows in layers so that a force applied on the upper layer is transferred to the next with a small defect due to friction. In this setup shear viscosity η is defined in terms of the friction force F per unit area A created by a shear flow with transverse flow gradient $\nabla_y v_x$:

$$\frac{F}{A} = \eta \nabla_y v_x. \tag{3.51}$$

In the field of QGP shear viscosity is one of the most important and much studied transport coefficients. As already discussed in the first Chapter, shear viscosity of strongly interacting matter is expected to be very close to the conjectured lower bound $\eta/s = 1/4\pi$ as predicted by AdS/CFT or extracted

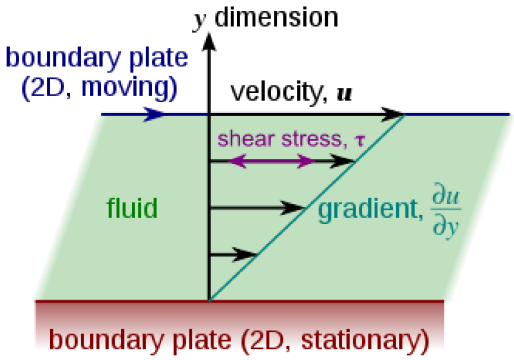

Figure 3.1: Shear flow of a 2-dimensional fluid.

by comparing experimental data of ellliptic flow v_2 with ideal hydrodynamical simulations results.

3.2.1 Perfect and dissipative fluid

The energy momentum tensor of a perfect fluid is diagonal in the local rest frame of the fluid ($u^\mu = (1,0,0,0)$):[55]

$$T^{\mu\nu}(x) = \begin{pmatrix} \varepsilon & 0 & 0 & 0 \\ 0 & P & 0 & 0 \\ 0 & 0 & P & 0 \\ 0 & 0 & 0 & P \end{pmatrix} \tag{3.52}$$

where ε is the local energy density and P is the local pressure. Eq. (3.52) is the Pascal law: the pressure exerted by a portion of the fluid is the same in all direction and is perpendicular to the area on which it acts (T^{ij} is the flux of the i-component of the momentum throught the surface orthogonal to the j direction). The energy momentum tensor for a fluid in motion with velocity flow $u^\mu = \gamma(1, \mathbf{v})$ is given by

$$T^{\mu\nu} = (\varepsilon + P)u^\mu u^\nu - g^{\mu\nu}P. \tag{3.53}$$

The conservation laws are:

$$\partial_\mu T^{\mu\nu} = 0, \qquad \partial_\mu j^\mu = 0 \tag{3.54}$$

which consist of 5 independent equations while the equation of state relating ε and P provides an extra equation. Solving these 6 equations, given an initial condition, one can determine the space time evolution of the 6 variables: ε, P, n and v_x, v_y, v_z. Using the thermodynamic relations one also obtains $\partial_\mu(su^\mu) = 0$ that is the entropy current conservation. The relativistic Euler equations are:

$$\frac{\partial \mathbf{v}}{\partial t} + (\mathbf{v}\cdot\nabla)\mathbf{v} = -\frac{1-v^2}{\varepsilon + P}\left(\nabla P + \mathbf{v}\frac{\partial P}{\partial t}\right) \tag{3.55}$$

where in the non-relativistic case the right hand side is $-\nabla P/\rho$ with ρ the mass density.

If the fluid is dissipative, the energy momentum tensor, the current and the entropy must be modified in order to include terms containing the derivatives of the flow velocity:

$$\begin{aligned} T^{\mu\nu} &= (\varepsilon + P)u^\mu - Pg^{\mu\nu} + \pi^{\mu\nu} \\ j^\mu &= nu^\mu + \nu^\mu \\ s^\mu &= su^\mu + \sigma^\mu \end{aligned} \tag{3.56}$$

where $\pi^{\mu\nu}$, ν^μ and σ^μ are the dissipative parts and hydrodynamical equations are derived from energy momentum and current conservations. There are two main definitions of the flow: the Landau-Lifshitz frame where u^μ is defined as the energy flow from $T^{\mu\nu}$ while the Eckart frame defined from the particle flow j^μ.

It is known that considering only linear order of the dissipative quantities one violates causality and acasual propagation takes place. Therefore in order to build up a consistent relativistic and dissipative hydrodynamics one needs to go beyond the linear order.[56,57]

However, it is possible to find the physical meaning of the dissipative part looking at linear order. Let us define the projector:

$$\Delta^{\mu\nu} = g^{\mu\nu} - u^\mu u^\nu \tag{3.57}$$

with $u_\mu \Delta^{\mu\nu} = 0$, that is perpendicular to the flow u^μ. Using the energy momentum conservation and the thermodynamical relations one obtains the following dissipative part of $T^{\mu\nu}$:

$$\pi^{\mu\nu} = \eta\left(D^\mu u^\nu + D^\nu u^\mu - \frac{2}{3}\Delta^{\mu\nu}\partial_\rho u^\rho\right) + \zeta\Delta^{\mu\nu}\partial_\rho u^\rho \tag{3.58}$$

where η is the shear viscosity and ζ is the bulk viscosity, $D_\mu = \partial_\mu - u_\mu u^\beta \partial_\beta$

is a derivative normal to u^μ. In the local rest frame $\Delta^{0\nu} = 0$, $\Delta^{ij} = \delta^{ij}$ and $D_0 = 0$, $D_i = \partial_i$. In this frame the divergency of entropy current is:

$$\partial_\mu s^\mu = \frac{\eta}{2T}\left(\partial_i u^j + \partial_j u^i - \frac{2}{3}\delta^{ij}\nabla\cdot\mathbf{u}\right)^2 + \frac{\zeta}{T}\left(\nabla\cdot\mathbf{u}\right)^2 \tag{3.59}$$

the non decreasing behaviour of entropy requires that both viscosities are non negative. The transport coefficients η and ζ can be derived by mean of a microscopic description. The energy-momentum tensor in kinetic theory can be written as

$$T^{\mu\nu}(x) = \sum_a \int \frac{d^3p}{(2\pi)^3}\frac{p_a^\mu p_a^\nu}{E_a} f_a(x,p) \tag{3.60}$$

where the sum runs over all species in the system. Assuming that the system is slightly out of equilibrium then we can write

$$f_a(x,p) = f_a^{eq}\left(\frac{u_\alpha p^\alpha}{T}\right)\left[1 + \phi_a(x,p)\right] \tag{3.61}$$

and the deviation from equilibrium for $T^{\mu\nu}$ is given by

$$\Delta T^{\mu\nu} = \sum_a \int \frac{d^3p}{(2\pi)^3}\frac{p_a^\mu p_a^\nu}{E_a} f_a^{eq}\left(\frac{u_\alpha p^\alpha}{T}\right)\phi_a(x,p) \tag{3.62}$$

where $|\phi_a| \ll 1$. Using the same temporal decomposition of Eq. (3.58) for ϕ_a as a function of space-time and momentum:[58]

$$\phi_a = -A_a \partial_\rho u^\rho + C_{\mu\nu}^a\left(D^\mu u^\nu + D^\nu u^\mu + \frac{2}{3}\Delta^{\mu\nu}\partial_\rho u^\rho\right) \tag{3.63}$$

where A_a in general will depend on the scalar $u_\alpha p^\alpha$ and $C_{\mu\nu}^a = C_a p_\mu p_\nu$ with C_a depending on the same scalar. Now, equating Eq. (3.58) with Eq. (3.62), using the decomposition of ϕ_a of Eq. (3.63), one obtains:[58]

$$\eta = \frac{2}{15}\sum_a \int \frac{d^3p}{(2\pi)^3}\frac{|\mathbf{p}|^4}{E_a} f_a^{eq}\left(\frac{E_a}{T}\right) C_a(E_a) \tag{3.64}$$

$$\zeta = \frac{1}{3}\sum \int \frac{d^3p}{(2\pi)^3}\frac{|\mathbf{p}|^2}{E_a} f_a^{eq}\left(\frac{E_a}{T}\right) A_a(E_a) \tag{3.65}$$

where we have used the local rest frame. In order to evaluate A_a and C_a it is necessary to use the Boltzmann equation as we will show in the next subsection.

3.2.2 Shear Viscosity from Relaxation Time Approximation

Let us suppose that the system is slightly out of equilibrium and consider a system of one species of particles so we can write:

$$f = f^{eq} + \delta f \tag{3.66}$$

suppressing the a index. We can approxiamte the Boltzmann equation as:

$$\frac{\partial}{\partial t} f + \mathbf{v} \cdot \nabla f = \mathcal{C}[f] \simeq -\omega(E)\delta f \tag{3.67}$$

where $\omega(E)$ is the frequency of interaction and $\omega^{-1}(E) = \tau(E)$ being $\tau(E)$ the equilibration time. As written explicitely, the frequency of interaction is energy and momentum dependent so the approximation made inEq. (3.67) is called momentum dependent Relaxation Time Approximation. The deviation δf is related to the function ϕ:

$$\delta f(x,p) = f^{eq}\phi(x,p). \tag{3.68}$$

The relaxation time $\tau(E) = \omega(E)^{-1}$ is given by

$$\tau^{-1}(E) = \omega(E) = \sum_{bcd} \frac{1}{2} \int \frac{d^3p_b}{(2\pi)^3} \frac{d^3p_c}{(2\pi)^3} \frac{d^3p_d}{(2\pi)^3} W(a,b|c,d)\, f^{eq} \ , \tag{3.69}$$

where the quantity $W(a,b|c,d)$ is defined as

$$W(a,b|c,d) = \frac{(2\pi)^4\delta^4\left(p_a + p_b - p_c - p_d\right)}{2E_a 2E_b 2E_c 2E_d} \left|\mathcal{M}\right|^2 \ . \tag{3.70}$$

$|\mathcal{M}|^2$ is the squared transition amplitude for the 2-body reaction $a + b \to c + d$. The collision frequency Eq.(3.69) can easily be expressed in terms of the total cross section σ_{tot}:

$$\omega(E) = \int \frac{d^3p_b}{(2\pi)^3} \frac{\sqrt{s(s-4m^2)}}{2E_a\, 2E_b} f^{eq}\, \sigma_{tot}. \tag{3.71}$$

After some calculations it can be found the expression for the shear and bulk

viscosities[58,59]

$$\eta = \frac{1}{15T}\int \frac{d^3p}{(2\pi^3)}\frac{|p|^4}{E^2}\tau(E)f^{eq}(E/T) \tag{3.72}$$

$$\zeta = \frac{1}{9T}\int \frac{d^3p}{(2\pi^3)}\frac{\tau(E)}{E^2}\left[(1-3v_s^2)E^2-m^2\right]^2 f^{eq}(E/T) \tag{3.73}$$

where v_s is the sound velocity and when considering different species of particles a sum has to be performed. Depending on the dynamics, the relaxation time may be highly momentum dependent: it is clear that the particles with the longest relaxation time dominate the viscosity since these particles can transport energy and momentum over greater distances before interacting. However one has also to consider that the impact of the relaxation time of high energy particles is exponentially damped by the $f^{eq}(E/T)$. Eq. (3.71) for a constant (energy independent) total cross section becomes energy independent and coincides with the standard mean relaxation time

$$\tau^{-1} = \rho\,\sigma_{tot}\,\langle v_{rel}\rangle \tag{3.74}$$

where $\langle v_{rel}\rangle$ is the thermal average of the relative velocity and for massless particles $\langle v_{rel}\rangle = 1$.

3.2.3 Shear viscosity from Chapman-Enskog method

In this section we will derive the shear viscosity using the Chapman-Enskog method and we will follow the derivation given in Refs.[41,60–62] Let us begin with the relativistic transport equation

$$p_\mu\partial^\mu f = \int (f'f_1' - ff_1)\,\sigma F d\Omega'\frac{d^3p_1}{p_1^0} \tag{3.75}$$

where we used the abbreviation $f \equiv f(x,p)$, $f' \equiv f(x,p')$, $f_1 \equiv f(x,p_1)$ and $f_1' \equiv f_1'(x,p_1')$. The differential cross section $\sigma = \sigma(P,\Theta)$ is defined in the center of mass frame with $P = [-(p^\alpha + p_1^\alpha)(p_\alpha + p_{1\alpha})]^{1/2}$ while the invariant flux $F = \left[(p_{1\alpha}p_1^\alpha)^2 - (mc)^4\right]^{1/2}$. $d\Omega'$ refers to the angle of $\mathbf{p}'$ in the center of mass frame. When the system is not too far from equilibrium one can write

$$f = f^{eq}(1+\phi). \tag{3.76}$$

The above equation does not define the rules for the approximation. In order to define the method in a closed way we must assume that the mean free path l is small compared to the typical length L over which the particle number

density, velocity flow and temperature vary in a significant way. Then ϕ is assumed to be of the order of l/L.

In the Chapman-Enskog method the deviation $f^{eq}\phi$ is determined from the Boltzmann integro-differential equation: inserting Eq. (3.76) in Eq. (3.75) and keeping only the leading terms in both sides of the resulting equation one obtains

$$p_\mu \partial^\mu f^{eq} = -f^{eq}\mathcal{L}[\phi] \tag{3.77}$$

where $\mathcal{L}[\phi]$ is the linearized collision integral and is given by

$$\mathcal{L}[\phi] = \int f_1^0(\phi + \phi_1 - \phi' - \phi_1')\sigma F d\Omega' \frac{d^3p_1}{p_1^0}. \tag{3.78}$$

and Eq. (3.77) is no more an integro-differential equation but an inhomogeneous integral equation for ϕ. The solution of the above equation is of fundamental importance in kinetic theory because it leads to the evaluation of transport coefficients. The solution has the general structure

$$\phi = A\partial_\alpha u^\alpha - B\Delta_{\alpha\beta}p^\beta \Delta^{\alpha\beta}\left(\frac{1}{T}\partial_\beta T + \frac{1}{c^2}Du_\beta\right) + C\langle p_\alpha p_\beta\rangle\langle\partial^\alpha u^\beta\rangle \tag{3.79}$$

with $D \equiv u^\alpha\partial_\alpha$, $\Delta^{\alpha\beta} = g^{\alpha\beta} + \frac{1}{c^2}u^\alpha u^\beta$, $\langle t_{\alpha\beta}\rangle = \Delta_{\alpha\beta\gamma\delta}t^{\gamma\delta}$, $\Delta_{\alpha\beta\gamma\delta} = \frac{1}{2}(\Delta_{\alpha\gamma}\Delta_{\beta\delta} + \Delta_{\alpha\delta}\Delta_{\beta\gamma}) - \frac{1}{3}\Delta_{\alpha\beta}\Delta_{\gamma\delta}$. The scalar functions A, B and C which depend on $p_\alpha u^\alpha$, ρ and T obey the integral equation[41, 60–62]

$$\mathcal{L}[A] = -\frac{1}{kT}Q \tag{3.80}$$

$$\mathcal{L}[B\Delta_{\alpha\beta}p^\beta] = \frac{1}{kT}(p_\gamma u^\gamma + mh)\Delta_{\alpha\beta}^{p^\beta} \tag{3.81}$$

$$\mathcal{L}[C\langle p_\alpha p_\beta\rangle] = -\frac{1}{kT}\langle p_\alpha p_\beta\rangle \tag{3.82}$$

where $Q = -\frac{(mc)^2}{3} + \frac{1}{c^2}p_\alpha u^\alpha[(1-\gamma)mh + \gamma kT] + \frac{1}{c^2}\left[\frac{4}{3} - \gamma\right](p_\alpha u^\alpha)$, $\gamma = c_p/c_v$ is the ratio of specific heats, $h = c^2K_3(z)/K_2(z)$ is the hentalpy. The energy momentum tensor can now be calculated with $f = f^{eq}(1+\phi)$ and the shear viscosity reads as

$$\eta = -\frac{c}{10}\int C\langle p_\alpha p_\beta\rangle\langle p^\alpha p^\beta\rangle f^{eq}\frac{d^3p}{p^0}. \tag{3.83}$$

The above inhomogeneous integral equation for the transport coefficient can be reduced to sets of algebraic equations by expanding the unknown scalar function $C(\tau)$ ($\tau = -(p_\alpha u^\alpha + mc^2)/kT$) in terms of orthogonal polynomials, e. g. Laguerre functions $L_n^\alpha(\tau)$ with α half integer for massive particles and $\alpha = 0$ for massless particles. Multiplying both sides of Eq. (3.82) by

$\left(p^0 f^0 L_n^{5/2}(\tau)\right)^{-1} \langle p^\alpha p^\beta \rangle$ and integrating over momentum one obtains

$$\left[C\langle p_\alpha p_\beta\rangle, L_n^{5/2}(\tau)\langle p^\alpha p^\beta\rangle\right] = \frac{m^2 kT}{\rho}\gamma_n \qquad (n = 0, 1, \dots) \tag{3.84}$$

where γ_n has been defined as:

$$\gamma_n \equiv \frac{c}{\rho k^2 T^2}\int f^0 L_n^{5/2}(\tau)\langle p_\alpha p_\beta\rangle\langle p^\alpha p^\beta\rangle \frac{d^3p}{p^0}. \tag{3.85}$$

Expanding $C(\tau) = \sum_{m=0}^{\infty} c_m L_m^{5/2}(\tau)$, Eq. (3.84) can be written as

$$\sum_{m=0}^{\infty} c_m c_{nm} = \frac{1}{\rho kT}\gamma_n \qquad (n = 0, 1, \dots) \tag{3.86}$$

and

$$c_{mn} = \frac{1}{(mkT)^2}\left[L_m^{5/2}(\tau)\langle p_\alpha p_\beta\rangle, L_n^{5/2}(\tau)\langle p^\alpha p^\beta\rangle\right] \qquad (m, n = 0, 1, \dots). \tag{3.87}$$

The shear viscosity can be written as

$$\eta = \frac{kT^2}{10}\sum_{m=0}^{\infty} c_m \gamma_m. \tag{3.88}$$

The first and second order approximations are:

$$\eta^{1^{st}} = \frac{1}{10} kT \frac{\gamma_0^2}{c_{00}} \tag{3.89}$$

$$\eta^{2^{nd}} = \frac{1}{10} kT \frac{\gamma_0^2 c_{00} - 2\gamma_0\gamma_1 c_{01} + \gamma_1^2 c_{00}}{c_{00}c_{11} - c_{01}^2} \tag{3.90}$$

where

$$\gamma_0 = -10\hat{h} \tag{3.91}$$

$$\gamma_1 = -\left[\hat{h}(10z-25)-10z\right] \tag{3.92}$$

$$c_{00} = 16\left(w_2^{(2)} - \frac{1}{z}\,w_1^{(2)} + \frac{1}{3z^2}w_0^{(2)}\right) \tag{3.93}$$

$$\begin{aligned} c_{01} = {} & 8\left(2z\left(w_2^{(2)} - w_3^{(2)}\right) + \left(-2w_1^{(2)} + 3w_2^{(2)}\right)\right. \\ & \left. + z^{-1}\left(\frac{2}{3}w_0^{(2)} - 9w_1^{(2)}\right) - \frac{11}{3z^2}w_0^{(2)}\right) \end{aligned} \tag{3.94}$$

$$\begin{aligned} c_{11} = {} & 4\left(4z^2\left(w_2^{(2)} - 2w_3^{(2)} + w_4^{(2)}\right)\right. \\ & + 2z\left(-2w_1^{(2)} + 6w_2^{(2)} - 9w_3^{(2)}\right) \\ & + \left(\frac{4}{3}w_0^{(2)} - 36w_1^{(2)} + 41w_2^{(2)}\right) \\ & \left. + z^{-1}\left(-\frac{44}{3}w_0^{(2)} - 35w_1^{(2)}\right) + \frac{175}{3z^2}w_0^{(2)}\right) \end{aligned} \tag{3.95}$$

with

$$z = \frac{mc^2}{kT} \quad \text{and} \quad \hat{h} = \frac{K_3(z)}{K_2(z)} \tag{3.96}$$

and the quantity $w_i^{(s)}$ is so-called the relativistic omega integral which is defined as

$$\begin{aligned} w_i^{(s)} = {} & \frac{2\pi z^3 c}{K_2(z)^2}\int_0^\infty d\psi \sinh^7\psi \cosh^i\psi K_j(2z\cosh\psi) \\ & \times \int_0^\pi d\Theta \sin\Theta\sigma(\psi,\Theta)(1-\cos^s\Theta)\ . \end{aligned} \tag{3.97}$$

3.3 Electric Conductivity

Being the QGP created in HICs a system far from equilibrium, the study of its transport coefficients is attracting a great interest. The η has been studied extensively.[58,59,62–69] Only very recently the electric conductivity, that represents the response of a system to the applied electric field, has captured a

significative importance in the field of strongly interacting matter for several motivations. Electric conductivity σ_{el} is a computable quantity on the Lattice from the correlation function. On the experimental side, Heavy Ion Collisions are generate very strong electric and magnetic fields ($eE \simeq eB \simeq m_\pi^2$, with m_π the pion mass) in the first 1 fm/c from the collision.[70–73] The value of σ_{el} would be of fundamental importance for the strength of the Chiral-Magnetic Effect,[74] a signature of the CP violation of the strong interaction. It has also been shown that in mass asymmetric collision the electric field has a privileged direction generating a current whose effects can be observed in collective flow and are directly related to σ_{el}.[71] Moreover σ_{el} can be related to the emission rate of soft photons[51] accounting for the measured raising spectra at low p_T.[75,76]

3.3.1 Electric conductivity from Relaxation Time Approximation

The starting point of our calculation is the Relativistic Boltzmann Transport (RBT) equation that in the presence of an external field can be written as:[55,77]

$$p^\mu \partial_\mu f(x,p) + qF^{\alpha\beta} p_\beta \frac{\partial}{\partial p^\alpha} f(x,p) = \mathcal{C}[f] \tag{3.98}$$

where $f(x,p)$ is the distribution function, $F^{\alpha\beta}$ is the electromagnetic field strength tensor, $C[f]$ is the collision integral which, considering only $2 \to 2$ scatterings, can be written as follows

$$\mathcal{C}(x,p) = \int_2 \int_{1'} \int_{2'} (f_{1'} f_{2'} - f_1 f_2) \, |\mathcal{M}_{1'2' \to 12}| \delta^4(p_1 + p_2 - p_1' p_2') \tag{3.99}$$

where $\mathcal{M}$ is the transition matrix for the elastic process linked to the differential cross-section $|\mathcal{M}|^2 = 16\pi s(s - 4M^2) d\sigma/dt$ and by $\int_j$ we mean $\int_j = \int d^3p_j/(2\pi)^3 p_j^0$. The possible extension to $2 \leftrightarrow 3$ processes has been thoroughly discussed in Ref.[67]

In order to obtain an analytical solution for the Boltzmann equation, it is necessary to approximate the Collision integral. The most simple scheme is the Relaxation Time Approximation which, noticing that $\mathcal{C}[f]$ is a $\Delta f/\Delta t$, assumes the following form:

$$\mathcal{C}[f] \simeq -\frac{p^\mu u_\mu}{\tau}(f - f_{eq}) \tag{3.100}$$

where u^μ is the velocity flow that in local rest frame is $(1, \mathbf{0})$, τ is the so-called relaxation time which determines the time scale for the system to relax toward the equilibrium state characterized by f_{eq}. Assuming that the distribution

function f is near the equilibrium one f_{eq}, one can write:

$$f(x,p,t) = f_{eq}(x,p)(1+\phi). \tag{3.101}$$

If we consider a uniform system and only an electric field $\vec{E}$, from Eq. (3.98) and Eq. (3.100) we obtain:

$$-q\left(p_0\vec{E}\cdot\frac{\partial f_{eq}}{\partial\vec{p}} - \vec{E}\cdot\vec{p}\frac{\partial f_{eq}}{\partial p^0}\right) = -\frac{p^0}{\tau}f_{eq}\phi \tag{3.102}$$

and solving for ϕ, assuming $\phi \ll f_{eq}$, one obtains:

$$\phi = \frac{1}{T}q\tau\,\vec{E}\cdot\frac{\vec{p}}{p^0} \tag{3.103}$$

The electric current is:

$$j^\mu = q\int\frac{d^3p}{(2\pi)^3}\frac{p^\mu}{p^0}\,f = q\int\frac{d^3p}{(2\pi)^3}\frac{p^\mu}{p^0}\,f_{eq}(1+\phi) \tag{3.104}$$

Using ϕ of the previous equation, considering the definition of electric conductivity and generalizing to a system of different charged particles one obtains:[78,79]

$$\sigma_{el} = \frac{e^2}{3T}\sum_{j=q,\bar{q}}q_j^2\int\frac{d^3p}{(2\pi)^3}\frac{\vec{p}^2}{E^2}\tau_j f_{eq} = \frac{e_\star^2}{3T}\left\langle\frac{\vec{p}^2}{E^2}\right\rangle\tau_q\rho_q \tag{3.105}$$

where q_j is the quarks charge $(\pm1/3, \pm2/3)$, τ_j is the relaxation time for quarks, ρ_q is the quark density, $e_\star^2 = e^2\sum_{j=\bar{q},q}q_j^2 = 4e^2/3$. We notice that in the classical limit Eq. (3.105) simplifies formally to the well known Drude formula $\tau e^2\rho/m$ while in the ultrarelativistic limit becomes $\tau e^2/3T$. However it has to be noticed that $\tau = 1/\rho\sigma$ in the Drude model while our expression is more general. We will see that indeed τ is quite larger than $(\rho\sigma)^{-1}$. Chapter 5 is dedicated to analyze the deviations from the Drude relaxation time.

3.4 Lattice calculations

In this section we report briefly the evaluation of shear viscosity and electric conductivity on Lattice QCD scheme and the latest results regarding this two transport coefficients.

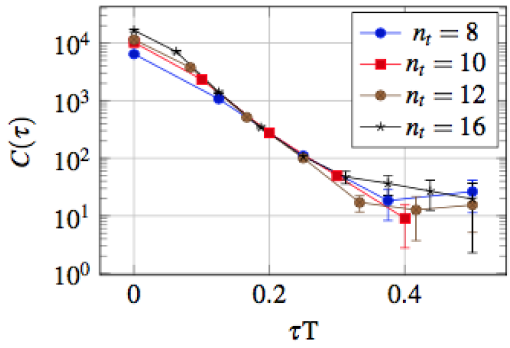

Figure 3.2: Correlation function $C(\tau) = \frac{1}{T^5}\int dx\,\langle\Theta_{12}(\tau,\mathbf{x}\Theta_{12}(0,\mathbf{0}))\rangle$ computed at $T = 1.5\,T_c$ for different values of lattice spacing.[80]

3.4.1 Shear viscosity

As discussed in previous sections, information about shear viscosity is encoded in correlators of the traceless part of $\Theta_{\mu\nu}$ of the energy momentum tensor $T_{\mu\nu}$ that for pure gauge theories is defined as:

$$\Theta_{\mu\nu} = F_{\mu\sigma}(x)F_{\nu\sigma}(x) - \frac{1}{4}\delta_{\mu\nu}F_{\rho\sigma}(x)F_{\rho\sigma}(x) \tag{3.106}$$

where $F_{\mu\nu}(x)$ is the field-strength tensor at $x = (\tau, \mathbf{x})$. The Euclidean correlators, which can be measured on the lattice, are defined as

$$C_{\mu\nu,\rho\sigma}(\tau, q) = \frac{1}{T^5}\int d^3x\, e^{iq\cdot x}\left(\langle\Theta_{\mu\nu}(x)\Theta_{\rho\sigma}(0)\rangle - \langle\Theta_{\mu\nu}(x)\rangle\langle\Theta_{\rho\sigma}(0)\rangle\right). \tag{3.107}$$

These correlators are connected to their spectral functions $\rho_{\mu\nu,\rho\sigma}(\tau, q)$ via integral transformation

$$C_{\mu\nu,\rho\sigma}(\tau, q) = \int_0^\infty d\omega\, K(\tau,\omega)\rho_{\mu\nu,\rho\sigma}(\omega, q) \tag{3.108}$$

$$K(\tau,\omega) = \frac{cosh\left(\omega(\tau - \frac{1}{2T})\right)}{sinh(\omega/(2T))} \tag{3.109}$$

with the finite temperature kernel $K(\tau, \omega)$. Transport properties then follow from the low energy limit of the spectral functions via Kubo formulae. In particular for the shear and bulk viscosities one obtains:

$$\eta = \pi \lim_{\omega\to 0}\lim_{q\to 0}\frac{\rho_{13,13}(\omega,1)}{\omega} \qquad \frac{4}{3}\eta + \zeta = \pi \lim_{\omega\to 0}\lim_{q\to 0}\frac{\rho_{33,33}(\omega,q)}{w} \tag{3.110}$$

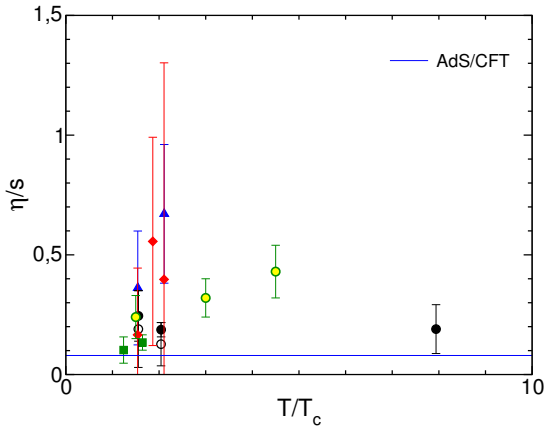

Figure 3.3: A collection of Lattice QCD calculations of shear viscosity over entropy density ratio: full squares,[81] diamonds and triangles,[82] open and full circles,[83] yellow circles.[80]

The Lattice calculations provide the Euclidean correlator but not the spectral functions so one has to apply inverse problem methods which usually give large systematic errors. The inversion is an ill-posed problem on the lattice because the Euclidean correlation function is only known at discrete number of space and time, while the spectral function is a continuous function. To solve this problem, one possibility is to use an ansatz for spectral function with a small number of fitting parameters and a constrained fitting procedure. For example, in Ref.[80] the following spectral functions have been chosed:

$$\begin{aligned} \frac{\rho_{13,13}(\omega,\mathbf{q})}{\omega} &\xrightarrow{\omega,\mathbf{q}\to 0} \frac{\eta}{\pi}\frac{\omega^2}{\omega^2+(\eta q^2/(\varepsilon+p))^2} \\ \frac{\rho_{33,33}(\omega,\mathbf{q})}{\omega} &\xrightarrow{\omega,\mathbf{q}\to 0} \frac{\Gamma_s}{\pi}\frac{(\varepsilon+p)\omega^4}{(\omega^2-\nu_s(q)^2q^2)^2+(\Gamma_s\omega q^2)^2} \end{aligned} \tag{3.111}$$

with the sound attenuation length $\Gamma_s = (\frac{4}{3}\eta+\zeta)/(\varepsilon+p)$ and the speed of sound $\nu_s(q)$.

In Fig. 3.2, taken from Ref.[80] it is shown the correlation function as a function of τT for different values of lattice spacing.
In Fig. 3.3 we show a collection of Lattice QCD calculations of η/s as a function of temperature: full squares,[81] diamonds and triangles,[82] open and full circles,[83] yellow circles.[80]

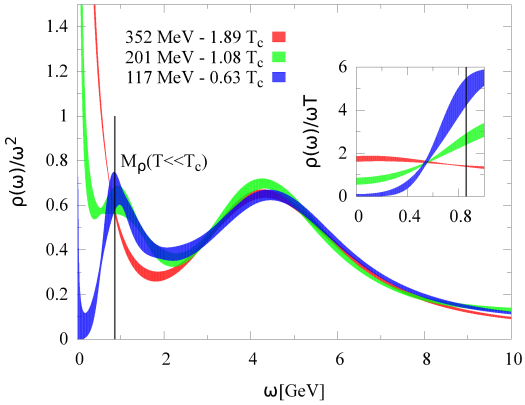

Figure 3.4: Spectral functions $\rho(\omega)/\omega^2$ and $\rho(\omega)/\omega T$ (inset) at three temperatures. The vertical line indicates M_ρ at $T = 0$, and the thickness of the lines represents the statistical jackknife error from MEM. The rise of the intercept at $\omega = 0$ in the inset indicates a temperature-dependent conductivity.[84]

3.4.2 Electric conductivity

The physical observable for computing electric conductivity on the Lattice is the Euclidean correlator G^{em}. It is built up from the electric current j^{em}_μ defined as

$$j^{em}_\mu = \sum_f (eq_f) j^f_\mu = \frac{2e}{3} j^u_\mu - \frac{e}{3} j^d_\mu - \frac{e}{3} j^s_\mu \tag{3.112}$$

where the sum runs over the up, down and strange contibutions and e is the elementary charge. The Euclidean correlator is related to the spectral function ρ via the integral relation

$$\begin{aligned} G^{em}_{\mu\nu}(\tau, \mathbf{p}) &= \int d^3x \, e^{i\mathbf{p}\cdot\mathbf{x}} \langle j^{em}_\mu(\tau, \mathbf{x}) j^{em}_\nu(0, \mathbf{0})^\dagger \rangle \\ &= \int_0^\infty \frac{d\omega}{2\pi} K(\tau, \omega) \rho^{em}_{\mu\nu}(\omega, \mathbf{p}) \end{aligned} \tag{3.113}$$

where we recognize the temperature dependent kernel $K(\tau, \omega)$ as in the previous subsection. The electric conductivity is given in terms of the spectral function via the Green-Kubo formula

$$\frac{\sigma_{el}}{T} = \frac{1}{6T} \lim_{\omega \to 0} \frac{\rho^{em}(\omega)}{\omega}, \qquad \rho^{em}(\omega) = \sum_{i=1}^{3} \rho^{em}_{ii}(\omega) \tag{3.114}$$

that is the slope of the spectral function at $\omega = 0$.

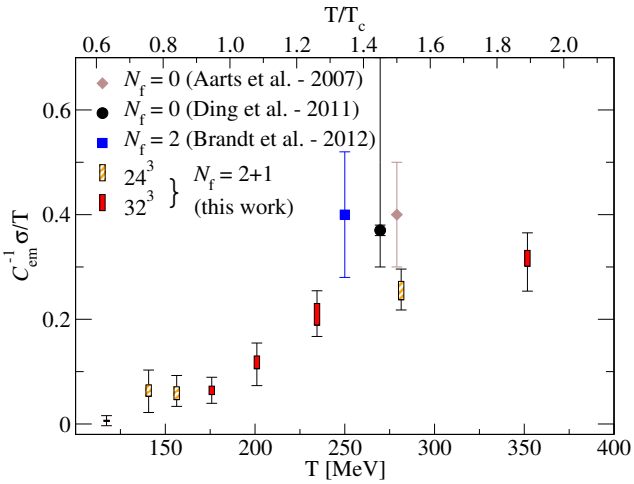

Figure 3.5: Figure adapted from Ref.[84] Temperature dependence of $C_{\rm em}^{-1}\sigma/T$, where $C_{\rm em} = 5/9e^2$ for two light flavours. Previously obtained results[85–87] are indicated as well: the $N_f = 0$ results are inserted matching the values of T/T_c.

In Fig. 3.4 from Ref.[84] are shown spectral functions for three different temperatures where the thickness represents the statistical error. In this work the problem of inverting the integral equation relating the correlator and the spectral function is solved using the Maximum Entropy Method (MEM) which aims to construct the most probable spectral function without requiring any assumptions of its functional form.

In Fig. 3.5 from Ref.[84] is shown a collection of Lattice results for the electric conductivity as a function of temperature.

3.5 AdS/CFT calculations

In this section we will briefly discuss the Anti-de-Sitter Conformal Field Theory (AdS/CFT) framework which is a powerful non-perturbative tool that can be used also to investigate the transport properties of strongly coupled gauge theories with a large number of colors N_c.

The AdS/CFT duality is an idea that originated from superstring theory and claims the equivalence between stronlgy coupled 4-D gauge theory and gravitational theory in 5-D AdS spacetime. It is also called *holographic theory* because encodes a five dimensional theory by a four dimensional theory.[88]

More explicitely AdS/CFT claims that the generating functionals (or partition functions) of the two theories are equivalent:[89]

$$\mathcal{Z}_{gauge} = \mathcal{Z}_{AdS}. \tag{3.115}$$

Therefore AdS/CFT enables one to analyze a strongly coupled gauge theory using AdS spacetime. In particular the last correspondance is for a gauge theory at finite temperature while on the gravitaional side one has to consider a AdS black hole. The black hole in this case helps to have the notion of temperature, because of Hawking radiation, and also the notion of entropy which is known to be equal to the area of the black hole horizon.

There are several differences between the realistic $SU(3)$ gauge theory and the gauge theory studied in AdS/CFT. First AdS/CFT typically considers a $SU(N_c)$ gauge theory where N_c plays the role of a parameter and the strong coupling is the so called *large N_c limit*. Second, AdS/CFT considers a supersymmetric gauge theory, in particularly $\mathcal{N} = 4$ Super-Yang-Mills (SYM) provides the simplest example of AdS/CFT.

Also in this framework transport coefficients are computed in Linear Response Theory by Green-Kubo formulae.

The hydrodynamic equations can be thought of as an effective theory describing the dynamics of the system at large lengths and time scales. Therefore one should be able to use these equations to extract information about the low momentum behaviour of Green's function in the original theory.[90] Coupling the sourc$J_a(\mathbf{x})$ to a set of operators $O_a(x)$ so that the new action can be written as

$$S = S_0 + \int_x J_a(x) O_a(x) \tag{3.116}$$

that the source will introduce a perturbation of the system. In particular the average value of O_a will differ from the equilibrium values, which can be assumed to be zero. If J_a are small, the perturbations are given by the linear response theory as

$$\langle O_a(x) \rangle = -\int_y G^R_{ab}(x-y) J_b(y) \tag{3.117}$$

where G^R_{ab} is the retarded Green's function

$$iG^R_{ab}(x-y) = \theta(x^0 - y^0) \langle [\theta_a(x), \theta_b(y)] \rangle. \tag{3.118}$$

The fact that the linear response is determined by the retarded Green's function comes from causality: the source can influence the system only after it has been turned on. Thus, in order to determine the correlation functions of $T^{\mu\nu}$, we

need to couple a weak source to the energy momentum tensor and determine the average value. One must generalize hydrodynamic equations to curved space time, treat the metric $g_{\mu\nu}$ as the source for $T^{\mu\nu}$ and then determine the response of the thermal medium to a weak perturbation of the metric. Recalling that the dissipative part of energy momentum tensor can be written as

$$\sigma^{\mu\nu} = P^{\mu\alpha}P^{\nu\beta}\left[\eta\left(\partial_\alpha u_\beta + \partial_\beta u_\alpha - \frac{2}{3}g_{\alpha\beta}\partial_\lambda u^\lambda\right) + \zeta g_{\alpha\beta}\partial_\lambda u^\lambda\right] \tag{3.119}$$

with $P^{\mu\nu} = g^{\mu\nu} + u^\mu u^\nu$. The previous equation has to be generalized to curved space-time as

$$\sigma_{\mu\nu} = P^{\mu\alpha}P^{\mu\beta}\left[\eta\left(\nabla_\alpha u_\beta + \nabla_\beta u_\alpha\right) + \left(\zeta - \frac{2}{3}\eta\right)g_{\alpha\beta}\nabla\cdot u\right]. \tag{3.120}$$

where ∇_α is the covariant derivative $\nabla_\alpha u_\beta = \partial_\alpha u_\beta + \Gamma^\gamma_{\beta\alpha}u_\gamma$. Using $u^\mu = (1,0,0,0)$ and $g_{\mu\nu}$, one obtains contributions only to the traceless spatial components and these contributions come from the Christoffel symbols in the covariant derivatives:

$$\sigma_{xy} = 2\eta\Gamma^0_{xy} = \eta\partial_0 h_{xy}. \tag{3.121}$$

By comparison with the expectation from linear response theory

$$G^R_{xy,xy}(\omega,\mathbf{0}) = \int dtd^3x\, e^{i\omega t}\theta(t)\langle[T_{xy}(t,\mathbf{x}),T_{xy}(0,\mathbf{0})]\rangle = -i\eta\omega \tag{3.122}$$

that is the Kubo formula for shear viscosity

$$\eta = -\lim_{\omega\to 0}\frac{1}{\omega}Im\, G^R_{xy,xy}(\omega,\mathbf{0}). \tag{3.123}$$

In order to compute holographically the retarded correlator of T^{xy} one can consider a general $d+1$ dimensional diagonal metric and perturb the metric by adding a non-diagonal element as:[91]

$$ds^2 = g_{tt}dt^2 + g_{zz}dz^2 + g_{xx}(\delta^{ij}dx^i dx^j + 2\phi dx^1 dx^2) \tag{3.124}$$

where ϕ is a small perturbation. The action fot the perturbation ϕ is

$$S_\phi = -\frac{1}{2}\int d^{d+1}x\,\sqrt{-g}\frac{1}{q(z)}g^{MN}\partial_M\phi\partial_N\phi. \tag{3.125}$$

where $q(z)$ can be considered as a space time dependent coupling constant. Transport coefficients are given by the Green-Kubo formula

$$\chi = -\lim_{k_\mu\to 0}\lim_{z\to 0} Im\left\{\frac{\Pi(z,k_\mu)}{\omega\phi(z,k_\mu)}\right\} \tag{3.126}$$

where Π is the canonical momentum of the field ϕ

$$\Pi = \frac{\delta S}{\delta \partial_z \phi} = -\frac{\sqrt{-g}}{q(z)} g^{zz} \partial_z \phi \tag{3.127}$$

and the equation of motion for Π is

$$\partial_z \Pi = -\frac{\sqrt{-g}}{q(z)} g^{\mu\nu} k_\mu k_\nu \phi. \tag{3.128}$$

In the vicinity of the horizon $z \to z_0$ one has

$$g_{tt} = -c_0(z_0 - z) \qquad g_{zz} = \frac{c_z}{z_0 - z}. \tag{3.129}$$

Solving the equation of motion and using Green-Kubo relation Eq. (3.126) one obtains:

$$\chi = \frac{1}{q(z_0)} \sqrt{\frac{-g}{-g_{zz} g_{tt}}}\Bigg|_{z_0} \tag{3.130}$$

which can be written as

$$\chi = \frac{1}{q(z_0)} \frac{A}{V} \tag{3.131}$$

where A is the area of the horizon and V the spatial volume of the boundary theory. The area of the horizon is related to the entropy of the boundary theory via

$$s = \frac{A}{V} \frac{1}{4G_N}. \tag{3.132}$$

Therefore for any theory with a gravity dual, the ratio of any transport coefficient to the entropy density depends only on the properties of the dual fields at the horizon:

$$\frac{\chi}{s} = \frac{4G_N}{q(z_0)}. \tag{3.133}$$

In the case of infinite coupling limit $\lambda \to \infty$, $q(z) = 16\pi G_N = const$, one gets the famous result

$$\frac{\eta_{\lambda=\infty}}{s_{\lambda=\infty}} = \frac{1}{4\pi} \tag{3.134}$$

that was first derived in Ref.[92] The result is universal because the derivation applies to any gauge theory with a gravity dual given by Einstein gravity coupled to matter fields. In particular, if large N_c QCD has a gravity dual, its η/s should also be given by $1/4\pi$ up to corrections due to the finiteness of the coupling. These corrections in $\mathcal{N} = 4$ SYM theory are given by

$$\frac{\eta}{s} = \frac{1}{4\pi} \left(1 + \frac{15\zeta(3)}{\lambda^{3/2}} + \dots\right). \tag{3.135}$$

However, in recent years, the conjecture that $\eta/s = 1/4\pi$ is a lower bound has

been questioned. When higher order corrections to Einstein gravity are taken into account, which corresponds to $1/N_c$ or $1/\sqrt{\lambda}$ corrections in the boundary gauge theory, $\eta/s = 1/4\pi$ will no longer be universal. In particular generic higher order derivatives corrections to Einstein gravity can violate the proposed bound.[93] Gauss-Bonnet gravity is an example in which this occurs leading to

$$\frac{\eta}{s} = \frac{(1 - 4\lambda_{GB})}{4\pi} \tag{3.136}$$

where λ_{GB} is the coupling for the Gauss-Bonnet higher derivative term. Thus for $\lambda_{GB} > 0$, η/s is smaller than $1/4\pi$.

Let us conclude this section with the Green-Kubo formula for electric conductivity

$$G^R_{\mu\nu}(\mathbf{k}) = \int d^4x\, e^{-ik\cdot x} \langle J^{EM}_\mu(0) J^{EM}_\nu(x)\rangle \tag{3.137}$$

$$\sigma_{el} = \lim_{k^0\to 0} \frac{e^2}{6T} g^{\mu\nu} G^R_{\mu\nu}(k^0, \mathbf{k} = 0) \tag{3.138}$$

and finally

$$\sigma_{el} = \frac{e^2 N_c^2 T}{16\pi} \tag{3.139}$$

showing that the electric conductivity is finite and coupling independent in the limit of large coupling.[94]

We note that far both η/s and σ_{el}/T predictions are temperature independent while Lattice QCD calculations have shown a sizable T dependence. This appears quite large in particular for σ_{el}/T. The understanding of these aspects in a kinetic theory framework constitutes a part of the results of the present thesis and is discussed in Chapter 5.

4

Shear Viscosity Results

"When analytic thought, the knife, is applied to experience, something is always killed in the process."
Robert M. Pirsig, Zen and the Art of Motorcycle Maintenance

Contents

This chapter is dedicated to the computation of shear viscosity η using Green-Kubo relation which gives us an exact formula for calculating transport coefficients. After checking numerical convergency of the method, we study the microscopic details dependence of shear viscosity, i. e. cross section dependence, and compare Green-Kubo results with the analytical formulas derived in Relaxation Time Approximation and in Chapman-Enskog scheme described in the previous Chapter. We will show that, in the general case of anisotropic cross section, Chapman-Enskog formula is in quite good agreement with the Green-Kubo results. This allows to implement a scheme in which $\mathcal{C}[f]$ in the transport equation is gauged to a fixed η/s. In such a way one can employ the transport theory to study the dynamics of a fluid with the the same language of hydrodynamics. We also study the shear viscosity of Quark-Gluon Plasma in a quasi-particle model.

4.1 Green-Kubo method at work

In this section we describe the Green-Kubo method for computing the shear viscosity. As shown in the previous chapter, Green-Kubo formula for shear viscosity can be written as follows:

$$\eta = \frac{V}{T}\int_0^\infty dt\langle\pi^{xy}(t)\pi^{xy}(0)\rangle \tag{4.1}$$

where V is the volume of the system, T the temperature, π^{xy} are the xy component of energy-momentum tensor, $\langle\dots\rangle$ denotes the thermal average at the equilibrium state. We note that in order to compute η from Eq. (4.1), we need to evaluate the time correlation function $\pi^{xy}(t)\pi^{xy}(0)$:

$$C(t) = \pi^{xy}(t)\pi^{xy}(0) = \lim_{T_{max}\to\infty}\frac{1}{T_{max}}\int_0^{T_{max}} dt'\pi^{xy}(t+t')\pi^{xy}(t') \tag{4.2}$$

where T_{max} is the maximum time of evolution of the system that has to be determined.

In order to apply the Green-Kubo method Eq. (4.1), we choose a system of relativistic particles in a static box with periodic boundary conditions in thermal equilibrium. The xy component of energy momentum tensor, in this case, can be written as:

$$\pi^{xy}(t) = \frac{1}{V}\sum_{i=1}^{N}\frac{p_i^x p_i^y}{p_i^0}(t) \tag{4.3}$$

where p_i^0 is the energy and $p^{x,y}$ are the x, y component of momentum of the $i-$th particle. As the sum in Eq. (4.3) runs over all test-particles, it is mandatory to determine also the number of test-particles that guarantees the convergency of the time correlation function.

4.1.1 Fluctuations and time-correlation functions

In Fig. 4.1 we plot p^{xy} as a function of time. As we can see, $p^{xy}(t)$ fluctuates around the mean value (red dashed line) that for a system in thermal equilibrium is zero being the energy momentum tensor diagonal $T^{\mu\nu} = diag(\varepsilon, P, P, P)$. Studying the time correlations of these kind of fluctuations one obtains an exponential decreasing function:[95]

$$\langle \pi^{xy}(t)\pi^{xy}(0)\rangle = \langle \pi^{xy}(0)\pi^{xy}(0)\rangle e^{-t/\tau} \tag{4.4}$$

where $\langle \pi^{xy}(0)\pi^{xy}(0)\rangle$ is the initial value of the correlator and τ is the decay time. Using the functional form of Eq. (4.4), Green-Kubo formula for shear viscosity η Eq. (4.1) simplifies to:

$$\eta = \frac{V}{T}\langle \pi^{xy}(0)\pi^{xy}(0)\rangle \tau \tag{4.5}$$

In Fig. 4.2 we show Green-Kubo correlator as a function of time: each black line represents an event of the ensemble, red line is the thermal average over all the events generated numerically. As we can see from the plot, the time correlation function is an exponential decreasing function as we expected for a system in thermal equilibrium whose fluctuations are gaussian.[95] Once the Green-Kubo correlator has been computed, one can perform a fit to the exponential decreasing function in order to obtain the decay time τ. In Fig. 4.3 it is shown an exponential fit (red line) to the time correlation function. Finally, using the initial value of the correlator $\pi^{xy}(0)\pi^{xy}(0)$ and the decay time τ, we can evaluate the shear viscosity using Eq. (4.5).

The decay time τ is calculated performing a fit on the temporal range where the correlation function assumes the exponential form, because at $t \gg \tau$ the correlation becomes too weak and the fluctuations starts to dominate. A key point is the evaluation of the error on the value of the viscosity as coming from the error on the initial value of the correlator and the error on the relaxation time τ extracted from the fit of the correlation function. Therefore possible deviations from the exponential law are evaluated through the error bars themselves.

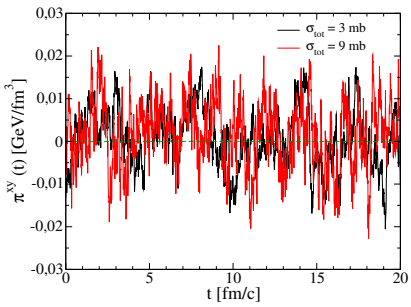

Figure 4.1: Time fluctuations of π^{xy}. Green dashed line is the thermal average. In this simulation we set total cross-section $\sigma_{tot} = 3\,mb$ black line and $\sigma_{tot} = 9\,mb$ red line, $T = 0.4\,GeV$.

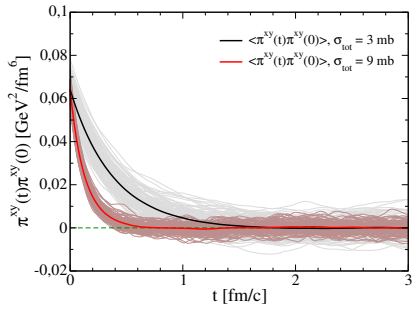

Figure 4.2: Gree-Kubo correlator as a function of time: black line is the thermal average for $\sigma_{tot} = 3\,mb$ while red line for $\sigma_{tot} = 9\,mb$. Thin lines represent each event of the ensemble. We set the temperature $T = 0.4\,GeV$

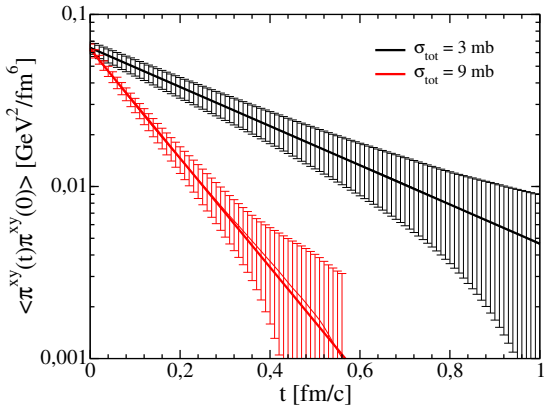

Figure 4.3: Gree-Kubo correlators as a function of time: black line is the fit for $\sigma_{tot} = 3\,mb$ while red line for $\sigma_{tot} = 9\,mb$. We set the temperature $T = 0.4\,GeV$.

4.1.2 Numerical Convergency

Being interested in a more quantitative and sistematic study about the microscopic details dependence of the shear viscosity, we have to check the numerical convergency of numerical implementation of Green-Kubo correlator in order to find the correct maximum time of evolution T_{max} and the correct number of test-particles.The maximum time T_{max} enters in the integral of Eq. (4.2) while the number of test-particles N_{test} are responsible for fluctuations of π^{xy}. In the following discussion, N_{test} is the number of test-particles per real particle.

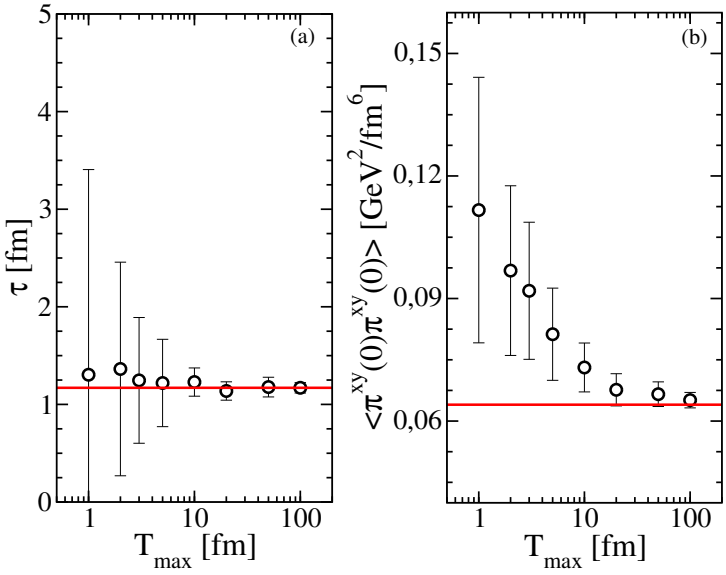

Figure 4.4: Left panel: convergency of decay time τ as a function of T_{max}. Right panel: convergency of initial value $\langle \pi^{xy}(0)\pi^{xy}(0)\rangle$ as a function of T_{max}

In Fig. (4.4) it is shown an example of study of the numerical convergence of the decay time τ and of the initial value of the correlator $\langle \pi^{xy}(0)\pi^{xy}(0)\rangle$ as a function of the maximum time of the simulation T_{max} for the case of isotropic and constant total cross section of $\sigma_{tot} = 0.1\,\mathrm{fm}^2$ and for a temperature of $T = 0.4\,\mathrm{GeV}$. We have performed such analysis using a large number of test particles $N_{test} = 1000$, the convergency with N_{test} will be described soon after. As shown in Fig. 4.4 (b) $\langle \pi^{xy}(0)\pi^{xy}(0)\rangle$ converges to the analytical value given by:

$$\langle \pi^{xy}(0)\pi^{xy}(0)\rangle = \frac{4}{15}\frac{\varepsilon T}{V} \tag{4.6}$$

where ε is the energy density, T the temperature and V the volume. This result is obtained analytically only for the case of massless particles. Eq. (4.6) is represented by red line in Fig: 4.4 showing that a very good accuracy is reached only at $T_{max} \approx 100\,\mathrm{fm/c}$, which is a very large time scale compared to the decay time for this case, $\tau \sim 1\,\mathrm{fm/c}$. The τ itself is instead always quite close to the exact value, but for small T_{max}, however, the evaluated error bars show that there is a large uncertainty on the exponential fit that again is reduced increasing the maximum time over which the temporal correlations are computed. The large error bars are essentially indicating that for small T_{max} it is not possible to have a defined exponential decay behavior according to Eq.(4.4).

We have checked also the numerical convergence as a function of the number

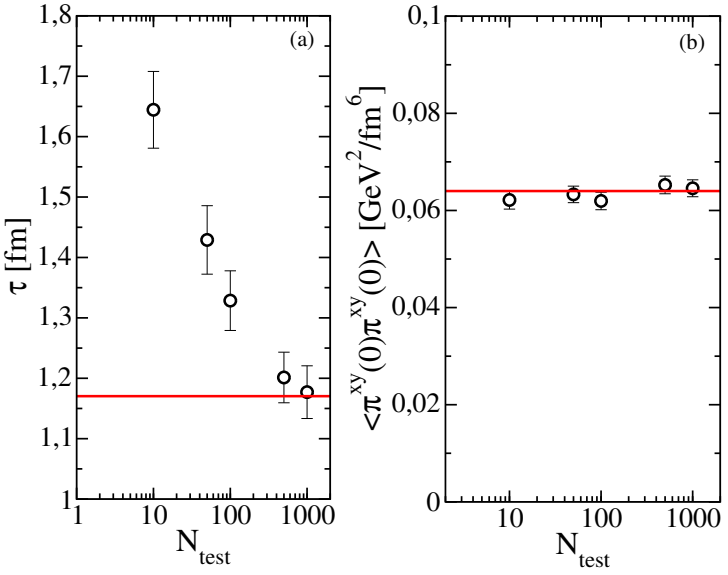

Figure 4.5: Left panel: convergency of decay time τ as a function of N_{test}. Right panel: convergency of initial value $\langle \pi^{xy}(0)\pi^{xy}(0)\rangle$ as a function of N_{test}

of test particles. In Fig.(4.5) we see that regarding τ it is very important to have a large number of test particle $N_{test} \geq 500$ to reduce the uncertainty on τ at the level of 2%. On the right panel of Fig.4.5 the $\langle \pi^{xy}(0)\pi^{xy}(0)\rangle$ is shown to be nearly indipendent on N_{test}, as one can expect considering that it is the initial value of the correlation hence less affected by the accuracy of the system evolution. At variance with the dependence of τ on T_{max}, the N_{test} is of crucial importance. This can be understood because a small number of N_{test} does not allow to properly map the phase space and consequently the dynamical evolution of the system.

A similar study have been performed for all the numerical calculations shown in this thesis both for shear viscosity and electric conductivity.

Once the numerical solution of both Transport Equation and Green-Kubo method are under control, one can study the microscopic details dependence of shear viscosity. In Fig. 4.6 we show an example of Green-Kubo correlators as a function of time for different values of total cross section. As the cross section increases, scatterings destroy time correlations and the decay time decreases.

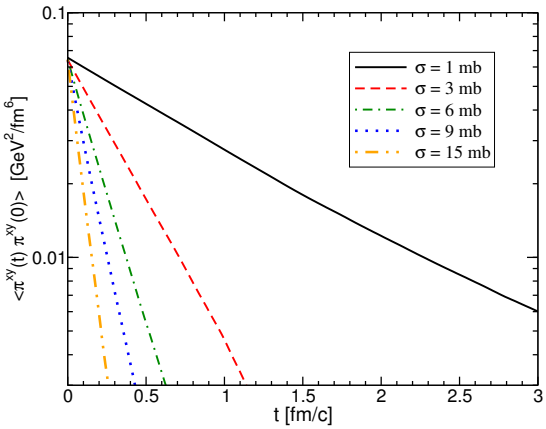

Figure 4.6: Green-Kubo correlator as a function of time for different value of two body cross-section σ_{tot}. The temperature is fixed to $T = 0.4\,GeV$. These results are for massless particles and for isotropic cross section.

4.2 Shear Viscosity: anisotropic scatterings

In this section our aim is to study the more realistic case of angular dependent cross section in the context of a gluon plasma. We choose a typical elastic pQCD inspired cross section with the infrared singularity regularized by Debye thermal mass m_D:

$$\frac{d\sigma}{dt} = \frac{9\pi\alpha_s^2}{2}\frac{1}{(t-m_D^2)^2}\left(1+\frac{m_D^2}{s}\right) \tag{4.7}$$

where s, t are the Mandelstam variables. Such kind of cross sections are those typically used in parton cascade approaches.[42,96–101] The total cross section corresponding to Eq. (4.7) is $\sigma_{tot} = 9\pi\alpha_s^2/(2m_D^2)$ which is energy and temperature independent. Here our objective is not to estimate the value of η but only to explore the impact of non-isotropic cross section on the comparison among Relaxation Time Approximation (RTA), Chapman-Enskog (CE) and Green-Kubo (GK) methods. In Eq.(4.7) the Debye mass m_D is a parameter that regulates the anisotropy of the scattering cross section. We will vary it to regulate the anisotropy, but fixing the total cross section by keeping constant the α_s^2/m_D^2 ratio, i.e. the total cross section. We note that for a plasma at temperature T the average momentum transfer $q^2 \approx (3T)^2$, hence for $m_D \gg 3T$ Eq. (4.7) acts as an almost isotropic cross section and we should recover the results of the previous Section. On the other hand, we notice that

the well known HTL estimate of a gluon plasma viscosity[102] is valid only in the limit of $g = m_D/T \ll 1$, i.e. for very anisotropic cross section.

We have seen that the modified Relaxation Time Approximation gives the same result of the first order Chapman-Enskog for isotropic cross section. In order to perform the same analysis for the non-isotropic case we have to calculate the transport cross section σ_{tr}:

$$\sigma_{tr}(s) = \int \frac{d\sigma}{dt} \sin^2\Theta \, dt = \sigma_{tot} \, h(a) \tag{4.8}$$

where $h(a) = 4a(1+a)\big[(2a+1)ln(1+1/a) - 2\big]$ and $a = m_D^2/s$. For $m_D \to \infty$ the function $h(a) \to 2/3$ and we recover the isotropic limit, $\sigma_{tr} = (2/3)\sigma_{tot}$, while for finite value of m_D the function $h(a) < 2/3$. One can generalize the concept of transport relaxation time $\tau_{tr}^{-1} = \langle \rho \, \sigma_{tr} \, v_{rel} \rangle$ that for isotropic cross section is equal to $(2/3)\langle \rho \, \sigma_{tot} \, v_{rel} \rangle$ writing

$$\tau_{tr}^{-1} = \langle \rho \, \sigma_{tr} \, v_{rel} \rangle = \rho \, \sigma_{tot} \, \langle v_{rel} \, h(a) \rangle \tag{4.9}$$

The shear viscosity η^*_{RTA} in the modified RTA is therefore given by

$$\eta^*_{RTA} = 0.8 \frac{1}{\langle v_{rel} \, h(a) \rangle} \frac{T}{\sigma_{tot}} \tag{4.10}$$

This is the same formula used in several transport calculation to fix the viscosity,[98, 103, 104] but also the formula used to evaluate the viscosity in effective lagrangian approaches.[64] The thermal average,$\langle h(a) \, v_{rel} \rangle$, can be written more explicitely, see also,[105] as:

$$\langle h(a) \, v_{rel} \rangle = \frac{8z}{K_2^2(z)} \int_1^\infty dy \, y^2 \, (y^2 - 1) \, h(2zy\,\overline{a}) \, K_1(2zy) = f(z, \overline{a}) \tag{4.11}$$

where in the function h we have re-written the argument as $a = 2zy\overline{a}$, with $\overline{a} = T/m_D$, just to make explicit the integration over the y variable. This leads to a compact formula for the viscosity in the RTA approximation:

$$\eta^*_{RTA} = 0.8 \frac{1}{f(z, \frac{T}{m_D})} \frac{T}{\sigma_{tot}} \tag{4.12}$$

with the function f, defined by Eq.(4.11), that essentially accounts for the ratio between the total and the transport cross section and therefore it is a function of value smaller than 2/3. Furthermore we notice that for massless particles it will be a function only of the T/m_D ratio.

In the CE approximation the situation is more complex, but for our case it is possible to write down the viscosity in a similar way obtaining, after some

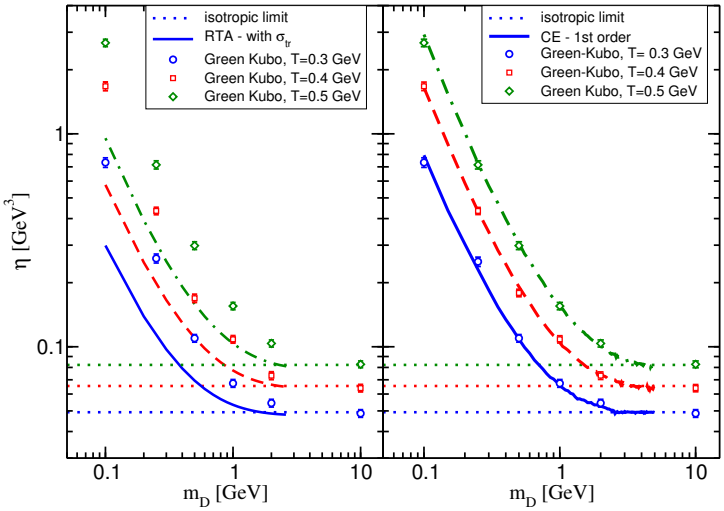

Figure 4.7: Left: Shear viscosity η as a function of the Debye mass m_D for two different values of the temperature $T = 0.3\,GeV$ (blue thick lines) and $T = 0.4\,GeV$ (red thin lines). The dotted line is the isotropic limit when $m_D \gg 1\,GeV$, the solid line is the relaxation time approximation with $\tau^{-1} = \langle \rho\, \sigma_{tr}\, v_{rel} \rangle$ and dashed line is the Chapman-Enskog approximation at firt order. Right: Dashed line represent Chapman-Enskog approximation at the first order for three different temperature ($T = 0.3, 0.4, 0.5\,\mathrm{GeV}$) while the open circles are the results obtained using the Green-Kubo relation.

manipulation of Eq. (3.89), the following form:

$$[\eta_s]^I_{CE} = 0.8\,\frac{1}{g(z,\overline{a})}\,\frac{T}{\sigma_{tot}} \tag{4.13}$$

with

$$\begin{aligned} g(z,\overline{a}) &= \frac{32}{25}\,\frac{z}{K_3^2(z)}\int_1^\infty dy(y^2-1)^3 h(2zy\overline{a}) \\ &\times \left[(z^2y^2+1/3)K_3(2zy) - zyK_2(2zy)\right] \end{aligned} \tag{4.14}$$

it is clear that the function $g(z, T/m_D)$ is quite different from the thermal average of the transport cross section as in the modified RTA, Eq. (4.11). From the results shown in Fig.4.7 comparing the lines on the left panel, evaluated from Eq. (4.12), and the lines on the right, evaluated from Eq.(4.13), we see that the $g(z, T/m_D)$ is generally smaller that the thermal average of the transport cross section.

In the left panel of Fig.(4.7) it is shown the shear viscosity η as a function of the Debye mass at fixed total cross section at $\sigma_{tot} = 3\,\mathrm{mb}$ and for three different temperatures $T = 0.3\,\mathrm{GeV}$, $T = 0.4\,\mathrm{GeV}$ and $T = 0.5\,\mathrm{GeV}$. The solid, dashed

and dot-dashed lines are the behavior of η in the modified RTA approximation, Eq.(4.10), while the symbols are the result with the Green-Kubo formula. It is evident that there is a strong disagreement between the two as soon as m_D is such to move from the isotropic limit indicated to guide the eye by dotted lines (which corresponds to the standard RTA). Therefore, we see in general that even if the total cross section is kept constant, the anisotropy of the cross section cause a strong enhancement of the viscosity η. However the increase is very strong and the difference between transport and total cross section is not able to account fully for such an increase. On the right panel of Fig. (4.7) we compare the Green-Kubo results (symbols) with the prediction of CE at first order (solid, dashed and dot-dashed lines). In this case we find a very good agreement between the two, hence the CE already at first order is able to account for the correct value of η even if the cross section is so forward-backward peaked to cause an increase of about an order of magnitude respect to the same total cross section but isotropic. The RTA approximation severely underestimate the viscosity. We can also see that for $m_D \sim 8-10T$ the isotropic limit is recovered and both CE and RTA coincide but this is essentially the limit discussed in the previous Section. We note that the calculation have been performed down to a quite low value of the screening mass, $m_D = 0.1\,\mathrm{GeV}$. This for $T = 0.5\,\mathrm{GeV}$ would correspond to anisotropic cross section that in the HTL approach corresponds to $g = m_D/T = 0.2$. Nonetheless within a precision of about 5% the first order CE is able to account for the correct value of η even for such forward-bacward peaked cross section. This result further validates the approach in Ref.[102]

4.3 Shear Viscosity: gluon plasma

In this section we want to apply the analysis performed for quite general case: the shear viscosity to entropy density ratio for a gluon plasma. Therefore we consider massless gluons in thermal equilibrium interacting via two-body collisions corresponding to direct $u-$ and $t-$ channel:

$$\frac{d\sigma^{gg\to gg}}{dq^2} = 9\pi\alpha_s^2 \frac{1}{(q^2+m_D^2)^2}. \tag{4.15}$$

where m_D is the Debye mass, $m_D = T\sqrt{4\pi\alpha_s}$ according to HTL calculations and

$$\alpha_s(T) = \frac{4\pi}{11\ln\left(\frac{2\pi T}{\Lambda}\right)^2} \quad , \qquad \Lambda = 200\,MeV \tag{4.16}$$

where Λ is the pQCD running coupling costant. A full pQCD calculation with HTL dressed propagator would include also the $s-$channel and all the interference terms, however it has been shown that the $u-$ and $t-$ channels are the dominant ones.[102] On the other a full HTL calculation as in Ref.[102] would require an energy dependent propagator with both longitudinal and transverse components, however our objective here it is not to have the best evaluation of η/s, but to discuss the comparison between CE, RTA and the numerical Green-Kubo method for a quite realistic case and also under the same condition of previous work based on the Green-Kubo method.[65]

The total cross section in this scheme is energy and temperature dependent:

$$\sigma_{tot} = \frac{9\pi\alpha_s^2}{m_D^2}\frac{s}{s+m_D^2}. \tag{4.17}$$

For this realistic case we have calculated the η/s as a function of the temperature for different temperatures in the range $0.2 \leq T \leq 1.0\,\mathrm{GeV}$ by mean of the numerical Green-Kubo method. The results shown by black symbols in Fig. 4.8 are compared to the CE (orange dashed line), the modified RTA (black dot-dashed line) described above and the simple RTA (green dotted line) with the relaxation time proportional to the total cross section and not to the transport one. We find again that the CE again is in excellent agreement with the Green-Kubo result at the level of accuracy of 4%, while the modified RTA significantly underestimates the η/s by about a 20% at $T \sim 0.2\,\mathrm{GeV}$. At increasing temperature the discrepancy tends to increase up to about a 50%; we can understand this result on the base of the discussion in the previous section because the $m_D^2/T^2 \propto \alpha_s(T)$ ratio becomes smaller at increasing temperature and therefore the cross section appear effectively less anisotropic.

We notice, as shown in Fig. 4.8, that for $T \sim 0.4\,GeV$ we predict a $\eta/s \sim 1$ in approximate agreement with the extrapolation of calculations in Ref.,[102] even if however we have not used the full HTL propagator.

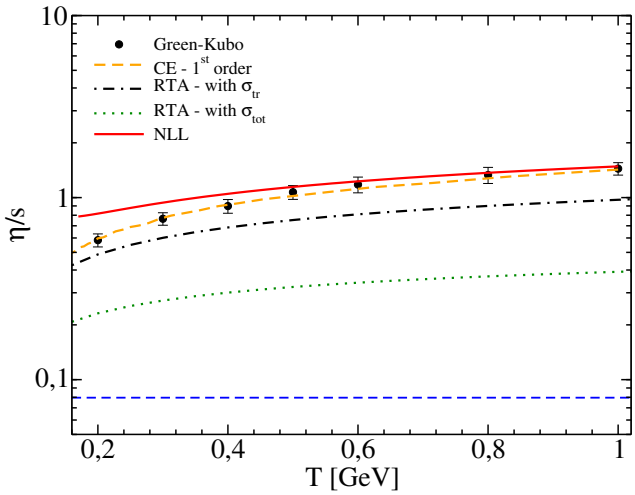

Figure 4.8: Shear viscosity to entropy density ratio η/s of a gluon plasma interacting through the differential cross section in Eq. (4.15) as a function of temperature T: black circles are the results obtained using Green-Kubo correlator, orange dashed line represents Chapman-Enskog first order approximation. The black dot-dashed line is the prediction with the modified RTA approximation and the green dotted lines is the standard RTA. Red solid line is the next to leading log order (NLL) from Ref.[102]

4.4 Impact of η/s on elliptic flow

Once we have found that the correct formula for shear viscosity is the one derived in Chapman-Enskog scheme, we are able to develope a Relativistic Boltzmann Transport (RBT) approach that, instead of focusing on specific microscopic calculations or modelings for the scattering matrix, fixes the cross section in order to have the wanted η/s. This is not the usual approach to transport theory that is generally employed by starting from cross sections and mean fields derived in microscopic models. The motivation for our approach is inspired by the success of the hydrodynamical approach that has shown the key role played by the η/s. Therefore on one hand we use the RBT equation as an approach converging to hydrodynamics for small scattering relaxation time $\tau \sim \sigma\rho$ (small η/s). On the other hand the RBT equation is naturally valid also at large η/s or $p_T \gg T$ in contrast to hydrodynamics and avoids uncertainties in the determination of the viscous correction, δf, to the distribution function $f(x,p)$, that usually becomes quite large at $p_T > 1.5\,\mathrm{GeV}$.[106]

The knowledge of the analytical relation between the shear viscosity η and the microscopic and macroscopic quantities $T, \sigma(\theta), \rho, M$ plays a role in building up

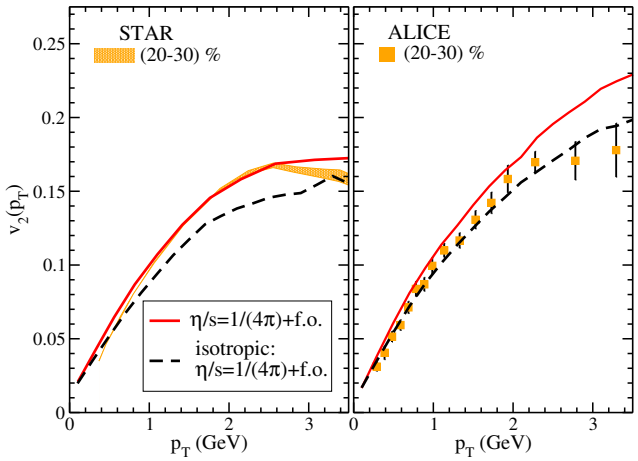

Figure 4.9: Differential elliptic flow $v_2(p_T)$ at mid rapidity for $20\% - 30\%$ collision centrality. Left panel: $Au + Au$ at $\sqrt{s} = 200\,GeV$ at RHIC. Right panel: $Pb + Pb$ at $\sqrt{s} = 2.76\,TeV$ at LHC. Red line is our simulation results keeping constant $\eta/s = 1/4\pi$ in the case of anisotropic cross section $m_D = 0.7\,GeV$ while black line is obtained with fixed $\eta/s = 1/4\pi$ and isotropic cross section.

a transport code that follows the evolution of a fluid at fixed η/s. First tentatives to develop such a transport approach were based on Eq. (4.12),[98–100, 103, 107] i.e. on the RTA approximation. Our work shows that for realistic case where the screening mass $m_D \sim 0.3 \div 1\,GeV$ for the temperature range $T \sim 0.15 \div 0.6\,GeV$ explored at RHIC and LHC energies, Eq. (4.13) provides a sufficiently correct expression within a 5%. Instead the use of Eq. (4.12) leads to underestimate the needed local cross section by about a factor $1.5 - 2$, because as we have seen from our study $f(\overline{a}) > g(\overline{a})$ except for the isotropic cross section case where they are equal.

Therefore, in order to study the expansion dynamics with a certain $\eta/s(T)$, we determine locally in space and time the total cross section σ_{tot} according to the Chapman-Enskog scheme:

$$\eta/s = \frac{1}{15}\langle p\rangle\,\tau_\eta = \frac{1}{15}\frac{\langle p\rangle}{g(a)\sigma_{tot}\rho}. \tag{4.18}$$

We notice that in the regime where viscous hydrodynamics applies the specific microscopic details of the cross section are irrelevant, and ours is the only effective way to employ transport theory to simulate a fluid at a given η/s.

In Fig. 4.9 we show the results of the elliptic flow for a realistic simulation 3+1D of the expanding fireball starting with a typical initial condition from Glauber model and keeping constant the value η/s during the evolution. We can see that v_2 does not depend on the microscopic details of the cross section

for $p_T < 1 \div 1.5\,GeV$, being η/s the physical quantity that determines the elliptic flow. However, at higher transverse momenta, microscopic details becomes relevant as we can see from Fig. 4.9 comparing red line (anisotropic cross section using $m_D = 0.7\,GeV$) with black line (isotropic cross section).

4.5 Shear Viscosity: Quark-Gluon Plasma

In this section we study the more realistic case of a plasma of quarks and gluons considering also the thermodynamics results from Lattice QCD calculations. Before entering the details of how to fix the equation of state, we briefly report general formulas for shear viscosity for a multi component sysyem. As shown in the previous sections, the shear viscosity η from the Green-Kubo relation is given by $\eta = V/T\,\langle \pi^2_{xy}(t=0)\rangle \cdot \tau$, where the initial value of the correlator of the transverse components of the energy-momentum tensor can be written as $\frac{\rho}{15T}\langle p^4/E^2\rangle$.[65,67,68] For a system with different species η can be written as:[58,59]

$$\eta = \frac{1}{15\,T}\left(\sum_q \int \frac{d^3p}{(2\pi)^3}\frac{p^4}{E^2}\tau_q f(p) + \int \frac{d^3p}{(2\pi)^3}\frac{p^4}{E^2}\tau_g f(p)\right) \tag{4.19}$$

where T is the temperature, the sum runs over all quark flavours, $\tau_{q,g}$ are quarks and gluons transport relaxation times. For a mixture, transport relaxation times can be generalized as a sum over all the components of the system weighted with cross-sections and densities, i.e.:

$$\tau^{-1}_{j,tr} = \sum_{i=q,\bar{q},g} \langle \rho_i v^{ij}_{rel} \sigma^{ij}_{tr}\rangle \tag{4.20}$$

where σ^{ij}_{tr} is the transport cross-section, v^{ij}_{rel} the relative velocity, ρ_i the density respectively of particles species i, j. Considering relaxation times momentum independent, the previous equation can be written as:

$$\eta = \frac{1}{15T}\left\langle \frac{p^4}{E^2}\right\rangle \left(\tau_q \rho^{tot}_q + \tau_g \rho_g\right) \tag{4.21}$$

where we implicitely assumed $\left\langle \frac{p^4}{E^2}\right\rangle_q \simeq \left\langle \frac{p^4}{E^2}\right\rangle_g$, we will explain this approximation soon after.

As done within the Hard-Thermal-Loop (HTL) approach, we will consider the total transport cross section regulated by a screening Debye mass $m_D = g(T)T$,

with $g(T)$ being the strong coupling:

$$\sigma_{tr}^{ij}(s) = \int \frac{d\sigma}{dt} \sin^2\Theta \, dt = \beta^{ij} \frac{\pi\alpha_s^2}{m_D^2} \frac{s}{s+m_D^2} h(a) \tag{4.22}$$

where $\alpha_s = g^2/4\pi$, the differential cross section is $\frac{d\sigma}{dt} = \frac{d\sigma}{dq^2} \simeq \alpha_s^2/(q^2 + m_D^2)^2$ where $q^2 = \frac{s}{2}(1-\cos\theta)$, the coefficient β^{ij} depends on the pair of interacting particles: $\beta^{qq} = 16/9$, $\beta^{qq'} = 8/9$, $\beta^{qg} = 2$, $\beta^{gg} = 9$. The function $h(a) = 4a(1+a)[(2a+1)\ln(1+1/a) - 2]$, where $a = m_D^2/s$, regulates the anisotropy of the scatterings: for $m_D \to \infty$, $h(a) \to 2/3$ and one recovers the isotropic limit while $h(a) < 2/3$ for finite value of m_D. We notice that these factors are directly related to the quark and gluon Casimir factor, for example $\beta^{qq}/\beta^{gg} = (C_F/C_A)^2 = (4/9)^2$.

The thermodynamical averages entering Eq. (4.21), will be fixed employing a quasi-particle (QP) model tuned to reproduce the lattice QCD thermodynamics,[108] similarly to.[109–112]

The quasi-particle approach represents a successful way to account for non-perturbative dynamics, encoding the interaction in quasiparticle masses. The mass of the particles can be viewed as arising from the energy contained in a strongly coupled volume determined by the correlation range of the interaction. Once the interaction is accounted for in this way, the quasiparticles behave like a free gas of massive constituents. The model is usually completed by introducing a finite bag pressure that can account for further nonperturbative effects. In order to be able to describe the main features of Lattice QCD thermodynamics, a temperature-dependent mass has to be considered. This also implies that the bag constant B has to be temperature-dependent in order to ensure thermodynamic consistency. In fact, when a temperature dependent mass is included in the pressure, its derivative with respect to the temperature will produce an extra term in the energy density, which does not have the ideal gas form. Therefore pressure and energy density contain additional medium contribution that is $B(T)$.

The pressure of the system can be written as:

$$P_{qp}(T) = \sum_{i=q,g} d_i \int \frac{d^3p}{(2\pi)^3} \frac{\vec{p}^2}{3E_i(p)} f_i(p) - B(T) \tag{4.23}$$

where d_i is the degeneracy factor, the quark and gluon masses are given by $m_g^2 = 3/4\, g^2T^2$ and $m_q^2 = 1/3\, g^2T^2$. In oder to have thermodynamic consistency, the following relationship has to be satisfied:

$$\left(\frac{\partial P_{qp}}{\partial m_i}\right)_T = 0, \qquad i = u, d, \ldots \tag{4.24}$$

which gives rise to a set of equations of the form

$$\frac{\partial B}{\partial m_i} + d_i \int \frac{d^3p}{(2\pi)^3} \frac{m_i}{E_i} f_i(E_i) = 0. \tag{4.25}$$

Only one of the above equations is independent, since the masses of constituents depend on the coupling g.
The energy density of the system is then obtained from the pressure through the thermodynamic relationship $\varepsilon(T) = TdP/dT - P$ and will have the form

$$\varepsilon_{qp}(T) = \sum_i d_i \int \frac{d^3p}{(2\pi)^3} E_i f(p) + B(T). \tag{4.26}$$

In the model there are therefore teo unknown functions, $g(T)$ and $B(T)$, but they are not independent: they are related through the thermodynamic consistency Eq. (4.24). Therefore, only one function needs to be determined, which we do by imposing the condition

$$\varepsilon_{qp}(T) = \varepsilon_{lattice}(T). \tag{4.27}$$

Performing a fit to the lattice energy density, as shown in Fig. 4.10 and 4.11, one obtains the following parametrization:[108]

$$g^2_{QP}(T) = \frac{48\pi^2}{(11N_c - 2N_f) \ln\left[\lambda\left(\frac{T}{T_c} - \frac{T_s}{T_c}\right)\right]^2} \tag{4.28}$$

with $\lambda = 2.6$, $T_s/T_c = 0.57$. We warn that the previous equation is a good parametrization only for $T > 1.1\,T_c$. We notice that a self-consistent dynamical model (DQPM), that includes also the pertinent spectral function, has been developed in[113] and leads to nearly the same behavior of the strong coupling $g(T)$. However, the simple QP model has the advantage to handle simpler analytical expression to pin down the core physics. We will consider the DQPM explicitly, showing that the considerations elaborated are quite general and can be only marginally affected by particle width. We notice that the correct thermal averages entering the transport coefficients, Eq. (4.21), have been determined fitting $g(T)$ to lQCD thermodynamics, but this does not imply that with the same $g(T)$ one has the correct description also of the scattering dynamics, unless one believes in QP model as a solid microscopic description of the correct one, which is not necessarily our point of view. We notice that the only approximation made in deriving Eq.(4.21) is to consider $\langle p^4/E^2\rangle$ equal for quarks and gluons. We have verified that $\langle p^4/E^2\rangle_g \simeq \langle p^4/E^2\rangle_q$ within a 5% in the QP model but also more generally even when m_q and m_g are largely different but $m_{q,g} \lesssim 3T$, which means that Eq. (4.21) is valid also for

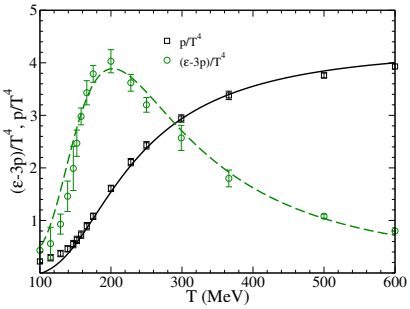

Figure 4.10: Equation of state from Lattice QCD as a function of temperature. Symbols represents Lattice QCD data:[114] green circles are the interaction measure $(\varepsilon - 3P)/T^4$; black squares represents the pressure p/T^4. Black line and green dashed line are the quasiparticle model prediction.

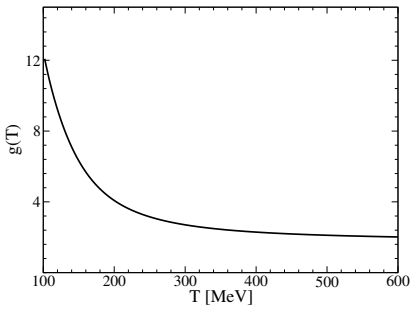

Figure 4.11: Running coupling $g(T)$ as a function of temperature deriverd in the quasiparticle model.

light and strange current quark masses and massless gluons. The $\langle p^4/E^2 \rangle$ in a massless approximation is simply $4\varepsilon\, T/\rho$, we have checked that the validity of this expression is kept using the QP model (i.e. massive excitation) with a discrepancy of about 2%. Hence the first term in Eq. (4.21) is determined by the lQCD thermodynamics and does not rely on the detailed $m_{q,g}(T)$ in the QP model. We note that even if the QP model is able to correctly describe the thermodynamics it is not obvious that it correctly describes dynamical quantities like the relaxation times with the same coupling $g(T)$ employed to fit the thermodynamics.

For its general interest and asymptotic validity for $T \to \infty$, we also consider the behavior of the pQCD running coupling constant for the evaluation of transport relaxation time: $g_{pQCD}(T) = \frac{8\pi^2}{9} \ln^{-1}\left(\frac{2\pi T}{\Lambda_{QCD}}\right)$. On one hand, close to T_c, such a case misses the dynamics of the phase transition, on the other hand it allows to see explicitly what is the impact of a different running coupling.

In Fig. 4.12 it is shown the temperature dependence of η/s: dashed line is the result for the QP model using $g_{QP}(T)$ (see Fig. 4.11) for relaxation times and transport coefficient, blue dot-dashed line labeled as g_{pQCD}, means that we used the pQCD running coupling for evaluating the relaxation time, green circles are our Green-Kubo results, green stars are the DQPM[115] and by symbols several lQCD results. We warn that the different lQCD data are obtained with different methods and actions. The main difference between our QP model and DQPM comes from the fact that the latter assumes isotropic scatterings which decrease the relaxation time by about $30 - 40\%$. Anyway, the η/s predicted is toward higher value with respect to the conjectured lower

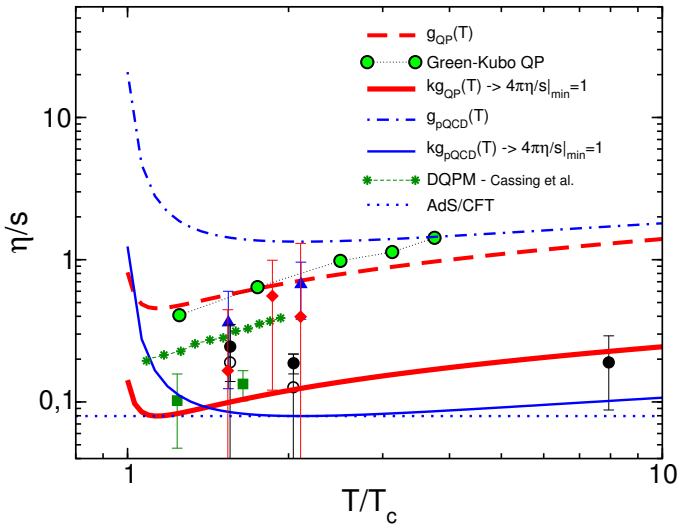

Figure 4.12: Shear viscosity to entropy density ratio η/s: dashed line represents QP model results, dot-dashed line is pQCD, stars is DQPM.[115] Red thick solid line and blue thin solid line are obtained rescaling $g(T)$. Blue dotted line is AdS/CFT result from.[92] Symbols are lattice date: full squares,[81] diamonds and triangles,[82] open and full circles.[83] Green full circles are Green-Kubo results for the Quasi-Particle model under study.

bound of $\eta/s = 1/4\pi$ shown by dotted line in Fig. 4.12, supported also by several phenomenological estimates.[98,116–119] However within the QP model it has been discussed in the literature also another approach for τ where the relaxation times are $\tau_{q,g} = C_{q,g}\, g^4 T \ln(a/g^2)$[120] with $C_{q,g}$ and a fixed to reproduce both the pQCD estimate asymptotically[102] and a minimum for $\eta/s(T) = 1/4\pi$.[108,111] In the T region of interest, the result is quite similar to upscaling the coupling $g(T)$ by a k-factor in such a way to have the minimum of $\eta/s(T) = 1/4\pi$. Therefore we do not employ the above parametrization but compute the transport coefficients using the definition of τ of Eq. (4.20), where enters the cross section in Eq. (4.22) with the coupling upscaled. The corresponding curves are shown in Fig. 4.12 by red thick solid line for the $g_{QP}(T)$ coupling (rescaled by $k = 1.59$) and by blue thin solid line for the $g_{pQCD}(T)$ (rescaled by $k = 2.08$). One obtains $\tau_g \simeq \tau_q/2 \sim 0.2\,\mathrm{fm/c}$ and also $\eta/s(T)$ roughly linearly rising with T in agreement with quenched lQCD estimates, full black circles.[83]

In the next chapter we will discuss also the relation between shear viscosity and electric conductivity employing the quasiparticle model.

5

Electric Conductivity Results

Q: How does a theoretical physicist milk a cow?
A: Well, first let us consider a spherical cow,...
However, milk the cow is not that easy and it is very good that someone does it.

Contents

Several processes occurring in ultra-relativistic heavy ion collisions as well as in the Early Universe are regulated by the electric conductivity σ_{el}. Indeed heavy ion collisions are expected to generate very high electric and magnetic field ($eE \simeq eB \simeq m_\pi^2$, with m_π the pion mass) in the very early stage of the collisions.[70,71] A large value of σ_{el} would determines a relaxation time for the electromagnetic field of the order of $\sim 1 - 2\, fm/c$,[72,73] which would be of fundamental importance for the strength of the Chiral-Magnetic Effect,[74] a signature of the CP violation of the strong interaction. Also in mass asymmetric collisions, like Cu+Au, the electric field directed from Au to Cu induces a current resulting in charge asymmetric collective flow directly related to σ_{el}.[71] Furthermore the emission rate of soft photons should be directly proportional to σ_{el}.[51,75,76] Despite its relevance there is yet only a poor theoretical and phenomenological knowledge of σ_{el} and its temperature dependence. First preliminary studies in lQCD has extracted only few estimates with large uncertainties[85,121] and only recently more safe extrapolation from the current correlator has been developed.[84,86,87]
In this chapter we present results about electric conductivity. In particular, as already done about shear viscosity, we study the electric conductivity dependence on microscopic details, i.e. mass, cross section and its angular dependence, using two methods: Green-Kubo correlator and the E-field method. The E-field method is based on the operative definition of the ratio between the xternal electric field applied and the induced electric current.
This study will allow us to discuss the relation of σ_{el} and shear viscosity discussed in the previous chapter.

5.1 Green-Kubo vs. E-field methods

The definition of electric conductivity $J = \sigma_{el} E$ suggests the experimental method for evaluating the electric conductivity simply inverting the relation $\sigma_{el} = J/E$: taking the ratio between the electric current measured and the electric field applied one obtains σ_{el}. Of course one needs also to verify that J/E is independent on E itself. In the following discussion we will call this method the *E-field method*.[79,122] We notice that recently such a method has been employed to evaluate σ_{el} in the parton-hadron-string dynamics (PHSD) transport approach[123]

To simulate a constant electric field $\vec{E}$ in the box, it is sufficient to modify the equation of motion of each particle as follows:

$$\frac{d}{dt} p_z^i = q_i e E_z \tag{5.1}$$

where q_j is the charge of the particle and we have chosen the electric field along the $z-$direction. The electric current in the z direction for a discrete system of particles has the following form:

$$j_z(t) = \frac{1}{V} \sum_i \frac{e q_i p_z^i(t)}{p_0^i} \tag{5.2}$$

where the sum is over particles, p_0 is the particle energy and V is the volume of the system.

We performed simulations in a uniform box of volume $V = 5^3\, fm^3$ with periodic boundary conditions using time step $\Delta t = 0.01\, fm/c$, spatial discretization $\Delta V_{cell} = 0.1^3\, fm^3$ and $N_{test} \times N_{real} \sim 5\, 10^5$ that ensures the numerical convergency; we have checked that results are independent on volume size. Particles are distributed uniformly in space and according to Boltzmann distribution function, $f(p) = e^{-E/T}$, in momentum.

In Fig. 5.1 we show an example of x, y, z components of the electric current $j(t)$ as a function of time. In this simulation we consider a system of massive quarks, antiquarks and gluons ($m = 0.4\, GeV$) at thermal and chemical equilibrium interacting with isotropic cross-section $\sigma_{tot} = 10\, mb$ and we have applied an electric field $eE = 0.05\, GeV/fm$ in the z direction. As we can see the z component (black solid line) reaches a saturation value while x and y components fluctuate around the equilibrium value zero.

In Fig. 5.2 is shown the ratio σ_{el}/T as a function of the applied electric field eE for two different temperatures $T = 0.2\, GeV$ (dark circles) and $T = 0.4\, GeV$ (green squares) for a system of massive particles with $m = 0.4\, GeV$ interacting via isotropic cross-section with $\sigma_{tot} = 10\, mb$. As shown σ_{el}/T is independent on the applied electric field which confirms the validity of its definition. Dashed lines are RTA predictions of Eq. (3.105). As we can see from Fig. 5.2 thermal fluctuations affect the uncertainties on electric conductivity because a greater temperature produces greater fluctuations in the saturation value of electric current. The increasing of the electric field has the effect of developing a more stable electric current that is easily noticeable in the decreasing of error bars. However, the electric field cannot be increased arbitrarily because one has to guarantee the linear response of the system: with a very high value of eE the system could not reach any equilibrium value of electric current and the definition itself of σ_{el} becomes meaningless. We have checked the correct behaviour of electric current for several value of electric field, temperature and cross-section presented in this work.[79, 122]

The other method we used to compute σ_{el} is the evaluation of Green-Kubo

formula Eq. (3.40) where the electric conductivity can be written as:

$$\sigma_{el} = \frac{V}{T}\int_0^\infty dt\,\langle j_z(t)j_z(0)\rangle. \tag{5.3}$$

The correlation function $\langle j_z(t)j(0)\rangle$ can be written as follows:

$$\langle j_z(t)j_z(0)\rangle = \left\langle \lim_{T_{max}\to\infty}\frac{1}{T_{max}}\int_0^{T_{max}} dt'\, j_z(t+t')j(t')\right\rangle = \tag{5.4}$$

$$= \left\langle \frac{1}{N_{T_{max}}}\sum_{j=1}^{N_{T_{max}}} j_z(i\Delta t + j\Delta t)j_z(j\Delta t)\right\rangle \tag{5.5}$$

where T_{max} is the maximum time chosen in our simulations, $N_{T_{max}} = T_{max}/\Delta t$ represents the maximum number of time-steps and $i\Delta t = t$, while $\langle\cdots\rangle$ denotes the average over events generated numerically. In Fig. 5.3 we plot an example of Green-Kubo correlation functions normalized to the initial value $\langle j_z(0)j_z(0)\rangle$ for a system of massless quarks and gluons interacting via isotropic cross-section ($\sigma_{tot} = 3\,mb$) for several temperatures in the range $T = 0.1 - 0.6\,GeV$. Correlation functions $\langle j_z(t)j_z(0)\rangle$ behave like decreasing exponential $\exp(-t/\tau)$ as it should be for a system in thermal equilibrium. Therefore the electric conductivity is given by

$$\sigma_{el} = \frac{V}{T}\langle j_z(0)j_z(0)\rangle\tau \tag{5.6}$$

and this is the formula used to evaluate the electric conductivity. As shown inf Fig. 5.3 as one increases the temperature, the slope τ decreases as expected from kinetic theory $\tau \sim 1/(\rho(T)\sigma)$.

We recall that for the calculation of σ_{el} and η using Green-Kubo relation the setup of the box is simply in thermal equilibrium, i.e. without any external electric field.

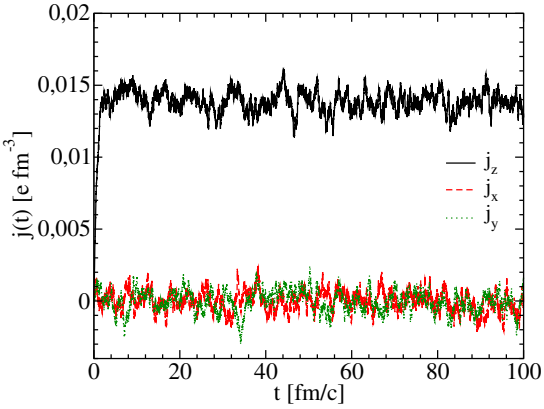

Figure 5.1: x, y, z components of electric current j as a function of time for electric field $eE = 0.05\,GeV/fm$ in the z direction. We fixed $T = 0.2\,GeV$, $m = 0.4\,GeV$ and $\sigma_{tot} = 10\,mb$ for all particles in this simulation. j_z reaches a saturation value proportional to E while x and y components fluctuate around 0.

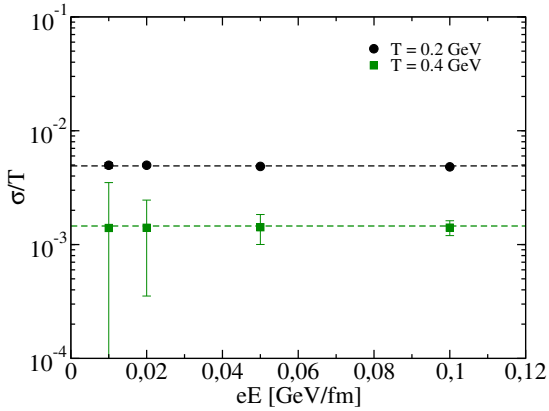

Figure 5.2: Electric conductivity σ_{el}/T as a function of electric field. We fixed $T = 0.2\,GeV$ (dark circles) and $T = 0.4\,GeV$ (green squares), $m = 0.4\,GeV$ and $\sigma_{tot} = 10\,mb$ isotropic for all particles in these simulations. Results are compatible with a constant ratio σ_{el}/T in the range of electric field explored. Dashed lines are RTA predictions.

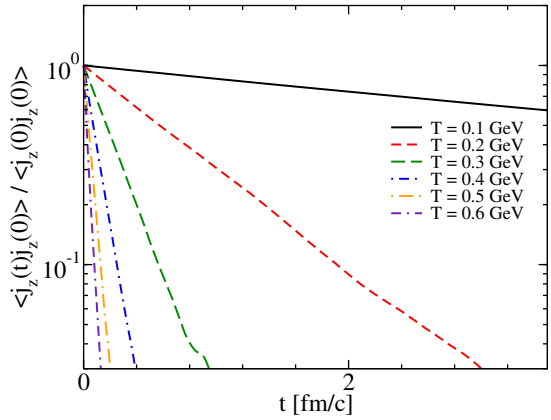

Figure 5.3: Green-Kubo correlators $\langle j_z(t) j_z(0) \rangle$ normalized to the initial value $\langle j_z(0) j_z(0) \rangle$ for a system of massless quarks and gluons interacting with isotropic cross-section ($\sigma_{tot} = 3\, mb$) for temperature $T = 0.1 - 0.6\, GeV$. We can see the typical behaviour of a decreasing exponential $\exp(-t/\tau)$.

5.2 Electric conductivity: isotropic scattering

In this section we consider the simplest case of a system of massless particles (quarks, anti-quarks and gluons) interacting via isotropic and elastic scatterings.[79,122] In this case the transport relaxation time has the following form:

$$\tau_{tr,i}^{-1} = \sum_{j=q,\bar{q},g} \langle \rho_j v_{rel}^{ij} \sigma_{tr}^{ij} \rangle = \frac{2}{3} \sigma_{tot} (\rho_q + \rho_{\bar{q}} + \rho_g) \tag{5.7}$$

where v_{rel} is the relative velocity of the two incoming particles and for massless particles $v_{rel} = 1$, σ_{tr} is the transport cross-section that for isotropic scatterings is equal to $\frac{2}{3}\sigma_{tot}$, $\rho_{q,\bar{q},g}$ is respectively quarks, antiquarks and gluons density. Assuming that all particles interact with the same cross-section, Eq. (3.105) simplifies as follows:

$$\frac{\sigma_{el}}{T} = \frac{e_\star^2}{3T^2} \frac{\gamma_q}{6\gamma_q + \gamma_g} \frac{1}{\frac{2}{3}\sigma_{tot}}. \tag{5.8}$$

where the factor 6 comes from the sum over quarks flavour $(u, d, s, \bar{u}, \bar{d}, \bar{s})$ and we used $\rho_{q,g} = \gamma_{q,g} T^3/\pi^2$, being γ the degeneracy factor.

In Fig. 5.4 we show electric conductivity σ_{el}/T as a function of temperature for a system of massless quarks, antiquarks and gluons interacting via the same isotropic cross-section $\sigma_{tot} = 3\,mb$: open circles are computed using Green-Kubo relation Eq. (5.3) while blue open squares are obtained with the E-field method ($eE = 0.01 - 1.0\,GeV/fm$ for $T = 0.1 - 0.6\,GeV$). Red dashed line represents Eq (5.8). We can see a very good agreement between Green-Kubo and E-field method as it should be in the framework of Linear Response Theory: both definition of σ_{el} are meaningful according to our results. However RTA tends to overestimate numerical results in particular for high temperatures, e.g. at $T = 0.6\,GeV$ there is a 30% of discrepancy. This shows that the relaxation time $\tau_{\sigma_{el}}$ for the electric conductivity is only approximatively determined by the transport cross-section σ_{tr}. We will show in the following that the discrepancy between τ_{tr} and $\tau_{\sigma_{el}}$ becomes more drastic in the more general case of non isotropic scatterings.

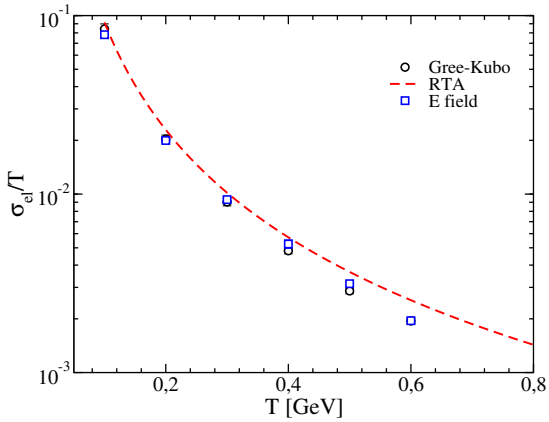

Figure 5.4: Electric conductivity σ_{el}/T as a function of Temperature T for a system of massless particles interacting via isotropic scatterings ($\sigma_{tot} = 3\,mb$). Circles are Green-Kubo results while blue squares represent the E-field method results. Red dashed line is Relaxation Time Approximation Eq. (5.8).

5.3 Electric Conductivity: anisotropic scatterings

In this section we consider a quark-gluon plasma of massive quarks, antiquarks and gluons interacting via anisotropic cross-section. In particular, we use the elastic pQCD inspired cross section with the infrared singularity regularized by Debye thermal mass m_D:[96]

$$\frac{d\sigma}{dt} = \frac{9\pi\alpha_s^2}{2} \frac{1}{\left(t - m_D^2\right)^2} \left(1 + \frac{m_D^2}{s}\right) \tag{5.9}$$

where s, t are the Mandelstam variables. This kind of cross-section is typically used in transport codes.[96,98,99,101] In our calculations the Debye mass m_D and the strong coupling constant α_s are both constant parameters. The total cross-section $\sigma_{tot} = 9\pi\alpha_s^2/(m_D^2)$ with the above prescription is energy and temperature independent. The Debye mass is a parameter that establishes the anisotropy of the collision, for small values of m_D we have that the distribution of the collision angle has a peak at small angles while in the opposite limit $m_D \gg T$, we recover the isotropic case. For a fixed total cross-section, the transport cross-section σ_{tr} can be written as

$$\sigma_{tr}(s) = \int \frac{d\sigma}{dt} \sin^2\Theta \, dt = \sigma_{tot}\, h(a) \tag{5.10}$$

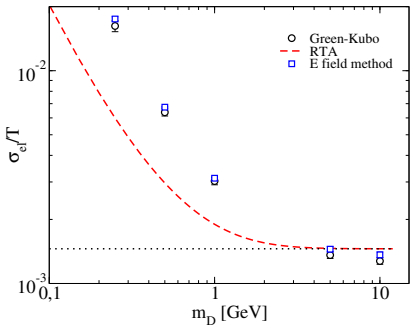

Figure 5.5: Electric conductivity as a function of Debye mass m_D. In this simulations we set $T = 0.4\,GeV$, $\sigma_{tot} = 10\,mb$ and $m = 0.4\,GeV$ for all particles. Circles are Green-Kubo results. Red dashed line is RTA Eq. (3.105) with τ_{tr} from Eq. (5.11). Dotted line represents the isotropic limit.

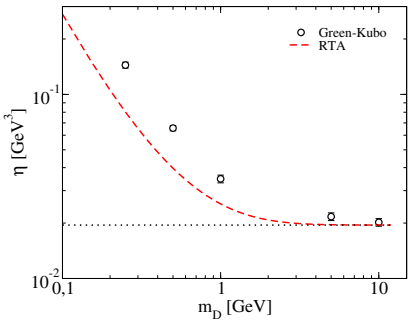

Figure 5.6: Shear viscosity as a function of Debye mass m_D. In this simulation we consider $T = 0.4\,GeV$, $\sigma_{tot} = 10\,mb$ and $m = 0.4\,GeV$ for all particles. Open circles are obtained using Green-Kubo correlator. Dashed line represents RTA while dotted line is the isotropic limit.

where $h(a) = 4a(1+a)\big[(2a+1)ln(1+1/a) - 2\big]$ and $a = m_D^2/s$. For $m_D \to \infty$ the function $h(a) \to 2/3$ and $\sigma_{tr} = (2/3)\sigma_{tot}$ we recover the isotropic limit, see the previous Sec., while for finite value of m_D the function $h(a) < 2/3$. The transport relaxation time in this case can be written as:

$$\tau_{tr,i}^{-1} = \sum_j \langle \rho_j \sigma^{ij_{tr}} v_{rel}^{ij} \rangle = \sigma_{tot} \langle v_{rel} h(a) \rangle \left(\rho_q + \rho_{\bar{q}} + \rho_g\right) \tag{5.11}$$

where for massive particles $\rho = \frac{\gamma}{2\pi^2} T^3 \left(\frac{m}{T}\right)^2 K_2\left(\frac{m}{T}\right)$, being K_2 the modified Bessel function. We performed simulations of a system of quarks, antiquarks and gluons with $m = 0.4\,GeV$, that is the same value obtained in quasi-particle model in the range of temperature $T = 0.2 \div 0.4\,GeV$. However at this point it represents only a systematic study: in the next section we will present quasi-particle model results with temperature dependent masses for quarks and gluons. In Fig. 5.5 we show σ_{el}/T as a function of m_D for a system of quarks and gluons interacting via the same cross-section described Eq. (5.9) with $\sigma_{tot} = 10\,mb$ and $T = 0.4\,GeV$: open circles represent Green-Kubo results while blue squares are obtained using the E-field method ($eE = 0.05\,GeV/fm$); red dashed line is RTA using Eq. (5.11) for the relaxation time; dotted line represent the isotropic limit, i.e. $\sigma_{tr} = \frac{2}{3}\sigma_{tot}$. We can see that RTA underestimates numerical results of σ_{el} by a factor of about 40% already at $m_D = 1\,GeV$ while in the isotropic limit $m_D > 5\,GeV$ it slightly overestimates numerical estimations as we know from the simple case of massless particles of the previous section.

The behaviour of σ_{el}/T as a function of m_D is similar to the one already

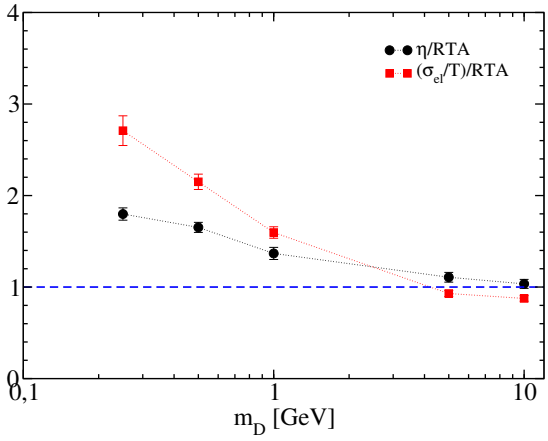

Figure 5.7: Green-Kubo results for shear viscosity η and electric conductivity (from results of Fig. 5.5 and Fig. 5.6) over RTA formulas as a function of Debye mass m_D. RTA is a quite good approximation for isotropic scatterings while for very anisotropic cross-section $m_D < 1\,GeV$ we can see that RTA underestimates in a more prominently way σ_{el}/T than η.

observed for shear viscosity in the case of massless gluons in Chapter 4 and Ref.[68] We show for η the corresponding plot in Fig. 5.6 where we show results for the same system studied for electric conductivity.[79,122] We compute shear viscosity η using Green-Kubo relation $\eta = V/T\langle\pi^{xy}(0)^2\rangle\tau$, as already done for single component system.[65,67,68] In Fig. 5.6 open circles are Green-Kubo results, dashed line is RTA and dotted line represents the isotropic limit. As found in[68] and in Chapter 5, RTA is a good approximation for η only for isotropic scatterings while for $m_D < 1\,GeV$ it underestimates Green-Kubo results by a factor of 25%.

If we look in details RTA estimations for both transport coefficients we find that σ_{el} is underestimated by RTA more considerably than η as the cross-section becomes more forward peaked. In Fig. 5.7 we plot the ratio of numerical results of both transport coefficients over the analytical predictions of RTA: black circles are Green-Kubo results for η, red squares are Green-Kubo results for σ_{el}/T. For $m_D < 1\,GeV$ we can see that RTA is a better approximation for η than for σ_{el}. From Fig. 5.7 we can say that relaxation time of σ_{el} is different from relaxation time of η in the sense that transport relaxation time τ_{tr} in Eq. (5.11) works better for η than for σ_{el}. It would be interesting to study the influence of $2 \to 3$ inelastic scatterings to relaxation time of electric conductivity as already done for η in.[67] This study is currently pursued within the BAMPS transport approach.[122] The effect of considering also $2 \to 3$ scatterings is to decrease η of about a factor 3.

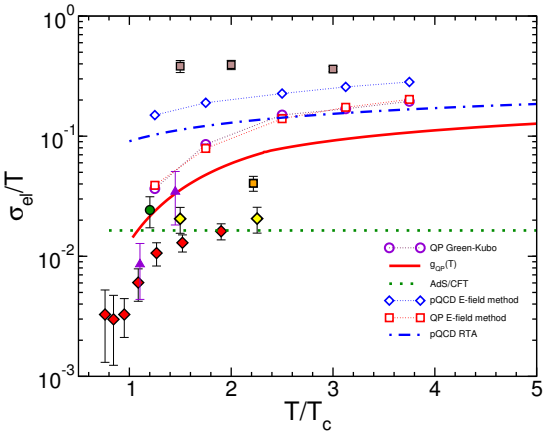

Figure 5.8: Electric conductivity σ_{el}/T as a function of T/T_c. Dark open circles are Green-Kubo results for QP model, red open squares are QP model results computed with the E-field method, violet open diamonds are pQCD results calculated with the E-field method; red line and violet line are RTA predictions respectively for the QP model and pQCD case. Symbols are Lattice data: grey squares,[121] violet triangles,[86] green circle,[87] yellow diamonds,[85] red diamonds[84] and orange square.[124]

5.4 Electric Conductivity: Quark-Gluon Plasma

In this section we investigate the more realistic case of quarks, antiquarks and gluons interacting via different anisotropic and energy dependent cross-section according to the pQCD-like scheme with a screening mass m_D as arising from HTL approach: $m_D \sim g(T)T$. The total cross-section used has the following form:

$$\sigma_{tot}^{ij} = \beta^{ij}\sigma(s) = \beta^{ij}\frac{\pi\alpha_s^2}{m_D^2}\frac{s}{s+m_D^2} \tag{5.12}$$

where $\alpha_s = g^2/4\pi$ and the coefficient β^{ij} depends on the species of interacting particles: $\beta^{qq} = 16/9$, $\beta^{qq'} = 8/9$, $\beta^{qg} = 2$, $\beta^{gg} = 9$.

We remind the formula for electric conductivity derived from Relaxation Time Approximation Eq. (3.105) from Chapter 3:

$$\sigma_{el} = \frac{e^2}{3T}\sum_{j=q,\bar{q}} q_j^2 \int \frac{d^3p}{(2\pi)^3}\frac{\vec{p}^2}{E^2}\tau_j f_{eq} = \frac{e_\star^2}{3T}\left\langle \frac{\vec{p}^2}{E^2}\right\rangle \tau_q \rho_q \tag{5.13}$$

where q_j is the quarks charge $(\pm 1/3, \pm 2/3)$, τ_j is the relaxation time for quarks, ρ_q is the quark density, $e_\star^2 = e^2\sum_{j=\bar{q},q} q_j^2 = 4e^2/3$.

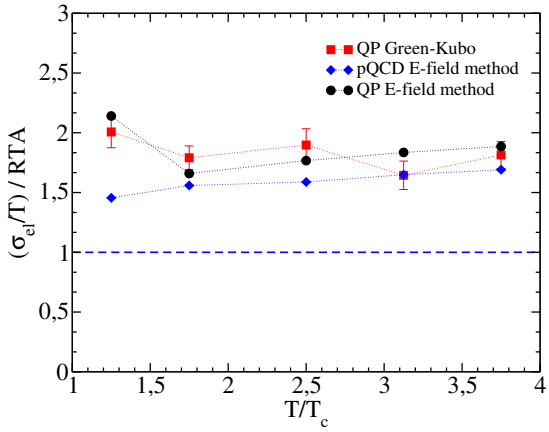

Figure 5.9: Ratio between numerical results of σ_{el}/T and RTA predictions as a function of T/T_c: red squares are obtained using Green-Kubo results for QP model, dark circles with E-field method for QP model, blue diamonds with E-field method for the pQCD case.

Furthermore, in order to take into account the thermodynamics from lQCD calculation, we employ the quasi-particle (QP) model as in the last section of Chapter 4 and Ref.[108] similarly to.[109–112] We recall that the aim of a quasi-particle model is to describe a strongly interacting systems in terms of quasi-particles weakly interacting whose masses are generated by the non-perturbative effects. The QP model, as a phenomenological way to describe microscopically the QGP, has become a quite solid approach for $T > 2 - 3\,T_c$ specifically using NNLO HTLpt.[125,126] As shown in the last section of Chapter 4 and in Ref.,[108] we remind the parametrization of the running coupling constant:

$$g^2(T) = \frac{48\pi^2}{(11N_c - 2N_f)\ln\left[\lambda\left(\frac{T}{T_c} - \frac{T_s}{T_c}\right)\right]^2} \tag{5.14}$$

with $\lambda = 2.6$ and $T_s/T_c = 0.57$. We notice that such a fit reproduce the exact result with a very good precision only for $T > 1.1\,T_c$. Quarks and gluons masses are given by $m_g^2 = 3/4g^2T^2$ and $m_q^2 = 1/3g^2T^2$.

We also study the behaviour of electric conductivity using the pQCD running coupling $g_{pQCD} = \frac{8\pi}{9}\ln^{-1}\left(\frac{2\pi T}{\Lambda_{QCD}}\right)$ considering massless particles: even if this case is not able to describe the phase transition, it is interesting to study the σ_{el} dependence on a different running coupling and also to consider an asymptotic limit valid for $T \gg T_c$. In Fig. 5.8, we show electric conductivity σ_{el}/T as a function of T/T_c.[79,122] Open circles are computed using Green-Kubo correlator, red open squares with the E-field method (applying an $eE = 0.02 \div 0.05\,GeV/fm$ to guarantee the saturation of electric current) for

the quasi-particle model, blue open diamonds represent result for the massless pQCD case that we have computed only with the E-field method. Red line is RTA for QP model, blue dot-dashed line RTA for the massless pQCD case. Symbols denotes Lattice data: grey squares,[121] violet triangles,[86] green circle,[87] yellow diamonds,[85] red diamonds[84] and orange square.[124] As shown, Green-Kubo results are in good agreement with E-field method in the range of temperature explored. Numerical results predicted by the QP model are about a factor of 4 greater then recent Lattice QCD calculations.[84] As we discussed in,[127] also η/s predicted by the QP model is about a factor $4-5$ greater than the minimum value $1/4\pi$ near T_c. This means that rescaling η/s, in order to reproduce the minimum value, one should obtain an electric conductivity σ_{el} very close to recent Lattice data.[84]

We note again that RTA underestimates σ_{el}/T for both QP model and pQCD case, as we could expect qualitatively from the previous section of anisotropic scattering considering that in the QP model $m_D \simeq 0.8-1.2\,GeV$ and in the pQCD case $m_D \simeq 0.4-1\,GeV$ for temperature $T = 0.2-0.6\,GeV$. We can see in details in Fig. 5.9 the ratio between numerical results of electric conductivity σ_{el}/T and RTA predictions as a function of T/T_c. Red squares are calculated taking the ratio between Green-Kubo results and RTA estimation for the QP model, black circles with the E-field method for QP model while blue diamonds with the E-field method for the pQCD case. We notice that QP results are underestimated by an average factor of 1.8 and pQCD results by 1.6 in the range of temperature explored.

5.5 Shear viscosity to electric conductivity ratio

As shown in the last section of Chapter 4, the η/s predicted is larger with respect to the conjectured minimum value of $\eta/s \sim 0.08$, supported also by several phenomenological estimates.[98,116–119] However within the QP model it has been discussed in the literature also another approach for τ where the relaxation times are $\tau_{q,g} = C_{q,g}\, g^4 T \ln(a/g^2)$[120] with $C_{q,g}$ and a fixed to reproduce both the pQCD estimate asymptotically[102] and a minimum for $\eta/s(T) = 1/4\pi$.[108,111] In the T region of interest, the result is quite similar to upscaling the coupling $g(T)$ by a k-factor in such a way to have the minimum of $\eta/s(T) = 1/4\pi$. Therefore we do not employ the above parametrization but compute the transport coefficients using the definition of τ of Eq. (5.16), where enters the cross section of Eq. (4.22) with the coupling upscaled. The corresponding curves were showed in Fig. 4.12 of Chapter 4 by red thick solid line for the $g_{QP}(T)$ coupling (rescaled by $k = 1.59$) and by blue thin solid line

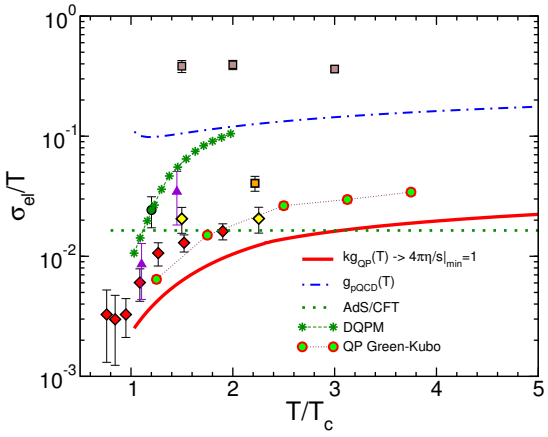

Figure 5.10: Electric conductivity σ_{el}/T as a function of T/T_c: red dashed line represents QP model results using the rescaled $g_{QP}(T)$, blue dot-dashed line is pQCD, red thick solid line and blue thin solid line are respectively QP and pQCD considering the rescaled $g(T)$ in order to reproduce the minimum of η/s. Green line are AdS/CFT results from.[94] Green stars represent DQPM.[115] Green circles are Green-Kubo results for the rescaled $g_{QP}(T)$. Symbols are Lattice data: grey squares,[121] violet triangles,[86] green circle,[87] yellow diamond,[85] orange square[124] and red diamonds.[84]

for the $g_{pQCD}(T)$ (rescaled by $k = 2.08$). One obtains $\tau_g \simeq \tau_q/2 \sim 0.2\,\mathrm{fm/c}$ and also $\eta/s(T)$ roughly linearly rising with T in agreement with quenched lQCD estimates, full circles.[83]

A main point we want to stress is that, once the relaxation time is set to give an $\eta/s(T) = 0.08$, the σ_{el}/T predicted by Green-Kubo results (green circles), with the same τ_q as for η/s, is in quite good agreement with most of the lQCD data, shown by symbols in Fig. 5.10 (see caption for details). Therefore a low σ_{el}/T is obtained at variance with the early lQCD estimate, Ref.,[121] as a consequence of the small $\tau_{q,g}$ entailed by $\eta/s \simeq 0.08$.[127]
In Fig. 5.10, we show also the predictions of DQPM (green stars).[115,123] We also plot by green dotted line the $\mathcal{N} = 4$ Super Yang Mills electric conductivity[94] that predicts a constant behavior for $\sigma_{el}/T = e^2 N_c^2/(16\pi)$. We note that in our framework one instead expects that, even if the η/s is independent on the temperature, the σ_{el} should still have a strong T-dependence. This can be seen noticing that, from Eq. (4.21), one can write approximately $\eta/s \simeq T^{-2}\tau\rho$, being $\langle p^4/E^2\rangle \simeq \varepsilon T/\rho$, and, from Eq. (5.13) $\sigma_{el}/T \simeq T/m(T)\eta/s$, being $\langle p^2/E^2\rangle \simeq T/m(T)$, which means an extra T dependence for σ_{el} leading to a steep decrease of σ_{el}/T close to T_c. We notice that $m(T)$ increases as $T \to T_c$ because it is fitted to reproduce the decrease of energy density ε and the non-vanishing $T^\mu_\mu = \varepsilon - 3P$ in Lattice QCD. For a gas of massless particles, one has $\varepsilon = 3P$ and $\sigma_{el}/T \sim \eta/s$ like found in AdS/CFT. It seems that the

large interaction measure is the origin of such extra T dependence of σ_{el}/T with respect to η/s. This indication is corroborated also by the recent result in AdS/QCD[128] that from one hand is able to reproduce the peak in $\varepsilon - 3P$ and from the other presents a similar strong T dependence for σ_{el}/T in the region $T > T_c$ at variance with AdS/CFT.

The σ_{el} of recent Lattice QCD calculations appears to be self-consistent with a minimal η/s, but the specific T dependence of both are largely dependent on the modeling of $\tau_{q,g}$, we point out that the ratio $(\eta/s)/(\sigma_{el}/T)$ can be written, from Eq. (3.105) and Eq. (4.21), as:

$$\frac{\eta/s}{\sigma_{el}/T} = \frac{6}{5}\frac{T\langle p^2/E^2\rangle^{-1}}{s\, e_\star^2}\left\langle \frac{p^4}{E^2}\right\rangle\left(1+\frac{\tau_g}{\tau_q}\frac{\rho_g}{\rho_q^{tot}}\right). \tag{5.15}$$

in terms of generic relaxation times. Eq.(5.15) is quite general and does not rely on specific features or validity of the quasi-particle model. A main feature of such a ratio is its independence on the k-factor introduced above, and, more importantly, even on the $g(T)$ coupling as we can see writing explicitly the transport relaxation time for quarks and gluons:

$$\begin{aligned}\tau_q^{-1} &= \langle\sigma(s)_{tr} v_{rel}\rangle(\rho_q \sum_{i=u,d,s}^{\bar{u},\bar{d},\bar{s}} \beta^{qi} + \rho_g \beta^{qg}) \\ \tau_g^{-1} &= \langle\sigma(s)_{tr} v_{rel}\rangle\left(\rho_q^{tot}\beta^{qg} + \rho_g\beta^{gg}\right)\end{aligned} \tag{5.16}$$

where the β^{ij} were defined above. Hence the ratio of transport relaxation times appearing in Eq. (5.15) can be written as:

$$\frac{\tau_g}{\tau_q} = \frac{C^q + \frac{\rho_g}{\rho_q}}{6 + \frac{\rho_g}{\rho_q}C^g} \tag{5.17}$$

where the coefficients $C^q = (\beta^{qq}+\beta^{q\bar{q}}+2\beta^{q\bar{q}'}+2\beta^{qq'})/\beta^{qg}$ and $C^g = \beta^{gg}/\beta^{qg}$ are the relative magnitude between quark-(anti-)quark and gg with respect to $q(\bar{q})g$ scatterings. Using the standard pQCD factors for β_{ij}, $C^q|_{pQCD} = \frac{28}{9} \simeq 3.1$ and $C^g|_{pQCD} = \frac{9}{2}$.

In Fig. 5.11 we show $(\eta/s)/(\sigma_{el}/T)$ as a function of T/T_c: the red thick solid line is the prediction for the ratio using $g_{QP}(T)$, but it is clear from the Eq. (5.15) that the ratio is completely independent on the running coupling itself; the result for $g_{pQCD}(T)$ is shown by blue dashed line; green circles are Green-Kubo results which are overestimated by RTA (red line) due to underestimation of σ_{el} as we know from the previous section; green stars are the DQPM from Ref.[115] The ratio is instead sensitive just to the relative strength of the quark (anti-quark) scatterings with respect to the gluonic ones

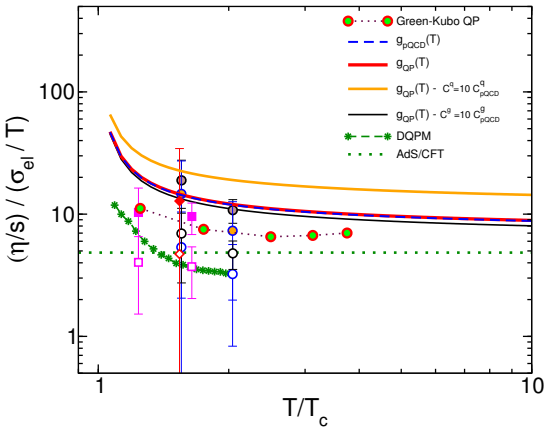

Figure 5.11: Shear viscosity η/s to σ/T ratio as a function of T/T_c: red solid line is the QP model, blue dashed line pQCD, green stars DQPM.[115] Orange line is obtained using $C^q = 10\, C^q_{pQCD}$, black thin line $C^g = 10\, C^g_{pQCD}$. Green circles are Green-Kubo results. Green dotted line represent AdS/CFT results.[92,94] Symbols are obtained using available lattice data (see text for details).

suggesting that a measurement in lQCD can shed light on the relative scattering rates of quarks and gluons, providing an insight into their relative role.[127] It is not known if such ratios, linked to the Casimir factors of $SU(3)_c$, are kept also in the non-perturbative regime, which may be not so unlikely.[129] We remark that we have computed the ratio in a very large temperature range $1 - 10\, T_c$: at large temperatures ($T > 5 - 10\, T_c$) deviation from the obtained value, $(\eta/s)/(\sigma_{el}/T) \simeq 6$, would be quite surprising, on the other hand for $T < 1.2 - 1.5\, T_c$ one may cast doubts on the validity of the Casimir coefficients. In the following we discuss also the impact of modified Casimir Coefficients. As $T \to T_c$ a steep increase is predicted that is essentially regulated by $\langle p^2/E^2 \rangle$. It is interesting to notice that in the massless limit (conformal theory) the factor before the parenthesis in Eq.(5.15) becomes a temperature independent constant and hence also the ratio. This is in quite close agreement with the AdS/CFT prediction shown by dotted line in Fig. 5.11.

We also briefly want to mention that one possible scenario could be that when the QGP approaches the phase transition, the confinement dynamics becomes dominant and the $q\bar{q}$ scattering, precursors of mesonic states, and di-quark qq states, precursor of baryonic states, are strongly enhanced by a resonant scattering with respect to other channels, as found in a T-matrix approach in the heavy quark sector.[130] For this reason, we explore the sensitivity of the ratio $(\eta/s)/(\sigma_{el}/T)$ on the magnitude of C^q and C^g. The orange solid line shows the behavior for an enhancement of the quark scatterings, $C^q = 10\, C^q_{pQCD}$. We can see in Fig. 5.11 that this would lead to an enhancement of the ratio

by about a 40%. We also see that instead the ratio is not very sensitive to a possible enhancement of only the gg scattering with respect to the $q\bar{q}, qq, qg$; in fact even for $C^g = 10C^g_{pQCD}$ one obtains the thin black solid line. This is due to the fact that already in the pQCD case $\tau_g/\tau_q \sim 0.3 - 0.4$. Furthermore already in the massless limit $\rho_g/\rho_q^{tot} \simeq d_g/d_{q+\bar{q}} = 4/9$ even not dwelling on the details of the QP model where the larger gluon mass further decreases this ratio. Therefore the second term in parenthesis in Eq. (5.15) is of the order of 10^{-1} and further decrease of its value would not be visible because the ratio is anyway dominated by the first term equal to one. We reported in Fig. 5.11 also the ratio from the DQPM model, as deduced from Ref.[115] and we can see that, even if it is not evaluated through Eq. (5.15), it is in very good agreement with our general prediction. In Fig. 5.11 we also display by symbols the ratio evaluated from the available lQCD data, considering for $4\pi\eta/s \lesssim 4$ while for σ_{el}/T we choose red diamonds[84] as a lower limit (filled symbols) and the others in Fig. 5.10 as an upper limit (open symbols), excluding only the grey squares being the only set more then one order of magnitude above all the other lQCD data. To compute $(\eta/s)/(\sigma_{el}/T)$ we do an interpolation between the data point of σ_{el}. We warn to consider these estimates only as a first rough indications, in fact the lattice data collected are obtained with different actions among them and have quite different T_c with respect to the most realistic one, $T_c \sim 160\, MeV$,[131,132] that we employed to tune the QP model.[108]

Finally, we point out the direct relation between the shear viscosity η and the electric conductivity σ_{el}. In particular, we have discussed why most recent lQCD data[84,86,87] predicting an electric conductivity $\sigma_{el} \simeq 10^{-2}T$ (for $T < 2\,T_c$) , appears to be consistent with a fluid at the minimal conjectured viscosity $4\pi\eta/s \simeq 1$, while the data of Ref.[121] appear to be hardly reconcilable with it. Also a steep rise of σ_{el}/T, in agreement with lQCD data, appears quite naturally in the quasi-particle approach as inverse of the self-energy determining the effective masses needed to correctly reproduce the lQCD thermodynamics. This result is at variance with the AdS/CFT,[94] but our analysis suggests that it is due to the conformal thermodynamics that does not reflect the QCD one. It is quite interesting that an AdS/QCD approach,[128] able to correctly describe the interaction measure of lQCD, also modify the AdS/CFT result predicting a strong T dependence of σ_{el}/T for $T < 2 - 3\,T_c$. We note that the extra T dependence predicted for σ_{el}/T with respect to η/s is determined by the $\langle p^2/E^2\rangle$ constrained to reproduce the lQCD thermodynamics. If instead one imposes conformality with $m = 0$, this leads to $\langle p^2/E^2\rangle = 1$ and the T dependence of η/s becomes quite similar to the one of σ_{el}/T apart from differences that can arise between quark and gluon relaxation times.

We identify the dimensionless ratio $(\eta/s)/(\sigma_{el}/T)$ as not affected by the uncertainties in the running coupling $g(T)$.[127] Moreover due to the fact that gluons

do not carry an electric charge, the ratio is regulated by the relative strength and chemical composition of the QGP through the term $(1 + \tau_g \rho_g / \tau_q \rho_q^{tot})$. Our analysis provides the baseline of such a ratio that in this decade will most likely be more safely evaluated thanks to the developments of lQCD techniques. This will provide a first and pivotal insight into the understanding of the relative role of quarks and gluons in the QGP. Deviations from our predictions for $(\eta/s)/(\sigma_{el}/T)$ especially at high temperature $T \gtrsim 2 - 3\,T_c$, where a quasi-particle picture can be derived from QCD within the HTL scheme,[125] would be quite compelling.

6

Early Time Dynamics and Schwinger Mechanism

"The Answer to the Great Question...
Of Life, the Universe and Everything...
Is...42"
Deep Thought

Contents

In this chapter we focus on the early time dynamics of heavy ion collisions. In particular we study the isotropization and thermalization of the system produced by the decay of a color electric flux tube.We couple the dynamical evolution of the initial color field to the dynamics of the many particles system, described by relativistic kinetic theory, produced by the decay thanks to the Schwinger mechanism. In details, we will show a systematic investigation starting from a static box calculation, to a 1+1D longitudinal expanding system to the more realistic case of a 3+1D expanding system. Using the results of Chapter 4 about shear viscosity, we focus on the effects that shear viscosity produces to the pressure isotropization and thermalization for all cases explored. Moreover, in the case of 3+1D expanding system, we will show also the impact of η/s on the elliptic flow.

6.1 Motivations

The understanding of early times dynamics is one of the most interesting and compelling problems of heavy ion collisions at ultrarelativistic energy. The common picture os such collisions goes as follows: at $t = 0^-$ the two high energy colliding nuclei are described as two sheets of Color Glass Condensate (CGC), as discussed in Chapter 1, which after the collision turns at $t = 0^+$ into an ensemble of strong longitudinal color electric and color magnetic coherent fields flux tubes, known as Glasma, on the top of which quantum fluctuations are produced and cause the decay of the glasma to a parton liquid as the system expands.[16–21] Quantum fluctuations in the glasma, which appear as inhomogeneities, are amplified by plasma instabilities, which eventually lead to loss of coherence of the color fields and to a locally partly isotropized particle plasma.[24, 133–139] Besides standard field theoretical methods used to study early time dynamics of classical color fields, the problem has been recently investigated also by means of AdS/CFT methods.[140–144]

Besides plasma instabilities, a mechanism responsible for the initial field decays might be the one introduced by Schwinger in the context of Quantum Electrodynamics,[145, 146] known as the Schwinger effect which consists in a vacuum instability towards the creation of particle pairs by a strong electric field, and it is related to the existence of an imaginary part in the quantum effective action of a pure electric field. The problem of pair formation in strong electric fields has been considered recently by means of real time lattice simulations.[147–149] Moreover non abelian generalizations of the Schwinger production rate has been found for the case of both static and time dependent field.[150–155] In the

context of quark-gluon plasma physics it has been considered as a mechanism for the color field decays.[?,156–175]

The purpose of the present study is to model early times dynamics of the system produced in relativistic heavy ion collisions by an initial color electric field which then decays to a plasma by the Schwinger mechanism. The focus of our study is to compute quantities which serve as indicators of thermalization and isotropization of the plasma. In particular, we couple the dynamical evolution of the initial color field to the dynamics of the many particles system produced by the decay, the latter being described by relativistic kinetic theory.[68,176–178] As in the previous studies on this subject we assume that the dynamics of the color field is abelian, hence it satisfies the classical field Maxwell equations.[?] Moreover in the present approach we neglect for simplicity initial longitudinal color magnetic fields which are present in the more complete description of the Glasma state. We consider three cases: the first one is a system evolving in a static box; then we consider a system with a longitudinal expansion which has a greater physical interest than the static box because it is closer to the picture of the early times dynamics of relativistic heavy ion collisions. Finally we extend our model to the more realistic case of a 3+1D expanding system allowing us the to study of collective flows.

Besides being the first study in which a Monte Carlo method is used to simulate the Schwinger effect in the context of early times dynamics of high energy collisions, we improve previous studies which mainly rely on Relaxation Time Approximation (RTA)[171,172] and/or on a linearization of the conductive electric current,[162] by avoiding any ansatz both on the electric current and on the collision integral in the Boltzmann equation which permits to go beyond the RTA. Even if we will discuss more details along this chapter, it is useful to mention since the very beginning that our approach has, among other things, the advantage to consider quantitatively the back-reaction of the plasma dynamics onto classical field evolution. On the one hand this back-reaction demands for tough numerical calculations; on the other hand, since we consistently study the interplay between the fields and the plasma, we can study quantitatively the effects of the initial field dynamics on observables relevant for experiments, like particle spectra and elliptic flow.

6.2 Schwinger mechanism

The problem of a quantum Dirac field interacting with an external uniform classical electric field was solved exactly by Schwinger.[146] The result of vacuum

persistence probability can be used to read off the probability of the e^+e^- pair creation in an external constant electric field

$$\frac{dN}{dtdV} = \frac{e^2\mathcal{E}^2}{4\pi^3}\sum_{n=1}^{\infty}\frac{1}{n^2}\exp\left(-\frac{\pi m^2 n}{e\mathcal{E}}\right) \tag{6.1}$$

where m is the electron mass and e the elementary charge. Later Eq. (6.1) was investigated further in the context of strong interactions interpreting $\mathcal{E}$ as the chromoelectric field and m as the quark mass arguing that confinement may be implemented by the generation of chromoelectric flux tubes with uniform energy density.[156] Moreover tunneling of quark pairs in such tubes represents the mechanism responsible for multiple hadron production.

As already mentioned, a simple way to understand Schwinger's formula Eq. (6.1) lies on the interpretation of vacuum decay as a quantum tunneling process. It is well known that quantum tunneling is equivalent to a propagation in imaginary time. The energy conservation gives:

$$\sqrt{p_\parallel^2(z) + p_\perp^2 + m^2} = Fz \tag{6.2}$$

where $F > 0$ is the force acting on the particle and z is the distance from the point of its first appearence. The longitudinal momentum is therefore

$$p_\parallel(z) = i\sqrt{m_\perp^2 - (Fz)^2} \tag{6.3}$$

where $m_\perp^2 = p_\perp^2 + m^2$ The action of one particle, integrated from the initial point to the point where it materializes with longitudinal momentum zero, is

$$S = i\int_0^{m_\perp/F} dz\ \left|p_\parallel(z)\right| = \frac{i\pi m_\perp^2}{4F}. \tag{6.4}$$

The probability for the tunneling of a virtual pair to a real state having transverse momentum $p_\perp$ is

$$P(p_\perp) = \left|e^{2iS}\right|^2 = \exp\left(-\frac{\pi(m^2 + p_\perp^2)}{F}\right). \tag{6.5}$$

The probability that no such tunneling process takes place is

$$\begin{aligned} |\langle 0_+|0_-|\rangle|^2 &= \prod_{\text{flavour}}\prod_{\text{spin}}\prod_{p_\perp}\prod_{\text{z}}\prod_{\text{t}}[1 - P(p_\perp)] = \\ &= \exp\left\{\sum_{\text{flavour}}\sum_{\text{spin}}\sum_{p_\perp}\sum_{\text{z}}\sum_{\text{t}}\ln\left[1 - P(p_\perp)\right]\right\}. \end{aligned} \tag{6.6}$$

Supposing that the spacetime volume available for tunneling is $L_xL_yL_zT$,

$\Delta z = 2m_\perp/F$ being the length required for materialization of the pair and $\Delta t = \pi/m_\perp$ the time interval for tunneling, we have

$$\begin{aligned} |\langle 0_+|0_-|\rangle|^2 &= \exp\left\{2\frac{T}{\Delta t}\frac{L_z}{\Delta z}\sum_{\text{flavour}} L_x L_y \int \frac{d^2p_\perp}{(2\pi)^2}\,\ln\left[1-P(p_\perp)\right]\right\} = \\ &= \exp(-L_x L_y L_z T p) \end{aligned} \tag{6.7}$$

being p the pair creation rate per unit volume

$$p = -\frac{F}{4\pi^2}\sum_{\text{flavour}}\int_{m_f^2}^{\infty} dm_\perp^2\,\ln\left[1-P(p_\perp)\right] = \frac{F^2}{4\pi^3}\sum_{\text{flavour}}\sum_{n=1}^{\infty}\frac{1}{n^2}\exp\left(-\frac{\pi m_f^2 n}{F}\right). \tag{6.8}$$

Eq. (6.8) can be written in the form

$$\frac{dN_f}{d^4x d^2p_\perp} = \frac{F}{4\pi^3}\left|\ln\left(1-\exp\left(-\frac{\pi m_{f\perp}^2}{F}\right)\right)\right|. \tag{6.9}$$

Taking into account that particles are produced with vanishing longitudinal momentum we can write the above equation as:

$$\frac{dN_f}{d\Gamma_{inv}} = \frac{F}{4\pi^3}\left|\ln\left(1-\exp\left(-\frac{\pi m_{f\perp}^2}{F}\right)\right)\right|\delta(p_\parallel)p^0 \tag{6.10}$$

where $d\Gamma_{inv}$ is the Lorentz invariant elemente of the phase space.

6.3 Abelian dominance approximation

Being the treatment of tunneling in the framework of QCD very complicated, several approximation are to be taken. In agreement with the glasma picture of the initial stage and following Ref.,[171] we assume that the gluon field can be separated in coherent part which can be interpreted as the classical mean field and an incoherent part:

$$F_{\mu\nu} = \langle F_{\mu\nu}\rangle + \delta F_{\mu\nu}. \tag{6.11}$$

Let assume that the mean-field part can be diagonalized in color space, i.e. there is a gauge transformation U which rotates $\langle F_{\mu\nu}\rangle$ into the abelian subgroup of the $SU(3)$ gauge group

$$F_{\mu\nu} \to U F_{\mu\nu} U^{-1} = F'_{\mu\nu} = \langle F'^3_{\mu\nu}\rangle\frac{\lambda_3}{2} + \langle F'^8_{\mu\nu}\rangle\frac{\lambda_8}{2} + \delta F'_{\mu\nu}. \tag{6.12}$$

One can see that $\langle F'_{\mu\nu}\rangle$ has two independent components which can be represented by a two-component vector

$$\mathbf{F}_{\mu\nu} = (\langle F'^{3}_{\mu\nu}\rangle, \langle F'^{8}_{\mu\nu}\rangle). \tag{6.13}$$

The fluctuating part $\delta F'_{\mu\nu}$ contains only non-diagonal terms while the diagonal components are smaller than $\mathbf{F}_{\mu\nu}$ and neglected. The mean-field part and the fluctuating part describe neutral and charged gluons respectively. Quarks couple to the field $\mathbf{F}_{\mu\nu}$ through the charges $\boldsymbol{\varepsilon}_i$ and the charged gluons couple to $\mathbf{F}_{\mu\nu}$ through the charges $\boldsymbol{\eta}_{ij}$, which we have introduced in Chapter 1. Moreover it is assumed that the color field configuration formed at the initial stage of a collision corresponds to the chromoelectric field $\boldsymbol{\mathcal{E}} = \mathbf{F}^{30}$. The Gauss law applied to the flux tubes gives

$$\boldsymbol{\mathcal{E}}\mathcal{A} = kg\mathbf{q} \tag{6.14}$$

where $\mathcal{A} = \pi r^2$ denotes the area of the transverse cross section of the tube, k is the number of color charges at the end of the tube and $g\mathbf{q} = g(q^3, q^8)$ is the color charge of a quark or a gluon. The energy of an elementary tube per unit length, the string tension, is

$$\sigma = \frac{1}{2}\mathcal{A}\boldsymbol{\mathcal{E}}\cdot\boldsymbol{\mathcal{E}} = \frac{g^2}{2\mathcal{A}}\mathbf{q}\cdot\mathbf{q} \tag{6.15}$$

and considering the quark and gluon charges one obtains

$$\sigma_q = \frac{g^2}{6\mathcal{A}}, \qquad \sigma_g = \frac{g^2}{2\mathcal{A}}. \tag{6.16}$$

The Gauss law can be rewritten as

$$\boldsymbol{\mathcal{E}} = \sqrt{\frac{2\sigma_g}{\pi r^2}}k\mathbf{q} = \sqrt{\frac{6\sigma_q}{\pi r^2}}k\mathbf{q} \tag{6.17}$$

which determines the value of initial chromoelectric field spanned by the two receding nuclei. For standard value $\sigma_q = 1\,GeV/fm$ one obtains

$$g^2 = 6\,\mathcal{A}\,\mathrm{GeV/fm} \approx 30\pi\frac{r^2}{\mathrm{fm}^2} \tag{6.18}$$

which, supposing the tube radius of the order of $1\,fm$, gives a coupling constant $g = 5.48$, excluding any perturbative treatment of the process. The number of color charges k may be obtained from the hypothesis of the random walk in color space[179]

$$k = \sqrt{\frac{d\nu}{d^2s}\pi r^2} \tag{6.19}$$

where $d\nu/d^2s$ is the number of collisions per unit transverse area.For example, for the cases which are relavant for simulations of initial stage of uRHICs one expects $k \approx 3$ for lead-lead collisions.

6.4 Abelian Flux Tube Model

In this Section we briefly summarize the abelian flux tube model (AFTm)[?, 156–172] which we implement in our simulations of the initial stage of relativistic heavy ion collisions. In our studies we do not insist on implementing the most realistic geometrical condition relevant for heavy ion collisions experiments, in which one should take into account several flux tubes in the transverse plane similar to the glasma configuration; rather we consider a simpler situation in which there is only one flux tube of a given transverse area, and study its dynamical evolution by coupling the field equations to relativistic kinetic theory for the particle quanta produced by the decay of the field itself, leaving to upcoming works the study of more realistic initial conditions.

The main assumptions of the AFTm are:

- In the initial condition a color electric field is present, which is produced by color charges in the colliding nuclei;
- The color electric field decays into particle quanta by the Schwinger mechanism;
- The particle quanta propagate in the medium colliding and interacting with the background of the color field;
- Particle creation as well as particle currents affect in a self-consistent way the color electric field;
- The field dynamics is abelian, namely it satisfies the abelian Maxwell equations.

The last assumption is quite strong because initial gauge fields are quite large, nevertheless it permits the easiest implementation of the coupling of classical field equations to relativistic kinetic theory in presence of the Schwinger mechanism, hence we will limit ourselves to consider abelian dynamics of the classical fields leaving the introduction of non abelian field dynamics to future works. We stress here that the name "abelian" just means that in the evolution equation for the classical part of the field, we neglect the classical Yang-Mills self-interaction terms; we still have quantum interactions of the classical gluon

field with gluon quanta arising both from the Schwinger effect and from the color currents produced by gluons.

In this Section we closely follow Ref.[171] at the same time adopting a slightly different notation which is more convenient for our case. Moreover we assume the initial color field to be polarized along the 3^{rd} direction of adjoint color space, meaning that only one particular color charge is present in the two colliding nuclei.[171] Moreover we assume only one component of the electric field is present, namely the one in the longitudinal direction, which we denote by E in the following. The latter is a consequence of the fact that in the initial condition we assume the field is purely longitudinal, and transverse currents are not produced during time evolution of the system if transverse expansion does not take place implying a vanishing transverse field. The number of pairs per unit of spacetime and invariant momentum space produced by the decay of the color field is obtained as a generalization of Eq. (6.10) to the QCD case:[171,180]

$$\frac{dN_{jc}}{d\Gamma} \equiv p_0 \frac{dN_{jc}}{d^4x d^2p_T dp_z} = \mathcal{R}_{jc}(p_T)\delta(p_z)p_0 \ , \tag{6.20}$$

with

$$\mathcal{R}_{jc}(p_T) = \frac{\mathcal{E}_{jc}}{4\pi^3} \left| \ln\left(1 \pm e^{-\pi p_T^2/\mathcal{E}_{jc}}\right)\right| \ , \tag{6.21}$$

the plus (minus) sign corresponding to the creation of a boson (fermion-antifermion) pair. In this equation j and c denote flavor and color indices respectively, p_T, p_z refer to each of the two particles created by the tunneling process; $\mathcal{E}_{jc}$ is the effective force which acts on the tunneling pair and it depends on color and flavor; it can be written as

$$\mathcal{E}_{jc} = (g|Q_{jc}E| - \sigma_j)\,\theta\,(g|Q_{jc}E| - \sigma_j) \ , \tag{6.22}$$

where σ_j denotes the string tension depending on the kind of flavor considered. Moreover $p_0 = \sqrt{p_T^2 + p_z^2}$ corresponds to the single particle kinetic energy.

The Q_{jc} are color-flavor charges which, in the case of quarks, correspond to the eigenvalues of the T_3 operator:

$$Q_{j1} = \frac{1}{2} \ , \quad Q_{j2} = -\frac{1}{2} \ , \quad Q_{j3} = 0 \ , \quad j = 1, N_f; \tag{6.23}$$

for antiquarks, corresponding to negative values of j, the color-flavor charges are just minus the corresponding charges for quarks; finally for gluons (which in our notation correspond to $j = 0$) the charges are obtained by building gluons up as the octet of the $3 \otimes \bar{3}$ in color space,

$$Q_{01} = 1 \ , \quad Q_{02} = \frac{1}{2} \ , \quad Q_{03} = -\frac{1}{2} \ , \tag{6.24}$$

and $Q_{04} = -Q_{01}$, $Q_{05} = -Q_{02}$, $Q_{06} = -Q_{03}$. We notice that we have only six gluons out of eight, corresponding to the non-diagonal color generators; the gluon fields corresponding to the diagonal color generators have vanishing coupling with the background field, hence they cannot be produced by the Schwinger effect.

6.5 Transport Theory coupled to Maxwell Equations

Our calculation scheme is based on the Relativistic Transport Boltzmann equation which, in the presence of a gauge field $F^{\mu\nu}$, can be written as follows:

$$\left(p^\mu \partial_\mu + g Q_{jc} F^{\mu\nu} p_\nu \partial_\mu^p\right) f_{jc}(x,p) = \frac{dN_{jc}}{d\Gamma} + \mathcal{C}_{jc}[f] \tag{6.25}$$

where $f_{jc}(x,p)$ is the distribution function for flavour j and color c, $F^{\mu\nu}$ is the electromagnetic tensor. On the right hand side we have the source term $dN/d\Gamma$ which describes the creation of quarks, antiquarks and gluons due to the decay of the color electric field and $\mathcal{C}[f]$ which represents the collision integral. Considering only $2 \to 2$ body elastic scatterings, the collision integral can be written as (see Chapter 2):

$$\begin{aligned} \mathcal{C}[f] \;=\; & \int \frac{d^3p_2}{2E_2(2\pi)^3} \frac{d^3p_{1'}}{2E_{1'}(2\pi)^3} \frac{d^3p_2'}{2E_2'(2\pi)^3} \left(f_{1'} f_{2'} - f_1 f_2\right) \\ & \times |\mathcal{M}|^2 \delta^4(p_1 + p_2 - p_{1'} - p_{2'}) \;, \end{aligned} \tag{6.26}$$

where we omit flavour and color indices for simplicity, $\mathcal{M}$ is the transition matrix for the elastic process linked to the differential cross section through $|\mathcal{M}|^2 = 16\pi s^2 d\sigma/dt$, being s the Mandelstam variable.

In our simulations we solve numerically Eq. (6.25) using the test particles method and the collision integral is computed using Monte Carlo methods based on the stochastic interpretation of transition amplitude[98,101,104,176–178,181,182] as discussed in Chapter 2.

The evolution of the electric field is given by the Maxwell equations:

$$\frac{\partial E}{\partial z} = \rho \;, \quad \frac{\partial E}{\partial t} = -j \;, \tag{6.27}$$

where ρ corresponds to the color charge density,

$$\rho = g \sum_{j,c} Q_{jc} \int d^3\mathbf{p} f_{jc}(p) \tag{6.28}$$

where the sum runs over quarks, antiquarks and gluons. On the other hand j corresponds to the color electric current which is given by the sum of two contributions: in fact the Schwinger effect can be described as a dielectric breakdown in which dipoles are produced by quantum tunneling hence changing the local dipole moment of the vacuum, and the charges move in the medium due to the residual electric field giving rise to a conductive current. Following Ref.[171] we name displacement current, j_D, and matter current, j_M:

$$j = j_M + j_D \ . \tag{6.29}$$

Here j_M is a colored generalization of the usual electric current density which in a continuum notation is given by

$$j_M^\mu = g \sum_{j,c} Q_{jc} \int \frac{d^3\mathbf{p}}{p_0} p^\mu f_{jc}(p) \ . \tag{6.30}$$

The displacement current arises from the polarization of the vacuum due to the decay of the electric field by the Schwinger mechanism: more precisely it is given by the time derivative of the local dipole moment induced by the particles pop-up, in the same way a time variation of the local dipole moment in a medium gives rise to a change in the local electric field.[183] According to the quantum tunneling interpretation of the Schwinger effect[156] the dipole moment can be computed as $2p_0/E$ where p_0 corresponds to the kinetic energy of the particles coming out from the vacuum; taking into account Eq. (6.20) j_D can be written, in the reference frame where particles are produced with vanishing longitudinal momentum, as

$$j_D = \sum_{j=0}^{N_f} \sum_{c=1}^{3} \int \frac{d^3\mathbf{p}}{p_0} \frac{dN_{jc}}{d\Gamma} \frac{2p_T}{E} \ , \tag{6.31}$$

where N_f corresponds to the number of flavors in the calculation. The color charge and current densities depend on the particle distribution function: hence they link the Maxwell equations Eq. (6.27) to the kinetic equation (6.25).

We use the CE approach to relate shear viscosity to temperature, cross section and density which is in agreement with Green-Kubo correlator results as already shown in Chapter 4 and Ref.[68] Therefore, we fix η/s and compute the pertinent total cross section by mean of the relation

$$\sigma_{tot} = \frac{1}{5} \frac{T}{\rho\, g(a)} \frac{1}{\eta/s} \ , \tag{6.32}$$

which is valid for a generic differential cross section $d\sigma/dt \sim \alpha_s^2/(t - m_D^2)^2$ as proved in Chapter 4 and in Ref.[68] In the above equation $a = m_D/2T$, with

m_D the screening mass regulating the angular dependence of the cross section, while

$$g(a) = \frac{1}{50}\int dy y^6 \left[(y^2+\frac{1}{3})K_3(2y) - yK_2(2y)\right] h\left(\frac{a^2}{y^2}\right) \tag{6.33}$$

We refer to Chapter 4 for the details of the previous formula reminding that Eq.(6.32) reduces to the relaxation time approximation with $\tau_\eta^{-1} = \tau_{tr}^{-1} = \sigma_{tr}\rho$, while for finite value of m_D, which means anisotropic scatterings, $g(a) < 2/3$.

We notice that, in the regime where viscous hydrodynamics applies, the specific microscopic details of the cross section are irrelevant, and our approach is an effective way to employ transport theory to simulate a fluid at a given η/s.[178, 184]

6.6 Static box

In this Section we study the chromoelectric flux tube decay in a static box. We assume the box is a cube with side of $5\,fm$. Moreover we assume periodic boundary conditions for particles propagating in the box. This case is of academic interest, nevertheless it is useful because it allows us to introduce concepts which will be useful when we will consider more interesting case of a longitudinally expanding background, as well as it provides a further test of the numerical solution of Eq. (6.25).

Given the symmetry of the problem, assuming at initial time a homogeneous electric field along the z direction, then the system will remain homogeneous along the whole dynamical evolution: the electric field at later times as well as the currents and the invariant distribution functions will depend only on time and not on space coordinates. Moreover it is easy to verify by Maxwell equations that neither magnetic fields nor transverse components of the electric field can develop during the evolution. Within these assumptions the evolution equation for the classical field relevant for our problem is given by

$$\frac{dE}{dt} = -j(t)\ . \tag{6.34}$$

In our simulations in the static box case we use Eq. (6.20) to create particle pairs from the color electric field: at each time step, the value of E and of the volume box being given, we compute the expected pair number, $\mathcal{N}$, integrating Eq. (6.20) over the volume box, then we distribute the $\mathcal{N}$ pairs uniformly in

the box and with transverse momentum p_T according to the distribution in Eq. (6.20); since the pairs have to pop out from the vacuum with vanishing total and longitudinal momenta, given p_T we extract randomly the azimuthal angle ϕ which uniquely determines $p_y = p_T \sin\phi$ and $p_x = p_T \cos\phi$ of one of the particles in the pair; finally the momentum direction of the second particle is given by $\pi - \phi$.

In Fig. 6.1 we show the time evolution of electric field E_z, current j_M and displacement current j_D for the case of $4\pi\eta/s = 3$. While the initial field, $E_z = 2.2\,GeV^2$, decays the current j_M developes due to the decay of the displacement current, meaning that particles were created. We also notice the presence of plasma oscillations, which are due to the continuous exchange among field and particles throughout the conduction current, as we discuss below in more details. Plasma oscillations will be discussed also later in the case of the expanding system and which characterize the evolution of the color field in the cases of intermediate to large values of η/s.

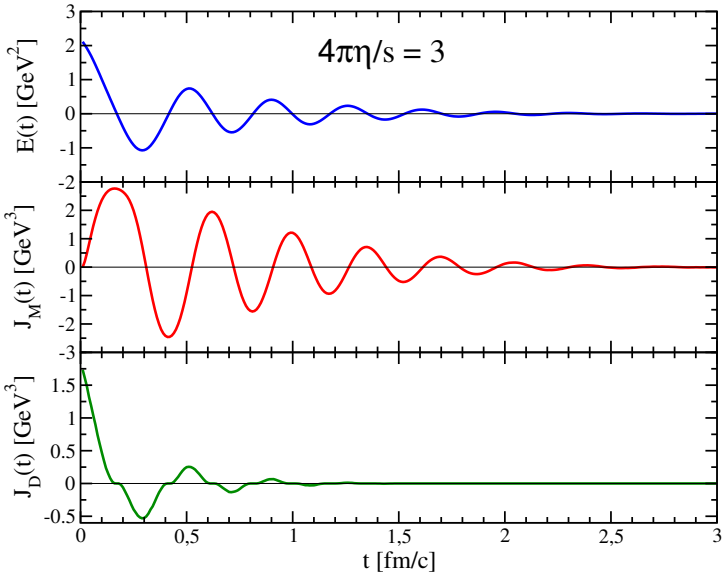

Figure 6.1: Time evolution of electric field E_z, current j_M and displacement current j_D for the case of a static box. In this calculation we have fixed shear viscosity over entropy density ratio as 4pieta/s=3.

In Fig. 6.2 we plot the early time evolution of the color-electric field for the cases of calculations at fixed total cross section while in Fig. 6.3 tha case of fixed η/s. The line labelled as ideal gas means a calculation with zero cross section.

From the results in Fig. 6.2 we notice that for small coupling among the

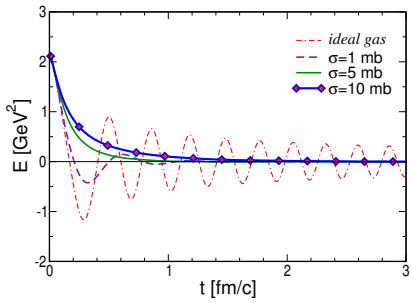

Figure 6.2: Early time evolution of the color-electric field for the cases of calculations at fixed total cross section.

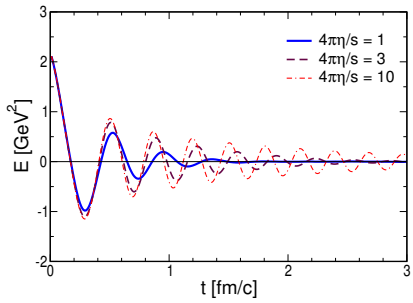

Figure 6.3: Early time evolution of the color-electric field for the cases of calculations at fixed η/s.

particles, the electric field rapidly decays through the Schwinger mechanism then it evolves with damped oscillations: the smaller the coupling is, the less efficient the damping is. Eventually for strong enough coupling the oscillations disappear and the color-electric fields just decays according to a power law. This dependence on the coupling strength is very easy to understand and is in last analysis due to the dependence of the electric conductivity of the plasma on the particle interaction strength as shown in Chapter 5 and in Ref.[79] In fact at initial times the particles are produced by the Schwinger effect with zero longitudinal momentum, then in case the coupling is small they are accelerated by the electric field thus generating an electric current j_M which at first gains energy from the field thus lowering its magnitude; because of the small coupling particles's momenta is not randomized thus currents are efficiently produced by the field. At some point of time the field is zero but the current j_M is still nonvanishing and positive hence causing a sign flip of the electric field and a negative acceleration of the charges, resulting eventually in $j_M < 0$ and an increase of the electric field. This process causes the field oscillations we observe in Fig. 6.2. On the other hand, for large values of the coupling the scattering processes among the particles randomize momenta hence causing $j_M \approx 0$ and the time evolution of the field is a pure decay by the Schwinger effect. To consider this point more closely we write down the analytical form of Eq. (6.31), namely

$$j_D = \frac{\zeta(5/2)}{4\pi^3 E}\left[\frac{4-\sqrt{2}}{4}\sum_{c=1}^{3}\mathcal{E}_{0c}^{5/2} + \sum_{j=1}^{N_f}\sum_{c=1}^{3}\mathcal{E}_{jc}^{5/2}\right] \tag{6.35}$$

For example in the case one considers only the decay into gluons and assuming for simplicity $\sigma_g = 0$ in Eq. (6.22) one has for $j_M = 0$ the equation

$$\frac{dE}{dt} = -\sigma_D E^{3/2}\,, \tag{6.36}$$

where we have introduced the quantity

$$\sigma_D = \frac{\zeta(5/2)}{4\pi^3}\frac{4-\sqrt{2}}{4}\sum_{c=1}^{3}|gQ_{0c}|^{5/2} \ , \tag{6.37}$$

which is related to the Schwinger effect and is independent on the coupling among the particles. The solution of Eq. (6.36) can be found as

$$E = \frac{E(0)}{(1+\sigma_D\sqrt{E_0}t)^2} \ , \tag{6.38}$$

showing that in absence of a conductive current the decay of the chromoelectric field is purely power law.

In Fig. 6.3 we plot the early time evolution of the color electric field keeping η/s fixed. The calculations have been performed assuming an isotropic cross section, and the relation among the total cross section and η/s is computed by the CE method, results of Chapter 4 and Ref.,[68] which is in agreement with the relaxation time approximation for the case of an isotropic differential cross section. From the qualitative point of view these results do not differ from those we obtain for calculations at fixed cross section, and they can be understood in the same way the results we obtained in the case of a fixed cross section.

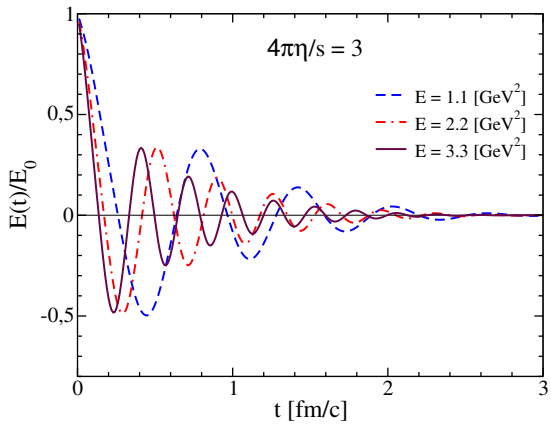

Figure 6.4: Time evolution of electric field E_z rescaled to the initial value E_0 for different values of E_0.

In Fig. 6.4 we plot time evolution of electric field for different intial value of E_0 keeping $\eta/s = 3/4\pi$: as we can see the decay time of E decreases for high value of E_0 causing also a faster damping of plasma oscillations. This picture figures out a possible interference among flux tubes with different electric field strength in a realistic collisions.

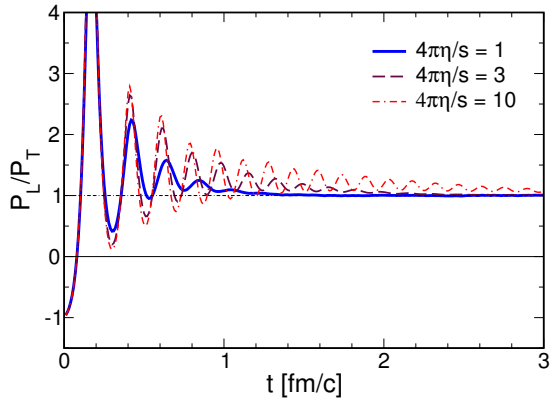

Figure 6.5: Time evolution of the ratio P_L/P_T for the static box, for several values of η/s.

We remind that one of the assumption of hydrodynamics calculations regards the fact that the system is isotropized at about $t = 0.6\, fm/c$, meaning that $P_L/P_T = 1$. It is mandatory to quantify how the system reaches dynamically such a state. In Fig. 6.5 we plot the time evolution of the ratio P_L/P_T for the case of the static box, for several values of η/s. As expected we find that for small values of η/s the system is very efficient in removing the initial anisotropy. We notice that the initial longitudinal pressure is negative and $P_L/\varepsilon = -1$; indeed at initial time the system is made of pure color electric field for which $T^{\mu\nu} = \mathrm{diag}\,(\varepsilon, P_T, P_T, P_L)$ with $\varepsilon = E^2/2$, $P_T = \varepsilon$ and $P_L = -\varepsilon$. On the other hand as soon as particles are produced by the Schwinger effect, they give a positive contribution to the longitudinal pressure and the field magnitude decreases, eventually leading to a positive pressure. Moreover because of the strong interactions among the particles produced, P_L and P_T tend to the same value within a very short time range, $\tau_{iso} \approx 1$ fm/c.

We notice that regardless of the value of η/s the system tends to remove the initial pressure anisotropy, which is quite natural in the case of the static box since collisions always lead to the equilibrium state. However isotropization times are different and indeed in the case of a weakly coupled system, see for example the case $4\pi\eta/s = 10$ in Fig. 6.5, the equilibrium state is reached in a much larger time than in the case of $4\pi\eta/s = 1$. Moreover the oscillations of the electric field strength in Fig. 6.3 lead to many oscillations of P_L/P_T in the case $4\pi\eta/s = 10$, such oscilations being damped effectively within the first fm/c in the case $4\pi\eta/s = 1$.

6.6.1 Energy conservation

In this subsection we check the energy conservation in our box calculations. Being the system initialized with a longitudinal electric field, the amount of total energy density is $\varepsilon_{tot} = E^2/2$. As the system evolves in time, the field energy decays due to particles creations while the particles energy increases because more particles account in the energy contribution of matter and because are accelerated by the electric field. In Fig. 6.6 we show the energy conservation as a function of time for three different value of $\eta/s = 1, 3, 10$. In each panel blue line is the energy density of the field, red line the energy density of particles while the green line is the total energy. As we can see, the method developed guaranties a excellent energy conservation also in the early time dynamics with only a 5% of discrepancy.

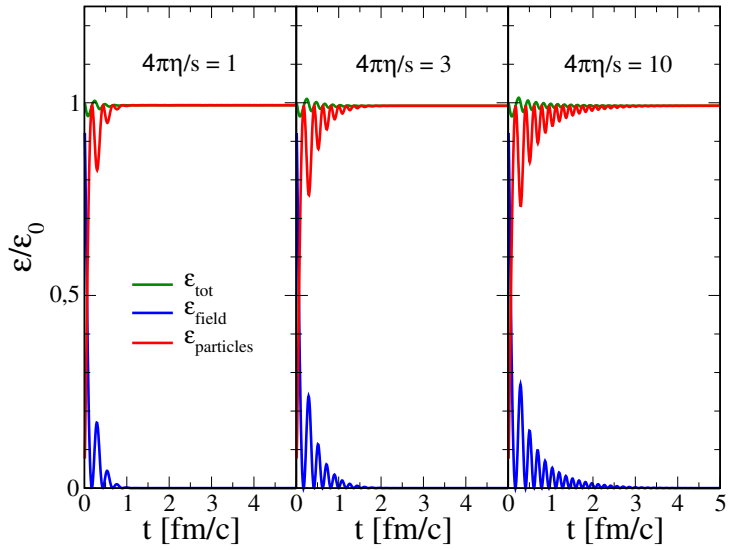

Figure 6.6: Energy density of the electric field, kinetic energy density of particles and the total kinetic energy as a function of time for three different values of shear viscosity $\eta/s = 1, 3, 10$.

6.7 Boost-invariant longitudinal expansion

In this Section we study the effect of a boost invariant longitudinal expansion on pair production from the decay of a chromoelectric flux tube. This case is interesting because a longitudinal expansion characterizes the very early stage of an ultra-relativistic collision process. We assume the expansion takes place along the direction of the electric field; moreover the dynamics is invariant for boosts along the longitudinal direction. For this case we will discuss more results because it is closer to the description of the central rapidity region in the early stages of a relativistic heavy ion collision.[180]

We remind very quickly the relevant equations in this case. The evolution equations for the color electric field are given by the pair of Maxwell equations

$$\frac{\partial E}{\partial z} = \rho \ , \qquad \frac{\partial E}{\partial t} = -j \ , \tag{6.39}$$

where both current and charge densities are computed in the laboratory frame. Assuming boost invariance along the longitudinal direction implies that $\mathcal{E}_z$ depends only on proper time $\tau = \sqrt{t^2 - z^2}$. We can combine the two Eqs. (6.39) to form a boost invariant equation, namely

$$\tau \frac{dE}{d\tau} = z\rho - tj \ , \tag{6.40}$$

which can be rewritten as

$$\frac{dE}{d\tau} = \rho \sinh\eta - j \cosh\eta \ , \tag{6.41}$$

where the right hand side corresponds to the (minus) electric current computed in the reference frame where the time is the proper time, namely the local rest frame of the fluid. Eq. (6.41) is in agreement with the boost invariant form of Maxwell equation used in Ref.[171]

To solve Eq. (6.41) we adopt a finite difference scheme and prepare a box with a square cross section in the transverse direction, with $-x_{max} \leq x \leq x_{max}$ and $-y_{max} \leq y \leq y_{max}$, and with cells in space-time rapidity, fixing the range of η in which we distribute the produced particles by $-\eta_{max} \leq \eta \leq \eta_{max}$ with $\eta_{max} = 2.5$. This implementation corresponds to have a box with a longitudinal expansion since from the well known equations of relativistic kinematics one gets $z_{max} = t \tanh\eta_{max}$ which, for η_{max} sufficiently large, corresponds to a wall moving at ultrarelativistic speed along the longitudinal direction. We

therefore distribute the pairs created by the decay of the flux tube with uniform probability in each of the cells in (x, y, η).

To take into account the longitudinal expansion Eq. (6.20) has to be modifed as[171, 180]

$$\frac{dN}{d^4x d^2p_T dy} = \mathcal{R}(p_T)\delta(w)v \ , \tag{6.42}$$

where y denotes the momentum rapidity; $\mathcal{R}(p_T)$ depends only on transverse momentum and it is not affected formally by the expanding geometry; moreover we have introduced the two boost-invariant variables

$$w = tp_z - zp_0 \ , \quad v = p_0 t - zp_z \ , \tag{6.43}$$

and $\delta(w)$ affects the longitudinal momentum distribution by forcing the condition

$$p_z = \frac{z}{t}p_0 = p_T \sinh\eta \tag{6.44}$$

for the produced pairs, with $p_0 = \sqrt{p_T^2 + p_z^2}$; such a condition is equivalent to assume that momentum rapidity of the produced pair is equal to space-time rapidity. The procedure we implement to create pairs in the case of the boost invariant longitudinal expansion is very similar to the one we have described in the case of the static box, the only difference being that in the present case we iterate the static box procedure for each rapidity cell.

6.7.1 Field decay, particle production and spectra

In Fig. 6.7 we plot the color electric field strength averaged in the central rapidity region $|\eta| < 0.5$ (main panel) and particle number produced per unit of transverse area and rapidity (inset panel) as a function of time. The calculations are shown for three different values of η/s (calculations at fixed total cross section give similar results); the relation among the total cross section and η/s we have used in the simulation is the CE relation with an isotropic cross section, see Eqs. (6.32) and (6.33). The electric field is averaged in the central rapidity region $|y| < 0.5$. The initial value we have used in the simulations is $E(t = 0) = 2.2\, GeV^2$ but we obtain similar results by changing this value within the range $0.5 \div 4\, GeV^2$. The initial value of the electric field is chosen in order to have a particle multiplicity in agreement with the expected multiplicity at a central RHIC collision, namely $dN/dy = 1040$ at midrapidity.

As for the case of the static box we find that for the case of boost invariant longitudinal expansion the chromoelectric field experiences a rapid decay for small values of η/s. Once again this is due to the fact that in this case

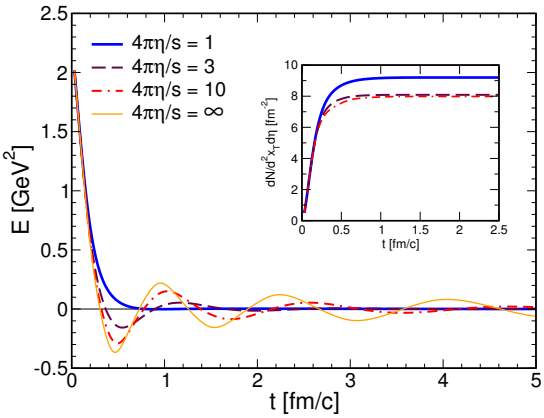

Figure 6.7: Chromoelectric field strength (main panel) and particle number produced per unit of transverse area and rapidity (inset panel) as a function of time. The electric field is averaged in the central rapidity region $|\eta| < 0.5$.

the coupling among particles is large, meaning collisions are very effective in randomizing particle momenta in each cell hence damping conductive currents that might sustain the field. On the other hand for intermediate and large values of η/s the electric field experiences stronger fluctuations during time evolution.

In the inset of Fig. 6.7 we plot the number of produced gluons per unit of transverse area and rapidity versus time. We find that regardless of the value of η/s we use in the simulation, the particles are produced at very early times, approximately within 0.5 fm/c, with the only expection of very few particles produced at later times in the case $4\pi\eta/s = 10$. We have checked that changing the initial value E_0 of the electric field does not modify the production time in a considerable way unless E_0 is very small, namely $E_0 \ll 1$ GeV^2. Moreover the value of η/s affects the conversion of the initial classical field to gluons only within a few percent: for example comparing the results for $4\pi\eta/s = 1$ and $4\pi\eta/s = 3$ we find in the latter case a lowering of less than 10% on the number of particles produced. We conclude that the Schwinger effect is a very efficient mechanism to produce a plasma from a classical color field.

In Fig. 6.8 we plot the proper kinetic energy density, ε_{kin}, at central rapidity ($|\eta| < 0.5$), versus laboratory time for three different values of η/s (calculations at fixed total cross section give similar results). The relation among η/s and cross section is fixed by the CE relation with an isotropic cross section. We find that in the case of small η/s, which corresponds to the case of a strongly coupled system, the energy density decays asymptotically as $\varepsilon_{kin} \propto t^{-4/3}$ which is what is expected in the ideal hydrodynamic limit in the case of a one-dimensional expansion, in agreement with Ref.[162] For the cases of larger

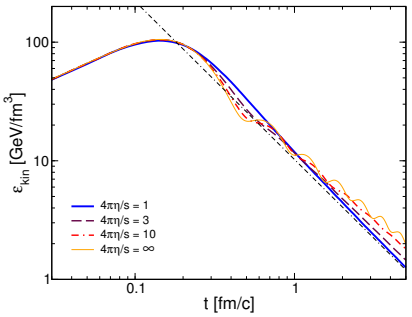

Figure 6.8: Proper kinetic energy density as a function of time averaged in the central rapidity region $|\eta| < 0.5$ and viscosity has been fixed using an isotropic cross section.

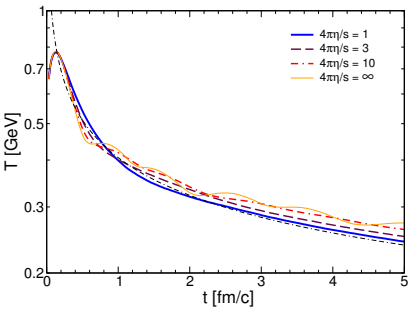

Figure 6.9: Local temperature as a function of time averaged in the central rapidity region $|\eta| < 0.5$ and viscosity has been fixed using an isotropic cross section.

η/s we find that a power law decay with a superimposed oscillation pattern is present. The thin dashed line in the figure corresponds to $t^{-4/3}$. These results are in good agreement with those of Ref.[171]

In Fig. 6.9 we plot the plasma temperature as a function of time; it is obtained by data shown in Fig. 6.8 by assuming a perfect gas equation of state which gives $T \propto \varepsilon_{kin}^{1/4}$ with proportionality constant being inversely proportional to the number of active degrees of freedom in the plasma. Our temperature is somehow larger than the one quoted in Ref.[171] because in the latter study both quarks and gluons have been considered in the plasma, while in our case we only include gluons. The thin dashed line corresponds to $t^{-1/3}$ which is the power law decay expected in the case of a one dimensional expansion of a non viscous fluid.

In Figs. 6.10, 6.11 and 6.12 we plot the gluon spectra at midrapidity $|y| < 0.5$, for three different values of η/s. For each value of η/s the spectrum at three different times is shown. The thin solid black line corresponds to a thermal spectrum, namely

$$\frac{dN}{p_T dp_T dy} \propto p_T e^{-\beta p_T}. \tag{6.45}$$

The above relation describes a thermalized system in three spatial dimensions at the temperature $T = 1/\beta$. In the figure the thermal spectrum is computed by taking the temperature at $t = 1$ fm/c from data plot in Fig. 6.9 . We find that for $4\pi\eta/s = 1$ the system efficiently thermalizes: in fact the spectrum at $t = 1$ fm/c is of the form Eq. (6.45) with temperature given (within a 2%) by the result in Fig. 6.9, as it is evident by comparing the thermal spectrum (black line) with simulation data (dot-dashed thin green line). For $4\pi\eta/s = 3$ and $4\pi\eta/s = 10$ the spectrum we obtain in the numerical calculation is in some

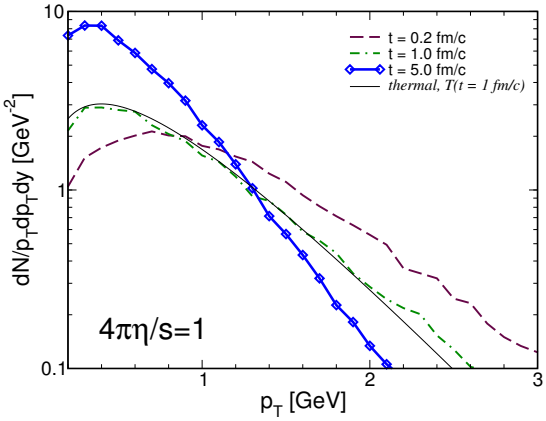

Figure 6.10: Gluon spectra at midrapidity $|y| < 0.5$, for $\eta/s = 1/4\pi$. The spectrum at three different times is shown. Black thin solid line corresponds to the thermal spectrum in Eq. (6.45) at $t = 1$ fm/c with temperature from data in Fig. 6.9.

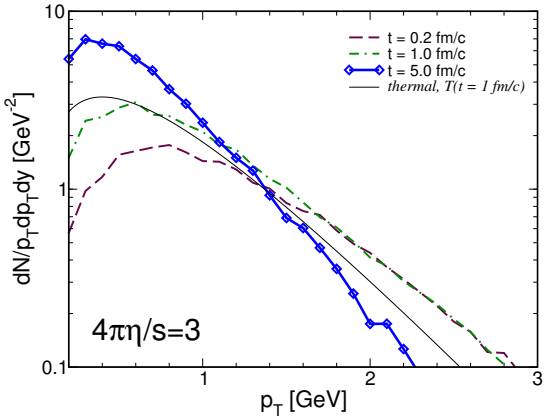

Figure 6.11: Gluon spectra at midrapidity $|y| < 0.5$, for $\eta/s = 3/4\pi$. The spectrum at three different times is shown. Black thin solid line corresponds to the thermal spectrum in Eq. (6.45) at $t = 1$ fm/c with temperature from data in Fig. 6.9.

disagreement with the thermal spectrum at the temperature plot in Fig. 6.9 at $t = 1$ fm/c, meaning the system is not completely thermalized in three dimensions. Moreover the very mild change in the slope of the spectrum we measure from $t = 1$ fm/c to $t = 5$ fm/c shows that the system does not cool down efficiently in this case, as it is expected because the large viscosity implies that a large part of energy dissipates into heat and the system cools down more slowly than the case of small viscosity.

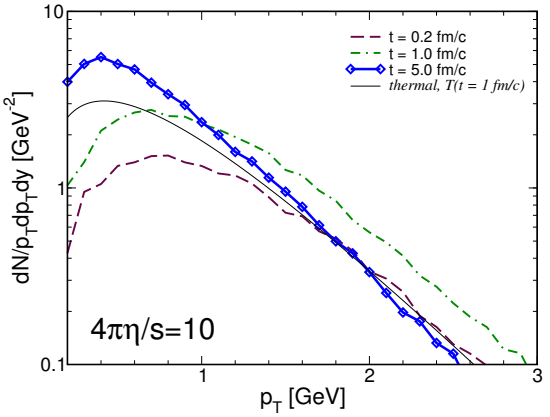

Figure 6.12: Gluon spectra at midrapidity $|y| < 0.5$, for $\eta/s = 10/4\pi$. The spectrum at three different times is shown. Black thin solid line corresponds to the thermal spectrum in Eq. (6.45) at $t = 1$ fm/c with temperature from data in Fig. 6.9.

6.7.2 Pressure isotropization

In this subsection we discuss pressure isotropization in the case with a longitudinal expanding geometry, which has a greater physical interest because it is closer to the picture of the early times dynamics of relativistic heavy ion collisions. Pressure isotropization is relevant to justify the initial time $\tau = 0.6\, fm/c$ in hydrodynamics calculations which assume that the system has reached $P_L/P_T = 1$. In Fig. 6.13 we plot the ratio P_L/P_T where once again P_L and P_T correspond to the longitudinal and transverse pressure respectively. These quantities are computed cell by cell in the local rest frame of the fluid, then averaged in the rapidity range $|\eta| < 0.5$. The initial longitudinal pressure at initial time is negative and $P_L/P_T = -1$ because at initial time the system is made of pure longitudinal chromoelectric field. On the other hand as soon as particles are produced, they give a positive contribution to the longitudinal pressure and the field magnitude decreases, eventually leading to a positive pressure. For all the value of η/s we consider in our simulations we find that the time needed to the total longitudinal pressure to be positive is about 0.2 fm/c. Moreover in the case $4\pi\eta/s = 1$ the strong interactions among the particles remove the initial pressure anisotropy quite efficiently and quickly: in this case $P_L/P_T = 0.7$ within 0.6 fm/c, then the ratio tends to increase towards 1 within the time evolution of the system. This would justify the use of viscous hydrodynamics with $\tau_0 \approx 0.6$ fm/c as commonly done.

On the other hand the larger the η/s of the fluid the larger the oscillations

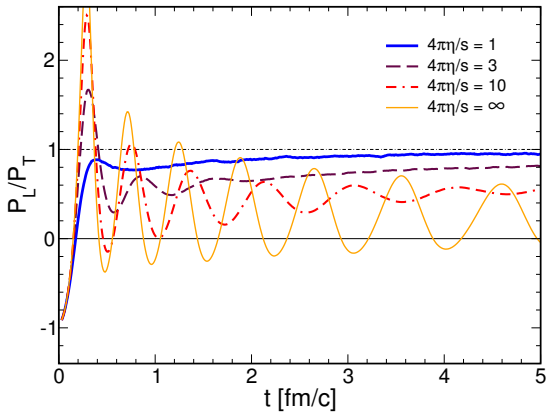

Figure 6.13: Proper kinetic energy density (upper panel), local temperature (middle panel) and the ratio P_L/P_T (lower panel) as a function of time. All the quantities are averaged in the central rapidity region $|\eta| < 0.5$ and viscosity has been fixed using an isotropic cross section.

of P_L/P_T, compare for example the cases $4\pi\eta/s = 1$ and $4\pi\eta/s = 10$ in Fig. 6.13: in the latter case P_L/P_T experiences several oscillations which follow the alternation of maxima of $|E|$ (corresponding to minima of P_L since the field gives a negative contribution to P_L) and zeros of E (corresponding to maxima of P_L); also, at large times P_L/P_T is quite smaller than 1. For intermediate values of η/s we still find some oscillation which become less important for smaller viscosities. On the same footing the asymptotic value of P_L/P_T approaches 1 when the viscosity becomes small.

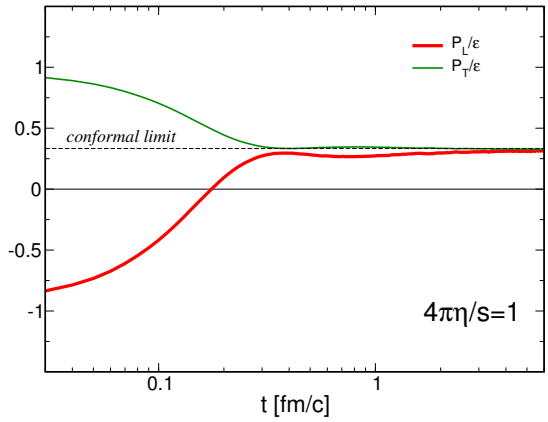

Figure 6.14: Ratios P_L/ε, P_T/ε against time for $4\pi\eta/s = 1$. All the quantities are averaged in the central rapidity region $|\eta| < 0.5$ and viscosity has been fixed using an isotropic cross section.

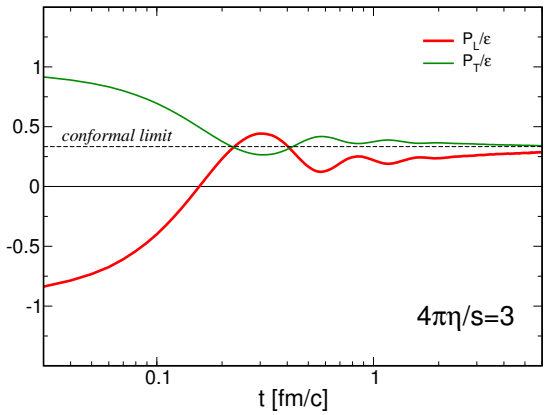

Figure 6.15: Ratios P_L/ε, P_T/ε against time for $4\pi\eta/s = 3$. All the quantities are averaged in the central rapidity region $|\eta| < 0.5$ and viscosity has been fixed using an isotropic cross section.

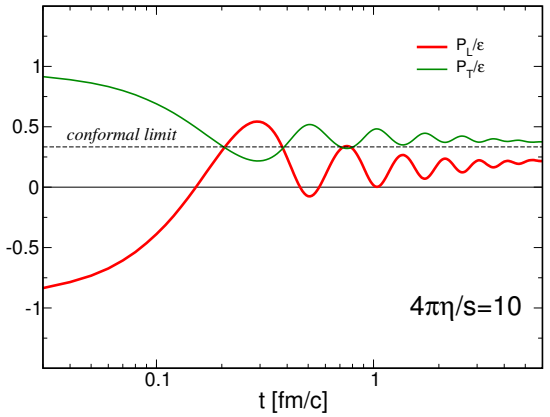

Figure 6.16: Ratios P_L/ε, P_T/ε against time for $4\pi\eta/s = 10$. All the quantities are averaged in the central rapidity region $|\eta| < 0.5$ and viscosity has been fixed using an isotropic cross section.

In Figs. 6.14, 6.15 and 6.16 we plot the ratios P_L/ε and P_T/ε as a function of time. Here ε corresponds to the total energy density, which takes into account energy density of both particles and field. We have shown results obtained for $4\pi\eta/s = 1$, $4\pi\eta/s = 3$ and $4\pi\eta/s = 10$. In Figs. 6.14, 6.15 and 6.16 the red solid line corresponds to P_L/ε and the thin green line to P_T/ε. The thin black dashed line corresponds to the conformal isotropic limit $\varepsilon = 3P$. One can compare the results of Figs. 6.14, 6.15 and 6.16 with those of,[135] where a classical Yang-Mills simulation with a $3+1$D expanding geometry is considered; in the weakest coupling case considered in Ref.,[135] namely $g = 0.1$, P_L asymptotically relaxes towards zero, which we might obtain if we introduce

a larger viscosity than the one we consider in the present study. On the other hand the case $g = 0.5$ from Ref.[135] produces P_L/ε and P_T/ε which lie in between our results for $4\pi\eta/s = 3$ and $4\pi\eta/s = 10$.

6.7.3 Anisotropic cross sections

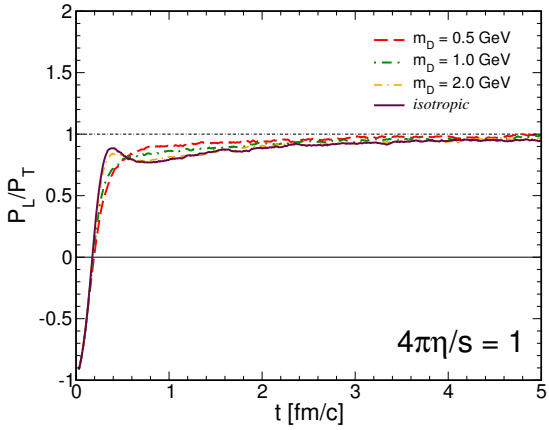

Figure 6.17: Ratio P_L/P_T versus time for several values of m_D for $\eta/s = 1/4\pi$. All the quantities are averaged in the central rapidity region $|\eta| < 0.5$.

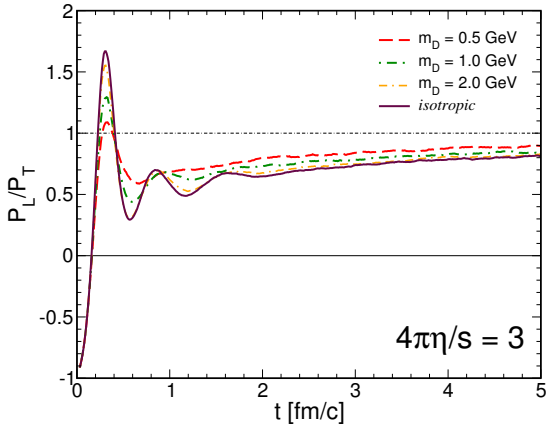

Figure 6.18: Ratio P_L/P_T versus time for several values of m_D for $\eta/s = 3/4\pi$. All the quantities are averaged in the central rapidity region $|\eta| < 0.5$.

In this subsection we study the effect of changing the microscopic cross section from isotropic to anisotropic. In our collision integral we achieve this by tuning the Debye screening mass in the two body cross section, leaving the value of

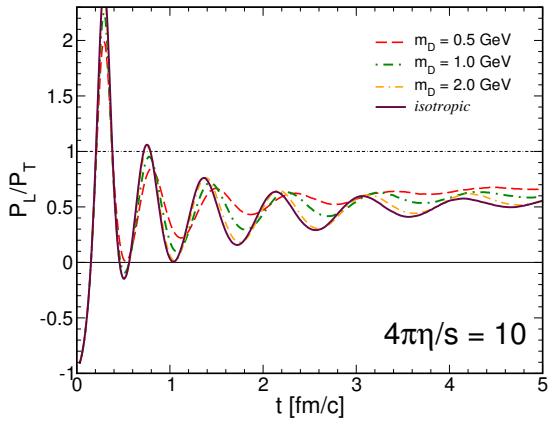

Figure 6.19: Ratio P_L/P_T versus time for several values of m_D for $\eta/s = 10/4\pi$. All the quantities are averaged in the central rapidity region $|\eta| < 0.5$.

η/s fixed. In Figs. 6.17, 6.18 and 6.19 we plot the time evolution of P_L/P_T for four different values of m_D for the case of $4\pi\eta/s = 1$, $4\pi\eta/s = 3$ and $4\pi\eta/s = 10$, and four different values of the Debye screening mass m_D. We remind that in our calculation the Debye mass is used as an infrared regulator of the differential cross section, and as a parameter which controls the anisotropy of the cross section: for very large values of m_D the differential cross section is isotropic, while for small values of m_D we get a forward peaked cross section. We find that lowering m_D for a given value of η/s the plasma oscillations tend to be damped. This can be understood because according to the study of Chapter 4 and Ref.[68] lowering m_D while keeping fixed η/s amounts to increase isotropization of the distribution function; as a consequence the conductive currents, which would sustain plasma oscillations in the late times evolution of the plasma, are damped. Nevertheless the effect on late time evolution of P_L/P_T is quite mild.

6.7.4 Chapman-Enskog vs. Relaxation Time Approximation

In this subsection we study the effect of shifting from the CE to RTA when we relate η/s to the total cross section. It has to be noticed that our RTA does not correspond to the RTA used in Ref.:[171] in fact in Ref.[171] RTA corresponds to an ansatz for the collision integral in the Boltzmann equation; on the other hand in our calculations, where we always solve the full collision integral in the Boltzmann equation, RTA refers only to an analytical equation which connects shear viscosity to microscopic cross section as in Chapter 4 and Ref.[68] We

limit ourselves to a particular value of η/s, namely $4\pi\eta/s = 3$ which is the intermediate case we have considered in the previous subsections. In Fig. 6.20 and Fig. 6.21 we plot P_L/P_T as a function of time for two values of m_D: on the left panel we consider $m_D = 0.5$ GeV and in the right panel $m_D = 2$ GeV. In each panel, the red dashed line corresponds to the CE formula while the dot dashed blue line to the RTA formula. In the case of $m_D = 0.5$ GeV the oscillations of P_L/P_T with CE are quite damped with respect to those of the RTA. This behaviour is easily understood by the results obtained in Chapter 4 and Ref.:[68] as a matter of fact a given η/s corresponds to a lower cross section for RTA, implying larger conductive currents which sustain plasma oscillations. In the case of $m_D = 2.0$ GeV the behaviour of P_L/P_T in RTA is similar to that in CE; in fact in this case the cross section is mostly isotropic, and it is known that RTA cross section is quite close to the CE one.

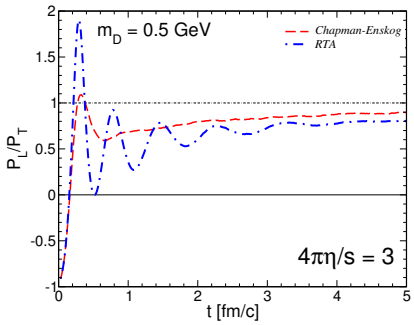

Figure 6.20: Ratio P_L/P_T versus time for $4\pi\eta/s = 3$ and for $m_D = 0.5$ GeV. We compare the Chapman-Enskog result (dashed red line) with the Relaxation time result (dot-dashed blue line).

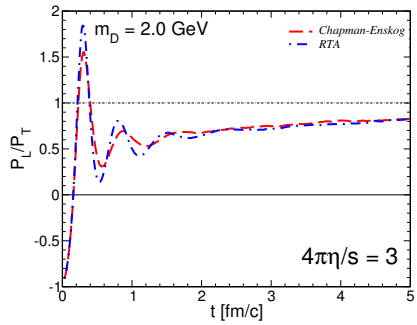

Figure 6.21: Ratio P_L/P_T versus time for $4\pi\eta/s = 3$ and for $m_D = 2.0$ GeV. We compare the Chapman-Enskog result (dashed red line) with the Relaxation time result (dot-dashed blue line).

6.8 3+1D expanding system

In this section we extend our previous results to the more realistic case of a 3+1D expanding system. While in the 1+1D geometry, due to the periodic boundary conditions in the transverse plane, no transverse components of the electric field develope since j_x and j_y are zero, in the 3+1D expansion we have to consider also transverse components of currents and electric field. We still neglect magnetic component of the color field. The evolution equations for the

color electric field are given by the following Maxwell equations:

$$\nabla \cdot \mathbf{E} = \rho \tag{6.46}$$

$$\frac{\partial \mathbf{E}}{\partial t} = -\mathbf{j} \tag{6.47}$$

where the current and charge density depend also on the transverse coordinate x and y. We still implement an initial condition in which only the longitudinal component of the field is non zero; transverse components will be generated by transverse currents in agreement with Eq. (6.47).

Assuming for sake of simplicity the boost invariance along the longitudinal direction implies that E_z depends on the proper time $\tau = \sqrt{t^2 - z^2}$. Combining Eqs. (6.46) and (6.47), one obtains the following equation for the z-component of the electric field:

$$\frac{\partial E_z}{\partial \tau} = \rho \sinh \eta - j_z \cosh \eta - \sinh \eta \left(\frac{\partial E_x}{\partial x} + \frac{\partial E_y}{\partial y} \right) \tag{6.48}$$

where the electric current and the charge density are computed in the local rest frame of the fluid. The equations for the transverse component electric field are:

$$\frac{\partial E_x}{\partial t} = -j_x \tag{6.49}$$

$$\frac{\partial E_y}{\partial t} = -j_y. \tag{6.50}$$

To solve Eqs. (6.48), (6.49) and (6.50), we use a finite difference scheme and a discretized spacetime using (x, y, η) coordinates. We choose the following cell dimensions in the transverse plane: $\Delta x = 0.5\, fm$ and $\Delta y = 0.5\, fm$. The time step is chosen as $dt = 0.01\, fm/c$. Regarding the space-time rapidity range, we choose $-\eta_{max} \leq \eta \leq \eta_{max}$ with $\eta_{max} = 2.5$. This implementation corresponds to the 1+1D expanding system of the previous section apart the fact that in this case there are no boundary conditions on the (x, y) plane. The procedure implemented in order to create pairs is equivalent to the one used for the longitudinal expansion, however Eq. (6.42) has to be evaluated in each $\Delta x \times \Delta y \times \Delta \eta$ volume.

We checked that the present implementation, restricted with the same boundary conditions of the 1+1D system, reproduces exactly the same results for the electric field time dependence, number of particles produced, particle spectra and isotropization for different values of shear viscosity.

6.8.1 Initial condition

In this subsection we discuss about the initial conditions for the color electric field. In our calculations we choose an initial condition that mimics the eccentricity obtained in the Glauber model at a given impact parameter. In details, the almond shape of the overlap region between the two colliding nuclei in the transverse plane gives the domain for the electric field: we assume a uniform electric field on the transverse plane, inside the overlap region, and also in the space-time rapidity region $|\eta| < 2.5$. We checked that the eccentricity of such a configuration is equal to the one obtained in the Glauber model. The only parameter to be fixed is the value of the initial color electric field which we fix in order to reproduce the particle multiplicity dN/dy from experimental results. In such a way we reproduce a system with a given initial eccentricity, which corresponds to a given impact parameter, and a given multiplicity due to the decay of the initial color electric field to a plasma.

6.8.2 Field decay, particles production and spectra

In FIg. 6.22 we plot the color electric field strength averaged in the central rapidity region $|\eta| < 0.5$ and in $|x|, |y| < 0.5\, fm$. Three different cases are shown which correspond to fixing $4\pi\eta/s = 1$ for the blue line, $4\pi\eta/s = 3$ maroon dashed line and $4\pi\eta/s = 10$ red dot-dashed line. Shear viscosity is fixed using our results of Chapter 4 as already done in the case of 1+1D expanding system of the previous section. As we can see in Fig. 6.22 the color electric field E_z has a rapid decay of about $1\, fm/c$ indipendently of the value of viscosity. The plasma oscillations that we see in Fig. 6.7 for high value of shear viscosity, in the present case are damped due to the transverse expansion of particles, or in other words due to the missing electric current which can sustain the electric field. In the inset of Fig. 6.22 we show the transverse component of the color electric field for the case $4\pi\eta/s = 1$: orange line represents E_x while green line E_y. As we can see such components do not have effects on the dynamic of the system since no electric currents develop in the transverse plane.

In Fig. 6.23 we show the total number of particles produced for the corresponding case of an impact parameter $b = 7.5\, fm/c$ using an initial color electric field $E_z = 2.2\, GeV^2$. Independently of the value of η/s, particles are produced in the first $0.5\, fm/c$. As in the 1+1D case (see Fig. 6.7), η/s affects in a small way the conversion of the initial color electric field to particles: comparing

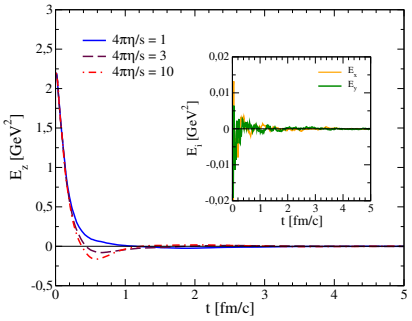

Figure 6.22: Color electric field z component as a function of time in the central region $\eta < 0.5$ and $x, y < 0.5\, fm$, for different value of η/s. Blue line corresponds to $\eta/s = 1$, maroon dashed line to $\eta/s = 3$ and red dot-dashed line to $\eta/s = 10$. In the inset x and y component for the case $\eta/s = 1$.

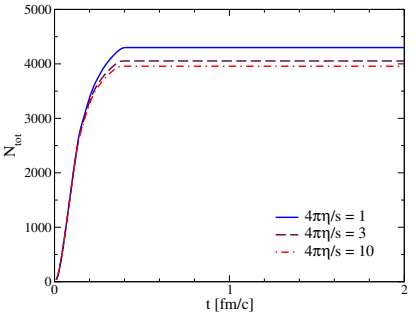

Figure 6.23: Total number of particles produced as a function of time for different values of η/s. In this simulations we set the initial color electric field $E_z = 2.2\, GeV^2$ and the impact parameter $b = 7.5\, fm$.

results for $4\pi\eta/s = 1$ with $4\pi\eta/s = 3$ there is a lowering of 6% in number of produced particles.

In Fig. 6.24 we plot the temperature as a function of time averaged in the central rapidity region $|\eta| < 0.5$ and $|x|, |y| < 0.5\, fm$. It has been computed in the local rest of the fluid assuming a perfect gas equation of state using $T \propto \varepsilon_{kin}^{1/4}$ with proportionality constant being inversely proportional to the degrees of freedom of the plasma. The temperature scales as $t^{-1/3}$ for $t < 6\, fm/c$ because the longitudinal expansion is the dominant one while at later times there is a change in the slope meaning that the transverse expansion begins having effects.

In Fig. 6.25 we show particles spectra in the midrapidity region $|y| < 0.5$ for the case of two different centralities corresponding to impact parameters $b = 2.5\, fm$ on the left panel and $b = 7.5\, fm$. In both simulations we fixed $4\pi\eta/s = 1$. The red line corresponds to the spectrum at $t = 0.1\, fm/c$. The system thermalizes in $4 \div 6\, fm/c$ as we can see comparing the maroon double-dot-dashed line with orange squares, which correspond to the spectrum at final time $t = 10\, fm/c$.

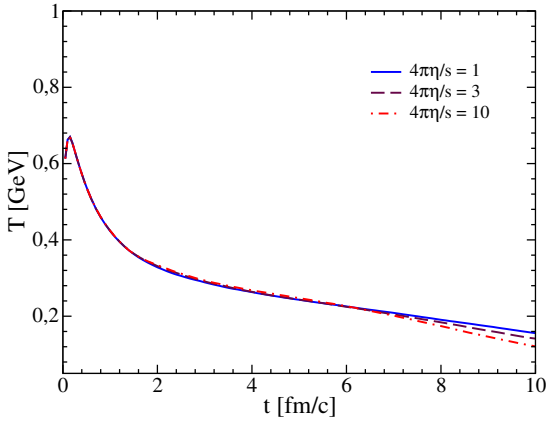

Figure 6.24: Local temperature, averaged in the central rapidity region $|\eta| < 0.5$ and $|x|, |y| < 0.5 fm$, as a function of time for different values of η/s.

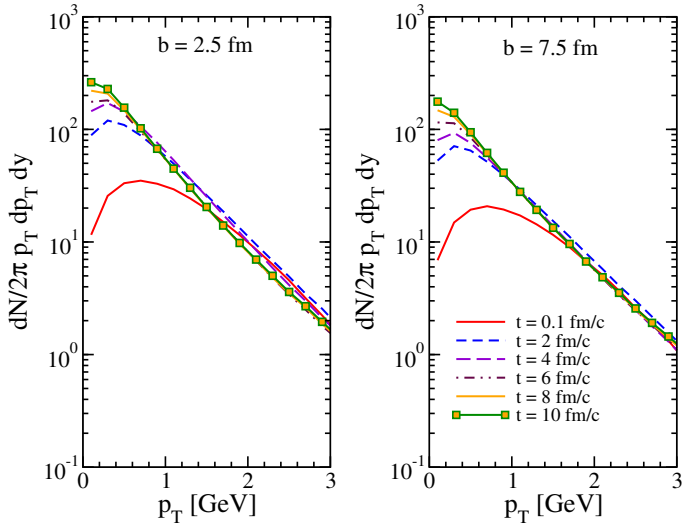

Figure 6.25: Particles spectra as a function of transverse momentum p_T. Left panel: results are obtained for an impact parameter $b = 2.5\, fm$. Right panel: results are obtained for an impact parameter $b = 7.5$. In these simulation η/s was fixed to $1/4\pi$.

6.8.3 Pressure isotropization

In Fig. 6.26 we plot the ratio of longitudinal pressure P_L over the transverse pressure P_T. Such quantities are computed in the local rest frame of the fluid cell by cell and averaged in the central rapidity region $|\eta| < 0.5$ and

$|x|, |y| < 0.5\, fm$. The initial $P_L/P_T = -1$ since the initial electric field E_z is purely longitudinal. As particles are produced, they contribute with a positive longitudinal pressure while the field strength decreases giving a positive pressure. Independently of η/s, P_L/P_T becomes positive in $0.2\, fm/c$. Comparing results of Fig. 6.26 with those of the 1+1D case in Fig. 6.14, we see that qualitatively P_L/P_T shows the same behaviour as the η/s is increased: large oscillations are obtained for $\eta/s = 10$ while, decreasing η/s oscillations are damped. However, as shown in the field decay in Fig. 6.22,oscillations of P_L/P_T are damped in the 3+1D case in the first $3\, fm/c$ for $4\pi\eta/s = 10$ down to $1\, fm/c$ for $4\pi\eta/s = 1$. The case $4\pi\eta/s = 1$ reaches $P_L/P_T = 0.6 \div 0.7$ in about $1\, fm/c$, within the same time scale of the 1+1D case while the other cases with higher value of viscosity mantain a greater state of non-isotropization respect with to the previous study.

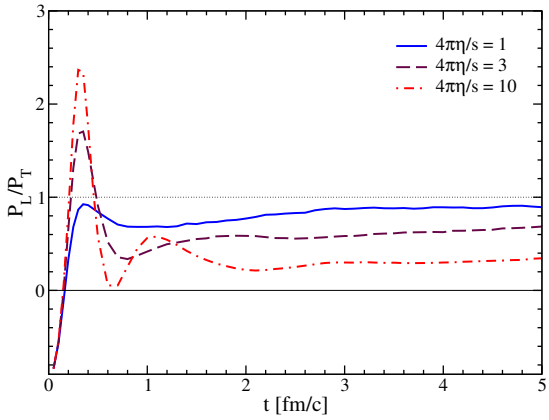

Figure 6.26: Longitudinal pressure P_L over transverse pressure P_T as a function of time for different values of η/s. The values calculated are average in the central rapidity region and $|x|, |y| < 0.5\, fm$.

6.8.4 Elliptic flow

In this subsection we discuss about the elliptic flow of the plasma produced by the decay of the initial color electric field with the aim of study the effects of initial non-equilibrium condition into the developing of momentum anisotropy. As already discussed in Chapter 1, the origin of the elliptic flow is the initial eccentricity in space coordinate

$$\varepsilon_x = \frac{\langle y^2 - x^2 \rangle}{\langle x^2 + y^2 \rangle} \tag{6.51}$$

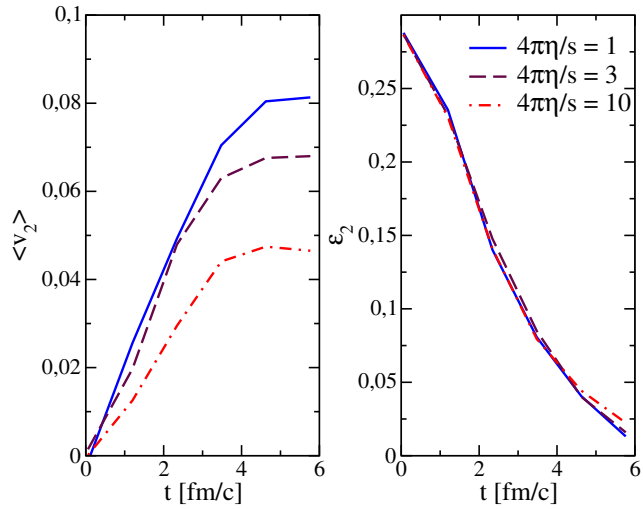

Figure 6.27: Left panel: averaged elliptic flow v_2 as a function of time for differen values of η/s. Right panel: eccentricity ε_2 as a function of time for different value of η/s. In these simulations the impact parameter is $b = 7.5\, fm$.

given by the overlap region of the two colliding nuclei in non-central collision. The eccentricity is responsible for different pressure gradients in the transverse plane favoring the flow along the x direction rather than the y direction. The eccentricity is converted into an anisotropy in momentum space which is measured by the elliptic flow v_2 defined as:

$$v_2 = \left\langle \frac{p_x^2 - p_y^2}{p_x^2 + p_y^2} \right\rangle . \tag{6.52}$$

In the left panel of Fig. 6.27 we show the averaged elliptic flow $\langle v_2 \rangle$ as a function of time for different value of η/s: blue line represents the system wiith $\eta/s = 1/4\pi$, maroon dashed line with $\eta/s = 3/4\pi$ and red dot-dashed line $\eta/s = 10$. The effect of a small η/s is to make the system more efficient in converting the initial eccentricity into the momentum anisotropy. Indeed as we can see from Fig. 6.27 as η/s is increased, the system produce less $\langle v_2 \rangle$. On the right panel of Fig. 6.27 we plot the eccentricity ε_2 as a function of time for three different values of viscosity corresponding to the simulations of the left panel in the same figure. The initial $\varepsilon_2 \simeq 0.28$ is equal to the ε_2 obtained in the Glauber model considering an impact parameter $b = 7.5\, fm$, as it has to be in according of our initial condition discussed in Subsection 6.8.1. Initial eccentricity decreases as the system evolves in time independently of the value of shear viscosity.

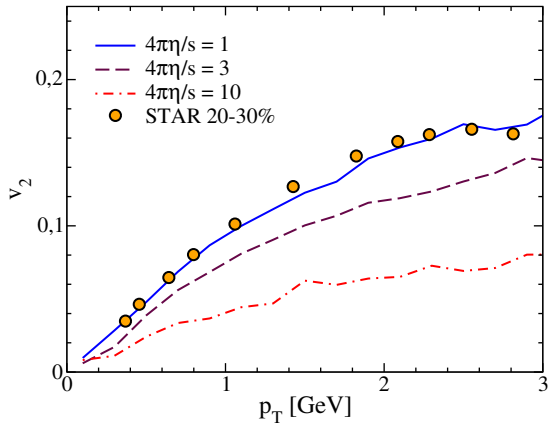

Figure 6.28: Elliptic flow $v_2(p_T)$ as a function of transverse momentum p_T. Blue line represents the case of $4\pi\eta/s = 1$, maroon dashed line of $4\pi\eta/s = 3$, red dot-dashed line $4\pi\eta/s = 10$. The impact parameter is $b = 7.5\, fm$.

In Fig. 6.28 we show our results for the differential elliptic flow for the case of $Au - Au$ at $\sqrt{s} = 200\, A\, GeV$ with an impact parameter $b = 7.5\, fm$, corresponding to the $20-30\%$ centrality class at RHIC. The blue line represents the simulations using $\eta/s = 1/4\pi$, maroon dashed line $\eta/s = 3/4\pi$ and red dot-dashed line $\eta/s = 10/4\pi$. We plot also experimental data for v_2 from the STAR Collaboration.[185]

We remind that in our simulations there is no hadronization process: to make a comparison we assume quark-hadron duality which implies that for each parton a single hadron is produced. So the agreement/disagreement with data is to be taken with caution nevertheless we see that the azimuthal asymmetries produced go in the right direction. Moreover, the initial condition for the color electric field, assumed in this work uniform in transverse plane, is a very rough description of the intial configuration of the fields in the overlap region. A more accurate description should include at least a Glauber-like profile in the transverse plane as one can figure out considering that in the central overlap region more color sources are present respect with the margins of the almond shape. Nonetheless we have set a space distribution that have the same eccentricity of the Glauber initial condition along with a similar average size R. This can allow a direct comparison for understanding the impact of the initial non-equilibrium field configuration. In Fig. 6.29 we show the evolution of the differential elliptic flow at fixed transverse momentum $p_T = 1.5\, GeV$ as a function of time. We compare our results to a study on the effects of non-equilibrium initial conditions on the elliptic flow.[178] In particular we show by green dashed line the factorized KLN, according to a modelization of the color Glass Condensate, which corresponds to an initial distribution far from

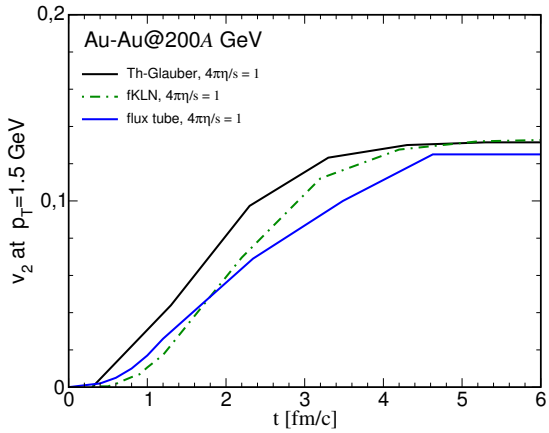

Figure 6.29: Evolution of v_2 as a function of time at fixed $p_T = 1.5\,GeV$ for different initial conditions for $Au - Au$ collisions at $\sqrt{s} = 200\,A\,GeV$ with impact parameter $b = 7.5\,fm$. Black line represents results starting with an initial condition from a thermalized Glauber model,[178] green-dashed line is a far from equilibrium initial condition fKLN,[178] blue line is our result using the flux tube model.

the thermalized one, black line in the figure denoting a thermalized Glauber model. The non-equilibrium initial condition has the effect of slowing the building up of the v_2 in the early stage of evolution ($t < 1\,fm/c$) while as the system evolves the v_2 of fKLN reaches the same momentum anisotropy of the Th-Glauber initial condition whose v_2 is larger then the previous case in the early stage, being the system already thermalized.
Our results, blue line, behaves in a similar way of the non-equilibrium initial condition fKLN: in the early stage the elliptic flow is built up very slowly however the system reaches a momentum anisotropy very close to the thermalized initial condition (black line).

We want to stress that, in order to have a more quantitative comparison with data, a more realistic initial configuration for the color electric field has to be taken into account exploring also other impact parameter. Nevertheless, the results in our explorative study are encouraging because they show that we are able to obtain the correct anisotropic flow even with a simplified initial configuration for the classical field, thus paving the way to more refined and realistic calculations.
Furthermore this first exploratory study shows that even if the initial-non equilibrium can slow down the build of the v_2 somehow the system is able to reach an almost identical elliptic flow with respect to the case of equilibrium initial conditions at a typical time of $0.5 \div 1\,fm/c$ as done in the hydrodynamical approach.

Conclusions and outlooks

In this thesis two main subjects directly related with the Quark-Gluon Plasma (QGP) and the ultra-relativistic heavy ions collisions were presented in the framework of Relativistic Boltzmann Transport equation. A study of transport coefficients, in particular shear viscosity η and electric conductivity σ_{el} with their dependence on microscopic details. A model on early time dynamics of the system produced in heavy ion collisions by an initial color electric field which then decays to a plasma by the Schwinger mechanism, with the aim of quantify the isotropization, thermalization and also the effects of the initial non-equilibrium condition on the elliptic flow.

The relevance of the study of transport coefficients resides in the importance of the shear viscosity and electric conductivity of the QGP.
Being η/s the most important physical quantity in the description of a fluid, our transport based approach focuses on keeping fixed η/s instead on dealing with all the specific amplitude scatterings one has to consider in the collision integral of the Boltzmann equation. Having this outlook in mind, the first task is to find the correct formula for shear viscosity which allows us to develop a very precise transport code simulating a fluid with a given η/s.
We compute the shear viscosity solving numerically the Relativistic Boltzmann Transport equation using the Green-Kubo relations. In Linear Response Theory Green-Kubo relations give us an exact formula for evaluate transport coefficients in terms of correlation functions of currents evaluated at the thermal equilibrium. After a convergency study of the numerical calculation of Gree-Kubo correlator, we compute shear viscosity for a generic anisotropic two body elastic cross section and compare our numerical results to analytical formulas derived in Relaxation Time Approxiamtion (RTA) and in Chapman-Enskog (CE) scheme. RTA is based on a crude approximation of the collision integral in the Boltzmann equation encoding all the informations in a relaxation time τ which represents the typical time scale to relax toward the equilibrium state. The CE scheme is based on a linearization of the collision integral.
We find that RTA is a good approximation only in the isotropic limit while the CE is in very good agreement with Green-Kubo results for all the range of temperature and anisotropy explored, in the range of interest for heavy ions collisions. Once the correct formula for shear viscosity has been selected, we are able to fix η/s in our transport code with very good accuracy and simulate the fireball evolution with the same language of hydrodynamics but in a wider range of transverse momentum of particles and also in out-of-equilibrium initial conditions.

The other transport coefficient under our investigation is the electric conductivity σ_{el} of the QGP. We compute σ_{el} using our numerical solution of the

Boltzmann equation and also in this case we study the microscopic dependence of σ_{el} on the particular scattering, isotropic or anisotropic cross section, exploring also massless and massive particles showing a very similar behavior of shear viscosity η. In general we discuss the relation between σ_{el} and the relaxation time τ which is underestimated by the Drude relaxation time $\tau = 1/\rho\sigma$, being ρ the density and σ the cross section. Being interested in a more realistic case and in a comparison with Lattice QCD results, we employed a quasi-particle model in order to take into account the thermodynamics of strongly interacting matter. We find that in this general case the Relaxation Time Approximation underestimates the electric conductivity Gree-Kubo results of about a factor 2. Moreover, for the first time, we investigated the connection between the shear viscosity to entropy density ratio and the electric conductivity fixing the thermodynamics using the Lattice QCD equation of state. We predicted that the recent Lattice QCD data of σ_{el} are compatible with the minimum value of η/s.
We discussed why the ratio of $(\eta/s)/(\sigma_{el}/T)$ supplies a measure of the quark to gluon scattering rates. We predicted that the ratio is independent of the running coupling $\alpha_s(T)$, is sensitive only on the quark scattering rates, increases near the critical temperature up to $\simeq 20$ while it goes down to a nearly flat behaviour around $\simeq 6$ for $T \geq 4\,T_c$. Moreover we in general found a stronger T dependence of σ_{el}/T with respect to η/s: in a our approach this extra temperature dependence is constrained by Lattice QCD thermodynamics while AdS/CFT calculations, instead, predicts a flat behaviour of both η/s and σ_{el}/T.

Employing our numerical solution of the Relativistic Boltzmann Transport equation we are able to calculate also the color conductivity which is very important in the early time dynamics of the QGP as it characterizes the response of the system to the strong chromoelectric and chromomagnetic fields present in the first stage of the collision. Our attention was captured by the early time dynamics of the QGP and in particular our challenge was to describe the QGP evolution starting from $t = 0^+$, when only color fields are present, to the final time, when collective flows are produced, using a single consistent scheme. The knowledge about the shear viscosity and the electric conductivity has allowed to pursue a key development of the partonic dynamics that incorporates the initial color electric fields following the dynamics of the color electric currents in the intial state of the collisions for a fluid with the scattering rates that merge into a fluid at $\eta/s \sim 0.1$. At the collision time $t = 0^+$ the Glasma is produced: it consists of an ensemble of strong longitudinal color electric and color magnetic coherent fields.
A mechanism responsible for the initial field decays is the one introduced by Schwinger in the context of Quantum Electrodynamics, known as the Schwinger effect which consists in a vacuum instability towards the creation of particle

pairs by a strong electric field.
We modelled early times dynamics of the system produced in relativistic heavy ion collisions by an initial color electric field which then decays to a plasma by the Schwinger effect studying the effects of η/s on the isotropization, thermalization and also on collective flows. According to the general understanding of high energy collision processes, this work is relevant both for heavy ion collisions, where a large number of flux tubes is expected, and for proton-nucleus and proton-proton collisions.

We extended our transport code in order to couple the dynamical evolution of the initial color field to the dynamics of the many particles system produced by the decay. Moreover, using our numerical solution of the Boltzmann equation, we improved previous studies which mainly rely on Relaxation Time Approximation (RTA) or on a linearization of the conductive electric current. We assume that the dynamics of the color field is abelian, hence it satisfies the classical field Maxwell equations and we neglect the longitudinal color magnetic field.
We have focused on the calculation of P_L/P_T, being P_L the longitudinal pressure and P_T the transverse one, in order to quantify the isotropization time, that in hydrodynamic calculation is assumed to be equal to $0.6 \div 0.8\, fm/c$. Thanks to the study of the shear viscosity in the first part of the thesis, we are able to study the effects of η/s on P_L/P_T. We have studied in a systematic way different cases starting from the static box with periodic boundary contitions. Such a case represents not only an achademic interest but also the guideline for interpreting the physical results obtained like for example the decay of the color electric field in about $1\, fm/c$ and the isotropization of the longitudinal pressure P_L over the transverse pressure P_T in $1\, fm/c$ for $\eta/s = 1/4\pi$. The cases with higher value of η/s show plasma oscillations and require a larger time to isotropize.
Then we considered a system with a longitudinal expansion which has a greater physical interest than the static box as it is closer to the picture of the early times dynamics of relativistic heavy ion collisions. In this case we found that the electric field exhibits a rapid decay for small η/s while for intermediate and high value of shear viscosity strong oscillations during the time evolution. The results obtained for the P_L/P_T show that the system reaches a state of isotropization in about $1\, fm/c$ for $\eta/s = 1/4\pi$. For $\eta/s = 3/4\pi, 10/4\pi$ the ratio experiences several oscillations and the aymptotic value of P_L/P_T is quite smaller than 1 indicating that the system does not isotropize. This would justify the use of viscous hydrodynamics with initial times $\tau_0 \simeq 0.6 \div 0.8\, fm/c$ for $4\pi\eta/s = 1 \div 3$. It remains to be understood if the oscillations of P_L/P_T for $t \leq 1\, fm/c$ affect some observables in ultrarelativistic heavy ion collisions. Our results imply that for a fluid with $4\pi\eta/s \leq 3$ isotropization time is less than $1\, fm/c$.

Finally we extend the longitudinal expansion case to a more realistic 3+1D expanding system. In this case we obtained that the oscillation of both color electric field and P_L/P_T are damped respect to the previous case because of transverse expansion. The ratio P_L/P_T saturates close to the isotropic limit within $1.5 \div 2\, fm/c$ for $\eta/s = 1/4\pi$ while for higher value of viscosity P_L/P_T is quite smaller than 1 meaning that the system does not isotropize. We found that indipendently of the value of shear viscosity the particles are produced in the first $0.5\, fm/c$.
Using our 3+1D code we also investigated the effects of the non-equilibrium initial condition and η/s on the building up of the elliptic flow. We calculated the elliptic flow for a case of interest of $Au-Au$ collision at $200\, GeV$, A at RHIC for an impact parameter of $b = 7.5\, fm$. In order to fix the initial eccentricity in our simulations, we assumed a uniform electric field on the transverse plane inside the overlap region of the two colliding nuclei. Such an initial condition is only a rough model however it gave us the possibility of investigating the elliptic flow and its dependence on shear viscosity. We found that the model predicts the decreasing of the differential elliptic flow with the increasing of the shear viscosity in agreement with hydrodynamics simulations. Moreover we found that the v_2 time evolution is compatible with other non-equilibrium initial conditions, namely fKLN. In details the v_2 in the early time evolution increases slowly with respect to a thermalized Glauber model however, at later time, the v_2 predicted in our model saturates to a value very close to the thermalized model one.

The results of the present work can be a starting point for further investigations both on the transport coefficients and early time dynamics sides. On one hand it would be very interesting to investigate the bulk viscosity of the QGP. The bulk viscosity represents the internal friction of a fluid when it rapidly expands as the QGP in heavy ion collisions. Furthermore, the study of electric conductivity can be extended to the case of color conductivity which is of great interest in the early time dynamics of ultra-relativistic heavy ion collisions.
On the other hand, our early time dynamics model needs improvements in particular on the initial condition of the color electric field in order to develop a more realistic framework devoted to study in a quantitative way collective flows. In addition the inclusion of fluctuations both in transverse plane and longitudinal direction would provide a systematic study on the higher harmonics v_n.
Furthermore isotropization and thermalization should be studied within the inclusion of the initial longitudinal color magnetic fields which in the present work was neglected.
In addition, using the approach developed in this thesis, it will be possible to investigate other observables such as the photon production. Photons represent one of the most important observables to understand the early time dynamics

since, even if produced in the early stage of the fireball evolution, they do not strongly interact with the QGP medium allowing a better access to the initial dynamics.

Appendix

.1 Natural units

Natural units are defined as $\hbar = c = 1$:

$$\hbar \equiv \frac{h}{2\pi} = 6.5821 \times 10^{-25}\, GeV\, s = 1 \tag{.53}$$

$$c = 2.9979 \times 10^{8} \frac{m}{s} = 1. \tag{.54}$$

These units have the following consequences: $[c] = [L][T]^{-1}$, i.e. $[L] = [T]$; $E^2 = p^2c^2 + m^2c^4$ leads to $[E] = [m] = [p]$. Furthermore $[\hbar] = [E][T]$ gives $[E] = [m] = [L]^{-1} = [T]^{-1}$. Therefore $[m]$, or equivalently $[E]$, can be chosen as a single independent dimension in natural units. From Eq. (.53) one obtains the following useful numerical relation:

$$\hbar c = 197.33\, MeV\, fm \simeq 200\, MeV\, fm. \tag{.55}$$

Moreover, we set also $k_B = 1$, with k_B the Boltzmann constant:

$$k_B = 8.6173 \times 10^{-14}\, GeV\, K^{-1} = 1 \tag{.56}$$

Thus a temperature of $1\, GeV$ is equal to

$$1\, GeV = 1.1605 \times 10^{13}\, K. \tag{.57}$$

.2 Rapidity and pseudorapidity

At relativistic energies, it is useful to use the rapidity instead of the standard velocity. It is defined as:

$$y = \frac{1}{2} \log \frac{E + p_\parallel}{E - p_\parallel} = \operatorname{arctanh}\left(\frac{p_\parallel}{E}\right) = \operatorname{arctanh}(v_\parallel) \tag{.58}$$

where E is the energy of a particle, $E = \sqrt{\mathbf{p}^2 + m^2}$, and $v_\parallel = p_\parallel / E$ is the longitudinal component of velocity. Rapidity is additive under Lorentz boosts along the longitudinal axis.

Using the rapidity and the transverse mass, one can calculate the energy and the longitudinal momentuma of a particle:

$$E = p^0 = m_\perp \cosh y \tag{.59}$$

$$p_\parallel = m_\perp \sinh y. \tag{.60}$$

In a similar way one defines the pseudorapidity variable η:

$$\eta = \frac{1}{2} \log \frac{|\mathbf{p}| + p_\parallel}{|\mathbf{p}| - p_\parallel} = \log \left(\cot \frac{\theta}{2} \right) = - \log \left(\tan \frac{\theta}{2} \right). \tag{.61}$$

One has:

$$|\mathbf{p}| = p_\perp \cosh \eta \tag{.62}$$

$$p_\parallel = p_\perp \sinh \eta. \tag{.63}$$

.3 Modified Bessel functions $K_n(x)$

The second-order ordinary differential equation

$$x^2 \frac{d^2 y(x)}{dx^2} + x \frac{dy(x)}{dx} - (x^2 + n^2) y(x) = 0 \tag{.64}$$

has a solution which is a linear combination of the modified Bessel functions of the first kind $I_n(x)$ and the second kind $K_n(x)$:

$$y(x) = c_1 I_n(x) + c_2 K_n(x). \tag{.65}$$

The modified Bessel function $K_n(x)$ has the following integral representation

$$K_n(x) = \frac{\sqrt{\pi} x^n}{2^n \Gamma\left(n + \frac{1}{2}\right)} \int_1^\infty dt\, e^{-xt} (t^2 - 1)^{n - \frac{1}{2}}. \tag{.66}$$

The importance of the functions $K_n(x)$ in relativistic thermodynamics comes from the fact that many relativistic phase space integral are reduced to the integral of the previous form.

The derivative of the Bessel function $K_n(x)$ can be expressed as:

$$\frac{\partial K_n(x)}{\partial x} = -\frac{1}{2} \left(K_{n-1}(x) + K_{n+1}(x) \right) \tag{.67}$$

which can also be expressed as

$$\frac{\partial K_n(x)}{\partial x} = -K_{n-1}(x) - \frac{n}{x}K_n(x). \tag{.68}$$

The series expansions of $K_n(x)$ for $x \to 0$ and for $n = 1, 2, 3$ are given by

$$K_1(x) = \frac{1}{x} + O(x^1) \tag{.69}$$

$$K_2(x) = \frac{2}{x^2} - \frac{1}{2} + O(x^2) \tag{.70}$$

$$K_3(x) = \frac{8}{x^3} - \frac{1}{x} + \frac{x}{8} + O(x^3). \tag{.71}$$

The asymptotic expansion for $x \to \infty$ has the following form:

$$K_n(x) = e^{-x}\left(\sqrt{\frac{\pi}{2x}} + O\left(x^{-\frac{3}{2}}\right)\right). \tag{.72}$$

Bibliography

[1] F. Wojciech. *Phenomenology of Ultra-relativistic Heavy-ion Collisions*. World Scientific.

[2] David J. Gross and Frank Wilczek. Ultraviolet behavior of non-abelian gauge theories. *Phys. Rev. Lett.*, 30:1343–1346, Jun 1973.

[3] H. David Politzer. Reliable perturbative results for strong interactions? *Phys. Rev. Lett.*, 30:1346–1349, Jun 1973.

[4] Siegfried Bethke. The 2009 World Average of alpha(s). *Eur. Phys. J.*, C64:689–703, 2009.

[5] Olaf Kaczmarek and Felix Zantow. Static quark anti-quark free and internal energy in 2-flavor QCD and bound states in the QGP. *PoS*, LAT2005:192, 2006.

[6] Alexander M. Polyakov. Thermal Properties of Gauge Fields and Quark Liberation. *Phys. Lett.*, B72:477–480, 1978.

[7] Leonard Susskind. Lattice Models of Quark Confinement at High Temperature. *Phys. Rev.*, D20:2610–2618, 1979.

[8] C. Borgs and E. Seiler. QUARK DECONFINEMENT AT HIGH TEMPERATURE. A RIGOROUS PROOF. *Nucl. Phys.*, B215:125–135, 1983.

[9] Szabolcs Borsanyi, Ydalia Delgado, Stephan Durr, Zoltan Fodor, Sandor D. Katz, Stefan Krieg, Thomas Lippert, Daniel Nogradi, and Kalman K. Szabo. QCD thermodynamics with dynamical overlap fermions. *Phys. Lett.*, B713:342–346, 2012.

[10] S. Aoki et al. Light hadron spectrum and quark masses from quenched lattice QCD. *Phys. Rev.*, D67:034503, 2003.

[11] Szabocls Borsanyi, Zoltan Fodor, Christian Hoelbling, Sandor D. Katz, Stefan Krieg, and Kalman K. Szabo. Full result for the QCD equation of state with 2+1 flavors. *Phys. Lett.*, B730:99–104, 2014.

[12] M. Ciminale, R. Gatto, N. D. Ippolito, G. Nardulli, and M. Ruggieri. Three flavor Nambu-Jona Lasinio model with Polyakov loop and competition with nuclear matter. *Phys. Rev.*, D77:054023, 2008.

[13] H. Abuki, R. Anglani, R. Gatto, G. Nardulli, and M. Ruggieri. Chiral crossover, deconfinement and quarkyonic matter within a Nambu-Jona Lasinio model with the Polyakov loop. *Phys. Rev.*, D78:034034, 2008.

[14] Raoul Gatto and Marco Ruggieri. Hot Quark Matter with an Axial Chemical Potential. *Phys. Rev.*, D85:054013, 2012.

[15] F. Gelis. Initial state and thermalization in the Color Glass Condensate framework. *Int. J. Mod. Phys.*, E24(10):1530008, 2015.

[16] T. Lappi and L. McLerran. Some features of the glasma. *Nucl. Phys.*, A772:200–212, 2006.

[17] Francois Gelis and Raju Venugopalan. Three lectures on multi-particle production in the glasma. *Acta Phys. Polon.*, B37:3253–3314, 2006.

[18] T. Lappi. The Glasma initial state at the LHC. *J. Phys.*, G35:104052, 2008.

[19] F. Gelis, T. Lappi, and L. McLerran. Glittering Glasmas. *Nucl. Phys.*, A828:149–160, 2009.

[20] Kenji Fukushima and Francois Gelis. The evolving Glasma. *Nucl. Phys.*, A874:108–129, 2012.

[21] Hideaki Iida, Teiji Kunihiro, Berndt Mueller, Akira Ohnishi, Andreas Schaefer, and Toru T. Takahashi. Entropy production in classical Yang-Mills theory from Glasma initial conditions. *Phys. Rev.*, D88:094006, 2013.

[22] F. D. Aaron et al. Combined Measurement and QCD Analysis of the Inclusive e+- p Scattering Cross Sections at HERA. *JHEP*, 01:109, 2010.

[23] Larry McLerran. Strongly Interacting Matter at High Energy Density. *Int. J. Mod. Phys.*, A25:5847–5864, 2010.

[24] Stanislaw Mrowczynski. Early stage thermalization via instabilities. *PoS*, CPOD2006:042, 2006.

[25] T. S. Biro, C. Gong, Berndt Muller, and A. Trayanov. Hamiltonian dynamics of Yang-Mills fields on a lattice. *Int. J. Mod. Phys.*, C5:113–149, 1994.

[26] I. G. Bearden et al. Nuclear stopping in Au + Au collisions at s(NN)**(1/2) = 200-GeV. *Phys. Rev. Lett.*, 93:102301, 2004.

[27] Ehab Abbas et al. Centrality dependence of the pseudorapidity density distribution for charged particles in Pb-Pb collisions at $\sqrt{s_{\rm NN}}$ = 2.76 TeV. *Phys. Lett.*, B726:610–622, 2013.

[28] Johann Rafelski and Berndt Muller. Strangeness Production in the Quark - Gluon Plasma. *Phys. Rev. Lett.*, 48:1066, 1982. [Erratum: Phys. Rev. Lett.56,2334(1986)].

[29] T. Matsui and H. Satz. J/ψ Suppression by Quark-Gluon Plasma Formation. *Phys. Lett.*, B178:416, 1986.

[30] Raimond Snellings. Elliptic Flow: A Brief Review. *New J. Phys.*, 13:055008, 2011.

[31] John Adams et al. Particle type dependence of azimuthal anisotropy and nuclear modification of particle production in Au + Au collisions at s(NN)**(1/2) = 200-GeV. *Phys. Rev. Lett.*, 92:052302, 2004.

[32] S. S. Adler et al. Elliptic flow of identified hadrons in Au+Au collisions at s(NN)**(1/2) = 200-GeV. *Phys. Rev. Lett.*, 91:182301, 2003.

[33] P. Huovinen, P. F. Kolb, Ulrich W. Heinz, P. V. Ruuskanen, and S. A. Voloshin. Radial and elliptic flow at RHIC: Further predictions. *Phys. Lett.*, B503:58–64, 2001.

[34] Peter F. Kolb. What did we learn and what will we learn from hydrodynamics at RHIC? *AIP Conf. Proc.*, 698:694–697, 2004. [,694(2003)].

[35] Matthew Luzum and Paul Romatschke. Conformal Relativistic Viscous Hydrodynamics: Applications to RHIC results at s(NN)**(1/2) = 200-GeV. *Phys. Rev.*, C78:034915, 2008. [Erratum: Phys. Rev.C79,039903(2009)].

[36] V. Greco, C. M. Ko, and P. Levai. Parton coalescence at RHIC. *Phys. Rev.*, C68:034904, 2003.

[37] Denes Molnar and Sergei A. Voloshin. Elliptic flow at large transverse momenta from quark coalescence. *Phys. Rev. Lett.*, 91:092301, 2003.

[38] K. Huang. *Statistical Mechanics*. John Wiley and Sons, 2000.

[39] R.K. Pathria and P.D. Beale. *Statistical Mechanics*. Elsevier Science, 1996.

[40] L. P. Csernai. *Introduction to relativistic heavy ion collisions*. 1994.

[41] S. R. De Groot. *Relativistic Kinetic Theory. Principles and Applications*. 1980.

[42] Zhe Xu and Carsten Greiner. Thermalization of gluons in ultrarelativistic heavy ion collisions by including three-body interactions in a parton cascade. *Phys. Rev.*, C71:064901, 2005.

[43] D. Vasak, M. Gyulassy, and H. T. Elze. Quantum Transport Theory for Abelian Plasmas. *Annals Phys.*, 173:462–492, 1987.

[44] H. T. Elze, M. Gyulassy, D. Vasak, H. Heinz, Horst Stoecker, and W. Greiner. Towards a Relativistic Selfconsistent Quantum Transport Theory of Hadronic Matter. *Mod. Phys. Lett.*, A2:451–460, 1987.

[45] Cheuk-Yin Wong. Dynamics of nuclear fluid. VIII. Time-dependent Hartree-Fock approximation from a classical point of view. *Phys. Rev.*, C25:1460–1475, 1982.

[46] G. F. Bertsch and S. Das Gupta. A Guide to microscopic models for intermediate-energy heavy ion collisions. *Phys. Rept.*, 160:189–233, 1988.

[47] W. Cassing, V. Metag, U. Mosel, and K. Niita. Production of energetic particles in heavy ion collisions. *Phys. Rept.*, 188:363–449, 1990.

[48] H. Kruse, B. V. Jacak, and Horst Stoecker. Microscopic theory of pion production and sidewards flow in heavy ion collisions. *Phys. Rev. Lett.*, 54:289–292, 1985.

[49] Andreas Lang, Hans Babovsky, Wolfgang Cassing, Ulrich Mosel, Hans-Georg Reusch, and Klaus Weber. A new treatment of boltzmann-like collision integrals in nuclear kinetic equations. *Journal of Computational Physics*, 106(2):391 – 396, 1993.

[50] Bin Zhang, Miklos Gyulassy, and Yang Pang. Equation of state and collision rate tests of parton cascade models. *Phys. Rev.*, C58:1175–1182, 1998.

[51] J.I. Kapusta and C. Gale. *Finite-Temperature Field Theory: Principles and Applications*. Cambridge Monographs on Mathematical Physics. Cambridge University Press, 2006.

[52] Ryogo Kubo. Statistical mechanical theory of irreversible processes. 1. General theory and simple applications in magnetic and conduction problems. *J. Phys. Soc. Jap.*, 12:570–586, 1957.

[53] Melville S. Green. Markoff Random Processes and Statistical MEchanics of Time-Dependent Phenomena. II. Irreversible Processes in Fluids. *The Journal of Chemical Physics*, 22(3):398–413, 1954.

[54] Sangyong Jeon and Ulrich Heinz. Introduction to Hydrodynamics. *Int. J. Mod. Phys.*, E24(10):1530010, 2015.

[55] K. Yagi, T. Hatsuda, and Y. Miake. *Quark-Gluon Plasma: From Big Bang to Little Bang*. Cambridge Monographs on Particle Physics, Nuclear Physics and Cosmology. Cambridge University Press, 2005.

[56] Ingo Muller. Zum Paradoxon der Warmeleitungstheorie. *Z. Phys.*, 198:329–344, 1967.

[57] W. Israel and J. M. Stewart. Transient relativistic thermodynamics and kinetic theory. *Annals Phys.*, 118:341–372, 1979.

[58] P. Chakraborty and J. I. Kapusta. Quasi-Particle Theory of Shear and Bulk Viscosities of Hadronic Matter. *Phys. Rev.*, C83:014906, 2011.

[59] C. Sasaki and K. Redlich. Bulk viscosity in quasi particle models. *Phys. Rev.*, C79:055207, 2009.

[60] F. Reif. *Fundamentals of Statistical and Thermal Physics:*. Waveland Press, 2009.

[61] S. Chapman and T.G. Cowling. *The Mathematical Theory of Non-uniform Gases: An Account of the Kinetic Theory of Viscosity, Thermal Conduction and Diffusion in Gases*. Cambridge Mathematical Library. Cambridge University Press, 1970.

[62] Anton Wiranata and Madappa Prakash. Shear Viscosities from the Chapman-Enskog and the Relaxation Time Approaches. *Phys. Rev.*, C85:054908, 2012.

[63] A. S. Khvorostukhin, V. D. Toneev, and D. N. Voskresensky. Viscosity Coefficients for Hadron and Quark-Gluon Phases. *Nucl. Phys.*, A845:106–146, 2010.

[64] Chihiro Sasaki and Krzysztof Redlich. Transport coefficients near chiral phase transition. *Nucl. Phys.*, A832:62–75, 2010.

[65] John Fuini, III, Nasser S. Demir, Dinesh K. Srivastava, and Steffen A. Bass. Shear Viscosity in a Perturbative Quark-Gluon-Plasma. *J. Phys.*, G38:015004, 2011.

[66] Azwinndini Muronga. Shear viscosity coefficient from microscopic models. *Phys. Rev.*, C69:044901, 2004.

[67] C. Wesp, A. El, F. Reining, Z. Xu, I. Bouras, and C. Greiner. Calculation of shear viscosity using Green-Kubo relations within a parton cascade. *Phys. Rev.*, C84:054911, 2011.

[68] S. Plumari, A. Puglisi, F. Scardina, and V. Greco. Shear Viscosity of a strongly interacting system: Green-Kubo vs. Chapman-Enskog and Relaxation Time Approximation. *Phys. Rev.*, C86:054902, 2012.

[69] V. Ozvenchuk, O. Linnyk, M. I. Gorenstein, E. L. Bratkovskaya, and W. Cassing. Shear and bulk viscosities of strongly interacting "infinite" parton-hadron matter within the parton-hadron-string dynamics transport approach. *Phys. Rev.*, C87(6):064903, 2013.

[70] Kirill Tuchin. Particle production in strong electromagnetic fields in relativistic heavy-ion collisions. *Adv. High Energy Phys.*, 2013:490495, 2013.

[71] Yuji Hirono, Masaru Hongo, and Tetsufumi Hirano. Estimation of electric conductivity of the quark gluon plasma via asymmetric heavy-ion collisions. *Phys. Rev.*, C90(2):021903, 2014.

[72] Umut Gursoy, Dmitri Kharzeev, and Krishna Rajagopal. Magnetohydrodynamics, charged currents and directed flow in heavy ion collisions. *Phys. Rev.*, C89(5):054905, 2014.

[73] L. McLerran and V. Skokov. Comments About the Electromagnetic Field in Heavy-Ion Collisions. *Nucl. Phys.*, A929:184–190, 2014.

[74] Kenji Fukushima, Dmitri E. Kharzeev, and Harmen J. Warringa. The Chiral Magnetic Effect. *Phys. Rev.*, D78:074033, 2008.

[75] Simon Turbide, Ralf Rapp, and Charles Gale. Hadronic production of thermal photons. *Phys. Rev.*, C69:014903, 2004.

[76] O. Linnyk, W. Cassing, and E. L. Bratkovskaya. Centrality dependence of the direct photon yield and elliptic flow in heavy-ion collisions at $\sqrt{s_{NN}} = 200$ GeV. *Phys. Rev.*, C89(3):034908, 2014.

[77] C. Cercignani and G.M. Kremer. *The Relativistic Boltzmann Equation: Theory and Applications*. Progress in Mathematical Physics. Birkhäuser Basel, 2012.

[78] D. Fernandez-Fraile and A. Gomez Nicola. The Electrical conductivity of a pion gas. *Phys. Rev.*, D73:045025, 2006.

[79] A. Puglisi, S. Plumari, and V. Greco. Electric Conductivity from the solution of the Relativistic Boltzmann Equation. *Phys. Rev.*, D90:114009, 2014.

[80] Simon W Mages, Szabolcs Borsányi, Zoltán Fodor, Andreas Schäfer, and Kálmán Szabó. Shear Viscosity from Lattice QCD. *PoS*, LATTICE2014:232, 2015.

[81] Harvey B. Meyer. A Calculation of the shear viscosity in SU(3) gluodynamics. *Phys. Rev.*, D76:101701, 2007.

[82] Atsushi Nakamura and Sunao Sakai. Transport coefficients of gluon plasma. *Phys. Rev. Lett.*, 94:072305, 2005.

[83] Sunao Sakai and Atsushi Nakamura. Lattice calculation of the QGP viscosities: Present results and next project. *PoS*, LAT2007:221, 2007. [AIP Conf. Proc.893,5(2007)].

[84] Alessandro Amato, Gert Aarts, Chris Allton, Pietro Giudice, Simon Hands, and Jon-Ivar Skullerud. Electrical conductivity of the quark-gluon plasma across the deconfinement transition. *Phys. Rev. Lett.*, 111(17):172001, 2013.

[85] Gert Aarts, Chris Allton, Justin Foley, Simon Hands, and Seyong Kim. Spectral functions at small energies and the electrical conductivity in hot, quenched lattice QCD. *Phys. Rev. Lett.*, 99:022002, 2007.

[86] H. T. Ding, A. Francis, O. Kaczmarek, F. Karsch, E. Laermann, and W. Soeldner. Thermal dilepton rate and electrical conductivity: An analysis of vector current correlation functions in quenched lattice QCD. *Phys. Rev.*, D83:034504, 2011.

[87] Bastian B. Brandt, Anthony Francis, Harvey B. Meyer, and Hartmut Wittig. Two-flavour lattice QCD correlation functions in the deconfinement transition region. 2013. [PoSConfinementX,186(2012)].

[88] M. Natsuume. *AdS/CFT Duality User Guide*. Lecture Notes in Physics. Springer Japan, 2015.

[89] Juan Martin Maldacena. The Large N limit of superconformal field theories and supergravity. *Int. J. Theor. Phys.*, 38:1113–1133, 1999. [Adv. Theor. Math. Phys.2,231(1998)].

[90] Dam T. Son and Andrei O. Starinets. Viscosity, Black Holes, and Quantum Field Theory. *Ann. Rev. Nucl. Part. Sci.*, 57:95–118, 2007.

[91] Alfonso V. Ramallo. Introduction to the AdS/CFT correspondence. *Springer Proc. Phys.*, 161:411–474, 2015.

[92] P. Kovtun, Dan T. Son, and Andrei O. Starinets. Viscosity in strongly interacting quantum field theories from black hole physics. *Phys. Rev. Lett.*, 94:111601, 2005.

[93] Mauro Brigante, Hong Liu, Robert C. Myers, Stephen Shenker, and Sho Yaida. Viscosity Bound Violation in Higher Derivative Gravity. *Phys. Rev.*, D77:126006, 2008.

[94] Simon Caron-Huot, Pavel Kovtun, Guy D. Moore, Andrei Starinets, and Laurence G. Yaffe. Photon and dilepton production in supersymmetric Yang-Mills plasma. *JHEP*, 12:015, 2006.

[95] L.P. Pitaevskii and E.M. Lifshitz. *Physical Kinetics*. Number v. 10. Elsevier Science, 2012.

[96] Bin Zhang, Miklos Gyulassy, and Che Ming Ko. Elliptic flow from a parton cascade. *Phys. Lett.*, B455:45–48, 1999.

[97] Denes Molnar and Miklos Gyulassy. Saturation of elliptic flow and the transport opacity of the gluon plasma at RHIC. *Nucl. Phys.*, A697:495–520, 2002. [Erratum: Nucl. Phys.A703,893(2002)].

[98] G. Ferini, M. Colonna, M. Di Toro, and V. Greco. Scalings of Elliptic Flow for a Fluid at Finite Shear Viscosity. *Phys. Lett.*, B670:325–329, 2009.

[99] V. Greco, M. Colonna, M. Di Toro, and G. Ferini. Anisotropies in momentum space at finite Shear Viscosity in ultrarelativistic heavy-ion collisions. 2008. [Prog. Part. Nucl. Phys.62,562(2009)].

[100] S. Plumari, V. Baran, M. Di Toro, and V. Greco. Collective Flows in a Transport Approach. *J. Phys. Conf. Ser.*, 270:012061, 2011.

[101] Zhe Xu and Carsten Greiner. Elliptic flow of gluon matter in ultrarelativistic heavy-ion collisions. *Phys. Rev.*, C79:014904, 2009.

[102] Peter Brockway Arnold, Guy D Moore, and Laurence G. Yaffe. Transport coefficients in high temperature gauge theories. 2. Beyond leading log. *JHEP*, 05:051, 2003.

[103] N. Armesto, N. Borghini, S. Jeon, U. A. Wiedemann, S. Abreu, V. Akkelin, J. Alam, J. L. Albacete, A. Andronic, D. Antonov, et al. Heavy Ion Collisions at the LHC - Last Call for Predictions. *J. Phys.*, G35:054001, 2008.

[104] S. Plumari and V. Greco. Elliptic Flow and Shear Viscosity within a Transport Approach from RHIC to LHC Energy. *AIP Conf. Proc.*, 1422:56–61, 2012.

[105] P. Koch, Berndt Muller, and Johann Rafelski. Strangeness in Relativistic Heavy Ion Collisions. *Phys. Rept.*, 142:167–262, 1986.

[106] Kevin Dusling, Guy D. Moore, and Derek Teaney. Radiative energy loss and v(2) spectra for viscous hydrodynamics. *Phys. Rev.*, C81:034907, 2010.

[107] Pasi Huovinen and Denes Molnar. The Applicability of causal dissipative hydrodynamics to relativistic heavy ion collisions. *Phys. Rev.*, C79:014906, 2009.

[108] Salvatore Plumari, Wanda M. Alberico, Vincenzo Greco, and Claudia Ratti. Recent thermodynamic results from lattice QCD analyzed within a quasi-particle model. *Phys. Rev.*, D84:094004, 2011.

[109] Peter Levai and Ulrich W. Heinz. Massive gluons and quarks and the equation of state obtained from SU(3) lattice QCD. *Phys. Rev.*, C57:1879–1890, 1998.

[110] A. Peshier, Burkhard Kampfer, and G. Soff. From QCD lattice calculations to the equation of state of quark matter. *Phys. Rev.*, D66:094003, 2002.

[111] M. Bluhm, B. Kampfer, and K. Redlich. Bulk and shear viscosities of the gluon plasma in a quasiparticle description. *Phys. Rev.*, C84:025201, 2011.

[112] M. Bluhm, Burkhard Kampfer, and G. Soff. The QCD equation of state near T(c) within a quasi-particle model. *Phys. Lett.*, B620:131–136, 2005.

[113] W. Cassing and E. L. Bratkovskaya. Parton-Hadron-String Dynamics: an off-shell transport approach for relativistic energies. *Nucl. Phys.*, A831:215–242, 2009.

[114] Szabolcs Borsanyi, Gergely Endrodi, Zoltan Fodor, Antal Jakovac, Sandor D. Katz, Stefan Krieg, Claudia Ratti, and Kalman K. Szabo. The QCD equation of state with dynamical quarks. *JHEP*, 11:077, 2010.

[115] Rudy Marty, Elena Bratkovskaya, Wolfgang Cassing, Jörg Aichelin, and Hamza Berrehrah. Transport coefficients from the Nambu-Jona-Lasinio model for $SU(3)_f$. *Phys. Rev.*, C88:045204, 2013.

[116] Paul Romatschke and Ulrike Romatschke. Viscosity Information from Relativistic Nuclear Collisions: How Perfect is the Fluid Observed at RHIC? *Phys. Rev. Lett.*, 99:172301, 2007.

[117] Huichao Song, Steffen A. Bass, Ulrich Heinz, Tetsufumi Hirano, and Chun Shen. Hadron spectra and elliptic flow for 200 A GeV Au+Au collisions from viscous hydrodynamics coupled to a Boltzmann cascade. *Phys. Rev.*, C83:054910, 2011. [Erratum: Phys. Rev.C86,059903(2012)].

[118] Bjoern Schenke, Sangyong Jeon, and Charles Gale. (3+1)D hydrodynamic simulation of relativistic heavy-ion collisions. *Phys. Rev.*, C82:014903, 2010.

[119] Harri Niemi, Gabriel S. Denicol, Pasi Huovinen, Etele Molnar, and Dirk H. Rischke. Influence of the shear viscosity of the quark-gluon plasma on elliptic flow in ultrarelativistic heavy-ion collisions. *Phys. Rev. Lett.*, 106:212302, 2011.

[120] A. S. Khvorostukhin, V. D. Toneev, and D. N. Voskresensky. Shear and bulk viscosities for pure glue matter. *Phys. Rev.*, C83:035204, 2011.

[121] Sourendu Gupta. The Electrical conductivity and soft photon emissivity of the QCD plasma. *Phys. Lett.*, B597:57–62, 2004.

[122] Moritz Greif, Ioannis Bouras, Carsten Greiner, and Zhe Xu. Electric conductivity of the quark-gluon plasma investigated using a perturbative QCD based parton cascade. *Phys. Rev.*, D90(9):094014, 2014.

[123] W. Cassing, O. Linnyk, T. Steinert, and V. Ozvenchuk. Electrical Conductivity of Hot QCD Matter. *Phys. Rev. Lett.*, 110(18):182301, 2013.

[124] P. V. Buividovich, M. N. Chernodub, D. E. Kharzeev, T. Kalaydzhyan, E. V. Luschevskaya, and M. I. Polikarpov. Magnetic-Field-Induced insulator-conductor transition in SU(2) quenched lattice gauge theory. *Phys. Rev. Lett.*, 105:132001, 2010.

[125] Jens O. Andersen, Lars E. Leganger, Michael Strickland, and Nan Su. NNLO hard-thermal-loop thermodynamics for QCD. *Phys. Lett.*, B696:468–472, 2011.

[126] Jean Paul Blaizot and Edmond Iancu. Soft collective excitations in hot gauge theories. *Nucl. Phys.*, B417:608–673, 1994.

[127] Armando Puglisi, Salvatore Plumari, and Vincenzo Greco. Shear viscosity η to electric conductivity σ_{el} ratio for the quark–gluon plasma. *Phys. Lett.*, B751:326–330, 2015.

[128] Stefano I. Finazzo and Jorge Noronha. Holographic calculation of the electric conductivity of the strongly coupled quark-gluon plasma near the deconfinement transition. *Phys. Rev.*, D89(10):106008, 2014.

[129] A. Nakamura and T. Saito. QCD color interactions between two quarks. *Phys. Lett.*, B621:171–175, 2005.

[130] H. van Hees, M. Mannarelli, V. Greco, and R. Rapp. Nonperturbative heavy-quark diffusion in the quark-gluon plasma. *Phys. Rev. Lett.*, 100:192301, 2008.

[131] Szabolcs Borsanyi, Zoltan Fodor, Christian Hoelbling, Sandor D Katz, Stefan Krieg, Claudia Ratti, and Kalman K. Szabo. Is there still any T_c mystery in lattice QCD? Results with physical masses in the continuum limit III. *JHEP*, 09:073, 2010.

[132] A. Bazavov et al. The chiral and deconfinement aspects of the QCD transition. *Phys. Rev.*, D85:054503, 2012.

[133] Paul Romatschke and Raju Venugopalan. The Unstable Glasma. *Phys. Rev.*, D74:045011, 2006.

[134] Hirotsugu Fujii, Kazunori Itakura, and Aiichi Iwazaki. Instabilities in non-expanding glasma. *Nucl. Phys.*, A828:178–190, 2009.

[135] Thomas Epelbaum and Francois Gelis. Pressure isotropization in high energy heavy ion collisions. *Phys. Rev. Lett.*, 111:232301, 2013.

[136] Jorgen Randrup and Stanislaw Mrowczynski. Chromodynamic Weibel instabilities in relativistic nuclear collisions. *Phys. Rev.*, C68:034909, 2003.

[137] Stanislaw Mrowczynski. Instabilities driven equilibration of the quark-gluon plasma. *Acta Phys. Polon.*, B37:427–454, 2006.

[138] Maximilian Attems, Anton Rebhan, and Michael Strickland. Instabilities of an anisotropically expanding non-Abelian plasma: 3D+3V discretized hard-loop simulations. *Phys. Rev.*, D87(2):025010, 2013.

[139] Anton Rebhan, Michael Strickland, and Maximilian Attems. Instabilities of an anisotropically expanding non-Abelian plasma: 1D+3V discretized hard-loop simulations. *Phys. Rev.*, D78:045023, 2008.

[140] L. Bellantuono, P. Colangelo, F. De Fazio, and F. Giannuzzi. On thermalization of a boost-invariant non Abelian plasma. *JHEP*, 07:053, 2015.

[141] Wilke van der Schee, Paul Romatschke, and Scott Pratt. Fully Dynamical Simulation of Central Nuclear Collisions. *Phys. Rev. Lett.*, 111(22):222302, 2013.

[142] Yuri V. Kovchegov and Anastasios Taliotis. Early Time Dynamics in Heavy Ion Collisions from AdS/CFT Correspondence. *Phys. Rev.*, C76:014905, 2007.

[143] Michal P. Heller, Romuald A. Janik, and Przemyslaw Witaszczyk. The characteristics of thermalization of boost-invariant plasma from holography. *Phys. Rev. Lett.*, 108:201602, 2012.

[144] Michal P. Heller, Romuald A. Janik, Michał Spaliński, and Przemysław Witaszczyk. Coupling hydrodynamics to nonequilibrium degrees of freedom in strongly interacting quark-gluon plasma. *Phys. Rev. Lett.*, 113(26):261601, 2014.

[145] W. Heisenberg and H. Euler. Consequences of Dirac's theory of positrons. *Z. Phys.*, 98:714–732, 1936.

[146] Julian S. Schwinger. On gauge invariance and vacuum polarization. *Phys. Rev.*, 82:664–679, 1951.

[147] Florian Hebenstreit, Jürgen Berges, and Daniil Gelfand. Real-time dynamics of string breaking. *Phys. Rev. Lett.*, 111:201601, 2013.

[148] Florian Hebenstreit, Jürgen Berges, and Daniil Gelfand. Simulating fermion production in 1+1 dimensional QED. *Phys. Rev.*, D87(10):105006, 2013.

[149] F. Gelis and N. Tanji. Formulation of the Schwinger mechanism in classical statistical field theory. *Phys. Rev.*, D87(12):125035, 2013.

[150] Gouranga C. Nayak. Schwinger Mechanism for Gluon Pair Production in the Presence of Arbitrary Time Dependent Chromo-Electric Field. *Eur. Phys. J.*, C59:715–722, 2009.

[151] Gouranga C. Nayak. Schwinger Mechanism for Quark-Antiquark Production in the Presence of Arbitrary Time Dependent Chromo-Electric Field. *Electron. J. Theor. Phys.*, 8:279–286, 2011.

[152] Fred Cooper and Gouranga C. Nayak. Schwinger mechanism for fermion pair production in the presence of arbitrary time dependent background electric field. 2006.

[153] Fred Cooper and Gouranga C. Nayak. Schwinger mechanism in the presence of arbitrary time dependent background electric field. 2006.

[154] Fred Cooper and Gouranga C. Nayak. Non-perturbative gluon pair production from a constant chromo-electric field via the Schwinger mechanism in arbitrary gauge. *Phys. Rev.*, D73:065005, 2006.

[155] Gouranga C. Nayak. Non-perturbative quark-antiquark production from a constant chromo-electric field via the Schwinger mechanism. *Phys. Rev.*, D72:125010, 2005.

[156] A. Casher, H. Neuberger, and S. Nussinov. Chromoelectric Flux Tube Model of Particle Production. *Phys. Rev.*, D20:179–188, 1979.

[157] N. K. Glendenning and T. Matsui. CREATION OF ANTI-Q Q PAIR IN A CHROMOELECTRIC FLUX TUBE. *Phys. Rev.*, D28:2890–2891, 1983.

[158] A. Bialas and W. Czyz. Boost Invariant Boltzmann-vlasov Equations for Relativistic Quark - Anti-quark Plasma. *Phys. Rev.*, D30:2371, 1984.

[159] A. Bialas and W. Czyz. Oscillations of Relativistic, Boost Invariant Quark - Anti-quark Plasma. *Z. Phys.*, C28:255, 1985.

[160] A. Bialas and W. Czyz. Conversion of Color Field Into $Q\bar{Q}$ Matter in the Central Region of High-energy Heavy Ion Collisions. *Nucl. Phys.*, B267:242, 1986.

[161] M. Gyulassy and A. Iwazaki. QUARK AND GLUON PAIR PRODUCTION IN SU(N) COVARIANT CONSTANT FIELDS. *Phys. Lett.*, B165:157–161, 1985.

[162] G. Gatoff, A. K. Kerman, and T. Matsui. The Flux Tube Model for Ultrarelativistic Heavy Ion Collisions: Electrohydrodynamics of a Quark Gluon Plasma. *Phys. Rev.*, D36:114, 1987.

[163] H. T. Elze, M. Gyulassy, and D. Vasak. Transport Equations for the QCD Quark Wigner Operator. *Nucl. Phys.*, B276:706–728, 1986.

[164] H. T. Elze, M. Gyulassy, and D. Vasak. Transport Equations for the QCD Gluon Wigner Operator. *Phys. Lett.*, B177:402–408, 1986.

[165] A. Bialas and W. Czyz. Production and Collective Motion of $q\bar{q}$ Plasma in Heavy Ion Collisions. *Acta Phys. Polon.*, B17:635, 1986.

[166] Wojciech Florkowski. Schwinger tunneling and thermal character of hadron spectra. *Acta Phys. Polon.*, B35:799–808, 2004.

[167] Katarzyna Bajan and Wojciech Florkowski. Boost invariant particle production in transport equations. *Acta Phys. Polon.*, B32:3035–3052, 2001.

[168] A. Bialas, W. Czyz, A. Dyrek, W. Florkowski, and Robert B. Peschanski. Intermittency and the Schwinger Tunneling Mechanism. *Phys. Lett.*, B229:398, 1989.

[169] A. Dyrek and W. Florkowski. PRODUCTION OF HEAVY QUARKS IN STRONG CHROMOELECTRIC FIELDS. *Nuovo Cim.*, A102:1013, 1989.

[170] A. Bialas, W. Czyz, A. Dyrek, and W. Florkowski. Oscillations of Quark - Gluon Plasma Generated in Strong Color Fields. *Nucl. Phys.*, B296:611, 1988.

[171] Radoslaw Ryblewski and Wojciech Florkowski. Equilibration of anisotropic quark-gluon plasma produced by decays of color flux tubes. *Phys. Rev.*, D88:034028, 2013.

[172] Wojciech Florkowski and Radoslaw Ryblewski. Thermalization of anisotropic quark–gluon plasma produced by decays of color flux tubes. *Nucl. Phys.*, A931:343–347, 2014.

[173] Naoto Tanji and Kazunori Itakura. Schwinger mechanism enhanced by the Nielsen–Olesen instability. *Phys. Lett.*, B713:117–121, 2012.

[174] Naoto Tanji. Dynamical view of pair creation in uniform electric and magnetic fields. *Annals Phys.*, 324:1691–1736, 2009.

[175] Naoto Tanji. Pair creation in boost-invariantly expanding electric fields and two-particle correlations. *Phys. Rev.*, D83:045011, 2011.

[176] Salvatore Plumari, Armando Puglisi, Maria Colonna, Francesco Scardina, and Vincenzo Greco. Shear viscosity and chemical equilibration of the QGP. 2012. [J. Phys. Conf. Ser.420,012029(2013)].

[177] M. Ruggieri, F. Scardina, S. Plumari, and V. Greco. Elliptic Flow from Non-equilibrium Initial Condition with a Saturation Scale. *Phys. Lett.*, B727:177–181, 2013.

[178] Marco Ruggieri, Francesco Scardina, Salvatore Plumari, and Vincenzo Greco. Thermalization, Isotropization and Elliptic Flow from Nonequilibrium Initial Conditions with a Saturation Scale. *Phys. Rev.*, C89(5):054914, 2014.

[179] T. S. Biro, Holger Bech Nielsen, and Joern Knoll. Color Rope Model for Extreme Relativistic Heavy Ion Collisions. *Nucl. Phys.*, B245:449–468, 1984.

[180] M. Ruggieri, A. Puglisi, L. Oliva, S. Plumari, F. Scardina, and V. Greco. Modeling early stages of relativistic heavy ion collisions: Coupling relativistic transport theory to decaying color-electric flux tubes. *Phys. Rev. C*, 92:064904, Dec 2015.

[181] Zhe Xu, Carsten Greiner, and Horst Stocker. PQCD calculations of elliptic flow and shear viscosity at RHIC. *Phys. Rev. Lett.*, 101:082302, 2008.

[182] E. L. Bratkovskaya, W. Cassing, V. P. Konchakovski, and O. Linnyk. Parton-Hadron-String Dynamics at Relativistic Collider Energies. *Nucl. Phys.*, A856:162–182, 2011.

[183] L.D. Landau, E.M. Lifshits, E.M. Lifshits, and L.P. Pitaevski. *Electrodynamics of continuous media:*. Pergamon international library of science, technology, engineering, and social studies. Pergamon, 1984.

[184] Salvatore Plumari, Giovanni Luca Guardo, Vincenzo Greco, and Jean-Yves Ollitrault. Viscous corrections to anisotropic flow and transverse momentum spectra from transport theory. *Nucl. Phys.*, A941:87–96, 2015.

[185] J. Adams et al. Azimuthal anisotropy in Au+Au collisions at s(NN)**(1/2) = 200-GeV. *Phys. Rev.*, C72:014904, 2005.